VOLUME 76 MARCH 30, 1972 NUMBER 7

JPCHAx

THE JOURNAL OF PHYSICAL CHEMISTRY

PUBLISHED BIWEEKLY BY THE AMERICAN CHEMICAL SOCIETY

THE JOURNAL OF

PHYSICAL CHEMISTRY

 Published biweekly by the American Chemical Society at 20th and Northampton Sts., Easton, Pa. 18042. Second-class postage paid at Washington, D. C., and at additional mailing offices.

All manuscripts should be sent to *The Journal of Physical Chemistry*, Department of Chemistry, University of Minnesota, Minneapolis, Minn. 55455.

Additions and Corrections are published once yearly in the final issue. See Volume 75, Number 26 for the proper form.

Extensive or unusual alterations in an article after it has been set in type are made at the author's expense, and it is understood that by requesting such alterations the author agrees to defray the cost thereof.

The American Chemical Society and the Editor of *The Journal of Physical Chemistry* assume no responsibility for the statements and opinions advanced by contributors.

Correspondence regarding accepted copy, proofs, and reprints should be directed to Editorial Production Office, American Chemical Society, 20th and Northampton Sts., Easton, Pa. 18042. Manager: CHARLES R. BERTSCH. Assistant Editor: EDWARD A. BORGER.

Advertising Office: Century Communications Corporation, 142 East Avenue, Norwalk, Conn. 06851.

Business and Subscription Information

Remittances and orders for subscriptions and for single copies, notices of changes of address and new professional connections, and claims for missing numbers should be sent to the Subscription Service Department, American Chemical Society, 1155 Sixteenth St., N.W., Washington, D. C. 20036. Allow 4 weeks for changes of address. Please include an old address label with the notification.

Claims for missing numbers will not be allowed (1) if received more than sixty days from date of issue, (2) if loss was due to failure of notice of change of address to be received before the date specified in the preceding paragraph, or (3) if the reason for the claim is "missing from files."

Subscription rates (1972): members of the American Chemical Society, $20.00 for 1 year; to nonmembers, $60.00 for 1 year. Those interested in becoming members should write to the Admissions Department, American Chemical Society, 1155 Sixteenth St., N.W., Washington, D. C. 20036. Postage to Canada and countries in the Pan-American Union, $5.00; all other countries, $6.00. Single copies for current year: $3.00. Rates for back issues from Volume 56 to date are available from the Special Issues Sales Department, 1155 Sixteenth St., N.W., Washington, D. C. 20036.

This publication and the other ACS periodical publications are now available on microfilm. For information write to: MICROFILM, Special Issues Sales Department, 1155 Sixteenth St., N.W., Washington, D. C. 20036.

Notice to Authors last printed in the issue of December 23, 1971

THE JOURNAL OF

PHYSICAL CHEMISTRY

Volume 76, Number 7 March 30, 1972

JPCHAx 76(7) 947–1088 (1972)

COMMUNICATIONS TO THE EDITOR

AUTHOR INDEX

In papers with more than one author the name of the author to whom inquiries about the paper should be addressed is marked with an asterisk in the by-line.

THE JOURNAL OF
PHYSICAL CHEMISTRY

VOLUME 76, NUMBER 7 MARCH 30, 1972

Molecular Beam Analysis Investigation of the Reaction between Atomic Fluorine and Carbon Tetrachloride

by C. E. Kolb and M. Kaufman*

Frick Chemical Laboratory, Princeton University, Princeton, New Jersey 08540 *(Received October 1, 1971)*

Publication costs assisted by the Office of Naval Research

Molecular beam analysis, a method for monitoring transient intermediates in gaseous reactions by a combination of molecular beam and mass spectrometric techniques, is employed to study the reaction of fluorine atoms with CCl_4. Atomic fluorine is generated by discharging either CF_4 or F_2–Ar mixtures. Titration with H_2 provides absolute measurements of the concentration of both atomic and molecular fluorine. The observation that very little CCl_3F is formed at low F_2 concentrations, such as are produced by discharging CF_4, establishes that at 25° the mechanism of the initial reaction is abstraction to produce FCl and CCl_3. The rate constant is 2.4×10^8 cm³/(mol sec) to within a factor of 2.

Introduction

Surprisingly few studies of the kinetics of atomic fluorine reactions have appeared in the literature, particularly in comparison with the voluminous amount of rate data available for nitrogen, oxygen, and the other halogens. In fact, prior to 1970, the only experimentally determined absolute rate constant for an atomic fluorine reaction was for $F + CCl_4$,[1] and this value is inconsistent with recent thermochemical measurements. Other reports on fluorine atom kinetics have included relative rates of hydrogen abstraction from hydrocarbons and their halogenated derivatives[2] and activation energies for the reactions $F + O_3$[3] and $F + ClF_3$.[4] In addition, vibrational energy distributions have been determined for HF and DF produced by the reaction of atomic fluorine with H_2 and D_2.[5]

The lack of convenient methods of generating, handling, and measuring the concentration of atomic fluorine is the principal reason that so few investigations of the kinetics of its reaction have been reported. In almost all the work summarized above, fluorine atoms were produced by thermal or photolytic decomposition of F_2. However, weakly bound molecular fluorine (D_0 = 37 kcal/mol[6]) is so reactive that careful consideration of its reactions is necessary in interpreting such kinetic data.

In an effort to overcome this difficulty, Wagner and coworkers have recently developed a fluorine atom source based on the reactions

$$N + NF_2 \longrightarrow N_2 + 2F \qquad (1)$$

The NF_2 radical is prepared by thermal dissociation

(1) D. T. Clark and J. M. Tedder, *J. Phys. Chem.*, **68**, 2018 (1964).

(2) P. C. Anson, P. S. Fredricks, and J. M. Tedder, *J. Chem. Soc.*, 918 (1959); G. C. Fettis, J. H. Knox, and A. F. Trotman-Dickenson, *ibid.*, 1064 (1960); R. Foon and N. A. McAskill, *Trans. Faraday Soc.*, **65**, 3005 (1969).

(3) E. H. Staricco, J. E. Sicre, and H. J. Schumacher, *Z. Phys. Chem. (Frankfurt am Main)*, **31**, 385 (1962).

(4) R. L. Krieger, R. Gatti, and H. J. Schumacher, *ibid.*, **51**, 240 (1966).

(5) J. H. Parker and G. C. Pimentel, *J. Chem. Phys.*, **51**, 91 (1969); J. C. Polanyi and D. C. Tardy, *ibid.*, **51**, 5717 (1969); T. P. Schafer, P. E. Siska, J. M. Parson, F. P. Tully, Y. C. Wong, and Y. T. Lee, *ibid.*, **53**, 3385 (1970).

(6) "Bond Dissociation Energies in Simple Molecules," NSRDS-NES 31, U. S. Government Printing Office, Washington, D. C., 1970.

of N_2F_4 and treated with nitrogen atoms produced by microwave discharge through N_2.[7] Using this source, Wagner, *et al.*, have measured the absolute rate constants for fluorine atoms reacting with H_2,[7] Cl_2,[8] and CH_4.[9] As a source of fluorine atoms, this scheme has the advantage of limiting the F_2 concentration to the small amount which results from atomic fluorine recombination. Neither the volume nor surface fluorine atom recombination rate has been measured. However, at pressures of a few Torr or less in glass or Teflon-coated systems, both processes seem to be quite slow. Unfortunately, the low efficiency with which N_2 is dissociated in microwave discharges limits the concentration of atomic fluorine that can be produced by Wagner's method and restricts this source to the study of fast reactions. Further disadvantages are the high cost of N_2F_4 and the necessity of pyrolyzing it to form NF_2. In addition, since both nitrogen atoms and NF_2 are reactive species, the excess of either must be kept to a minimum and accounted for in the analysis.

These limitations have led us to investigate alternative methods of producing fluorine atoms for rate studies. We have found that the microwave discharge through CF_4 is a simple and convenient source of atomic fluorine almost completely free of F_2. In addition, when considerable F_2 can be tolerated, discharges through F_2–Ar mixtures can be employed to produce higher concentrations of fluorine atoms.

These discharge systems have been characterized by molecular beam analysis, a novel technique for identifying and monitoring transient intermediates in gaseous systems that has recently been developed in our laboratory. Since quantitative kinetic studies often require knowledge of absolute atom concentrations, we have developed a gas-phase titration with H_2 which converts the relative concentrations of F and F_2 provided by molecular beam analysis to absolute values.

Finally, these techniques of generating atomic fluorine and measuring its concentration have been employed to study the rate and mechanism of the F + CCl_4 reaction. Although recent studies had suggested that a displacement mechanism predominates for this reaction at flame temperatures, at 25° it is shown to proceed by abstraction to form FCl and CCl_3. Our measured rate constant of the reaction is far more compatible with its endothermic nature than the value obtained in a previous investigation.[1]

Experimental Section

In ordinary mass spectrometry, the detection of gas-phase reaction intermediates is often precluded owing to interference from dissociative ionization of stable molecules. These interferences may sometimes be avoided by careful control of the energy of the ionizing electrons. However, owing to the weak F_2 bond, this procedure is particularly ineffective in removing F_2 contributions when monitoring fluorine atoms by mass spectrometry. In addition, much of the inherent sensitivity of mass spectrometry is sacrificed by use of low-energy electrons and the small electron currents that are necessary for precise energy control.

The molecular beam analyzer employed in this work is a mass spectrometer equipped with a high-efficiency Weiss-type[10] ionizer, which ionizes with *ca.* 250 mA of 100-V electrons. No attempt is made to identify the neutral parent of each ion by appearance-potential discrimination. Instead, a number of molecular beam techniques are employed to separate these neutrals before they enter the ionizer. The most important of these techniques in the present work is magnetic deflection. A beam obstacle and inhomogeneous magnetic field are arranged so that only paramagnetic species are directed into the ionizer. Some diamagnetic molecules (*ca.* 2% of the unblocked beam) are scattered into the ionizer, but the net result is greatly increased sensitivity for detecting free atoms or radicals. The magnetic field is produced by a small permanent hexapole magnet. Comparisons with the field off and on are made by raising the magnet and then lowering it onto a kinematic mount which reproducibly aligns it on the beam axis. The beam is modulated and a hybrid detection system, consisting of pulse amplification and phase-sensitive detection, is generally employed. By substituting an electric quadrupole field for the magnet, electric deflection can be used to separate polar from nonpolar species. Velocity distributions of neutrals may also be determined, either by pulsing the beam and measuring the time dependence of the ion signal or by modulating the beam in a pseudorandom manner and employing correlation techniques. Repetitive multiscaling is used to increase the signal-to-noise ratio of the measured velocity distributions. Figure 1 shows a schematic representation of the molecular beam analyzer. A more detailed description of the method may be found in ref 11.

In this work, fluorine atom concentrations were taken as proportional to the paramagnetic component of the m/e 19 ion current. Velocity distribution measurements showed that this signal results from a neutral with a mass of roughly 20, thus substantiating that it arises from fluorine atoms.

The conventional discharge-flow system, consisting of a quartz discharge tube and a Pyrex flow reactor, was found to be unsuitable for studying fluorine atom kinetics. Atomic fluorine reacts rapidly with Pyrex, producing an etched appearance, and very few fluorine

(7) K. H. Homann, W. C. Solomon, J. Warnatz, H. Gg. Wagner, and C. Zetzsch, *Ber. Bunsenges. Phys. Chem.*, **74**, 585 (1970).

(8) J. Warnatz, H. Gg. Wagner, and C. Zetzsch, *ibid.*, **75**, 119 (1971).

(9) H. Gg. Wagner, J. Warnatz, and C. Zetzsch, in preparation.

(10) R. Weiss, *Rev. Sci. Instrum.*, **32**, 397 (1961).

(11) C. E. Kolb and M. Kaufman, *Chem. Instrum.*, **3**, 175 (1971); C. E. Kolb, Ph.D. Thesis, Princeton University, 1971; C. E. Kolb and M. Kaufman, ONR Report No. AD-721400, Jan 1971.

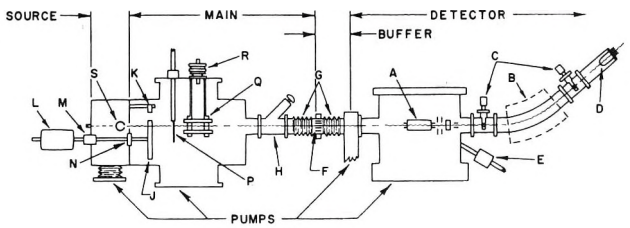

Figure 1. Side view of molecular beam analyzer: (A) electron bombardment ionizer, (B) magnet pole tips, (C) variable slits, (D) electron multiplier, (E) variable leak value, (F) directional entrance, (G) flexible metal bellows, (H) straight-through valve, (J) pulser or modulator, (K) magnetic pickup, (L) motor, (M) rotary motion feedthrough, (N) bearing, (P) movable obstacle, (Q) electric quadrupole field, (R) high voltage terminal, (S) reactor [reproduced with permission from *Chem. Instrum.*, **3**, 175 (1971)].

atoms remain after flowing through 80 cm of Pyrex tubing. The reaction between fluorine atoms and quartz is considerably slower, but some "clouding" can be noted after several hours of exposure. Within the discharge region, corrosion is even more severe, and usually a hole penetrates the 1-mm thick quartz wall of the discharge tube within 10 hr of operation. (We employ an Evenson-type discharge cavity,[12] operating with 50–100 W of 2450-MHz power in the pressure range 0.2–2 Torr.) The molecular beam analyzer indicates large amounts of SiF_4 and COF_2 in such systems, with smaller amounts of $SiOF_2$, O_2, CO_2, OF_2, BF_3, C_2F_6, and F_2.

Teflon is the material of choice for handling atomic fluorine. We have successfully employed both Teflon liners and Teflon coatings in quartz and Pyrex flow systems to greatly reduce wall reactions. The coatings are applied by a technique similar to that used by Berg and Kleppner to coat hydrogen maser storage bulbs,[13] and generally withstand serious deterioration for 50 hr or more of exposure to the discharge products. Unfortunately, Teflon is not suitable within the discharge cavity, where it is quickly vaporized, with the production of many low molecular weight fluorocarbons (and very few fluorine atoms). For the discharge section of the flow system, we have thus employed a 0.5-in. diameter cast alumina tube, similar to that used by Rosner and Allendorf.[14] In such tubes, production of OF_2 and COF_2 rapidly drops to extremely low levels. Presumably, a layer of nonvolatile AlF_3 is formed, which protects the discharge tube from further attack. No aluminum-containing species was ever detected mass spectrometrically. However, a very small O_2 signal was persistent, probably indicating some tendency for fluorine and oxygen atoms to diffuse through the AlF_3 coating. Oxygen and oxygen-containing compounds appear to be catalytic for production of fluorine atoms in both the F_2–Ar and CF_4 discharges. Thus, while discharges in alumina tubes are a much "cleaner" source of fluorine atoms, they generally produce lower

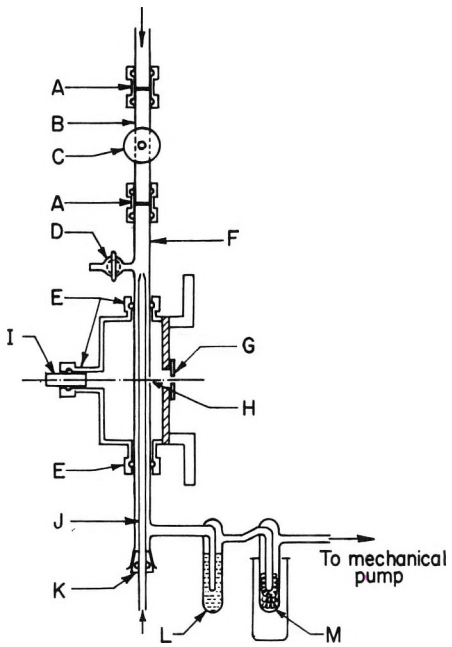

Figure 2. Diagram of discharge flow system: (A) nylon O ring "quick connects" with Teflon inserts, (B) 0.5-in. o.d. cast alumina tube, (C) Evenson-type microwave cavity, (D) stopcock connection to McLeod gauge, (E) O ring "quick connects", (F) 19-mm Teflon-coated glass tubing, (G) beam collimator, (H) sampling orifice, (I) sight tube, (J) movable gas inlet tube (7-mm o.d.), (K) Teflon O ring vacuum seal, (L) vacuum trap filled with 8–14 mesh activated alumina, (M) vacuum trap with Cu turnings, liquid N_2 cooled.

concentrations of atomic fluorine than discharges in quartz tubes. In addition, the dielectric loss factor of alumina is somewhat greater than that of quartz.[15] Thus, discharges through alumina are more difficult to maintain and a greater portion of the microwave power is lost as heat.

A diagram of the discharge-flow system is shown in Figure 2. The O-ring-sealed connector between the discharge and flow tubes is lined with Teflon. The movable inlet tube is either Teflon or Teflon coated. Two traps, the first containing 8–14-mesh activated alumina and the second containing copper turnings at liquid N_2 temperature, were employed to remove F and F_2 from the gases entering the Duo-Seal Model 1397 mechanical pump.

Gas flows were measured either with displacement-type (CF_4, Ar) or calibrated capillary (H_2) flow meters, or by measuring the rate of pressure drop in a known volume (CCl_4). Pressures were determined with a McLeod gauge or, in the presence of F_2, with a calibrated thermocouple gauge.

(12) F. C. Fehsenfeld, K. M. Evenson, and H. P. Broida, *Rev. Sci. Instrum.*, **36**, 294 (1965), commercially available from the Opthos Instrument Co.

(13) H. C. Berg and D. Kleppner, *ibid.*, **33**, 248 (1962).

(14) D. E. Rosner and H. D. Allendorf, *J. Phys. Chem.*, **75**, 308 (1971).

(15) "Handbook of Chemistry and Physics," 49th ed, Chemical Rubber Publishing Co., Cleveland, Ohio, 1968, pp E 63, 64.

Matheson Gas Products F_2, CF_4 (99.7%), and Ar (prepurified grade, dried over P_2O_5) were employed. The F_2 was passed through a NaF trap to remove HF and transported from a barricaded cylinder to the flow system through passivated copper tubing and Matheson valves specially treated for fluorine handling. Matheson Coleman and Bell spectral grade CCl_4 (frozen and pumped on before use) and Liquid Carbonic Co. hydrogen (99.9%) were employed. Only halogenated hydrocarbon grease (Halocarbon Products Corp.) was used on vacuum fittings.

Results and Discussion

Discharged CF_4 as a Source of Atomic Fluorine. The low cost and toxicity of CF_4 make it an attractive candidate for a discharge source of fluorine atoms. Carrington, Levy, and Miller used discharged CF_4 to obtain the esr spectrum of gas-phase atomic fluorine.[16] They detected both the $^2P_{3/2}$ ground state and the $^2P_{1/2}$ first excited state, which lies just 404 cm^{-1} above the ground state. The intensity of the lines indicated a somewhat higher population of the excited state than that expected from a Boltzmann distribution. Wagner, *et al.*, have observed that it is likely that $N + NF_2$ also produces a non-Boltzmann population of the $^2P_{1/2}$ state.[7] Polanyi and Tardy also used a CF_4 discharge in their study of the chemiluminescence of the $F + H_2$ reaction.[5]

When the alumina discharge section and Teflon-coated flow tube were used, the only species present in quantity 30 cm downstream of the discharge were undissociated CF_4, C_2F_6, and atomic and molecular fluorine. Under typical conditions (0.2–0.6 Torr of CF_4, 50–100 W of discharge power, and linear flow rates of 50–150 cm/sec), titration with H_2 indicated that atomic fluorine concentrations were $0.4–1.0 \times 10^{-9}$ mol/cm^3 and were three to ten times the concentration of molecular fluorine. Magnetic and electric deflection gave no indication of any CF, CF_3, or CF_2 in this system, although we must admit to having very low sensitivity for the latter species due to its singlet ground state and rather weak Stark effect.[17] We thus conclude that discharged CF_4 is a convenient source of fluorine atoms, suitable for kinetics studies where it is important to minimize interference from the reactions of F_2.

Discharged F_2–Ar Mixtures as a Source of Atomic Fluorine. In view of the weakness of the F–F bond, it is not surprising that an electrodeless discharge through molecular fluorine produces large concentrations of fluorine atoms. Atomic fluorine has been generated in this manner for several paramagnetic resonance studies.[18] In addition, Rosner and Allendorf have recently employed F_2–Ar mixtures, discharged in an alumina tube, to produce fluorine atoms for investigation of the kinetics of their reactions with refractory solids.[14]

In our work, Ar:F_2 ratios between 5 and 20 were employed, at total pressures of 0.5–1.5 Torr. At linear flow rates of 50–100 cm/sec, titration 30 cm downstream of the discharge indicated atomic fluorine concentrations of $1–5 \times 10^{-9}$ mol/cm^3, but generally in the presence of two to five times as much F_2. (Rosner and Allendorf, using higher flow rates and more dilute F_2–Ar mixtures, have achieved much higher per cent decomposition in a similar system.) These high concentrations of atomic fluorine are extremely useful for studying the slower reactions of this species.

$F + CCl_4$, Reaction Mechanism. At thermal energies, reactions between atoms and alkanes and their halogenated derivatives generally proceed by an abstraction mechanism.[19] By contrast, highly energetic "hot atoms," produced photochemically or by nuclear reactions, can displace atoms attached to carbon, as well as abstract such species.[20] On the basis of diffusion-flame studies at *ca.* 1500°K, Homann and MacLean recently suggested that atomic fluorine might provide an exception to these generalizations.[21] In flames of F_2 with CCl_4, CCl_3F, and CCl_2F_2, they were unable to detect mass spectrometrically products containing two or more carbon atoms, such as would be formed by reactions of the type

$$2CCl_3 \longrightarrow C_2Cl_6 \qquad (2)$$

Thus, they concluded that fluorine atoms reacted by exothermic displacement

$$F + CCl_4 \longrightarrow CCl_3F + Cl$$
$$\Delta H_{298} = -36 \pm 10 \text{ kcal/mol}^{22} \qquad (3)$$

rather than by endothermic abstraction

$$F + CCl_4 \longrightarrow FCl + CCl_3$$
$$\Delta H_{298} = 8.8 \pm 5 \text{ kcal/mol}^{22} \qquad (4)$$

Since both Cl and CCl_3 rapidly react with molecular fluorine, in the presence of considerable F_2, both (3) and (4) would give the same final products, FCl and CCl_3F, and would be indistinguishable. Thus, to establish the room-temperature mechanism of the reaction, we added CCl_4 to atomic fluorine produced by discharging CF_4. At the low F_2 concentrations existing in this system, FCl was observed, but no CCl_3F, a primary product of the displacement mechanism,

(16) A. Carrington, D. H. Levy, and T. A. Miller, *J. Chem. Phys.*, **45**, 4093 (1966).

(17) F. X. Powell and D. R. Lide, Jr., *ibid.*, **45**, 1067 (1966).

(18) M. Vanderkooi and J. S. MacKenzie, *Advan. Chem. Ser.*, **No. 36**, 98 (1962); H. E. Radford, V. W. Hughes, and V. Beltran-Lopez, *Phys. Rev.*, **123**, 153 (1961).

(19) A. F. Trotman-Dickenson, "Gas Kinetics," Butterworths, London, 1955, pp 237–242.

(20) R. Wolfgang, *Ann. Rev. Phys. Chem.*, **16**, 15 (1965).

(21) K. H. Homann and D. I. MacLean, *Combust. Flame*, **14**, 409 (1970).

(22) $D°_{298}$: CCl_3–F, 106 ± 5; CCl_3–Cl, 70 ± 5; Cl–F, 61.2 ± 0.5 kcal/mol; see ref 6.

was detected. A concentration of CCl_3F one-tenth as large as the FCl concentration would have been easily observable. Since there is no reasonable mechanism by which CCl_3F would be removed in this system, the reaction must proceed primarily by abstraction at room temperature. At higher F_2 concentrations, such as are produced by discharging F_2–Ar mixtures, CCl_3F signals comparable to those from FCl were obtained.

Magnetic deflection of the parent of the m/e 35 and 37 ions indicated the presence of chlorine atoms in these systems. However, these probably arise, not from an initial displacement, but from secondary reactions of the type

$$F + CCl_3 \longrightarrow CCl_3F^* \longrightarrow CCl_2F + Cl \qquad \Delta H_{298} \approx -30 \text{ kcal/mol} \quad (5)$$

Such reactions between two radical species are extremely rapid. Very few of the excited CCl_3F molecules would be stabilized by collisions at these pressures, and thus they would decompose in the most energetically favorable manner, illustrated by (5). The atomic chlorine partial pressures were estimated to be between 0.01 and 0.1 μ. The detection of such low concentrations of chlorine atoms in the presence of 10–50 μ of CCl_4, as well as other chlorine-containing species, is an indication of the utility of molecular beam analysis in observing transient intermediates. Although we have detected CX_3 radicals in other systems,[11] the $F + CCl_4$ reaction is too slow to produce observable concentrations of these radicals. Most of the CCl_3 is probably converted to CF_4 by a series of reactions similar to (5), followed by reaction with F_2. The rapidity of reaction 5 is evidenced by our observation of some CF_3^+ ions being produced even at the higher F_2 concentrations of the F_2–Ar fluorine atom source.

Although the room-temperature mechanism does not necessarily prevail at flame temperatures, the endothermicity of the abstraction reaction indicates that it should markedly accelerate at higher temperatures. Since in diffusion flames reaction 2 is in competition with very efficient scavenging of CCl_3 radicals by F_2 and FCl, it is possible that even if the initial reaction were abstraction, unobservable quantities of C_2Cl_6 would be produced.

Atomic Fluorine Concentration. Since the reaction of atomic fluorine with CCl_4 proceeds by abstraction, with eventual regeneration of most of the fluorine atoms by reaction of CX_3 radicals with F_2, first-order decay of the atomic fluorine concentration cannot be expected in this system. The kinetics can most easily be studied by monitoring the CCl_4 decay under conditions at which it is first order. However, this procedure requires absolute measurements of the fluorine atom concentration. Although in molecular beam analysis the intensity of the paramagnetic contribution to the m/e 19 ion is a sensitive measure of the relative concentration of atomic fluorine, conversion of this to an absolute basis involves rather dubious estimates of instrumental factors such as gathering power of the magnetic field, ionization efficiency and multiplier gain. Alternatively, one could make the conventional assumption that the decrease in the m/e 38 ion produced by the discharge is due completely to F_2 being converted to fluorine atoms. This would neglect changes in the fragmentation pattern of F_2 which result from its being vibrationally excited (as might be expected as a consequence of the discharge or recombination reaction), and loss of a small amount of fluorine due to reaction with surfaces.

A third possibility for determining absolute atomic fluorine concentrations would involve titrating the fluorine atoms with a stable molecule which rapidly reacts with it according to a known stoichiometry. In chemiluminescent titration reactions, such as those for atomic oxygen, nitrogen, and hydrogen, the endpoint of the titration is indicated by a "color change." Alternatively, the disappearance of the atomic reactant or the cessation of product formation may be monitored directly by a technique such as molecular beam analysis.

No light-producing titration reaction for fluorine atoms has yet been successfully developed. One chemiluminescent sequence

$$F + NOCl \longrightarrow NO + FCl \quad (6)$$

$$F + NO \longrightarrow NOF + h\nu \quad (7)$$

is complicated with F_2 present by

$$F_2 + NO \longrightarrow NOF + F \quad (8)$$

and by the possible reaction of F_2 with NOCl.[14] Wagner, *et al.*,[7] have titrated fluorine atoms with NOCl by following the formation of FCl mass spectrometrically. They assumed no interference from F_2, which was only a minor constituent of their system.

Since no compound was found which would react quickly with fluorine atoms but not produce products which would react with F_2, the titration used in this study was based upon the reaction sequence

$$H_2 + F \longrightarrow HF + H \quad (9)$$

$$H + F_2 \longrightarrow F + HF \quad (10)$$

The literature values for the room-temperature rate constants of reactions 9 and 10 are 1.0×10^{13}[7] and 2.3×10^{12} cm^3/(mol sec),[23] respectively.

If loss of hydrogen atoms other than by reaction with F_2 is negligible, eq 9 and 10 predict no depletion of the fluorine atoms until all the F_2 is consumed. Hydrogen atoms can be lost by recombination or by combination

(23) R. G. Albright, A. F. Dodonov, G. K. Lavrovskaya, I. I. Morosov, and V. L. Tal'roze, *J. Chem. Phys.*, **50**, 3632 (1969).

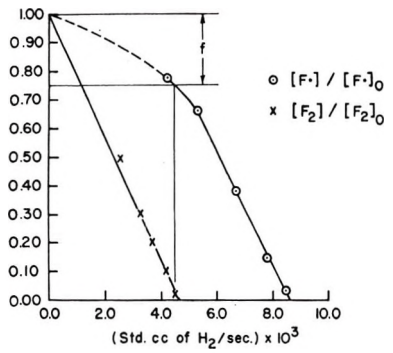

Figure 3. H_2 titration curve for F atoms and F_2.

with fluorine atoms, either homogeneously or on the flow tube walls. The average rate constant for homogeneous atomic hydrogen recombination (with H_2 as the third body) from a number of recent determinations[24,25] is 4.4×10^{15} cm^6/(mol^2 sec). Using a typical system density of 4×10^{-8} mol/cm^3, this can be converted to an equivalent bimolecular rate constant of 1.8×10^8 cm^3/(mol sec), which is more than a factor of 10^4 slower than k for reaction 10. Teflon is probably the least effective surface for catalyzing recombination of hydrogen atoms. The reported recombination efficiency is *ca.* 10^{-6}, and indicates that this loss mechanism is negligible.[25] Rate constants for association of hydrogen atoms with fluorine atoms are not available. However, unless atomic fluorine forms stable complexes with some component of the system (*e.g.*, FHF with HF[26]), there is no reason to expect that such rates are much faster than those between hydrogen atoms.

Figure 3 shows a typical titration of atomic and molecular fluorine in a discharged F_2–Ar mixture. As predicted by eq 9 and 10, F_2 is titrated before F. However, the atomic fluorine signal usually drops by a fraction, f (0.15–0.30), before the F_2 is completely removed. This effect is undoubtedly partly instrumental—these fairly large additions of H_2 causing increased scattering of fluorine atoms in the vicinity of the sampling orifice and resulting in their being somewhat less efficiently gathered by the magnetic field. Addition of comparable amounts of He show that such instrumental factors are less than 10%, and thus f probably also includes contributions from H-atom removal processes other than (10). These two explanations of the drop in the atomic fluorine signal require somewhat different interpretations of the titration data. If instrumental factors are dominant, the difference in the H_2 flows needed to remove F and F_2 would be equal to the flow of atomic fluorine. If other H-atom removal processes are dominant, the difference would equal $(1 - f)$ times the atomic fluorine flow. (Only $1 - f$ of the fluorine atoms would remain when the F_2 was titrated.) Since it is difficult to assess the relative contribution of the two effects, we have taken the average of the results provided by the two interpretations, and consider f to be an estimate of the possible systematic errors involved in the titration. Additional confidence in this procedure is gained from the good agreement between the total fluorine flows (molecular + 0.5 atomic) obtained from the titration and the measured flow of F_2 being added to the system.

F + CCl_4, Rate Constant. At 25°, the reaction of atomic fluorine with CCl_4 is so slow that, in order to achieve appreciable consumption (30–60%) of the CCl_4 in the 30-cm long reaction zone, fairly slow flows (25–50 cm/sec) and the higher concentrations of atomic fluorine produced by discharging F_2–Ar mixtures were necessary. Since CCl_4 gives no parent ion, the extent of its reaction between the movable inlet and the sampling orifice was determined by monitoring the CCl_3^+ ion with the discharge alternately on and off. No interference from product CCl_3F is expected, since CCl_3^+ is a very minor fragmentation ion of CCl_3F.[27] With these high concentrations of fluorine atoms, and with their being regenerated by the reaction

$$F_2 + CCl_3 \longrightarrow CCl_3F + F \qquad (11)$$

less than 15% of the atomic fluorine was lost upon addition of the CCl_4. Thus, semilogarithmic plots of the fraction of CCl_4 that was unreacted *vs.* inlet position (and reaction time) yielded straight lines, as shown in Figure 4. The failure of the data to extrapolate exactly to unity when the CCl_4 is added right at the orifice is probably due to axial diffusion at these fairly low flows.

The results of room-temperature rate constant determinations are shown in Table I. The mean is 2.4×10^8 cm^3/(mol sec), and one standard deviation is 0.9×10^8 cm^3/(mol sec). Unfortunately, only rather limited variation of the reaction conditions were compatible with obtaining sufficient depletion of the CCl_4 to measure the rate constant. Some systematic variation of k with CCl_4 concentration is possible, but this may be

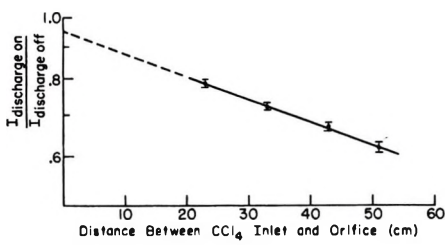

Figure 4. First-order plot of consumption of CCl_4.

(24) F. S. Larkin and B. A. Thrush, *Discuss. Faraday Soc.*, **No. 37**, 112 (1964); J. E. Bennett and D. R. Blackmore, *Proc. Roy. Soc., Ser. A*, **305**, 553 (1968); D. O. Ham, D. W. Trainor, and F. Kaufman, *J. Chem. Phys.*, **53**, 4395 (1970).

(25) J. E. Bennett and D. R. Blackmore, *ibid.*, **53**, 4400 (1970).

(26) V. Bondybey, G. C. Pimentel, and P. N. Nobel, *ibid.*, **55**, 540 (1971); R. N. Kortzeborn and P. N. Noble, *ibid.*, **52**, 5375 (1970).

(27) A. Cornu and R. Massot, "Compilation of Mass Spectral Data," Heyden, 1966.

due to diffusion effects. Considering possible systematic errors involved in measuring the concentration of atomic fluorine, this result can be considered reliable to within a factor of two. The reaction is almost definitely occurring homogeneously, since adsorption on Teflon surfaces is generally very weak, and the rate constant is independent of large changes in the Pyrex to Teflon ratio as the Teflon coating deteriorates.

Table I: Rate Data for F + CCl_4

Total concn[a]	Initial $[CCl_4]$[a]	[F][a]	$[F_2]$[a]	k, $cm^3/(mol\ sec)$
37.5	0.8	2.0	7.6	1.1×10^8
42.8	0.9	0.9	3.4	1.6×10^8
53.6	0.5	1.4	2.3	2.9×10^8
53.6	1.0	1.4	2.3	2.8×10^8
53.6	1.7	1.4	2.3	1.3×10^8
33.2	2.5	1.1	3.1	2.5×10^8
33.2	1.5	1.1	3.1	2.4×10^8
33.2	1.0	1.1	3.1	3.2×10^8
33.2	0.8	1.1	3.1	3.8×10^8

[a] Units, 10^{-9} mol/cm^3.

This value of k differs from that measured by Clark and Tedder,[1] 2×10^{13} $cm^3/(mol\ sec)$ (at 20°), by almost five orders of magnitude. Clark and Tedder mixed F_2 and CCl_4 in a N_2 diluent at roughly atmospheric pressure and assumed that the atomic fluorine concentration would be determined by the equilibrium with F_2. However, in their experiments, the CCl_3 radicals produced in the initial abstraction would react with F_2, with an exothermicity of approximately 70 kcal/mol. Since this is almost twice the strength of the F_2 bond, there is a possibility of a small amount of branching due to an energy chain[28] (*e.g.*, vibrationally excited CCl_3F collisionally dissociating F_2 molecules). If such branching occurs, the fluorine atom concentration in Clark and Tedder's experiment would have been larger than the value they calculated from the F_2 dissociation equilibrium. As a result, their reported rate constant would be far too high. A branching chain of this type could be detected by measuring the atomic fluorine concentration directly, something Clark and Tedder were not able to do. The ability to directly monitor intermediates, and thus avoid errors in mechanism, is the principal advantage of using a technique such as molecular beam analysis for kinetic studies.

Assuming a normal preexponential factor of 10^{14} $cm^3/(mol\ sec)$, our rate constant corresponds to an activation energy of 7.3–8.2 kcal/mol. Since $D°_{298}$ of ClF is probably very close to 61.2 kcal/mol,[29] our rate constant would tend to favor a value for $D°_{298}$ (CCl_3–Cl) close to that measured by Farmer, *et al.* (67.9 kcal/mol).[30]

Acknowledgment. The authors would like to thank Dr. J. M. Tedder for an interesting discussion and J. Bozzelli and B. Hertzler for considerable aid with the experimental work. This work was supported by the Office of Naval Research under Contract No. N00 14-67-A-0151-0013.

(28) N. N. Semenov and A. E. Shilov, *Kinet. Katal.*, 6, 3 (1965).

(29) A. L. Wahrhaftig, *J. Chem. Phys.*, 10, 248 (1942); H. Schnutz and H. J. Schumacher, *Z. Naturforsch.*, 29, 359 (1947). By analogy to IF [R. A. Durie, *Can. J. Phys.*, 44, 337 (1966)], the dissociation limit is probably $Cl(^2P_{3/2}) + F(^2P_{1/2})$, giving good agreement between the spectroscopic and thermochemical dissociation energy; see ref 6.

(30) J. B. Farmer, H. S. Henderson, F. P. Lossing, and D. G. H. Marsden, *J. Chem. Phys.*, 24, 348 (1956).

Nonequilibrium Unimolecular Reactions and Collisional Deactivation of Chemically Activated Fluoroethane and 1,1,1-Trifluoroethane

by H. W. Chang, N. L. Craig, and D. W. Setser*

Chemistry Department, Kansas State University, Manhattan, Kansas 66502 *(Received November 1, 1971)*

Publication costs assisted by the National Science Foundation

Highly vibrationally excited fluoroethane and 1,1,1-trifluoroethane molecules were generated by combination of CH_2F and CF_3 radicals with CH_3. The radicals were produced by cophotolysis of acetone and 1,3-difluoroacetone and by photolysis of trifluoroazomethane. The nonequilibrium unimolecular rate constant for HF elimination from $CH_3CH_2F^*$ was measured using the acetone mixture as the bath gas. The rate constants for $CH_3CF_3^*$ were measured with C_2F_6, $CH_3N_2CF_3$, c-C_4F_8, C_6F_{14}, and C_8F_{18} as bath gases. RRKM calculations were done using a four-centered activated complex model and currently favored thermochemical values; good agreement was found between the calculated and both thermal and chemical activation rate constants for CH_3CH_2F. For the high $D(CH_3-CF_3)$ value of $\sim$99 kcal mol^{-1}, the chemical activation data support a high threshold energy, 68 $\pm$ 2 kcal mol^{-1}, for HF elimination from CH_3CF_3. RRKM calculations for the dissociation reactions of $CH_3CF_3^*$ and $CH_3CH_2F^*$ indicate that radical dissociation should compete with HF elimination at energies near 110 kcal mol^{-1}. The low pressure data for $CH_3CF_3^*$ were analyzed according to a cascade stepladder deactivation model to obtain estimates of the average energy lost per collision. An upper limit of 10–12 kcal mol^{-1} is implied for even the larger bath gas molecules.

Introduction

The combination reactions of methyl and halomethyl radicals provide excellent chemical activation systems for studying unimolecular four-centered HX (X = F, Cl, Br) elimination reactions and vibrational energy transfer near 90 kcal mol^{-1} of energy.[1-3] The chloro- or bromomethyl radicals[1] are more difficult to produce than fluoromethyl radicals,[2,3] and molecules formed from the latter offer greater potential for study of energy transfer. Methyl and fluorinated methyl radicals mainly have been produced by photolysis of ketones.[2-4] In this work we used 1,1,1-trifluoroazomethane in an attempt to obtain a better source of these radicals. Our eventual goal is to use this chemical activation system for studies of vibrational energy transfer. To do this, it first is necessary to fully characterize the unimolecular reaction which competes with the collisional stabilization. For this purpose the C_2H_5F reaction was first investigated since it corresponds most closely with the previously studied C_2H_5Cl and C_2H_5Br reactions.[1a,b] The Arrhenius parameters[5] and $D_0°(CH_3-CH_2F)$ are known for fluoroethane so these data provide another consistency test for the general validity of the model used for the four-centered elimination reactions. The transition state model that was formulated for C_2H_5F was extended to CH_3CF_3. Since the Arrhenius parameters[6] for CH_3CF_3 have been measured, the threshold energy is relatively well known and the chemical activation data can be used to provide an estimate of $D(CH_3-CF_3)$.

The nonequilibrium unimolecular reactions of fluoroalkanes are of importance for activation by displacement reactions of hot fluorine and tritium atoms.[7] For this reason the HF elimination reaction channel was compared to the radical dissociation channel, and both were extended to relatively high energies using RRKM calculations. Energy partitioning information[1a,8] has been obtained for the HF product of the CF_3CH_3 reaction and it is desirable to have the more conventional chemical activation data available as background information.

Previous chemical activation data were interpreted[1c,d] as showing that highly vibrationally excited haloethanes transfer, on the average, 10 $\pm$ 3 kcal mol^{-1}

(1) (a) W. G. Clark, K. Dees, and D. W. Setser, *J. Amer. Chem. Soc.*, **93**, 5328 (1971); (b) R. L. Johnson and D. W. Setser, *J. Phys. Chem.*, **71**, 4366 (1967); (c) H. W. Chang and D. W. Setser, *J. Amer. Chem. Soc.*, **91**, 7648 (1969); (d) W. G. Clark, D. W. Setser, and E. E. Siefert, *J. Phys. Chem.*, **74**, 1670 (1970).

(2) (a) G. O. Pritchard and M. J. Perona, *Int. J. Chem. Kinet.*, **2**, 281 (1970); (b) G. O. Pritchard and R. L. Thommarson, *J. Phys. Chem.*, **71**, 1674 (1967).

(3) (a) J. A. Kerr, B. V. O'Grady, and A. F. Trotman-Dickenson, *J. Chem. Soc. A*, 275 (1969); (b) A. W. Kirk, A. F. Trotman-Dickenson, and B. L. Trus, *ibid.*, 3058 (1968).

(4) R. D. Giles and E. Whittle, *Trans. Faraday Soc.*, **61**, 1425 (1965).

(5) (a) P. Cadman, M. Day, and A. F. Trotman-Dickenson, *J. Chem. Soc. A*, 2498 (1970); (b) M. Day and A. F. Trotman-Dickenson, *ibid.*, 223 (1969).

(6) (a) P. Cadman, M. Day, A. W. Kirk, and A. F. Trotman-Dickenson, *Chem. Commun.*, 203 (1970); (b) E. Tschuikow-Roux and W. J. Quiring, *J. Phys. Chem.*, **75**, 295 (1971); (c) D. Sianesi, G. Nelli, and R. Fontanelli, *Chim. Ind. (Milan)*, **50**, 619 (1968).

(7) (a) N. J. Parks, K. A. Krohn, and J. W. Root, *J. Chem. Phys.*, **55**, 5785 (1971); (b) C. F. McKnight, N. J. Parks, and J. W. Root, *J. Phys. Chem.*, **74**, 217 (1969).

(8) (a) P. N. Clough, J. C. Polanyi, and R. T. Taguchi, *Can. J. Chem.*, **48**, 2919 (1970); (b) M. J. Berry and G. C. Pimentel, *J. Chem. Phys.*, **49**, 5190 (1968).

of energy per collision with molecules of intermediate size, *e.g.*, CH_3Cl or CH_2ClF. Large perfluoroalkane molecules were used with CH_3CF_3* to test whether or not the average energy removed per collision increased with increasing size of the bath gas molecule. In addition to providing information about vibrational energy transfer, data from several "efficient" bath gases provide a better estimate for the unit deactivation rate constant. Although the experiments giving C_2H_5F are not quite as convenient as those giving CH_3CF_3, energy transfer studies with CH_3CH_2F are possible and desirable.

Experimental Section

Trifluoroazomethane was prepared using a procedure similar to that of Haszeldine and Dinwoodie.[9] To minimize polymer formation from reaction of methylamine with the trifluoroazomethane, the methylamine was slowly metered through a central jet into the reaction bulb containing gaseous trifluoronitrosomethane. When polymer formation appeared to be the main reaction, the reaction was stopped even though some of the blue nitroso compound remained in the reaction bulb. The azo compound was separated from the unreacted trifluoronitrosomethane using a pentane slush bath and was purified by gas chromatography using a Porapak-T column.

The methylamine and C_2F_6 were obtained from Matheson Co., and the trifluoronitrosomethane, perfluorocyclobutane, perfluorohexane, and perfluorooctane were purchased from Peninsular Chemresearch Corp. The 1,3-difluoroacetone was purchased from Pfaltz and Bauer, Inc., and the acetone was obtained from Fisher. Gas chromatographic analysis showed that these reagents contained negligible impurities; therefore, after degassing they were used without further treatment.

Experiments consisted of photolyzing trifluoroazomethane diluted in a $\sim$10:1 ratio with a bath gas and measuring the product yields. Samples were made up by introducing measured quantities of trifluoroazomethane and bath gas into Pyrex vessels of known volumes using standard vacuum techniques. After shaking the vessels, which contained small glass beads, to obtain a homogeneous mixture, the samples were photolyzed for $\sim$2 hr using unfiltered light from a water-cooled General Electric AH6 high-pressure lamp. When no bath gas was used, photolysis times of a few minutes gave sufficient yields for analysis. The wavelength region between 3500 and 3800 Å was responsible for at least 75% of the photodissociation. Since the CH_3 and CF_3 radicals are formed at very low concentrations in the bath gas, they are thermalized before recombination, and the wavelength spread of the photolysis lamp is not important for our measurements. The temperature of the reaction vessels was maintained at room temperature by blowing a stream of air over the surface of the Pyrex vessels. After photolysis the condensable products were recovered by pumping the photolyzed sample through a glass wool packed trap at 77°K. These products were then transferred to a gas chromatograph inlet and injected into a 16-ft Porapak-T column. At 55°, the low-boiling products had the following retention times: C_2F_6, 3 min; C_2H_6, 6 min; CF_2CH_2, 9 min; and CF_3CH_3, 24 min. To elute C_6F_{14}, C_8F_{18}, and trifluoroazomethane within a reasonable time, the column temperature was raised to 160° after the appearance of the trifluoroethane peak. When *c*-C_4F_8 was used as a bath gas, a column composed of 3 ft of Porapak S and 6 ft of Porapak T was used to separate the C_4F_8 from trifluoroethane. Even with this modification the C_4F_8 appeared on the tail of the trifluoroethane peak. In addition to the radical recombination products higher boiling products, which were mainly hydrazines resulting from the addition of CF_3 and CH_3 to $CH_3N_2CF_3$, were observed.

Vibrationally excited CH_3CH_2F was generated by cophotolysis of CH_3COCH_3 and CH_2FCOCH_2F using the lamp mentioned above. The irradiation time was normally $\sim$20 min. Since the extinction coefficient of CH_2FCOCH_2F is five times larger than that of CH_3COCH_3, a 5:1 ratio of acetone to 1,3-difluoroacetone was used. Since CH_2FCOCH_2F has a low vapor pressure, the samples were heated to $\sim$90° during the photolysis. This was done by placing the sealed Pyrex vessels of known volume in an enclosed pipe; the lamp output was sufficient to heat the sample to $\sim$90°. The temperature was regulated by passing a flow of air through the pipe. After the photolysis the condensable products were recovered by pumping the sample through a glass wool packed trap at 77°K. These products then were transferred to the gas chromatograph inlet and analyzed with a 16-ft column containing ethylene glycol saturated with $AgNO_3$ followed by a 2-in. Porapak-S column, which was heated slightly above room temperature.

For both photolysis systems the gas chromatograph was calibrated with mixtures containing known quantities of the products. A number of these standards, containing markedly different ratios of compounds, were used to ensure that the peak height was proportional to the amount of compound present.

Experimental Results

*Rate Constants for CF_3CH_3**. The photolysis of trifluoroazomethane gave ethane, hexafluoroethane, difluoroethylene, trifluoroethane, and some high-boiling hydrazine products arising from radical addition to the parent compound. Hydrogen abstraction reactions by CF_3 or CH_3 were found to be negligible at room temperature. Typical radical combination product yields are shown in Table I. These products are consistent with

(9) A. H. Dinwoodie and R. N. Haszeldine, *J. Chem. Soc.*, 2266 (1965).

Table I: Radical Combination Products[a,b] from Photolysis of 1,1,1-Trifluoroazomethane with c-C_4F_8

Pressure, Torr	C_2F_6	C_2H_6	CF_2CH_2	CF_3CH_3	$\frac{(CF_3CH_3 + CF_2CH_2)}{(C_2F_6 \cdot C_2H_6)^{1/2}}$
750.0	0.011	0.058	0.0019	0.070	2.9
621.0	0.014	0.061	0.0019	0.074	2.6
436.0	0.0065	0.044	0.0017	0.047	2.9
150.0	0.0073	0.046	0.0051	0.043	2.6
110.0	0.038	0.073	0.0071	0.11	3.4
87.9	0.035	0.062	0.012	0.093	2.3
60.5	0.029	0.075	0.028	0.085	2.4
40.7	0.053	0.094	0.057	0.11	2.4
40.4	0.015	0.015	0.014	0.025	2.6
26.9	0.041	0.062	0.066	0.083	3.0
15.5	0.054	0.079	0.095	0.063	2.4
10.9	0.042	0.059	0.092	0.039	2.6
9.2	0.0081	0.011	0.019	0.0054	2.6

[a] Product yields are in cubic centimeters at STP and were measured with a gas chromatograph having a thermal conductivity detector. [b] In addition to these products, hydrazine products resulting from addition of CF_3 and CH_3 to the double bond of trifluoroazomethane were found in yields comparable to the above quantities.

the reactions shown below.

$$CF_3N_2CH_3 \xrightarrow{h\nu} CF_3 + CH_3 + N_2 \quad (1)$$

$$CF_3 + CF_3 \longrightarrow C_2F_6^* \quad (2)$$

$$CH_3 + CH_3 \longrightarrow C_2H_6^* \quad (3)$$

$$CF_3 + CH_3 \longrightarrow CF_3CH_3^* \quad (4)$$

$$CF_3CH_3^* \xrightarrow{k_a} CF_2CH_2 + HF \quad (5)$$

$$\xrightarrow{k_M[M]} CF_3CH_3 \quad (6)$$

Our primary concern here is the unimolecular decomposition of vibrationally excited 1,1,1-trifluoroethane. The photochemistry of $CF_3N_2CH_3$ and other details, such as the formation of the hydrazines and mass balance, will be reported elsewhere. Even with these additional reactions, which favor removal of CF_3 relative to CH_3, the value of $(CF_3CH_3 + CF_2CH_2)/(C_2F_6 + C_2H_6)^{1/2}$ should remain constant and equal to $k_4/(k_3k_2)^{1/2}$. The constancy of this ratio can be seen from Table I. At lower pressures the dissociation of ethane would be expected, as has been reported by Kobrinsky, *et al.*[10] Our value of $k_4/(k_3k_2)^{1/2}$ is larger than 2 and is in close agreement with other work.[10] Except for experiments with c-C_4F_8 as the bath gas, most analyses were done with a hydrogen flame detector which has a very low response for C_2F_6. Hence information about the C_2F_6 yield was lost in gaining the enhanced sensitivity for $C_2H_2F_2$ and CH_3CF_3.

The photolysis of $CF_3N_2CH_3$ is a clean source of vibrationally excited $CH_3CF_3^*$, which either is stabilized by collision or decomposes to give 1,1-difluoroethylene and HF. The nonequilibrium rate constant is defined as $k_a = \omega D/S$; S being the amount of stabilized product (CF_3CH_3), D the amount of decomposition product (CF_2CH_2), and $\omega = k_M[M]$ with k_M being the collision number and [M] the number of bath gas molecules per cubic centimeter. Since ω is proportional to the pressure, k_a can be redefined in pressure units, and $k_a = P[D/S]$. Thus for *unit deactivation* a plot of D/S *vs.* $1/P$ gives a straight line and the slope is the chemical activation rate constant. For cascade deactivation the plots show upwards curvature; however, for the relatively efficient gases used here the higher pressure points show linear behavior.

These plots for various bath gases are shown in Figures 1 and 2. The slopes of the linear portion of the

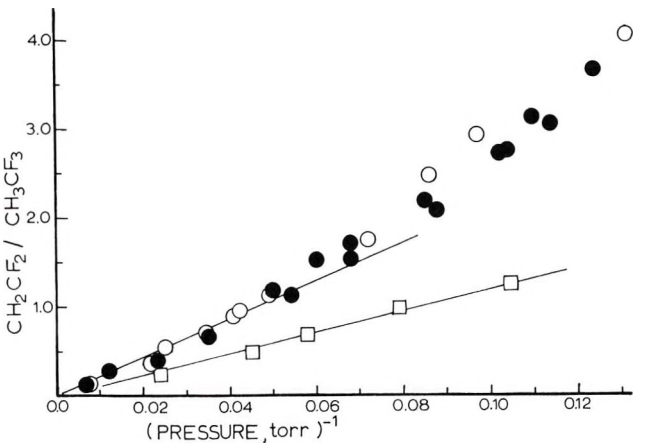

Figure 1. Plot of CH_2CF_2–CH_3CF_3 yield ratios *vs.* pressure^{-1} for C_2F_6, ○, $CF_3N_2CH_3$, ●, and n-C_6F_{14}, □, as bath gases at 300°K.

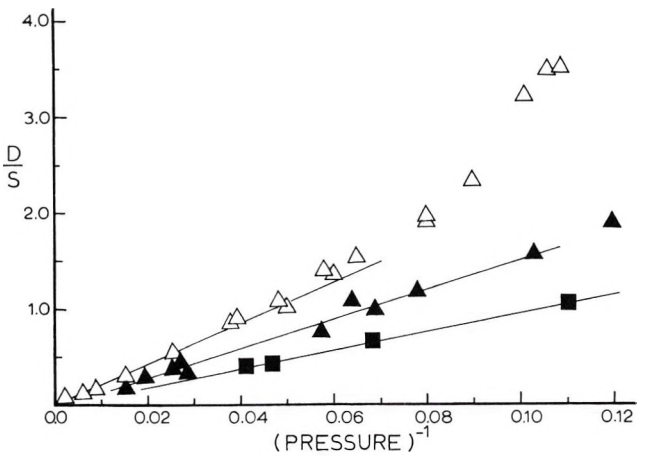

Figure 2. Plot of decomposition–stabilization yield ratios *vs.* pressure for $CF_3CH_3^*$ with c-C_4F_8, △, and C_3F_{18}, ■, as bath gases at 300°K; the pressure scale is in units of Torr^{-1}. The ▲ symbols are for $CH_3CH_2F^*$ at 363°K with the pressure scale in units of cm^{-1} of Hg.

(10) P. C. Kobrinsky, G. O. Pritchard, and S. Toby, *J. Phys. Chem.*, 75, 2225 (1971).

Table II: Experimental Rate Constants for CH_3CF_3* and CH_3CH_2F*

Molecule	Bath gas	Torr	Experimental rate constants a 10^8 sec^{-1}	b	σ(M), 10^{-8} cm	ϵ/k(M), °K	$[\Omega_{AM}^{(2,2)*}]^{1/2}$
CF_3CH_3[c]	C_2F_6	21	1.9	2.8	5.1	238	1.20
	c-C_4F_8	21	2.0	3.4	5.8	400	1.28
	$CF_3N_2CH_3$	21	2.0	3.4	5.3	400	1.28
	C_6F_{14}	11	1.2	2.2	6.8	575	1.36
	C_8F_{18}	9	1.1	2.2	7.6	850	1.42
CH_2FCH_3[c]	$(CH_3)_2CO/(CH_2F)_2CO$ = 5/1	151	12.8	20.2	4.7/5.0	519	1.26

[a] For $S_{AM} = (\sigma(CF_3CH_3 \text{ or } CH_2FCH_3) + \sigma(M))/2$. [b] For $S_{AM} = [(\sigma CF_3CH_3 \text{ or } CH_2FCH_3) + \sigma(M)/2][\Omega_{AM}^{(2,2*)}]^{1/2}$. [c] For CF_3CH_3 and CH_2FCH_3 σ = 5.0 and 4.0 Å, respectively; ϵ/k = 270° was used for both molecules. The rate constants for CF_3CH_3 were measured at room temperature; that for CH_3CH_2F were measured at 363°K.

graphs, $D/S \leq 1.5$, and plots of k_a *vs.* pressure were used to fix the values of the high-pressure rate constants. These values were converted to units of reciprocal seconds by using Lennard-Jones collision diameters and $\Omega^{(2,2)*}$ integrals to obtain the collision number, $k_M = S_{AM}^2(8\pi kT/\mu)^{1/2}$ and the results are summarized in Table II.

Root[11] has tabulated values for collision diameters based on molecular excluded volumes from critical property data; and these were used for CF_3CH_3, C_2F_6, C_4F_8, C_6F_{14}, and C_8F_{18}. The collision diameter for trifluoroazomethane was not covered by any other work. Basing this molecule on *cis*-butene[12] and estimating from trifluorobutane the amount that a trifluoromethyl group might add,[12] we obtained a value of 5.5 Å. As noted by Rabinovitch[13] the literature values for ϵ/k are incomplete and inconsistent. The ϵ/k values for the fluoroalkanes, which correlated best with our data, were based on reduced second virial coefficients.[14] Values of 238° for C_2F_6 and 575° for C_6F_{14} were obtained directly from published tables;[14] a value of 850° was obtained for C_8F_{18} by extrapolation. A value of 400° was selected for $CF_3N{=}NCH_3$ based on C_4F_{10} data;[14] the 270° value for CF_3CH_3 was increased somewhat over C_2F_6 or C_2H_6 to take into account the polar effect.

Rate Constant for C_2H_5F. The following products were observed from the photolysis of CH_3COCH_3 with CH_2FCOCH_2F: CH_3F, C_2H_4, C_2H_6, CH_3CH_2F, and CH_2FCH_2F. Even if present methane would not have been observed. These products are consistent with the production of CH_3 and CH_2F radicals by the known photodissociation reactions of ketones.[2] These radicals then combine or abstract hydrogen.

$$CH_2F + CH_2FCOCH_2F \text{ or } CH_3COCH_3 \longrightarrow CH_3F + CHFCOCH_2F \text{ or } CH_2COCH_3$$

$$CH_3 + CH_2FCOCH_2F \text{ or } CH_3COCH_3 \longrightarrow CH_4 + CHFCOCH_2F \text{ or } CH_2COCH_3$$

$$CH_3 + CH_3 \longrightarrow CH_3CH_3^*$$

$$CH_2F + CH_2F \longrightarrow CH_2FCH_2F^*$$

$$CH_3 + CH_2F \longrightarrow CH_3CH_2F^* \xrightarrow{k_a} CH_2{=}CH_2 + HF$$

$$CH_3CH_2F^* \xrightarrow{\omega} CH_3CH_2F$$

Since the photochemistry of acetone and difluoroacetone has been studied previously,[2] our objective was to obtain the chemical activation rate constant for C_2H_5F*, and only the yields of C_2H_4 and C_2H_5F were measured. A plot of CH_2CH_2/CH_3CH_2F *vs.* $1/P$ is shown in Figure 2, and least-squares analysis gave 151 ± 10 Torr for the slope. This slope was converted into the rate constant in reciprocal seconds[1] units using σ and ϵ/k values from ref 12, and the final result is shown in Table II.

Low-Pressure, Energy Transfer Results for CH_3CF_3.* Since the D/S *vs.* $1/P$ plots show curvature at low pressure, a unit deactivation mechanism is not completely adequate, and a cascade mechanism must be considered. For the gases studied here the simple stepladder model, which is based on the removal of a constant increment, $\langle\Delta E\rangle$, of energy per collision, is appropriate. To assign the $\langle\Delta E\rangle$ values, the low-pressure data must be fitted to computed results. For this calculation unimolecular rate constants, which are discussed in the next section, are needed. The low-pressure data shown in Figure 3 were matched to stepladder calculated curves to identify the average energy lost per collision. Further details regarding the calculations are given in the energy transfer section; the results are summarized in Table III.

Calculated Results

HF Elimination Rate Constants. Since the molecular frequencies of CH_3CH_2F[15] and CH_3CF_3[16] are known,

(11) J. W. Root, *J. Phys. Chem.*, in press.

(12) J. O. Hirschfelder, C. F. Curtiss, and R. B. Bird, "Molecular Theory of Gases and Liquids," Wiley, New York, N. Y., 1959.

(13) S. C. Chan, J. T. Bryant, L. D. Spicer, and B. S. Rabinovitch, *J. Phys. Chem.*, **74**, 2058 (1970).

(14) E. M. Dantzler and C. M. Knobler, *ibid.*, **73**, 1335 (1969).

(15) (a) B. Bak, S. Detoni, L. Hansen-Nygaard, J. T. Nielsen, and J. Rastrup-Anderson, *Spectrochim. Acta*, **16**, 376 (1960); (b) NSRDS-NBS 11, Part 2, U. S. Government (1968).

(16) (a) D. M. Minkin and A. A. Vvedenskii, *Russ. J. Phys. Chem.*, **41**, 841 (1967); (b) J. R. Nielsen, H. H. Claassen, and D. C. Smith, *J. Chem. Phys.*, **18**, 1471 (1950).

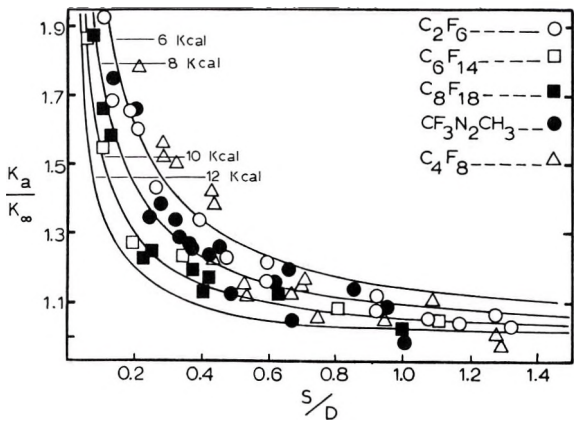

Figure 3. Plot of low pressure data in the form of k_a/k_a^∞ *vs.* S/D for CF_3CH_3*: ○, C_2F_6; ●, $CF_3N_2CH_3$; △, *c*-C_4F_8; □, C_6F_{18}; and ■, C_8F_{18}. The curves are the calculated results from the stepladder model with the $\langle\Delta E\rangle$ values indicated.

Table III: Summary of Energy Transfer for CF_3CH_3*

Bath gas	$\langle\Delta E\rangle$[a]	k_a^∞ (exptl)[c] Torr	k_a^∞ (exptl)[c] 10^6 sec^{-1}	k_a^∞ (calcd),[b] 10^6 sec^{-1}
n-C_8F_{16}	10	9	2.2	2.6
n-C_6F_{14}	10	11	2.2	2.6
c-C_4F_8	7	21	3.4	3.0
$CF_3N_2CH_3$	7	21	3.4	3.0
C_2F_6	7	19	2.8	3.0

[a] Assigned from matching the curves and data points of Figure 3; all are for a stepladder model. [b] Calculated from the stepladder model with $\langle\Delta E\rangle$ of column 2. The calculated $k_a^\infty(\Delta E)$ obtained with k_E values of Figure 4 were scaled by a factor of 0.67 to provide a better absolute fit to experimental values. Relative to the unit deactivation rate constant the $k_a^\infty(\Delta E)$ values increase by factors of 1.04, 1.14, 1.23, 1.42, and 1.81 for $\langle\Delta E\rangle$ = 14, 10, 8, 6, and 4 kcal mol^{-1}. [c] The experimental values obtained with $S^2 = \sigma^2\Omega^{(2,2)*}$ are favored over those from $S = \sigma^2$.

RRKM rate constants may be calculated by choosing a model of the activated complex and assigning the energy of formed molecules and threshold energy for the reactions. The model chosen for the activated complex was of the same type as used for C_2H_5Cl[1a] and C_2H_5Br.[1b] The frequencies of the four-centered transition state were divided into three categories: (i) the 12 out-of-ring frequencies associated with the four atoms attached to the carbon atoms; (ii) the five in-plane frequencies of the four atom ring; and (iii) the one ring-puckering frequency.

The 12 out-of-ring frequencies of $CH_3CH_2F^\dagger$ are the wagging, rocking twisting, and scissoring of the CH_2 groups, which were assigned by analogy with CH_3CH_2F, cyclobutane, and to a lesser extent with ethene. For $CH_3CF_3^\dagger$, these frequencies were chosen by analogy with CH_3CF_3 and CH_2CF_2. The in-plane frequencies were calculated by assigning bond orders of 1.1, 0.8, 0.1, and 0.1 to the C–C, C–F, F–H, and C–H bonds, respectively, and following the procedure described in earlier papers.[1,17] We have previously used a C–C bond order assignment of ~1.9, which was set to conserve a total bond order of 3. The recent energy partitioning data[1a,8] suggest that the C–C double bond formation occurs after crossing the barrier configuration. The lowering of this C–C bond order reduces one ring frequency, but this has no serious effect upon the calculated rate constants.[1a] The ring-puckering frequency was set at 450 cm^{-1} as was done for the 1,2-$C_2H_4F_2$[1c] transition state. The grouped frequencies are given in Table IV.

Table IV: Frequencies[a] and Moments of Inertia[a] for Molecules and Transition States

Molecule	Transition states: HF elimination	Transition states: Radical association[d]
C_2H_5F[b]		
2972 (5)	3000 (4)	3095 (5)
1472 (5)	1423 (3)	1398 (4)
1270 (1)	1241 (3)	1171 (1)
1067 (3)	1021 (3)	606 (2)
845 (2)	948 (2)	86 (2)
415 (1)	698 (1)	63 (2)
243 (1)	450 (1)	
14.0; 53.9; 61.6	19.1; 43.4; 55.6	21.6; 105; 118
		I_r = 3.02
	HF elimination	Radical association[e]
CH_3CF_3[c]		
3000 (3)	3000 (2)	3122 (3)
1431 (3)	1339 (2)	1322 (4)
1248 (3)	1050 (3)	1087 (1)
921 (3)	932 (3)	655 (2)
560 (3)	806 (2)	512 (2)
365 (2)	598 (3)	71 (2)
238 (1)	424 (2)	41 (2)
91.7; 97.4; 97.4	94.9; 99.6; 115	168; 168; 113
		I_r = 3.5

[a] The last entry, or last two entries for the association transition states, of each column are the moments of inertia in amu Å^2. The frequencies are in cm^{-1} units and the number of frequencies having a given magnitude are indicated by parentheses. The reaction path degeneracy is 2 for C_2H_5F and is 6 for CH_3CF_3. [b] Reference 15. [c] Reference 16. [d] References 22 and 23. [e] References 22 and 24.

The threshold energy was chosen to agree with the E_0 deduced from the Arrhenius activation energies; the dependency of k_E upon E_0 is shown in Figures 4 and 5. The E_{min} values were set at $D(R_1\text{–}R_2)$ + 1 kcal mol^{-1} by analogy with previous work. The $D(CH_3\text{–}CH_2F)$ value of 87.2 kcal mol^{-1} is known with reasonable certainty. The $D(CH_3\text{–}CF_3)$ value of 98.9 kcal mol^{-1} is rather high but may be accepted with some reservation pending further investigation of $\Delta H_f°(CH_3CF_3)$. These thermochemical values have been discussed by us ear-

(17) K. Dees, D. W. Setser, and W. G. Clark, *J. Phys. Chem.*, **75**, 2231 (1971).

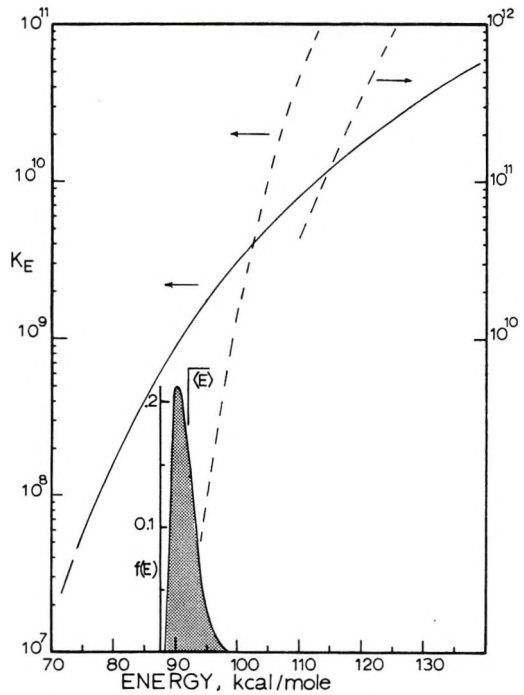

Figure 4. Calculated dissociation, —, and HF elimination, ——, rate constants from the RRKM formula, $k_E = \sigma/hP_1^+/P_1 \Sigma_{E_v \leq E^+} P(E_v)/N(E_0 + E^+)$; E_0 is the threshold energy and $E^+ = E - E_0$. The harmonic oscillator sums and densities were calculated using the frequencies of Table IV. The distribution function is for $CH_3 + CH_2F \rightarrow C_2H_5F$ at 360°K.

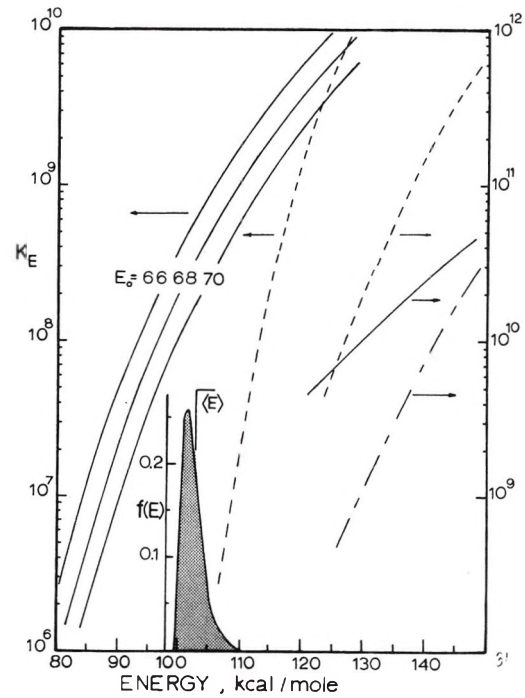

Figure 5. Calculated rate constants and distribution functions for CH_3CF_3. This distribution function is for $CH_3 + CF_3$ at 300°K. Dissociation rate constant, — (model of Table IV); — — — (model in text); ——, elimination rate constants for various E_0. Only the $E_0 = 68$ curve was extended to higher energy.

lier[1c] and by others.[18] The k_E values were computed from harmonic densities and sums in the same way as previously reported.[1]

Dissociation Rate Constants. These rate constants are needed to obtain the distribution function of $C_2H_5F^*$ and $CH_3CF_3^*$ formed by radical combination. Since intramolecular competition between dissociation and elimination may exist at high energies, some effort was put into obtaining realistic models for dissociation. Since the radical combination rates can be predicted[19] and since the equilibrium constant for

$$R_1R_2 \rightleftharpoons R_1 + R_2$$

can be accurately calculated, the thermal unimolecular rate constant can be obtained from $k_{uni} = K_{eq}k_{bi}$. At the present time it is not possible to formulate a transition state which satisfies both the unimolecular data and the radical combination bimolecular rate constant for simple alkanes.[20,21] In general the unimolecular results favor tighter transition state models than those required by the bimolecular combination step. However a recent study[10] of $C_2H_6^*$ formed by radical association claims agreement with calculations based on a loose transition state.

Our purpose was to estimate the dissociation rate constants. For this we calculated the equilibrium constants at 800°K and used typical values ($\sim 10^{13.3}$ cm^3 mol^{-1} sec^{-1}) of bimolecular rate constants[19] to fix the preexponential factor of the unimolecular step. We retained 1 kcal mol^{-1} for the threshold energy of radical combination for consistency with prior work.[1] This has the effect of making the low-temperature bimolecular rate constants too small relative to current experimental measurements. It would, however, be unrealistic to compensate for the 1 kcal mol^{-1} by selecting an even looser transition state model. The transition state model (see Table IV) consists of the frequencies of CH_3,[22] CH_2F,[23] or CF_3[24] radicals plus four low bending modes, which were assigned to obtain the desired preexponential factor. The results are summarized in Figures 4 and 5 and in Table V. The k_E values were calculated using the RRKM form of k_E which includes

(18) (a) G. O. Pritchard and M. J. Perona, *Int. J. Chem. Kinet.*, 1, 509 (1969); (b) J. A. Kerr and D. M. Timlin, *Trans. Faraday Soc.*, 67, 1376 (1971).

(19) (a) N. Basco, D. G. L. James, and R. D. Suart, *Int. J. Chem. Kinet.*, 2, 215 (1970); (b) H. E. van Den Berg, A. B. Callear, and R. Norstrom, *Chem. Phys. Lett.*, 4, 101 (1969); (c) T. Ogawa, G. A. Carlson, and G. C. Pimentel, *J. Phys. Chem.*, 74, 2090 (1970).

(20) E. V. Waage and B. S. Rabinovitch, *Int. J. Chem. Kinet.*, 3, 105 (1971).

(21) (a) W. L. Hase and J. W. Simmons, *J. Chem. Phys.*, 54, 1277 (1971); (b) W. L. Hase, R. L. Johnson, and J. W. Simons, *ibid.*, in press.

(22) (a) D. E. Milligan and M. E. Jacox, *ibid.*, 47, 5146 (1967); (b) A. Snelson, *J. Phys. Chem.*, 74, 537 (1970).

(23) The frequencies of CH_2F were constructed by analogy with CH_3 and 1,2-$C_2H_4F_2$.

(24) D. E. Milligan and M. E. Jacox, *J. Chem. Phys.*, 48, 2265 (1968).

Table V: Comparison of Calculated and Experimental[a] Results

Reaction	E_0, kcal	$\langle E \rangle$, kcal[c]	Preexponential factor,[b] sec^{-1}	Chemical activation rate constant,[c] sec^{-1}	Equilibrium constant, mol/cm^3
CH_3CH_2F	$(58.4 \pm 1.0)^e$		$(1.13 \times 10^{13})^e$	$(1.8 \pm 0.3 \times 10^9)$	
	$(57.0 \pm 1.3)^f$		$(0.96 \times 10^{13})^f$		
$\xrightarrow{800°} C_2H_4 + HF$	57	92.1	1.64×10^{13}	1.24×10^9	
					$2.8 \times 10^3 \exp(-E_0°/RT) =$
$\xrightarrow{800°} CH_3 + CH_2F$	88.2		1.4×10^{17}	See Figure 4	4.3×10^{-21}[d]
$\xrightarrow{400°} CH_3 + CH_2F$	88.2		1.3×10^{16}	See Figure 4	$1.1 \times 10^3 \exp(-E_0°/RT) = 2.5 \times 10^{-45}$
CH_3CF_3	$(67 \pm 2)^g$		$(3.8 \times 10^{13})^g$	$(2.3 \pm 0.4 \times 10^8)$	
$\xrightarrow{800°} CH_2CF_2 + HF$	68	102.4	5.29×10^{13}	3.4×10^8	
					$4.3 \times 10^3 \exp(-E_0°/RT) =$
$\xrightarrow{800°} CH_3 + CF_3$	98.9		1.7×10^{17}	See Figure 5	7.7×10^{-24}[d]
					$2.72 \times 10^3 \exp(-E_0°/RT) =$
$\xrightarrow{400°} CH_3 + CF_3$	98.9		2.2×10^{16}	See Figure 5	8.7×10^{-51}

[a] Experimental numbers are enclosed in parentheses; calculated values are not. [b] Preexponential factors are in the partition function form $(\sigma kt/h)(Q_{vr}^+/Q_{vr})$. The torsionial mode was treated as a vibration frequency for this calculation. A hindered rotor model would lower the preexponential factor by 0.81. [c] The calculated values are the unit deactivation limiting high pressure form of $\langle k_E \rangle$; $\langle E \rangle$ is the average energy of molecules formed by radical combination. The experimental values are from Table II and have been reduced to a unit deactivation basis. [d] The calculated values of the bimolecular rate constants (k_{uni}/K_{eq}) are 2.7×10^{13} (C_2H_5F) and 2.1×10^{13} (CH_3CF_3) $cm^3\ mol^{-1}\ sec^{-1}$ at 800°K. The slight difference in the bimolecular rate constants results from the choices made for the bending modes in the transition states and has no physical significance. The $E_0°$ was set at 1 kcal mol^{-1} lower than E_0. This 1 kcal mol^{-1} threshold energy, which was included for consistency with previous work, has the effect of making k_{bi} more strongly dependent on temperature than suggested by current experimental evidence. [e] Arrhenius value of ref 5a converted into a threshold energy and partition function preexponential factor. [f] Arrhenius values of ref 5b converted into a threshold energy and partition function preexponential factor. [g] Arrhenius values of ref 6b converted into a threshold energy and partition function preexponential factor.

the overall rotational partition functions and harmonic sums and densities. A more explicit accounting of centrifugal effects[20] would lower the k_E values by ~50%. However, this is an unnecessary detail since the rate constants can be altered much more severely by selecting different values of the bending frequencies. For example a CH_3–CF_3 model[25] having bending frequencies of 150(2) and 100(2) was used for comparison, and the results are shown in Figure 5. This model, which has a preexponential factor of 7.8×10^{15} sec^{-1}, gives a radical combination rate constant of 1.2×10^{12} $cm^3\ mol^{-1}\ sec^{-1}$ at 800°. This model should be viewed as giving lower limits to the values of the dissociation rate constants for CH_3CF_3*; whereas, the rate constants from the other model are close to the upper limit. Fortunately the distribution function for molecules formed by radical combination is not very sensitive to the dissociation rate constants.

The unimolecular reaction data and various transition state models for C_2H_6 have recently been reviewed by Waage and Rabinovitch.[20] They favored a model having a preexponential factor (partition function form) of $10^{17.0}$ sec^{-1} at 873°K, which is similar to that selected for C_2H_5F and CH_3CF_3. It is worth noting that inclusion of anharmonicity in the computation of N_E and $\Sigma P(E_v)$ could significantly lower the k_E values for the radical dissociation channel of the alkanes or fluoroethane because E is large and $E - E_0$ is small.

Calculation of Experimental Rate Constants for Stepladder Cascade Deactivation. For unit deactivation the experimental rate constant is obtained from

$$k_a = k_M[M] \frac{\int_{E_{min}}^{\infty} \frac{k_E}{k_E + k_M[M]} f(E)dE}{\int_{E_{min}}^{\infty} \frac{k_M[M]}{k_E + k_M[M]} f(E)dE}$$

The distribution function, which was obtained in the usual way,[1] is shown in Figures 4 and 5 for C_2H_5F* and CH_3CF_3*. Since $\langle E \rangle - E_0$ is relatively large and since $f(E)$ is narrow, there is little variation in k_a(unit) with pressure and for simplicity the high pressure value was tabulated in Table V. For the stepladder cascade calculations the full distribution was used; however, for

(25) The k_E values from the lower limit model were the ones used by Root and coworkers in their recent study of $^{18}F + CH_3CF_3$; ref 7. Use of the larger k_E values for radical dissociation does not affect their arguments.

simplicity in presentation a monoenergetic excitation at $\langle E \rangle$ will be discussed below. The equations[26] for calculating S, D, and k_a at a pressure corresponding to [M] are

$$S_T = \prod_{t=1}^{T} \frac{\beta k_M[M]}{\beta k_M[M] + k_{Et}}; \quad D = 1 - S_T$$

and

$$k_a^T = k_a(\Delta E) = k_M[M][(\beta k_M[M])^{-1} \prod_{t=1}^{T} (\beta k_M[M] + k_{Et}) - 1]$$

T is the number of cascade steps of magnitude $\langle \Delta E \rangle$ in the energy region $E - E_0$. Another way of stating this is that $\langle \Delta E \rangle$ is the average energy lost per collision. The factor β allows for uncertainty in the knowledge of cross sections. The calculations were done by assuming that $\beta = 1$ and that $S_{AM}^2 = \sigma_{AM}^2 \Omega^{(2,2)*}$. The $k_a(\Delta E)$ values were calculated using the specific rate constants tabulated in Figure 5 for various $\langle \Delta E \rangle$ over an extended pressure range. The results are shown as the solid curves of Figure 3. In addition to the increase in $k_a(\Delta E)$ with declining pressure, the high-pressure limiting values depend on $\langle \Delta E \rangle$ as shown in the footnote of Table III.

Discussion

Experimental Rate Constants. Our value of 151 Torr for the rate constant (in pressure units, which corresponds to the half-quenching pressure) or $C_2H_5F^*$ at 363°K agrees well with the measurements (142 Torr at 300°K) of Trotman-Dickenson and coworkers.[3] Pritchard and Thommarson's values are high by about a factor of 2; this also was true of their rate constant for 1,2-$C_2H_4F_2$ and implies that some systematic error exists in the data. All of these studies employed ketones as the bath gas.

Pritchard and Perona[2a] reported a rate constant of 29 Torr for CH_3CF_3 with trifluoroacetone as the bath gas at 425°K. Using the data of their Table I, a rate constant of 18–22 Torr seems appropriate at 300°K. McKnight, Parks, and Root[7b] photolyzed[14] CH_3COCH_3 and CF_3COCF_3 in a bath gas of CH_3CF_3 at 300°K and reported a rate constant of 29 Torr; however, examination of their data suggest that 25 Torr may be a better value. Based upon limited data, Giles and Whittle[4] deduced rate constants of 67 Torr (CH_3COCH_3), 29 Torr (CF_3COCF_3), 360 Torr (N_2), and 19 Torr (c-C_6F_{12}) at 423°K. These values are in approximate agreement with our data for comparable gases even though much of Giles and Whittle's data were obtained at pressures corresponding to relatively high D/S and, thus, cannot be directly equated to k_a^∞ values. These data, as well as our own,[27] point out that quite significant differences may exist for vibrational quenching by supposedly efficient gases and that considerable care must be exercised in selection of collision diameters to obtain unimolecular rate constants for even "efficient" deactivating gases.

Comparison of Calculated and Experimental Rate Constants. RRKM computations for C_2H_5F, with an E_0 of 57 kcal, have been done by Kirk and coworkers.[3b] Our k_E and preexponential factor values are lower by 10–20% since they assigned the frequencies of the transition state in a slightly different way. The thermal and chemical activation data of Table V fit either calculation quite well, although the calculations tend to underestimate the chemical activation rate constant and overestimate the preexponential factor. However, the calculated chemical activation rate constant is within the uncertainty of the possible collision diameters used to obtain the experimental value.

The agreement between the experimental and calculated unit deactivation chemical and thermal activation data for CH_3CF_3 also is satisfactory, see Table V. Since $D(CH_3\text{–}CF_3)$ is not well established, the agreement between the data and the calculations may be taken in support of the surprisingly high value of the bond energy. As pointed out by Tschuikow-Roux,[6b] increasing fluorine substitution raises the threshold energy for HF elimination from fluoroethanes. The enhanced preexponential factor of CH_3CF_3 relative to C_2H_5F mainly arises from the larger reaction path degeneracy.

It is quite interesting that the rate constant for dissociation of CH_3CH_2F is predicted to exceed that for HF elimination at energies above ~105 kcal mol^{-1}. This may explain why the rate constant for "decomposition" of $C_2H_5F^*$ formed by insertion of CH_2 with CH_3F exceeded the predicted HF rate constant value, by nearly a factor of 3.[5,28]

According to our calculations, radical dissociation for $CH_3CF_3^*$ should complete with HF elimination at ~125 kcal mol^{-1}. This higher energy, relative to C_2H_5F, primarily arises from the higher threshold energy for radical dissociation by CH_3CF_3. However, even taking this into consideration the energy required for the two rates to be of similar magnitudes is somewhat smaller for C_2H_5F than for CH_3CF_3. Obtaining experimental data at higher energies for the purpose of ascertaining the reliability of the radical dissociation models would be worthwhile. Roux and coworkers[29]

(26) D. W. Setser and J. C. Hassler, *J. Phys. Chem.*, 71, 1364 (1967).

(27) D. W. Setser, E. E. Siefert, and N. L. Craig, 162nd American Chemical Society National Meeting, Washington, D. C., Abstract 93 of the Physical Division, Sept 1971.

(28) The insertion reaction of CH with CHF is 99 kcal mol^{-1} exothermic at 0°K for $\Delta H_f°(CH_2)$ = 93 kcal mol^{-1}. If 3 kcal mol^{-1} of thermal energy and 6 kcal mol^{-1} of excess energy carried by CH_2 from the photolysis step is added, the total energy is 108 kcal mol^{-1}. The experimental rate was 1.5×10^{10} sec^{-1} which is a factor of 2–3 above the value predicted in Figure 4. A similar conclusion was reached in ref 5.

(29) (a) G. E. Millward, R. Hartig, and E. Tschuikow-Roux, *J. Phys. Chem.*, 75, 3195 (1971); (b) E. Tschuikow-Roux, G. E. Millward, and W. J. Quiring, *ibid.*, 75, 3493 (1971).

recently observed the radical dissociation reaction in competition with HF elimination for pentafluoroethane and 1,1,2,2-tetrafluoroethane in shock tube experiments. Although the preexperimental factors have significant standard deviations, they certainly support a loose transition state model which would be similar to those described in Table IV.

The excellent agreement between experimental and calculated results from the same basic transition state model for chemical and thermal activation of C_2H_5Cl, C_2H_5F, and many other chloro- and fluoroalkanes provides support for the postulates of the RRKM theory as applied to the computation of rate constants. Rynbrandt and Rabinovitch[30] recently reported evidence for nonrandomization of energy in chemically activated hexafluorobicyclopropane. Their chemical activation system was explicitly designed to test for nonrandomization of energy, and it is doubtful that the haloethanes experiments would have detected a small nonrandom component, even if it were present. However, considering the many molecules examined, a *large* contribution to the decomposition product *via* a nonrandom component should have been noted. Root and coworkers[7a] have suggested that $CH_3CF_2{}^{18}F$ formed by hot ^{18}F atom displacement decomposes before the energy is randomized because they found only HF elimination even at high energies[31] such that radical dissociation should have been important. It may be that molecules formed by the high kinetic energy impact of ^{18}F atoms do decompose before the energy can randomize;[31] however, our evidence at $\sim$102 kcal mol^{-1} indicates that CH_3CF_3* behaves in a way that is consistent with the postulates of RRKM theory.

No evidence was found for the decomposition of CH_2CF_2 following reaction 5. Since the threshold[32] for HF elimination from CH_2CF_2 is 86 $\pm$ 7 kcal mol^{-1} and since $\leq^2/_3$ of the available energy is partitioned to the olefin,[1a] further unimolecular reaction would not be expected.

Although the empirical parameters for application of the RRK theory may be chosen (or adjusted) such that a useful description of a given piece of data is obtained, *e.g.*, thermally activated fall-off data,[33] a *single* set of parameters are not adequate to describe a given unimolecular reaction over a wide range of excitation energies. Previous attempts[2] to use the RRK theory to interpret the chemical activation data for the fluoroethanes has not been notably successful for reasons which already have been discussed.[1c] Isotope effects[1] also cannot be adequately described by the RRK theory.

Energy Transfer Probabilities and Collision Diameters. The plots of Figure 3 unmistakably show cascade deactivation, even for the large perfluoroalkane bath gas molecules. The average amount of energy lost per collision cannot be assigned with high reliability, but it is about 10 kcal mol^{-1} according to a stepladder model, and the C_6 and C_8 alkanes are more efficient than the other bath gases. The C_4F_8 data have the worst scatter because of difficulty with the gas chromatography separation of C_4F_8 and CF_3CH_3 and that energy assignment is the least reliable. There are very few other data available for comparison because interest usually is focused on the less efficient bath gas molecules. The only other well-documented example[34] having similar quantities of energy is the deactivation of dimethylcyclopropane by *cis*-butene-2 for which $\langle\Delta E\rangle$ = 11.4 kcal mol^{-1}. Unfortunately our studies[1d] of 1,2-$C_2H_4Cl_2$* with *c*-C_4F_8 could not be carried to sufficiently low pressure to identify $\langle\Delta E\rangle$. We do have tentative evidence[27] that 1,2-$C_2H_4Cl_2$* is deactivated more easily than CH_3CF_3* by the same bath gas. Further experiments are certainly needed with different excited molecules and with a larger variety of bath gases; however, the present data suggest an upper limit to the amount of internal energy removed from vibrationally excited polyatomic molecules. This may vary from one case to another but for CH_3CF_3* the limit appears to be in the 10–12 kcal mol^{-1} range.

The question of the collisional efficiency of the parent molecule with a vibrationally excited molecule often arises in thermally activated unimolecular reaction studies. The decomposition and stabilization product yields of $^{14}CH_3CF_3$ formed by ketone photolyses in a bath gas of CH_3CF_3 have been measured[35] down to $S/D \sim 0.05$. The plot of k/k_∞ *vs.* S/D, with the experimental k_∞ of 25 Torr, is very similar to those shown in Figure 3 and fit a calculated curve corresponding to $\langle\Delta E\rangle \sim 8$ kcal mol^{-1}. Thus as a bath gas, CH_3CF_3 is consistent with similar molecules investigated in this work and does not show any evidence for having a special efficiency. We[17] previously reached the same conclusion about 1,2-$C_2H_4Cl_2$, but with less direct evidence. For most thermally activated unimolecular reactions, the average energy above the threshold is less than 10 kcal mol^{-1}; therefore, for such cases the unit efficiency assumption should be good.[36]

After assignment of the $\langle\Delta E\rangle$ values, a consistent set of collision diameters for the fluoroalkanes was sought. For the $\langle\Delta E\rangle$ values chosen, the range of experimental k_n^∞ values exceeded that for the calculated results (which were scaled downward by 0.67 to obtain a better absolute fit to the experimental result). The scaling

(30) J. D. Rynbrandt and B. S. Rabinovitch, *J. Phys. Chem.*, **75**, 2164 (1971).

(31) The possible role of excited electronic states should not be overlooked for haloalkanes formed at very high energies.

(32) J. M. Simmie and E. Tschuikow-Roux, *J. Phys. Chem.*, **74**, 4075 (1970).

(33) D. M. Golden, R. K. Solly, and S. W. Benson, *ibid.*, **75**, 1333 (1971).

(34) J. D. Rynbrandt and B. S. Rabinovitch, *ibid.*, **74**, 1679 (1970).

(35) J. W. Root and C. F. McKnight, private communication (1971).

(36) D. C. Tardy and B.S. Rabinovitch, *J. Chem. Phys.*, **45**, 3720 (1966); **48**, 1282 (1968).

corresponds to reducing all the k_E values by this factor. It is possible that the smaller $\langle \Delta E \rangle$ values should be associated with a more complex transition probability model than the stepladder case. However, this is just speculation at this time. To fit the data, large collision diameters (S_{AM}) are required for the C_6 and C_8 fluoroalkanes. Dividing S_{AM} into σ and ϵ/k can be done in several ways, and we chose to follow the trend suggested by second virial coefficient data.[14] Rabinovitch and coworkers[13] successfully used a constant ϵ/k value of 160° and an increase in σ of 0.54 Å per CF_2 group to obtain collision diameters for thermal activation studies of perfluoroalkanes and CH_3NC. Their collision diameters corresponding to $\sigma_{AM}[\Omega^{(2,2)*}]^{1/2}$ are 6.7 and 7.3 Å for C_6F_{14} and C_8F_{18}, respectively. The difference from our choices (8.0 and 8.9 Å) could be reduced by using a larger ϵ/k for CF_3CH_3; however, this would not alleviate our problem of fitting the relative rate constants in the series C_2F_6–C_8F_{18}.

Conclusions

Unimolecular rate constants for elimination of HF from chemically activated CH_3CF_3 and CH_3CH_2F fit the pattern for other chloro-, bromo-, and fluoroethanes. Consequently, we conclude that the elimination reactions at 90–100 kcal mol^{-1} are adequately described by RRKM theory. The amount of energy removed from CH_3CF_3* per collision with perfluoroalkane bath gases ranged from 7 to 10 kcal mol^{-1}; the parent molecule also followed a similar collisional deactivation[35] pattern and did not show an unusually high efficiency.

Acknowledgment. We wish to thank Dr. J. W. Root for sending us the data cited in ref 35 and for giving us permission to quote the results. Mr. E. E. Siefert assisted with some of the energy transfer computations. This work was supported by the National Science Foundation under Grants GP-9245 and -27536X and by the Kansas State University Bureau of General Research.

Thermal Decomposition of Cyclobutanone

by T. Howard McGee* and A. Schleifer

York College of the City University of New York, Jamaica, New York 11432 *(Received October 8, 1971)*

Publication costs borne completely by The Journal of Physical Chemistry

The thermal decomposition of cyclobutanone has been reinvestigated in a static system between 360.0 and 406.3°. The products observed were ethylene, ketene, cyclopropane, and carbon monoxide. The formation of both ethylene and cyclopropane were found to be first order, and the rates were not affected by the addition of nitric oxide or propylene. The Arrhenius expressions are: $k(C_2H_4) = (3.6 \times 10^{14})e^{-51,900/RT}$ sec^{-1} and $k(c\text{-}C_3H_6) = (6.3 \times 10^{13})e^{-56,300/RT}$ sec^{-1}. A concerted molecular mechanism for the formation of ethylene and cyclopropane is shown to be consistent with the observed Arrhenius parameters.

Introduction

The kinetics and mechanisms of the photolysis and thermal decomposition of cyclic ketones have been investigated and discussed recently.[1] The photolysis of cyclobutanone has been shown to yield ethylene, ketene, cyclopropane, propylene, and carbon monoxide, and both singlet and triplet states have been demonstrated to be the precursors of these products.[2,3]

The thermal decomposition of cyclobutanone has been investigated by Walters[4] and yields essentially ethylene and ketene as reaction products. A rearrangement mechanism is supported by Walters, *et al.*, who found[4] that propylene and nitric oxide do not decrease the rate of reaction. However, recent thermochemical calculations by O'Neal and Benson[5] support a biradical mechanism for the decomposition of most small-ring compounds. The thermal decomposition of cyclopentanone,[6,7] by contrast, consists of at least four sep-

(1) R. Srinivasan, *Advan. Photochem.*, **1**, 83 (1963).

(2) T. H. McGee, *J. Phys. Chem.*, **72**, 1621 (1968).

(3) (a) H. O. Denschlag and E. K. C. Lee, *J. Amer. Chem. Soc.*, **89**, 4795 (1967); (b) *ibid.*, **90**, 3628 (1968); (c) N. E. Lee, H. O. Denschlag, and E. K. C. Lee, *J. Chem. Phys.*, **48**, 3334 (1968); (d) N. E. Lee and E. K. C. Lee, *J. Chem. Phys.*, **50**, 2094 (1969); (e) D. C. Montague and F. S. Rowland, *J. Amer. Chem. Soc.*, **91**, 7230 (1969).

(4) M. N. Das, F. Kern, T. D. Coyle, and W. D. Walters, *ibid.*, **76**, 6271 (1954).

(5) H. E. O'Neal and S. W. Benson, *J. Phys. Chem.*, **72**, 1866 (1968).

(6) E. R. Johnson and W. D. Walters, *J. Amer. Chem. Soc.*, **76**, 6266 (1954).

(7) F. M. Delles, L. T. Dodd, L. F. Lowden, F. J. Romano, and L. G. Daignault, *ibid.*, **91**, 7645 (1969).

arate reactions yielding ethylene, but-1-ene, carbon monoxide, pent-4-enal, cyclopent-2-en-1-one, and hydrogen. The mechanistic pathways for these reactions are not defined.

The current investigation of the thermal decomposition of cyclobutanone was undertaken to study further the products and kinetics of the pyrolysis and to clarify the mechanism of the decomposition of cyclic ketones.

Experimental Section

Apparatus. The pyrolysis was investigated in a static system using an 80-ml quartz reaction cell connected to a high-vacuum system with metal valves. The reaction cell was heated in an asbestos-packed furnace and the temperature was controlled by a Leeds and Northrup Thermocouple Electromax. A chromel–alumel thermocouple was used to measure the temperature.

The reaction cell pressure was measured by a Consolidated Electrodynamics Corp. pressure transducer maintained at 40°, and the transducer output was continuously recorded on a Leeds and Northrup Speedomax H Azar recorder.

Analysis. Products were collected in liquid nitrogen cooled traps and identified by gas chromatography and infrared analysis. In most experiments the products and unreacted cyclobutanone were mixed with a known amount of ethane, which served as an internal standard, and then transferred through the vacuum line directly to a gas sample loop connected to a Varian-Aerograph Model 1200 gas chromatograph with a hydrogen flame detector. In this manner the analysis for ethylene and cyclopropane was conducted using a 6 ft × 0.125 in. column packed with Porapak Q. The vpc peak areas were measured and recorded by a Leeds and Northrup Model H recorder and analog integrator.

Materials. Cyclobutanone was obtained from the Aldrich Chemical Co., Inc., purified, dried, and stored under vacuum in a blackened vessel. The sample was degassed by pumping at liquid nitrogen temperature before each run.

Ethylene, cyclopropane, carbon monoxide, propylene, and ethane were obtained from the Matheson Co., Inc., and were used directly after degassing. Nitric oxide, obtained from the Matheson Co., Inc., was first purified by removing NO_2 and N_2O impurities at −127°.

Results

Measurement of total reaction pressure *vs.* time gave smooth curves (Figure 1), from which the times required for definite pressure increases, $t_{25\%}$ and $t_{50\%}$, were obtained. No initial pressure decrease was observed in any of these experiments as was reported in the pyrolysis of cyclopentanone.[7] Plots of $1/t_{25\%}$ *vs.* $P_i(C_4H_6O)$ showed first-order dependence at all

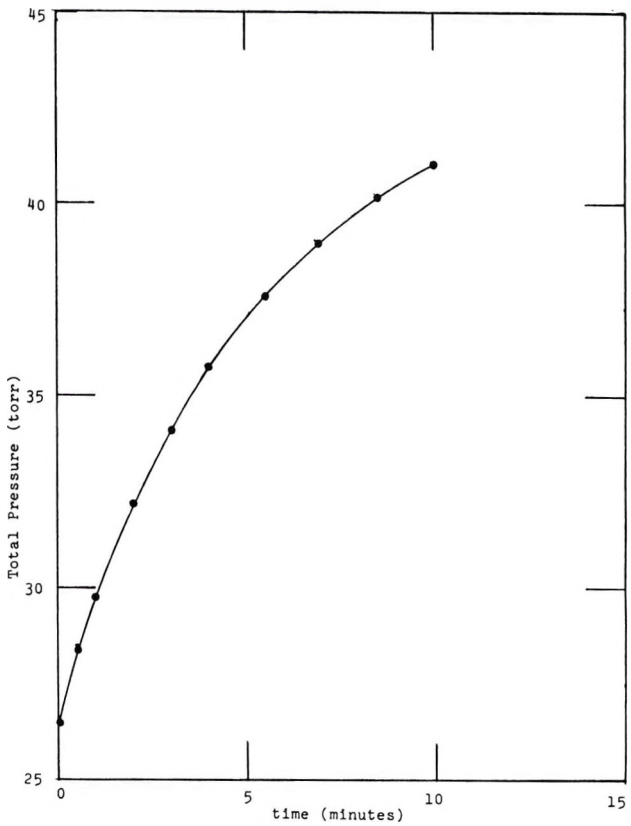

Figure 1. Pressure–time curve for decomposition of cyclobutanone at 397.2° ($P_i(C_4H_6O)$ = 26.5 Torr).

temperatures, and an Arrhenius plot of log $1/t_{25\%}$ *vs.* $1/T$ (°K) gave a straight line whose slope yielded an activation energy of 54 kcal/mol, in fair agreement with the value of 52.0 kcal/mol reported by Walters.[4]

Analysis of the products of the thermal decomposition of cyclobutanone indicated the formation of ethylene, ketene, cyclopropane, and carbon monoxide. The formation of ethylene and cyclopropane were measured as a function of reaction time, initial pressure (Figures 2 and 3), and temperature. The curves obtained from plots of $n_{C_2H_4}$ and $n_{c\text{-}C_3H_6}$ *vs.* time were fitted by a least-squares program on an IBM 1130 computer. The initial rate of formation of C_2H_4 and c-C_3H_6 was obtained from the initial slopes of these curves. Plots of log $R_i(C_2H_4)$ or log $R_i(c\text{-}C_3H_6)$ *vs.* log $[C_4H_6O]_i$ gave straight lines, as in Figure 4, and the order and rate constants for these processes were obtained from the slopes and intercepts, respectively, of these graphs. The average order for the formation of C_2H_4 was 1.01 and that for c-C_3H_6 was 0.99 over the temperature range 360.0–406.3° and initial pressures of 1.5–38.0 Torr of cyclobutanone. The activation energies and frequency factors for the formation of C_2H_4 and c-C_3H_6 were then determined from rate constants derived from initial rates of formation. The resulting Arrhenius expressions are: $k(C_2H_4) = (3.6 \times 10^{14}) \cdot e^{-51,900/RT}$ sec^{-1} and $k(c\text{-}C_3H_6) = (6.3 \times 10^{13})e^{-56,300/RT}$ sec^{-1} (Figure 5).

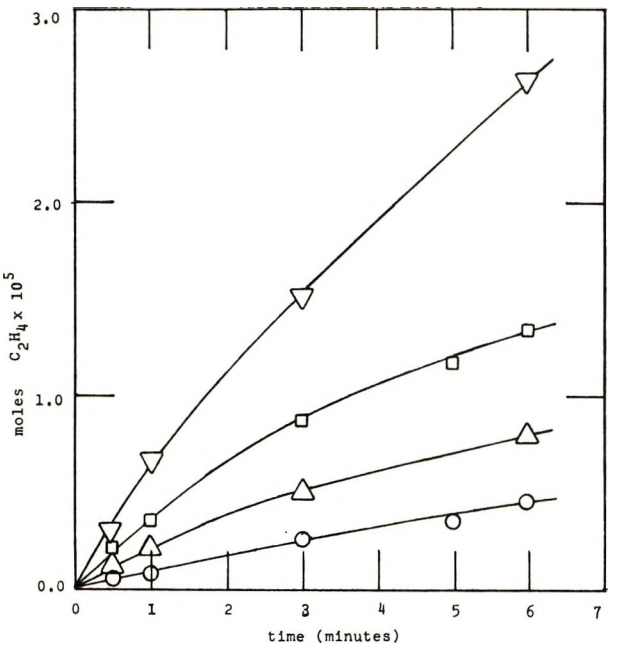

Figure 2. Formation of C_2H_4 *vs.* time at several pressures at 383°: (○) P_i = 5 Torr, (△) P_i = 11 Torr, (□) P_i = 20 Torr, (▽) P_i = 39 Torr.

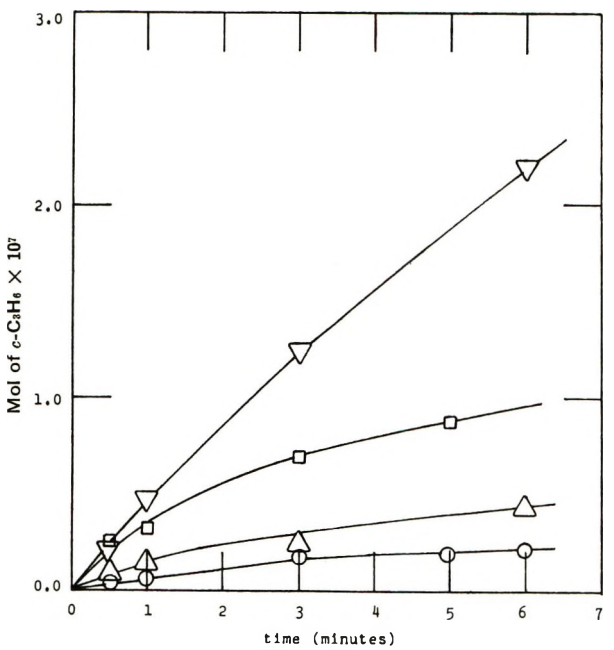

Figure 3. Formation of c-C_3H_6 *vs.* time at several pressures at 383°: (○) P_i = 5 Torr, (△) P_i = 11 Torr, (□) P_i = 20 Torr, (▽) P_i = 39 Torr.

First-order plots (log $[a_0/a_0 - x]$ *vs.* t) for the disappearance of cyclobutanone, calculated from the initial concentration of cyclobutanone and the amounts of C_2H_4 and c-C_3H_6 formed, also gave straight lines. First-order rate constants, k', calculated from the slopes of these plots were obtained, and a graph of log k' *vs.* $1/T$ (°K) gave the Arrhenius expression $k' = (4.2 \times 10^{14})e^{-52,300/RT}$ sec^{-1}. This compares quite favorably with that given by Walters, $k = (3.6 \times 10^{14}) \cdot e^{-52,000/RT}$ sec^{-1}.

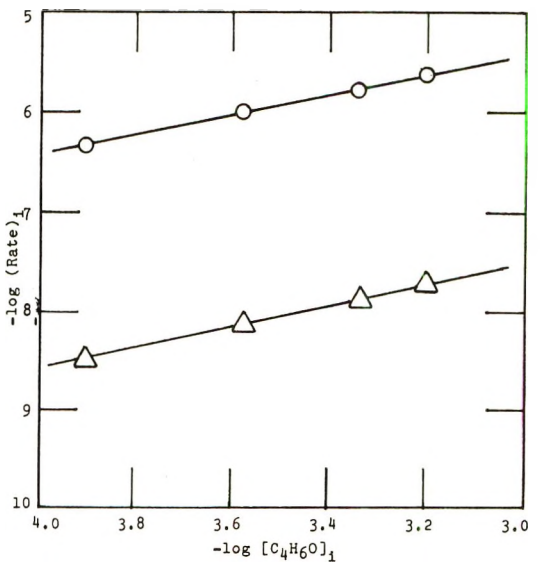

Figure 4. Determination of the order of reaction for the formation of ethylene (○), and cyclopropane (△); 356.5°.

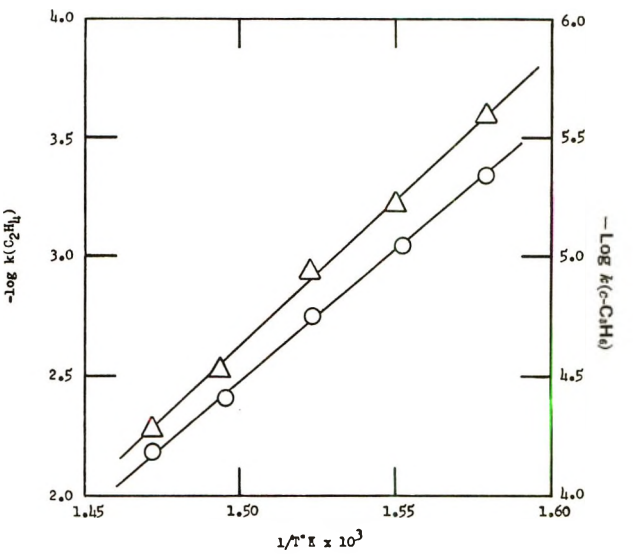

Figure 5. Variation of log $k(C_2H_4)$ (○) and log $k(c$-$C_3H_6)$ (△) with reciprocal of the absolute temperature.

In separate experiments at 372°, C_3H_6 and NO were found to have no effect on the rates of formation of either C_2H_4 or c-C_3H_6.

Discussion

The results indicate that besides the previously reported ethylene and ketene, cyclopropane and carbon monoxide are formed in the pyrolysis of cyclobutanone. Walters[4] had detected a trace of cyclopropane in a mass spectrometric analysis of products from one experiment carried to 33% pressure increase. Cyclopropane may be formed directly from the decomposition of cyclobutanone or through secondary reactions involving possibly ketene.

The thermal decomposition of ketene has been investigated between 396 and 563° [8] and has been found to be second order, resulting in the formation of carbon monoxide, ethylene, methane, carbon dioxide, and allene. The decomposition apparently does not produce methylene in a simple unimolecular process.[9] Ketene easily dimerizes[10] in the gas phase to form β-methylene cyclic lactone.

The formation of cyclopropane from cyclobutanone was observed at very small per cents decomposition and has been found to be first order. The decomposition does not exhibit an induction period which might result if cyclopropane were formed in secondary reactions involving ketene. Neither methane nor allene was detected in the vpc analysis, and the rate of ketene decomposition *via* a bimolecular process at the lower temperatures and pressures must be very small, if not zero. Finally, if cyclopropane were formed by reaction of methylene with ethylene, the appearance of propylene should also be observed. At 300°, Benson[10] estimates that about 10% of the trimethylene diradicals formed in such a reaction should lead to propylene. A similar calculation at 650°K, the average temperature of the experiments reported above, again yields the result that about 10% of the products of such a reaction should be propylene. No propylene was observed in any of the vpc analyses under the experimental conditions employed. It thus appears that cyclopropane is formed directly from the decomposition of cyclobutanone.

A mechanism including the intermediate diradicals, I and II, in the formation of ethylene and ketene can be advanced. O'Neal and Benson[5,11] have made extensive thermochemical calculations of activation energies and frequency factors for dissociation and isomerization reactions of small ring compounds. In predicting activation energies, enthalpy changes for the following processes are evaluated:[11] (a) ring opening to the diradical at 298°K; (b) inclusion of resonance, if any, in the diradical; (c) a temperature correction from 298°K to the average reaction temperature; and (d) formation of the transition state from the diradical. The results of these calculations are consistent with a reaction mechanism that includes a diradical intermediate for the large majority of these reactions. In a similar manner, the activation energies for reactions 1 and 2 can be estimated using the available thermochemical data.

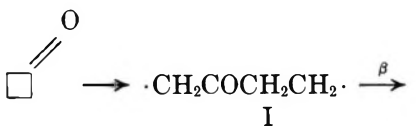

$$\xrightarrow{\beta} CH_2CO + C_2H_4 \quad (1)$$

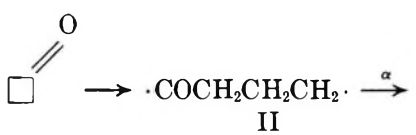

$$\xrightarrow{\alpha} CH_2CO + C_2H_4 \quad (2)$$

The heat of formation of diradical I, $\Delta H_f°(\mathrm{I})$, may be estimated from the heat of reaction for (3). $\Delta H_f°$(2-

$$CH_3COCH_2CH_3 \longrightarrow 2H\cdot + \cdot CH_2COCH_2CH_2\cdot \quad (3)$$

butanone) can be estimated from group additivity tables[11-13] to be −56.7 kcal/mol, and a value of 98 kcal/mol can be assigned for the C–H bond strength.[14] Thus, $\Delta H_f°(\mathrm{I}) = 2(98) - 104 - 56.7 = 35.3$ kcal/mol. This, together with $\Delta H_f°(c\text{-}C_4H_6O) = -20.3$ kcal/mol, results in a value of 55.6 kcal/mol for step a in the above sequence. The resonance stabilization energy for $\cdot CH_2CH_2COCH_2\cdot$ can be taken to be zero, as has been determined for the acetonyl radical.[14] A previous value of −7.9 kcal/mol[11] estimated from rate constant parameters for the decomposition of methyl cyclobutyl ketone appears high in the present case. An upper limit on this resonance stabilization is probably −2.7 kcal/mol, as estimated for the methylacetonyl radical.[15] Tabulated $C_p°$ values[11] have been used in step c and the C_4 ring-closing activation energy of 6.6 kcal/mol[5,11] has been used in step d. This gives $E_a(\beta) = 63.3$ kcal/mol (60.6 kcal/mol if −2.7 kcal/mol is used for the resonance energy), significantly higher than the observed value.

Similarly, $\Delta H_f°(\mathrm{II})$ can be estimated from the heat of reaction of 4, using $\Delta H_f°$(butanal) = −49.6 and

$$CH_3CH_2CH_2COH \longrightarrow 2H\cdot + \cdot CH_2CH_2CH_2CO\cdot \quad (4)$$

bond energies of 98 kcal/mol for (–CH_2–H) and 86 kcal/mol for (–CO–H).[16] This gives $\Delta H_f°(\mathrm{II}) = 30.4$ kcal/mol. Again assuming no resonance energy stabilization energy for $\cdot COCH_2CH_2CH_2\cdot$ and proceeding as above, the estimated activation energy for reaction 2 is $E_a(\alpha) = 58.5$ kcal/mol. Thus, it appears that neither diradical I nor II is an intermediate in the formation of C_2H_4 and CH_2CO, and that the decomposition to these products occurs by a concerted reaction.

Although β cleavage to diradical I cannot lead to formation of cyclopropane and carbon monoxide, α cleavage should be considered as a possible mechanism.

(8) W. B. Guenther and W. D. Walters, *J. Amer. Chem. Soc.*, **81**, 1310 (1959).

(9) J. R. Young, *J. Chem. Soc.*, 2908 (1958).

(10) W. B. De More and S. W. Benson, *Advan. Photochem.*, **2**, 219 (1964).

(11) S. W. Benson and H. E. O'Neal, "Kinetic Data on Gas Phase Unimolecular Reactions," NSRDS-NBS 21, 1970.

(12) S. W. Benson, "Thermochemical Kinetics," Wiley, New York, N. Y., 1968.

(13) H. E. O'Neal and S. W. Benson, *Int. J. Chem. Kinet.*, **1**, 221 (1969).

(14) R. K. Solly, D. M. Golden, and S. W. Benson, *ibid.*, **2**, 11 (1970).

(15) R. K. Solly, D. M. Golden, and S. W. Benson, *ibid.*, **2**, 381 (1970).

(16) J. A. Devore and H. E. O'Neal, *J. Phys. Chem.*, **73**, 2644 (1969).

Diradical II can further dissociate to the trimethylene diradical

$$\cdot COCH_2CH_2CH_2\cdot \longrightarrow CO + \cdot CH_2CH_2CH_2\cdot \quad (5)$$

Taking $\Delta H_f^\circ(\cdot CH_2CH_2CH_2\cdot) = 67$ kcal/mol,[17] with data given above, reaction 5 requires an additional 10.0 kcal/mol. The activation energy for the reverse reaction, -5, is approximately 8 kcal/mol, and the mole change introduces a factor of RT.[18] This, together with the C_3 ring-closing activation energy of 9.3 kcal/mol,[5] raises the activation energy for c-C_3H_6 formation to $E_a = 77.9$ kcal/mol, much higher than the E_a (obsd) = 56.3 kcal/mol determined in this work. Additionally, as discussed above, propylene would be expected to be observed among the products if the trimethylene diradical were formed.

A second possible route to c-C_3H_6 and CO is through a concerted rearrangement of diradical II without formation of $\cdot CH_2CH_2CH_2\cdot$. For such a sequence, the normal C_4 ring-closing activation energy, 6.6 kcal/mol, is not valid. Any approximation of the activation energy for such a reaction is likely to be much higher and to result in a total estimated E_a much greater than the observed experimental value. No evidence has been reported for this type of reaction.

The concerted decomposition of cyclobutanone into c-C_3H_6 and CO must be the dominant reaction. The absence of propylene in the reaction products can now be explained if c-C_3H_6 is formed directly in the decomposition. The activation energy for the isomerization of c-C_3H_6 to propylene is about 65 kcal/mol,[19-21] with a frequency factor of 1.6×10^{15}. This gives $k_{isom} = 2.5 \times 10^{-7}$ at 650°K and will result in a negligible rate of propylene formation.

The entropies of activation have been calculated from (6) to be: $\Delta S^{\ddagger}(C_2H_4 + CH_2CO) = 4.6$ gibbs/mol

$$A = (ekT/h)e^{\Delta S^{\ddagger}/R} \quad (6)$$

and $\Delta S^{\ddagger}(c\text{-}C_3H_6 + CO) = 1.1$ gibbs/mol. These values appear to be consistent with the proposed concerted mechanism.

Finally, a mechanism other than one involving an intermediate diradical must be involved in other reactions of cyclic ketones. The formation of unsaturated aldehydes[1,22] in the photolysis of cyclobutanone and other cyclic ketones probably proceeds through a cyclic transition state. The pyrolysis of cyclopentanone,[7] reactions 7–10, probably also proceeds by a concerted

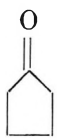

$$\longrightarrow CO + 2C_2H_4 \quad (7)$$

$$\longrightarrow CO + CH_2{=}CHCH_2CH_3 \quad (8)$$

$$\longrightarrow CH_2{=}CHCH_2CH_2C{-}H \quad (9)$$

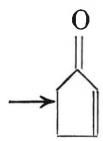

$$+ H_2 \quad (10)$$

rearrangement mechanism, especially in reactions 9 and 10.

Acknowledgments. We wish to acknowledge support from the National Science Foundation, Grant No. GY-5616, and from a City University of New York Doctoral Faculty Research Grant. We also wish to thank Dr. Duli Jain for his assistance in the computer programming.

(17) S. W. Benson, *J. Chem. Phys.*, **34**, 521 (1961).

(18) J. A. Kerr and A. C. Lloyd, *Quart. Rev. Chem. Soc.*, **22**, 549 (1968).

(19) W. E. Falconer, T. F. Hunter, and A. F. Trotman-Dickenson, *J. Chem. Soc.*, 609 (1961).

(20) E. S. Corner and R. N. Pease, *J. Amer. Chem. Soc.*, **67**, 2067 (1945).

(21) T. S. Chamber and G. B. Kistiakowsky, *ibid.*, **56**, 399 (1934).

(22) R. Srinivasan, *ibid.*, **81**, 5541 (1959).

The Oxidation of Carbon at the Surface of Nickel[1a]

by Jerome W. McAllister[1b] and John M. White*

Department of Chemistry, University of Texas at Austin, Austin, Texas 78712 *(Received September 16, 1971)*

Publication costs assisted by the National Science Foundation

The production of CO by oxidation of carbon at the surface of polycrystalline nickel has been investigated over the temperature range 300 to 800°K. Heating the nickel subsequent to oxygen exposure at room temperature produced gas phase CO molecules. The experimental data are interpreted in terms of a mechanism in which the rate-controlling step is the diffusion of carbon atoms to the surface of the nickel.

Many techniques are available for the study of chemisorption on nickel but, prior to the use of any one of these, the nickel surface must be cleaned. In cleaning, difficulty arises because surface impurity atoms are not removed by high temperature heating under vacuum. Germer, *et al.*,[2] reported that when a carbon-contaminated nickel surface is heated to near the melting point, the nickel atoms vaporize freely without removing the carbon. Sickafus[3] suggested that outgassing a Ni (110) surface at above 450° removes carbon atoms but that upon cooling a new growth of surface carbon occurs. After treating a Ni (111) sample at 700°, Dalmai-Imelik, *et al.*,[4] observed LEED patterns produced by surface carbon atoms and Auger spectra produced by carbon and sulfur atoms. LEED[5] and field emission[6] studies suggest that surface carbon can be partially removed by oxidation and removal as CO. Onchi and Farnsworth[7] have noted the evolution of CO from (100) nickel after room temperature oxygen exposure when the nickel sample was heated to temperatures above 200°.

Many details of the carbon oxidation process have not been investigated. For example, the rate-controlling step in the process is not known; neither are most of the mechanistic details of the overall oxidation–desorption process. We present here data characterizing in more detail the process of CO formation and the binding state of the resulting CO.

Our experiments were performed in an ultrahigh vacuum system capable of attaining base pressures below 10^{-10} Torr. The polycrystalline nickel target (geometric area = 6.3 cm²) was cut from 0.005-in. thick foil of 99.97% purity. It was mounted on two tungsten electrical feedthroughs which allowed resistive heating; the feedthroughs were coated with Pyrex glass to prevent the tungsten from interacting with gas phase species. An iron–constantan thermocouple spotwelded to the nickel monitored the sample temperature. Linear heating rates were utilized throughout this work. An Aero Vac Model 610-611 magnetic deflection type mass spectrometer monitored partial pressures during these experiments; the mass spectrometer was calibrated for CO with an NRC cold cathode ionization gauge which read in Torrs of air equivalent.

The sample was prepared by prolonged high-temperature outgassing under vacuum. Oxygen was then admitted to the system by means of a calibrated leak valve. Mass spectrometer measurements ensured that a given pressure of oxygen was maintained for a given length of time. After oxygen exposure, the pressure was lowered to less than 10^{-9} Torr; then the target was heated at a linear rate of 7.6 ± 0.5°K sec^{-1}. Calculations using simple heat transfer equations and known conductivity values indicated that during the course of sample heating, the portion of the thermocouple leads undergoing significant heating had a negligible geometric surface area (<0.4 cm²) compared to that of the nickel target. During heating the partial pressure was monitored at $m/e = 28$ by the mass spectometer and the bulk temperature was monitored by the thermocouple.

The resulting plot of CO partial pressure *vs.* time was analyzed to obtain the total number of CO molecules desorbed and the temperature where the desorption was a maximum. The analysis was accomplished as follows. During desorption the pressure is given as a function of time by the following equation

$$\frac{dp}{dt} = \frac{AQ(t)}{V} - \frac{s(p - p_0)}{V} \qquad (1)$$

where p is the pressure, p_0 is the initial pressure, t the time, A the geometric sample area, V the volume, $Q(t)$ the rate of desorption (Torr l. sec^{-1} cm^{-2}) at time t, and s the pumping speed (l. sec^{-1}). The surface cover-

(1) (a) Supported in part by NSF Grant GP-20370; (b) NSF Trainee 1967–1970 and Jefferson Chemical Co. Fellow (1970–1971).

(2) L. H. Germer and A. U. MacRae, *Proc. Nat. Acad. Sci. U. S.*, **48**, 997 (1962).

(3) E. N. Sickafus, *Surface Sci.*, **19**, 181 (1970).

(4) G. Dalmai-Imelik, J. C. Bertonlini, and J. Rousseau, *ibid.*, **27**, 379 (1971).

(5) A. U. MacRae, *Science*, **139**, 379 (1963).

(6) R. Gomer, *J. Chem. Phys.*, **21**, 293 (1953).

(7) M. Onchi and H. E. Farnsworth, *Surface Sci.*, **11**, 203 (1968).

age Θ is obtained by solving eq 1 for the rate and integrating numerically from $t = 0$ to $t = \infty$ during desorption.

The partial pressure *vs.* time curves revealed two distinct states from which CO desorbed. The first state desorbed between 300 and 400°K, the second between 400 and 800°K. For the low energy state the maximum desorption rate occurred at 350°K and the coverage was always small, near 10^{11} molecules cm^{-2}. The high energy state was characterized by coverages as large as 10^{15} molecules cm^{-2}. For this state the temperature corresponding to the maximum desorption rate varied from 550 to 700°K.

If the target was prepared as described above and the experiment was performed without the admission of oxygen, a small amount of CO ($\sim 10^{11}$ molecules/cm^2) was always desorbed in the same temperature range as the above low energy state. If CO rather than oxygen was admitted following sample preparation, desorption always indicated the low energy state was occupied, but no desorption from the above high energy state was noted. Therefore, since the high temperature CO desorption species observed after oxygen exposure has experimental characteristics quite different from the CO desorption produced by either residual gas exposure or deliberate CO exposure, we conclude that this species resulted from the interaction of oxygen with carbon atoms in the nickel. Furthermore, since the pressure of oxygen was immeasurably small immediately preceding each thermal desorption measurement, the carbon monoxide desorption resulted entirely from the influence of bulk nickel heating upon carbon and oxygen species sorbed to the surface or contained in the bulk lattice.

The CO desorption produced by oxygen exposure demonstrated the following experimental characteristics. The amount of CO desorbed at temperatures above 400°K was not affected either by prior carbon monoxide exposure or by the pressure of carbon monoxide during oxygen exposure. The number of CO molecules desorbed increased monotonically with the oxygen exposure; the amount varied from 0.01×10^{15} to 1.3×10^{15} molecules cm^{-2} for oxygen exposures from 10^{-6} to 10^{-1} Torr sec. Repeated cycles of oxygen exposure followed by thermal desorption did not measurably diminish the amount of CO desorbed after a given oxygen exposure. After oxygen exposure, the observed O_2 desorption was small; for exposures of 500×10^{-6} Torr sec, the O_2 desorption was less than 10^{11} molecules cm^{-2}.

The number of CO molecules thermally desorbed, θ, was measured for several oxygen exposures between 1 and 500×10^{-6} Torr sec. For each thermal desorption experiment, the temperature where the desorption attained a maximum T_m was measured also. In Figure 1, the experimental values of θ are plotted *vs.* the oxygen exposure. The number of desorbing CO molecules

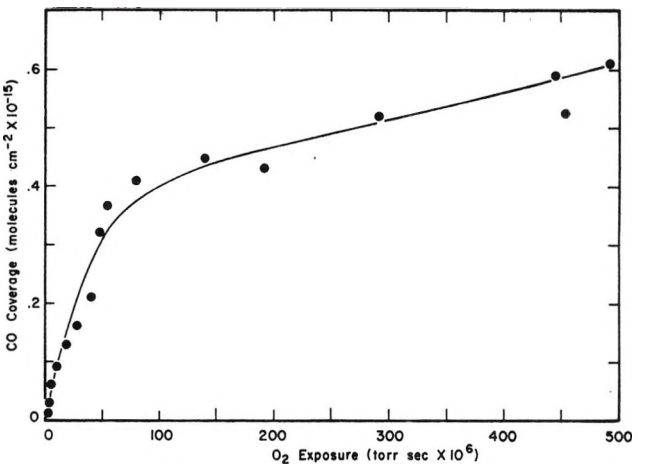

Figure 1. The variation of the carbon monoxide surface coverage with the oxygen exposure.

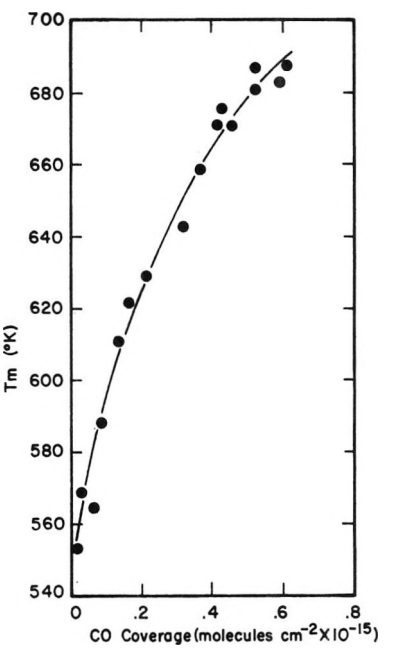

Figure 2. The variation of the temperature of maximum desorption rate, T_m, with the carbon monoxide surface coverage.

increases rapidly with exposure up to about 75×10^{-6} Torr sec of O_2 and more slowly for larger exposures. Figure 2 shows the dependence of T_m upon θ; T_m increased from 550 to almost 700°K as θ went from 0.01 to 0.60×10^{15} molecules cm^{-2}. In the kinetic theories of thermal desorption,[8,9] T_m is independent of the surface coverage for first-order desorption and a decreasing function for second-order desorption. Therefore, the magnitude of the rate of desorption of CO in these experiments must be governed by something other than relevant surface concentrations and the activation energy of desorption.

(8) G. Ehrlich, *J. Appl. Phys.*, **32**, 4 (1961).
(9) P. A. Redhead, *Vacuum*, **12**, 203 (1962).

The anomalous dependence of T_m upon θ can be explained by a model which considers the diffusion of carbon through the bulk to be important. Smithells and Ransley (SR)[10] studied the diffusion of carbon, oxygen, and carbon monoxide through nickel, and they concluded that C and O atoms diffuse readily while CO diffuses only very slowly if at all. SR observed that CO desorption originated from dissolved oxygen and carbon and that the diffusion of carbon was the rate-limiting step in the desorption process.

The results of our experiment are well explained by the conclusions of SR. Assuming the carbon was distributed uniformly throughout the target, there was enough carbon in the bulk to desorb 10^{15} molecules cm^{-2} of CO as many as 10^4 times (based on a 0.02% carbon impurity concentration). After each oxygen exposure at room temperature, the oxygen is localized at or near the surface and, upon heating the target at 7.6°K sec^{-1}, the carbon diffuses to the surface and reacts with oxygen to form carbon monoxide which desorbs. T_m increases with θ because the diffusion of carbon is the rate-controlling step in the oxidation process. Larger oxygen coverages lead to the consumption of larger amounts of carbon, and the latter requires additional time; thus a larger T_m.

(10) C. J. Smithells and C. E. Ransley, *Proc. Roy. Soc., Ser. A*, **155**, 195 (1936).

Concerning the Isotope Effect in the Decomposition of Ammonia on Tungsten Surfaces

by R. Sheets and G. Blyholder*

Department of Chemistry, University of Arkansas, Fayetteville, Arkansas 72701 *(Received July 1, 1971)*

Publication costs borne completely by The Journal of Physical Chemistry

It has been stated in the literature that NH_3 decomposition on W being 1.6 times faster than ND_3 precludes N_2 desorption being the rate-determining step as has been suggested from kinetic measurements. Having found ND_3 is a better electron donor than NH_3 we present a simple molecular orbital model of bonding to the surface which suggests the isotope effect can be explained as a β-secondary isotope effect which is compatible with N_2 desorption being rate limiting.

Although thermal decomposition of ammonia on tungsten surfaces has been studied for nearly half a century, the identity of the rate-determining step has not yet been established. Early investigations by Jungers and Taylor[1] and by Barrer[2] of the rates of decomposition of ammonia and deuterioammonia on tungsten showed that, while both rates were nearly zero order with respect to ammonia and hydrogen, ammonia decomposed 1.6 times as fast as deuterioammonia. This isotope effect seemed to imply that the breaking of a N–H or N–D bond is involved in the rate-determining step. A more recent study of ammonia decomposition has led Tamaru[3a] to conclude that decomposition occurs through consecutive reactions comprising nitride layer formation to produce H_2, followed by the rate-limiting decomposition of the nitride layers to give N_2. A recent paper by Matsushita and Hansen[3b] supports the conclusion that nitrogen desorption is the limiting step although Szostak and Germer[4] and Ozaki, Taylor, and Boudart[5] have maintained that the observed zero-order decomposition of ammonia on tungsten, unaffected by N_2 or H_2, when taken together with the isotope effect, is not explicable in terms of the theory which predicts that N_2 desorption is rate limiting. They argue that the zero order means the surface is completely covered with N atoms, and thus the rate should be equal to N_2 desorption and no isotope effect should be observed. Peng and Dawson[6] on the basis of desorbed gas analysis state that the surface contains W_2N_3H and claim that N–H bond breaking is involved

(1) J. Jungers and H. S. Taylor, *J. Amer. Chem. Soc.*, **57**, 679 (1935).

(2) R. Barrer, *Trans. Faraday Soc.*, **32**, 490 (1936).

(3) (a) K. Tamaru, *ibid.*, **57**, 1410 (1961). (b) K. Matsushita and R. S. Hansen, *J. Phys. Chem.*, **52**, 4877 (1970).

(4) J. May, R. Szostak and L. Germer, *Surface Sci.*, **15**, 37 (1969).

(5) A. Ozaki, H. S. Taylor, and M. Boudart, *Proc. Roy. Soc., Ser. A*, **258**, 47 (1960).

(6) Y. K. Peng and P. T. Dawson, *J. Chem. Phys.*, **54**, 950 (1971).

in the rate-determining step of NH_3 decomposition. However establishing the ratio of W, N, and H atoms on the surface in no way establishes that a N–H bond even exists on the surface and so their conclusion that N–H bond breaking is rate determining cannot be a necessary conclusion from their data.

We believe the isotope effect can be explained as a β-secondary isotope effect, a process which does not involve the breaking of a N–H or N–D bond, and thus the observed isotope effect and a zero-order NH_3 decomposition with N_2 desorption rate limiting can be compatible. The causes of β-isotope effects, which have had magnitudes around 1.5,[7,8] are not well understood. Halevi and coworkers[9,10] concluded that the CD_3 group is a better electron donor than the CH_3 group and that in their work this electron donation could account for most of the β effect.

We have found[11] that ND_3 is similarly a better electron donor than NH_3. Spectra of chemisorbed CO show one or more strong bands in the 1800–2100-cm^{-1} region which are attributed to C=O stretching vibrations.[12] It is known[12,13] that simultaneous chemisorption of electron-donating species causes a shift in the positions of these bands and a theoretical explanation of these shifts has been given by Blyholder.[14] We found that when CO and NH_3 were coadsorbed on iron or nickel films, the CO bands were shifted in the direction (to lower energy) and by an amount which indicated that the chemisorbed ammonia species were strongly donating electrons to the metal surface. The spectra indicated that the chemisorbed ammonia was undissociated. Similar experiments with ND_3 showed shifts in the same direction but of larger magnitude. The conclusion followed that ND_3 is a better electron donor than NH_3.

Since N_2 is isoelectronic with CO, the same molecular orbital picture which applies to CO also applies to N_2. In this picture the highest partially filled molecular orbital, which is bonding for the metal–adsorbate bond would receive more charge when an electron-donating group is coadsorbed. Desorption of N_2 would therefore be slower from a surface with coadsorbed ND_3 than from one with coadsorbed NH_3. Thus, desorption of N_2 as the slow step in ammonia decomposition would have a β-isotope effect. Furthermore, the β-isotope hypothesis does not require exact knowledge of what the coadsorbed species is, whether ND_3, ND_2, or ND, as long as such species are better electron donors than the corresponding NH_3, NH_2, or NH species.

As Schwab[15] has pointed out, in gas–solid catalysis it is difficult to draw definite conclusions as to the mechanism from the magnitude of the observed isotope effect. Nevertheless, we feel that the explanation we propose brings harmony to isotope and kinetic measurement which had previously appeared to be inconsistent.

Acknowledgment. This investigation was supported in part by Research Grant No. 00818-02 from the Air Pollution Control Office, Environmental Protection Agency. We thank the National Science Foundation for financial support to R. Sheets.

(7) The discussion of primary and secondary isotope effects taken from J. March, "Advanced Organic Chemistry," McGraw-Hill, New York, N. Y., 1968, pp 213–216.

(8) K. T. Leffek, J. A. Lewellyn, and R. E. Robertson, *Can. J. Chem.*, **38**, 2171 (1960).

(9) E. A. Halevi, M. Nussim, and A. Ron, *J. Chem. Soc.*, 866 (1963).

(10) E. A. Halevi and M. Nussim, *ibid.*, 876 (1963).

(11) R. Sheets, Ph.D. Dissertation, University of Arkansas, 1970.

(12) L. H. Little, "Infrared Spectra of Adsorbed Species," Academic Press, New York, N. Y., 1966.

(13) C. R. Guerra, *J. Colloid Interface Sci.*, **29**, 229 (1969).

(14) G. Blyholder, *J. Phys. Chem.*, **68**, 2772 (1964).

(15) G. M. Schwab and A. M. Watsen, *Trans. Faraday Soc.*, **60**, 1833 (1964).

Promoted Adsorption of Pyridine on Nickel[1]

by Ralph W. Sheets and Robert S. Hansen*

Institute for Atomic Research and Department of Chemistry, Iowa State University, Ames, Iowa 50010
(Received August 20, 1971)

Publication costs assisted by Ames Laboratory, U. S. Atomic Energy Commission

Ultraviolet and infrared spectroscopy were used to investigate the adsorption of pyridine on oil-covered nickel films and to study the effects of coadsorbed catalyst poisons. No chemisorption of pyridine was detected on unpoisoned films, but on films previously exposed to oxygen, carbon monoxide, or carbon disulfide, pyridine was coordinately adsorbed. A model for poisoning of metal surfaces by promoted or induced irreversible adsorption of the reactants is presented.

I. Introduction

There are many metal-catalyzed reactions which are severely inhibited by adsorption of oxygen- or sulfur-containing species on the catalyst surface.[2] These species are strongly chemisorbed, and it is thought that they poison the surface by blocking catalytically active sites, thereby preventing adsorption of the reactants.[3] There is, however, evidence that this is not the only method by which poisoning of metal catalyst occurs. An early study by White and Benton[4] established that, although carbon monoxide poisons nickel for hydrogenation, the amount of hydrogen adsorbed on the poisoned nickel catalyst is actually greater than the amount adsorbed on the unpoisoned catalyst. Other investigators have reported reactions in which preadsorption of hydrogen on metal catalysts has promoted adsorption of carbon monoxide[5a] or oxygen[5b] (although in the latter case, "poisoning" by hydrogen increased, rather than inhibited, the catalyzed reaction). Evidence of this sort suggests a second general mechanism in which the poison acts not by preventing adsorption of a reactant, but by inducing irreversible chemisorption of the species. In this case an "induced self-poisoning" occurs.

The present paper reports the investigation of another example of induced adsorption: the promoted adsorption of pyridine on nickel by oxygen, carbon monoxide, or carbon disulfide.

II. Experimental Section

The cell used to obtain both infrared and ultraviolet spectra is shown in Figure 1. The films were prepared by Blyholder's[6] method. This technique consists of evaporating nickel from a resistively heated tungsten filament in the evacuated cell. The metal is deposited in a mineral oil film on the salt windows of the cell. The resulting dispersion of nickel particles in oil transmits ir and uv light well and shows little change in scattering properties over periods of several hours. The oil greatly decreases the rate of sintering and protects the metal from contamination by water from the ambient. Films prepared in this manner are not "clean," and the data obtained are the result of competition among various species for chemisorption sites on the nickel surface.

Cell pressures were maintained below 10^{-6} Torr during evaporation. After evaporation, the gas to be studied was admitted to the cell at a pressure of several Torr for periods of 15 min to 24 hr and then evacuated. Spectra were recorded before and after admission of the gas and after various periods of evacuation. Pumping for 1 hr was adequate to remove all traces of gas phase pyridine from ir spectra, but a period of 6 hr was required to eliminate the uv gas phase bands. All spectra of chemisorbed pyridine reported in this study were recorded after evacuating the cell for at least 18 hr at 10^{-6} Torr.

Use of CaF_2 windows allowed successive uv and ir spectra of the same sample to be recorded. Infrared spectra were recorded on a Perkin-Elmer Model 21 spectrophotometer. Useful spectra over all of the 4000–1000-cm^{-1} region were obtained by placing a cell with oil-covered CaF_2 windows in the reference beam. Ultraviolet spectra were recorded on a Cary Model 12 spectrophotometer in the 210–400-mμ region. Wire screens were used to attenuate the reference beam.

The pyridine was Fisher Certified reagent grade and the carbon disulfide was Baker Analyzed reagent grade. Both were subjected to fractional distillation under vacuum. The carbon monoxide was supplied in a breakseal flask by Air Reduction Co. and was used without further purification. The purity of the nickel wire supplied by Alfa Inorganics was 99.97%.

(1) Work was performed in the Ames Laboratory of the Atomic Energy Commission; Contribution No. 3084.

(2) E. B. Maxted, *Advan. Catal.*, **3**, 129 (1951).

(3) P. G. Ashmore, "Catalysis and Inhibition of Chemical Reactions," Butterworths, London, 1963, p 188.

(4) T. A. White and A. F. Benton, *J. Phys. Chem.*, **35**, 1784 (1931).

(5) (a) G. W. Keulks and A. Ravi, *ibid.*, **74**, 783 (1970); (b) R. L. Goldsmith, M. Modell, and R. F. Baddour, *ibid.*, **75**, 2065 (1971).

(6) G. Blyholder, *J. Chem. Phys.*, **36**, 2036 (1962).

Table I: Infrared Bands (cm^{-1}) for Pyridine Chemisorbed on Poisoned Nickel Films

Py + CO on nickel	Py + CO + O_2 on nickel	Py + O_2 on nickel	Py + CS_2 on nickel	Py + CS_2 + O_2 on nickel	$NiPy_4(NCS)_2$[a]	Liquid Py[b]	Assignment[c]
						3083 vs	20b
~3075 b, m	~3075 b, m	~3075 w	~3075 m, b	~3075 m, b		3054 s	2, 7b, 13
						3036 vs	20a
1605 s	1610 m	1600 s	1600 s	1610 s	1603 s	1580 vs	8a
						1572 m	8b
d	*d*	*d*	*d*	*d*	1488 s	1482 s	19a
1450 s[e]	1450 m[e]				1445 s	1439 vs	19b
d	*d*	*d*	*d*	*d*	1356 vw	1375 m	14
1220 s	1220 m	1220 m	1215 s	1225 s	1215 s	1218 s	3, 9a
1160 s	1160 w	1150 m	1150 s	1160 s	1151 m	1148 s	15
1070 s	1070 m	1075 m	1065 s	1070 s	1068 s	1068 s	18a, 18b
1050 m	1050 m	1050 m	1045 s	1050 s	1043 s	1029 vs	12
2000 vs							CO stretch
1870 vs							CO stretch
	1560 s						Carbonate species
	1330 s						Carbonate species

[a] Reference 9. [b] Reference 12. [c] Numbers denote vibrational modes of pyridine as assigned in ref 12. [d] Region obscured by background oil bands. [e] Appears as shoulder on background oil band.

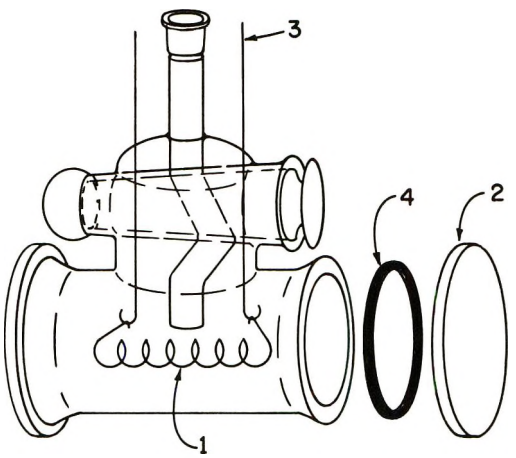

Figure 1. Infrared and ultraviolet cell: 1, filament; 2, CaF_2 window; 3, tungsten lead; 4, "O" ring.

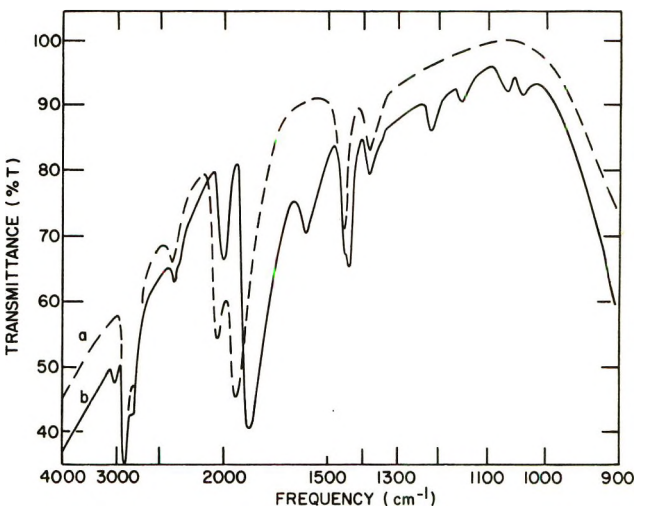

Figure 2. Infrared spectra of pyridine chemisorbed on a CO-poisoned nickel film: a, CO added, evacuated; b, pyridine added, evacuated.

III. Experimental Results

Infrared and ultraviolet spectra of nickel films exposed to pyridine vapor for periods of up to 24 hr showed no bands due to chemisorbed species. Spectra of similar films exposed to carbon monoxide showed the bands at 2080 and 1940 cm^{-1} assigned to chemisorbed CO[7] (Figure 2) but no bands in the uv region. Subsequent exposure of these poisoned films to pyridine vapor for 30 min produced ir spectra typical of coordinately adsorbed pyridine[8] or metal–pyridine complexes[9,10] (Figure 2, Table I). The adsorbed CO bands were shifted 70–80 cm^{-1} toward lower frequencies, indicating the presence of a coadsorbed species which is a strong electron donor.[11] Two bands appeared in the uv region at 255 and 310 mμ (Figure 3b). When these samples were then exposed to air at a pressure of 100 Torr for 15 min, the adsorbed CO species were oxidized to carbonate species, as was shown by the disappearance of the 2000- and 1870-cm^{-1} bands and the appearance of new bands at 1560 and 1330 cm^{-1}.[7] Only minor changes occurred in the positions and intensities of the uv and ir pyridine bands (Figure 3c, Table I).

In the next series of experiments, freshly evaporated nickel films were first exposed to air and then, after

(7) G. Blyholder, "Proceedings of the Third International Congress on Catalysis, Amsterdam, 1964," W. Sachtler, *et al.*, Ed., North-Holland Publishing Co., Amsterdam, 1965.

(8) L. H. Little, "Infrared Spectra of Adsorbed Species," Academic Press, New York, N. Y., 1966, p 193.

(9) F. Herbelin, J. D. Herbelin, J. P. Mathieu, and H. Poulet, *Spectrochim. Acta*, 22, 1515 (1966).

(10) P. C. H. Mitchell, *J. Inorg. Nucl. Chem.*, 21, 382 (1961).

(11) G. Blyholder, *J. Phys. Chem.*, 68, 2772 (1964).

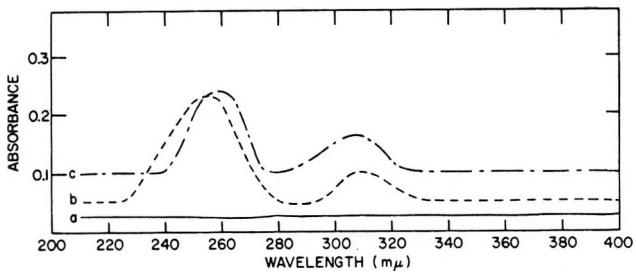

Figure 3. Ultraviolet spectra of pyridine chemisorbed on a CO-poisoned nickel film: a, CO added, evacuated; b, pyridine added, evacuated; c, air added, evacuated.

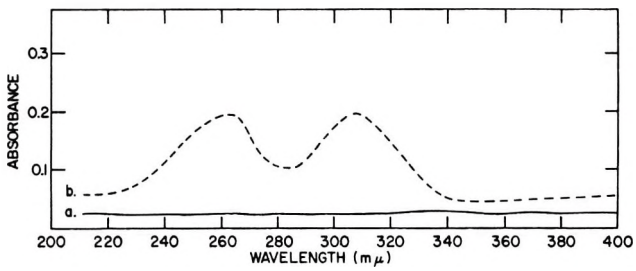

Figure 4. Ultraviolet spectra of pyridine chemisorbed on an oxygen-poisoned nickel film: a, air added, evacuated; b, pyridine added, evacuated.

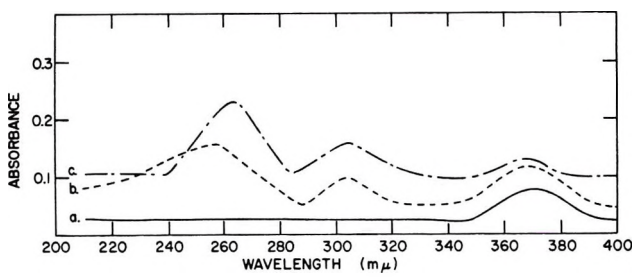

Figure 5. Ultraviolet spectra of pyridine chemisorbed on a CS_2-poisoned nickel film: a, CS_2 added, evacuated; b, pyridine added, evacuated; c, air added, evacuated.

evacuation, to pyridine. The resulting spectra were similar to those obtained with carbon monoxide and pyridine, although no bands due to oxide species were observed (Table I, Figure 4). No spectral changes occurred when these samples were finally exposed to carbon monoxide.

The third series of experiments was carried out in the same manner as the first except that carbon disulfide was used instead of carbon monoxide. Spectra of CS_2 adsorbed alone on nickel had one band at 370 mμ (Figure 5a). Spectra of adsorbed pyridine in the presence of coadsorbed CS_2 were much like those for the two systems described above (Table I, Figure 5b, c).

Finally, freshly evaporated films were exposed to water vapor and subsequently to pyridine. There was no spectral evidence that either substance was chemisorbed.

Table I gives ir frequencies for all of the investigated systems together with corresponding frequencies for a nickel–pyridine complex[10] and for liquid pyridine.[12] Table II shows uv band positions for all chemisorbed species, for a nickel–pyridine complex,[13] and for pyridine vapor.[14] All spectra in Figures 3–5 are difference spectra obtained by subtracting the absorbance of the background spectra of the oil-covered films from that of the apparent spectra observed. The spectra have been displaced along the ordinate for the sake of clarity.

IV. Discussion

A. Infrared Spectra. Infrared spectroscopic studies of pyridine adsorbed on silica gel, alumina, and silica–alumina cracking catalysts[15] and on cation-substituted montmorillonite[16] have demonstrated that changes in absorption in the 1700–1400-cm^{-1} region can be used to distinguish between coordinately bonded pyridine and pyridine bonded to surface hydrogens (pyridinium ion surface complexes). A band in the 1440–1465-cm^{-1} region is characteristic of a coordination surface complex, whereas bands near 1640 and especially 1540 cm^{-1} are indicative of pyridinium ion complexes.[15] Differences in infrared band positions have similarly been used to distinguish between ligand (coordinated) pyridine and the pyridinium cation in metal–pyridine complexes,[10] with bands near 1440 and 1215 cm^{-1} considered due to coordinated pyridine, and bands at 1530 and 1200 cm^{-1} due to pyridinium ion.

The ir spectrum of pyridine adsorbed on a CO-poisoned nickel film (Figure 2) shows bands at 1450 and 1220 cm^{-1}, and no bands in the 1530–1540-cm^{-1} region. Since these are characteristics of pyridine in coordinately bonded pyridine–metal complexes, the ir spectrum provides strong evidence that pyridine is chemisorbed on nickel by coordinate bonding. The spectra of pyridine on oxygen- and CS_2-poisoned films are similar (Table I) indicating that here, too, the molecules are coordinately bonded. Resolution of the 1450-cm^{-1} pyridine band from the strong CH_2 band at 1475 cm^{-1} was practicable on the CO-poisoned surface (see Figure 2) but not on the O_2 and CS_2 poisoned surfaces.

B. Ultraviolet Spectra. In the ultraviolet spectrum of pyridine vapor[14] there is a strong π-π^* band with a maximum at 249.5 mμ (Table II). This band shows considerable vibrational structure. In metal–pyridine complexes the vibrational structure is diminished, and a second band often appears in the 280–420-mμ re-

(12) L. Corrsin, B. J. Fax, and R. C. Lord, *J. Chem. Phys.*, **21**, 1170 (1953). Vibrational modes are denoted by numbers following scheme illustrated in Figure 1 of C. H. Kline, Jr., and J. Turkevich, *ibid.*, **12**, 300 (1944).

(13) E. Koenig and H. L. Schlaefer, *Z. Phys. Chem. (Frankfurt am Main)*, **26**, 371 (1960).

(14) K. Kishi and S. Ikeda, *J. Phys. Chem.*, **73**, 2559 (1969).

(15) E. P. Parry, *J. Catal.*, **2**, 371 (1963).

(16) Yu. I. Tarasevich, V. P. Telichkun, and F. D. Ovcharenko, *Teor. Eksp. Khim.*, **6** (6), 804 (1970).

Table II: Ultraviolet Bands (mμ) for Pyridine Chemisorbed on Poisoned Nickel Films

Py + CO on nickel	Py + CO + O_2 on nickel	Py + O_2 on nickel	Py + CS_2 on nickel	Py + CS_2 + O_2 on nickel	$NiCl_2Py_2$[a]	Py vapor[b]	Assignment
310	310	310	305	305	310[c]		Ni–Py charge-transfer
					280[c]		
					264	260.5	Py 0
					258	254	Py 1
255	260	265	257	262	252	249.5[d]	Py 2
					246	244.5	Py 3
						239	Py 4
			370	370			Sulfur charge-transfer

[a] Reference 12. [b] Reference 14. [c] Assigned in ref 12 as either a pyridine or a Cl charge-transfer band. [d] Most intense peak in band.

gion.[13,17] The latter (charge-transfer) band is caused by transfer of electrons from the metal to antibonding orbitals on the pyridine molecule. Ultraviolet spectra of pyridine adsorbed on various metals, including nickel, were obtained by Kishi and Ikeda[14] in a study of adsorption on bare evaporated films. They reported that in the spectrum of pyridine on nickel, the uv band position was not shifted much from that of pyridine vapor; the band showed well-defined vibrational structure, and its intensity decreased after prolonged evacuation (liquid nitrogen trap). For pyridine on iron, on the other hand, they observed two broad bands at 258 and 297 mμ, neither of which showed vibrational structure. The 297-mμ band was attributed to a charge transfer from the iron to the pyridine. The authors concluded that on iron the pyridine was bonded much as in metal–pyridine complexes, but that the bonding on nickel was weaker.

In the present study all uv spectra of pyridine adsorbed on poisoned nickel films indicate that the pyridine is strongly bonded in molecular form (Figures 3–5). In every case there are two bands which have no vibrational structure, and the band intensities do not decrease after evacuation for 24 hr. After comparing these spectra with those of metal–pyridine complexes[13] we have assigned the 255–265-mμ band to a π-π^* transition of the adsorbed pyridine and the 305–310-mμ band to nickel–pyridine charge transfer (Table II).

C. Promoted Adsorption by Poisoning. If it is supposed that a pyridine molecule reacts with a metal surface primarily by donating electrons to incompletely filled orbitals on the surface, then the ease with which the reaction occurs (and the stability of the bond formed) must decrease as the number of electrons already in these surface orbitals increases. There is, in general, such an increase in electrons on going from left to right across the transition metal series, and this may be used to explain the findings of Kishi and Ikeda[14] that pyridine chemisorbed strongly on Ti and Fe, less strongly on Ni, and not at all on Cu.

For a specific metal, the number of electrons in the unbonded orbitals of a surface atom must decrease upon adsorption of oxidizing, or electron-withdrawing, species on neighboring surface atoms; *i.e.*, the inductive effects are transmitted through the surface, at least over short distances. It should therefore be possible to increase the acid strength of nickel atoms toward pyridine by partially oxidizing the nickel surface.

For the case of oil-covered films, since the reaction between pyridine and nickel is weak to begin with,[14] interactions between the metal and the oil prevent formation of pyridine–nickel surface complexes. (Diffusion of pyridine through the oil cannot be the limiting factor since, with poisoned films, pyridine readily penetrates the oil and reacts with the metal.) Partial oxidation of the nickel with CO, a good electron-withdrawing species, makes the metal atoms stronger Lewis acids and permits reaction with pyridine to occur (Figures 2 and 3). Exposing the CO-poisoned film to air, and thereby removing the chemisorbed carbon monoxide, has little effect on the coadsorbed pyridine because the metal surface adsorbs oxygen, another electron-withdrawing species, during the process (Figure 3). This is shown by the ease with which pyridine chemisorbs on films exposed previously only to air (Figure 4).

After exposure of freshly evaporated nickel films to CS_2 and evacuation, no bands are detected in the ir region.[18,19] This has been interpreted as being due to dissociation of the CS_2 and formation of surface metal sulfides.[19] The cause of the band which appears at 370 mμ after exposure of the nickel film to CS_2 is uncertain, but we tentatively assign it to a charge transfer

(17) H. L. Schlaefer and E. Koenig, *Z. Phys. Chem. (Frankfurt am Main)*, **30**, 145 (1961).

(18) C. W. Garland, *J. Phys. Chem.*, **63**, 1423 (1959).

(19) G. Blyholder and G. W. Cagle, *Environ. Sci. Technol.*, **5**, 158 (1971).

between surface nickel atoms and dissociated sulfide species (Table II). CS_2 has a major uv band at 290–380 mμ (maximum at 320 mμ)[20] in the gas phase, at 260–300 mμ (maximum at 280 mμ) in CCl_4 solution,[21] and at 250–357 mμ (maximum at 330 mμ) in heptane.[22] Uv spectra for NiS appear to be unavailable in the literature. The presence of this electronegative sulfur species increases the acid strength of the nickel so that reaction with pyridine occurs (Figure 5).

Poisoning of the nickel films with electron-donating species should inhibit rather than enhance pyridine adsorption. In trying to chemisorb other Lewis bases, however, one encounters the same difficulties as with pyridine itself. As expected, the attempted poisoning with H_2O did not produce any evidence that the water chemisorbed. Subsequent exposure of the film to pyridine again failed to produce chemisorbed species, although when the film was finally exposed to carbon monoxide, chemisorption of CO readily occurred.

These results suggest a model for catalytic poisoning which may be generally applicable to reactions of Lewis bases. According to this model, inhibition of catalytic reactions involving such bases is due to induced irreversible adsorption of the reactants, caused by inductive effects of the adsorbed poison. This is consistent with the observation[2] that often only small amounts of poison are required to inhibit reactions, since most of the surface sites are blocked, not by the poison, but by the reactant.

Finally, it should be noted that while the poisoning mechanism proposed here is probably quite important on transition metals toward the right of the series (*e.g.*, Ni and Cu), it becomes less important on going to the left across the series (depending on the strength of the base involved). For Ti and V the mechanism probably does not operate at all, simply because on these metals the surface orbitals were already empty to permit stable coordination bonds to be formed.

Acknowledgment. We are grateful to Richard N. Kniseley and George D. Blyholder for their enlightening (R. N. K.) as well as entertaining (G. D. B.) suggestions.

(20) R. S. Mulliken, *J. Chem. Phys.*, **13**, 720 (1935).
(21) N. Slagg and R. A. Marcus, *ibid.*, **34**, 1013 (1961).
(22) E. Treiber, J. Gierer, J. Rehnstrom, and K. E. Almin, *Acta Chem. Scand.*, **11**, 752 (1957).

Influence of Specific Adsorption of Reactant and Product upon Charge-Transfer Processes in Voltammetry. The Tl^{3+}/Tl^{+} Couple in 1 *M* $HClO_4$ on Smooth and Platinized Platinum

by Rolando Guidelli,* Giovanni Pezzatini, and Maria Luisa Foresti

Institute of Analytical Chemistry, University of Florence, Florence, Italy *(Received August 2, 1971)*

Publication costs assisted by Istituto di Chimica Analitica

The voltammetric behavior of thallous and thallic ions in 1 *M* $HClO_4$ on smooth and on variously platinized platinum is investigated. Experimental conditions suitable for a quantitative examination of the voltammetric curves of Tl^{3+} and Tl^{+} are determined. Some conclusions about the mechanism of the overall electrode process $Tl^{3+} + 2e \rightleftharpoons Tl^{+}$ are drawn. Furthermore, the adsorptivities of Tl^{3+} and Tl^{+} on oxide-free smooth platinum and on oxide-covered both smooth and variously platinized platinum are determined from the shift of the half-wave potential of the voltammetric curves of Tl^{3+} and Tl^{+} with a change in the bulk concentration of the reactant.

Introduction

The voltammetric behavior of the Tl^{3+}/Tl^{+} couple on smooth platinum has been investigated by several researchers[1-5] in perchloric as well as in sulfuric acid. Vetter and Thiemke,[1] as well as Catherino and Jordan,[2] drew some conclusions about the mechanism of the overall electrode process $Tl^{3+} + 2e \rightleftharpoons Tl^{+}$ on the basis

(1) K. J. Vetter and G. Thiemke, *Z. Elektrochem.*, **64**, 805 (1960).
(2) H. A. Catherino and J. Jordan, *Talanta*, **11**, 159 (1964).
(3) S. D. James, *Electrochim. Acta*, **12**, 939 (1967).

of an examination of the voltammetric curves of Tl^{3+} and Tl^{+}. Both James[3] and Ulstrup[4] observed that the current–potential curves given by solutions of Tl^{3+} and Tl^{+} in $HClO_4$ are extremely sensitive to electrode pretreatments and exhibit a notable hysteresis when the direction of the potential sweep is inverted. The specific adsorption of thallous ion on smooth platinum from solutions of hydrochloric acid[6,7] and of sulfuric acid[8,9] was studied by several authors both by the radiotracer method and by the galvanostatic transient method.

In the present paper conditions which are suitable to a quantitative examination of the voltammetric curves given by Tl^{3+} and by Tl^{+} in $HClO_4$ both on smooth and variously platinized platinum are first determined; second, from an examination of the voltammetric curves recorded under these conditions, some conclusions are drawn about the mechanism of the electrode process $Tl^{3+} + 2e \rightleftharpoons Tl^{+}$ as well as about the influence exerted on this process by the specific adsorption of Tl^{3+} and Tl^{+}.

Experimental Section

The working electrodes employed in the measurements were prepared by melting the end of a platinum wire (Metalli Preziosi, 99.98% pure) in a hydrogen flame until a small sphere, 2 mm in diameter, was obtained. The hydrogen eventually absorbed into platinum during melting was removed by heating the electrode for about 3 hr at 500° in vacuum and then letting it cool to room temperature, still in vacuum, as suggested by Trasatti.[10] The roughness factor of an electrode so prepared, as measured with the method proposed by Will and Knorr,[11] was about 1.5. The variously platinized electrodes were obtained by electrolyzing freshly prepared smooth platinum electrodes in a 2% solution of chloroplatinic acid in 2 N HCl for differing times at a current density of about 20 mA/cm^2.

The cell employed in the measurements was described by Cozzi and coworkers.[12] In this cell a Teflon-finned piston containing an iron nucleus is moved by a magnet coil at regular intervals of time, causing a rapid laminar flow of the solution around a hemispherical platinum microelectrode. This flow, which reduces the thickness of the diffusion layer around the microelectrode to a value as low as 5×10^{-4} cm, ceases abruptly after about 30 msec (washing period) from its start. The washing period is followed by a much longer period of time (3–9 sec) during which the solution is perfectly still so that the reactant reaches the electrode surface by simple diffusion. Therefore the measured instantaneous current is a potentiostatic current at a stationary spherical electrode. Owing to the periodical renewal of the diffusion layer, once the cell in question is connected with a conventional polarograph a current–potential curve is obtained which is analogous to a polarographic wave, the only difference being represented by the fact that here the average current is recorded at a stationary spherical electrode rather than at a growing drop. The current–potential curves were recorded with a Beckmann TM30 Electroscan, employing the three-electrode system. As reference electrode and as counterelectrode, two saturated mercurous sulfate electrodes were used. Since we noted that impurities of sulfate ions alter the behavior of the voltammetric curves (particularly of the cathodic one), a solution of 1 M $HClO_4$ was interposed between the solution under study and each saturated Hg_2SO_4 electrode. All potentials reported in what follows are referred to the nhe.

The solutions of Tl^{+} were obtained starting from reagent-grade Merck Tl_2CO_3 and BDH Analar $HClO_4$. The solutions of Tl^{3+} were prepared starting from $Tl(OH)_3$ obtained by the method described by Huttig and Mytizek[13] and were titrated iodometrically. Since impurities of chlorides alter the behavior of the voltammetric curves, the precipitate of $Tl(OH)_3$ was purified by dissolving it with $HClO_4$ and precipitating it again with NaOH; this procedure was repeated several times until no visible turbidity was observed after addition of $AgNO_3$. Triply distilled water was employed, the first two distillations having been performed from alkaline permanganate. The solutions in the electrolysis cell were deaerated with nitrogen 99.999% pure.

In order to obtain reproducible data it was found necessary to pretreat the electrode before each single recording. The pretreatments, consisting in evolving hydrogen either at controlled current or at controlled potential for a given period of time (in order to obtain an oxide-free electrode) or in evolving oxygen (in order to obtain an oxide-covered electrode), revealed themselves unsatisfactory. The irreproducible results obtained by the above drastic pretreatments are largely due to a rapid increase in the electrode roughness factor, which has a remarkable effect upon the rate of the charge-transfer process $Tl^{3+} + 2e \rightleftharpoons Tl^{+}$. Thus 4 or 5 pretreatments consisting in evolving hydrogen on the electrode surface are sufficient to increase the roughness factor from the initial value 1.5 to a value of about 2. For the above reasons, in order to obtain an oxide-free electrode we used a milder pretreatment, which consists

(4) J. Ulstrup, *Electrochim. Acta*, **13**, 535 (1968).

(5) D. Cozzi and G. Raspi, *Atti Soc. Toscana Sci. Nat. Pisa, Proc. Verbali Mem., Ser. A*, **70**, 131 (1963).

(6) B. J. Bowles, *Electrochim. Acta*, **10**, 717 (1965).

(7) B. J. Bowles, *ibid.*, **10**, 731 (1965).

(8) G. N. Mansurov, N. A. Balashova, and V. E. Kazarinov, *Elektrokhimiya*, **4**, 641 (1968).

(9) G. N. Mansurov and N. A. Balashova, *ibid.*, **2**, 1358 (1966).

(10) S. Trasatti, *Electrochim. Metal.*, **1**, 267 (1966).

(11) F. G. Will and C. A. Knorr, *Z. Elektrochem.*, **64**, 258 (1960).

(12) D. Cozzi, G. Raspi, and L. Nucci, *J. Electroanal. Chem.*, **12**, 36 (1966).

(13) G. F. Huttig and R. Mytizek, *Z. Anorg. Allgem. Chem.*, **192**, 187 (1930).

in applying a potential varying linearly from 0.300 V to 1.300 V and *vice versa* with a frequency of 0.05 Hz for 3 min to the electrode immersed in the electrolysis cell. The pretreatment was arrested at 0.300 V and immediately after the cathodic curve was recorded from 0.300 V toward more positive potentials. Analogously, the anodic curves on smooth oxide-covered platinum were obtained by applying a potential varying linearly from 0.85 V to 1.85 V and *vice versa* with a frequency of 0.05 Hz for 3 min to the electrode immersed in the electrolysis cell, arresting the pretreatment at 1.85 V, and proceeding immediately after to the recording of the anodic curve toward less positive potentials. The variously platinized electrodes were submitted to an analogous anodic pretreatment; the only difference was that the value of the positive extreme of the potential range chosen for the pretreatment was decreased with an increase in the platinization, in order that the current density at such an extreme should not exceed 4 mA/cm^2.

In order to avoid appreciable changes in the electrode roughness factor during the recordings, each single series of recordings was carried out within one day starting from a freshly prepared electrode and ascertaining that the value for the roughness factor of this electrode at the end of the series was equal to the initial value. Whenever recording cathodic curves on smooth prereduced platinum, the potential sweep-rate was kept above a certain limit (100–150 mV per min) in order to avoid the incipient surface oxidation of the electrode during the recording of the lower portion of these curves.

Results

The potential range enclosing both the cathodic curve of Tl^{3+} to Tl^+ and the anodic curve of Tl^+ to Tl^{3+} on smooth platinum is too wide for the state of the platinum surface to remain unchanged within this range (see Figure 1). Thus, starting with a prereduced electrode and shifting the applied potential toward more positive values, the surface oxidation of platinum begins at about +0.900 V and proceeds gradually up to oxygen evolution. This is clearly shown in curve a of Figure 2, given by 1 *M* $HClO_4$ alone on platinized platinum with a roughness factor of 8 (it should be noted that the voltammogram given by the supporting electrolyte alone does not change its shape appreciably with an increase of the roughness factor of platinum, but simply increases in height). Conversely, if we start with a preoxidized electrode and we proceed toward less positive potentials, the electroreduction of the surface oxide takes place in a relatively narrow potential range (0.900–0.600 V), revealing itself by the appearance of a cathodic peak at about +0.700 V. This peak is clearly shown in curve a of Figure 3, given by 1 *M* $HClO_4$ on platinized platinum with a roughness factor of 8.

The voltammogram given by a solution of 10^{-3} *M* Tl^{3+} and 10^{-3} *M* Tl^+ in 1 *M* $HClO_4$ on smooth platinum starting with a prereduced electrode and proceeding toward more positive potentials is shown in Figure 1, curve a. The cathodic curve develops entirely at an oxide-free electrode and therefore can be analyzed quantitatively. Conversely, the anodic curve develops at an electrode which is undergoing simultaneous progressive surface oxidation. Consequently, the anodic curve recorded under such experimental conditions cannot be profitably analyzed. Among other things, the cathodic limiting current of the voltam-

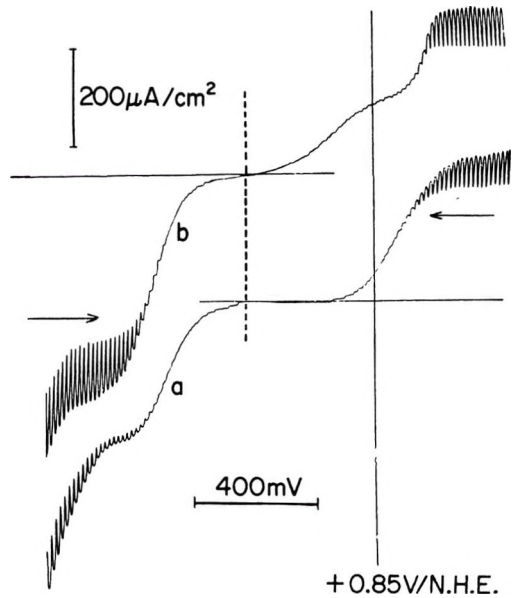

Figure 1. Voltammograms of 10^{-3} *M* Tl^+ + 10^{-3} *M* Tl^{3+} in 1 *M* $HClO_4$ on smooth platinum. Curve a was recorded starting with a prereduced electrode and proceeding toward more positive potentials. Curve b was recorded starting with a preoxidized electrode and proceeding toward less positive potentials. The dashed vertical line refers to the standard potential of the Tl^{3+}/Tl^+ system.

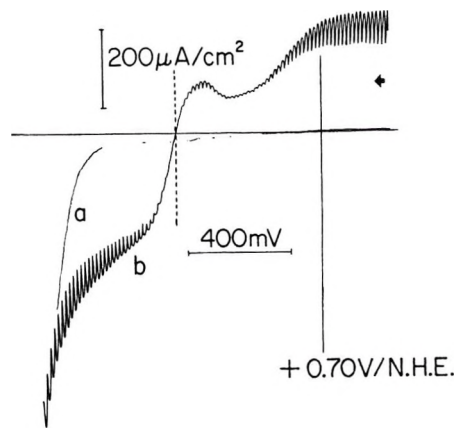

Figure 2. Voltammograms of 1 *M* $HClO_4$ alone (curve a) and of 10^{-3} *M* Tl^+ + 10^{-3} *M* Tl^{3+} in 1 *M* $HClO_4$ (curve b) on platinized platinum with a roughness factor of 8, as obtained starting with a prereduced electrode and proceeding toward more positive potentials. The dashed vertical line refers to the standard potential of the Tl^{3+}/Tl^+ system.

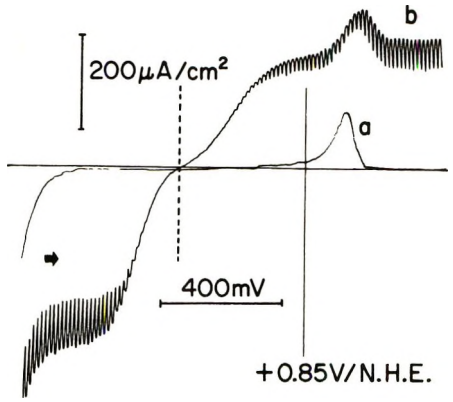

Figure 3. Voltammograms of 1 M $HClO_4$ alone (curve a) and of 10^{-3} M Tl^+ + 10^{-3} M Tl^{3+} in 1 M $HClO_4$ (curve b) on platinized platinum with a roughness factor of 8, as obtained starting with a preoxidized electrode and proceeding toward less positive potentials. The dashed vertical line refers to the standard potential of the Tl^{3+}/Tl^+ system.

mogram in Figure 1 is diffusion-controlled, whereas the anodic limiting current of the same voltammogram is not. In fact an oscillographic examination of the instantaneous potentiostatic current at the cathodic plateau shows that this current obeys the Cottrell equation corrected for sphericity, whereas this is not the case for the instantaneous current at the anodic plateau. A different situation is encountered whenever we record the voltammogram of the same solution of Tl^{3+} and Tl^+ starting with a preoxidized electrode and proceeding toward less positive potentials (curve b in Figure 1). In this case the anodic curve develops at an electrode covered by a stable layer of surface oxides and its limiting current is diffusion-controlled. Conversely the cathodic curve splits into two partial waves, only the second of which is diffusion-controlled. The first cathodic wave was also observed by James,[3] who refers to it as to a "prewave." Its rising portion develops at an oxide-covered electrode but its ill-defined limiting current falls within the potential range in which the surface layer of platinum oxides is reduced.

The standard potential of the Tl^{3+}/Tl^+ couple is about equal to 1.260 V[14] and therefore is much closer to the rising portion of the anodic curve at an oxide-covered electrode (voltammogram b in Figure 1) than to the rising portion of the cathodic curve at an oxide-free electrode (voltammogram a in Figure 1). This observation suggests that the rate for the electrode process $Tl^{3+} + 2e \rightleftharpoons Tl^+$ is greater at an oxide-covered than at an oxide-free platinum electrode. This conclusion is further supported by the peculiar shape of voltammogram b of Figure 1. Here the point of zero current coincides to a good approximation with the standard potential of the Tl^{3+}/Tl^+ couple; in addition, the rising portion of the anodic curve and that of the cathodic prewave (both developing at an oxide-covered electrode) are practically antisymmetrical with respect to such a point, apart from the difference in their heights. In this respect the plateau of the cathodic prewave can be regarded as having originated from the mutual compensation of two conflicting tendencies: they are, on the one hand, the natural tendency to an increase in the reduction current of Tl^{3+} as a consequence of a decrease in the applied potential, and, on the other hand, the tendency to a decrease in the same cathodic current following the gradual reduction of platinum surface oxides and the consequent decrease in the exchange current for the cathodic process $Tl^{3+} + 2e \rightarrow Tl^+$. The second cathodic partial wave develops on an electrode almost completely free from oxides. From the above it is evident that in the voltammogram b of Figure 1 only the anodic curve can be analyzed quantitatively.

The preceding qualitative considerations are confirmed by the voltammetric behavior of the Tl^{3+}/Tl^+ system on variously platinized platinum electrodes. With an increase in the roughness factor of platinum the voltammogram of 10^{-3} M Tl^+ + 10^{-3} M Tl^{3+}, as recorded toward less positive potentials starting with a preoxidized electrode, undergoes the following changes with respect to voltammogram b of Figure 1: (a) the anodic curve shifts gradually toward less positive potentials approaching the standard potential; (b) the cathodic prewave shifts toward more positive potentials, at the same time increasing in height, the more the greater is the distance of its rising portion from the reduction peak of platinum oxides (see for instance voltammogram b of Figure 3, recorded at an electrode with a roughness factor of 8). The preceding behavior indicates that the rate for the $Tl^{3+} + 2e \rightarrow Tl^+$ reaction at an oxide-covered electrode increases remarkably as the roughness factor of platinum is increased. In practice, even for a roughness factor as low as 8, the cathodic prewave reaches a height quite close to that of the corresponding diffusion limiting current, which in voltammogram b of Figure 3 is actually attained at potentials more cathodic than those corresponding to the reduction peak of platinum oxides. In practice on preoxidized platinized platinum with a roughness factor of 36 a solution of 10^{-3} M Tl^{3+} and 10^{-3} M Tl^+ already yields a cathanodic curve which intersects the zero-current axis at the standard potential and which develops entirely at an oxide-covered electrode.

As the roughness factor of platinum is gradually increased the voltammogram of 10^{-3} M Tl^{3+} + 10^{-3} M Tl^+, as recorded toward more positive potentials starting with a prereduced electrode, undergoes the following changes with respect to voltammogram a of Figure 1. The cathodic curve shifts gradually toward more positive potentials, showing that the exchange current for the $Tl^{3+} + 2e \rightarrow Tl^+$ reaction also increases on oxide-free platinum. As soon as the above shift brings the

(14) M. S. Sherrill and J. Haar, Jr., *J. Amer. Chem. Soc.*, 58, 952 (1936).

rising portion of the cathodic curve to potentials at which a detectable oxidation of the electrode surface starts to take place (~+1.00 V; see for instance curves a and b in Figure 2), the cathodic current ceases to decrease with increasing potential and begins to increase, exhibiting a minimum. Subsequently the current falls rapidly in the proximity of the standard potential intersecting the residual current at this potential. The rise in the cathodic current occurring at the potential of incipient oxidation of the electrode surface must be attributed to the increase in the exchange current for the $Tl^{3+} + 2e \rightarrow Tl^{+}$ reaction following the gradual surface oxidation of platinum. Incidentally, in the following we will show that the adsorptivity of thallic ion is greater on oxide-covered than on oxide-free platinum. Quite probably the increase in the surface concentration of Tl^{3+} accompanying the progressive surface oxidation of platinum as we proceed toward more positive potentials contributes in causing the relatively rapid increase in the cathodic current shown in curve b of Figure 2. Obviously, when the standard potential of the Tl^{3+}/Tl^{+} couple is closely approached, the anodic component of the current, which is due to the electrooxidation of thallous ion, starts to become appreciable and the current decreases again, becoming zero at the standard potential. As the roughness factor of platinum is increased beyond 8, the potential at which the cathodic current starts to decrease perceptibly with respect to its diffusion limiting value continues shifting toward more positive values; consequently, the minimum in the cathodic current increases so as to disappear almost completely for roughness factors higher than 12.

In conclusion, upon recording the voltammogram of 10^{-3} *M* $Tl^{3+} + 10^{-3}$ *M* Tl^{+} toward more positive potentials on variously platinized platinum, either the whole or part of the cathodic curve, as well as the whole anodic curve, develop at an electrode undergoing a gradual surface oxidation. Likewise, the cathodic curve recorded on platinized platinum starting with a preoxidized electrode develops at an electrode on which electroreduction of surface platinum oxides is in progress. Hence only the anodic curve recorded toward less positive potentials starting with a preoxidized electrode (see curve b in Figure 3) can be examined quantitatively on platinized platinum.

Voltammetric curves similar to those in Figures 2 and 3 were obtained by James[3] at an apparently smooth platinum electrode. Since curves of similar shape were obtained by us even on platinum electrodes having roughness factors appreciably lower than 8 (*e.g.*, 2.5) and since a smooth electrode submitted to an excessive number of pretreatments increases appreciably its roughness factor, it is probable that the electrode employed by James had a roughness factor higher than 1.5. It must be noted that the conclusions drawn by James are opposite to ours. In fact he assumes that

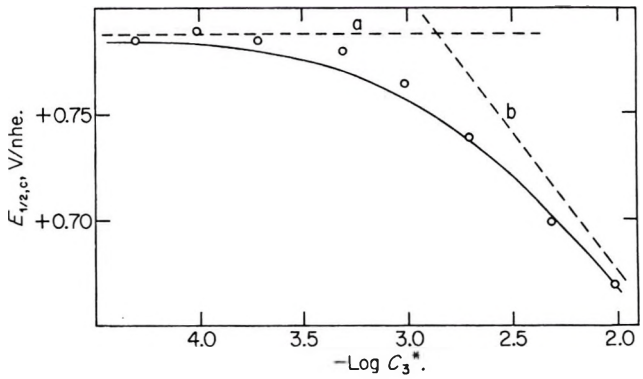

Figure 4. Plot of the half-wave potential $E_{1/2,c}$ for the cathodic curve of Tl^{3+} on smooth prereduced platinum against log C_3^*. The small circles denote experimental values, whereas the solid curve expresses the theoretical behavior. The broken lines a and b express the asymptotic behavior of $E_{1/2,c}$ at low and high values of log C_3^*, respectively.

the process $Tl^{3+} + 2e \rightleftharpoons Tl^{+}$ occurs more rapidly on oxide-free than on oxide-covered platinum.

In the present paper we will examine from a quantitative point of view the irreversible cathodic curve of Tl^{3+} on oxide-free prereduced smooth platinum as well as the anodic curve of Tl^{+} on both smooth and platinized oxide-covered preoxidized platinum. When using platinized platinum, in order to simplify the interpretation of data, we will confine ourselves to the examination of the voltammograms recorded on electrodes with roughness factors sufficiently low (ρ = 1.5–31) to yield totally irreversible anodic curves.

The cathodic curve recorded on prereduced smooth platinum exhibits a particular behavior with increasing the bulk concentration of Tl^{3+}, C_3^*. For concentrations less than 5×10^{-4} *M* the half-wave potential remains constant (see Figure 4); furthermore a plot of log $[\bar{i}_c/(\bar{i}_{c,d} - \bar{i}_c)]$ against the applied potential E (where $\bar{i}_c$ is the mean cathodic current at the potential E and $\bar{i}_{c,d}$ the corresponding mean diffusion limiting current) is linear along the whole rising portion of the curve and exhibits a reciprocal slope of −130 mV. Upon increasing C_3^* above 5×10^{-4} *M* the half-wave potential $E_{1/2,c}$ of the cathodic curve tends to shift toward less positive values, at first slowly and subsequently more rapidly. Accompanying the shift of $E_{1/2,c}$ the slope of the cathodic curve increases. Thus the value of $E_{1/4} - E_{3/4}$, which for $C_3^* = 5 \times 10^{-5}$ *M* is about equal to 125 mV, becomes 72 mV when C_3^* is increased to 10^{-2} *M*. Figure 5 shows two cathodic curves, recorded at different sensitivities; curve a is given by a 10^{-4} *M* solution and curve b by a 10^{-2} *M* solution of Tl^{3+}. Furthermore, Figure 6 shows the ratio $\bar{i}_c/\bar{i}_{c,d}$ of the mean cathodic current $\bar{i}_c$ at a given potential E to the corresponding mean diffusion limiting current $\bar{i}_{c,d}$ as a function of E for three different concentrations of Tl^{3+}. The presence of Tl^{+} in concentrations as high as 10^{-1} *M* does not alter either the shape or the position of the

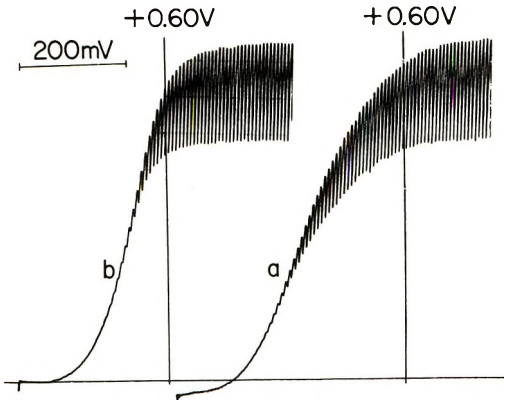

Figure 5. Cathodic voltammograms of 10^{-4} M Tl^{3+} (curve a) and of 10^{-2} M Tl^{3+} (curve b) in 1 M $HClO_4$ on smooth prereduced platinum. The vertical lines on each curve refer to +0.60 V. The sensitivity at which curve a was recorded is $^1/_{100}$ of the sensitivity at which curve b was recorded.

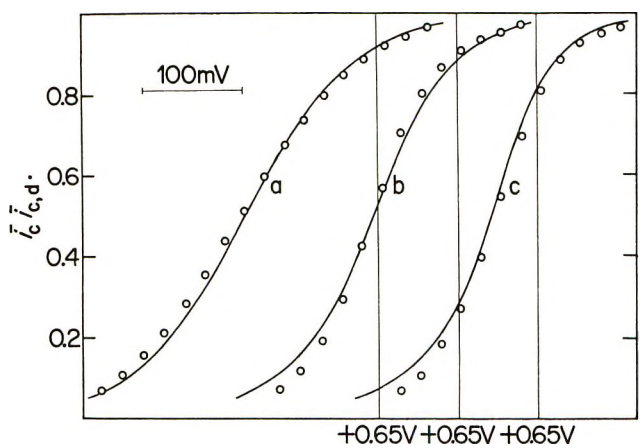

Figure 6. Plot of $\bar{i}_c/\bar{i}_{c,d}$ against E as obtained from the cathodic voltammograms of 5×10^{-5} M Tl^{3+} (curve a), 2×10^{-3} M Tl^{3+} (curve b), and 5×10^{-3} M Tl^{3+} (curve c) in 1 M $HClO_4$ on smooth prereduced platinum. The small circles denote experimental values whereas the solid curves denote the theoretical behavior as expressed by eq 12 and 14. The vertical lines on each curve refer to +0.65 V.

cathodic curve furnished by a given solution of Tl^{3+} on smooth prereduced platinum.

The anodic curve of Tl^+ on smooth preoxidized platinum shifts toward more positive potentials with an increase in the bulk concentration C_1^* of thallous ions. In this latter case the shift in the half-wave potential, $E_{1/2,a}$, is already appreciable at the lowest experimentally accessible concentrations of Tl^+. This is clearly shown in curve a of Figure 7, which reports $E_{1/2,a}$ against the common logarithm of C_1^*. For 10^{-5} $M \leq C_1 \leq 10^{-2}$ M the plot of $E_{1/2,a}$ *vs.* log C_1^* is linear with a slope of 110 mV. The slope of the anodic curve on preoxidized smooth platinum, expressed by an $E_{3/4} - E_{1/4}$ value of about 105 mV, does not change appreciably with a change of C_1^* and therefore of $E_{1/2,a}$, as opposed to what observed with the cathodic curve. Furthermore, the plot of log $[\bar{i}_a/(\bar{i}_{a,d} - \bar{i}_a)]$ *vs.* the applied potential

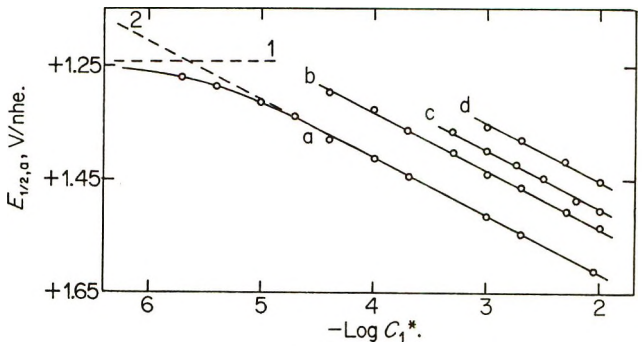

Figure 7. Plot of the half-wave potential $E_{1/2,a}$ for the anodic curve of Tl^+ on smooth preoxidized platinum (curve a) and on platinized preoxidized platinum with a roughness factor of 7 (curve b), 14 (curve c) and 31 (curve d) against log C_1^*. The broken lines 1 and 2 express the asymptotic behavior of $E_{1/2,a}$ on smooth platinum at low and high values of log C_1^*, respectively.

E (where $\bar{i}_a$ is the mean anodic current at the potential E and $\bar{i}_{a,d}$ the corresponding mean diffusion limiting current) is linear and exhibits a reciprocal slope of about 110 mV at all the concentrations of Tl^+ investigated. If we add to a solution of Tl^+ of a given concentration C_1^* a comparable amount of Tl^{3+}, then the half-wave potential of the anodic curve shifts appreciably toward more positive values.

The anodic curve furnished by a Tl^+ solution of a given concentration on variously platinized preoxidized platinum shifts toward decreasing overpotentials with an increase in the roughness factor of platinum as a consequence of the increased exchange current density. Nevertheless, for a given roughness factor, the anodic curve shifts toward more positive potentials with an increase in the bulk concentration of Tl^+, C_1^*, analogously to what is observed on smooth platinum. Curves b, c, and d of Figure 7 show the linear variation of $E_{1/2,a}$ with log C_1^* on platinized platinum of roughness factor 7, 14, and 31, respectively. As the electrode roughness is increased, the minimum value of C_1^* for which the anodic curve is still totally irreversible also increases. In Figure 7 such a minimum value, for each roughness factor, is expressed by the lowest C_1^* value for which the experimental value of $E_{1/2,a}$ is reported.

Discussion and Conclusions

Mechanism of the Overall Electrode Process $Tl^{3+} + 2e \rightleftharpoons Tl^+$. On the basis of a theoretical treatment formulated by one of us in a preceding paper,[15] we can state, prior to further discussion, that the shift in the half-wave potential both of the anodic curve on preoxidized platinum (Figure 7) and of the cathodic curve on prereduced platinum (Figure 4) is due to the influence of the specific adsorption of the reactant and the product of electrolysis. A detailed quantitative examination of this shift will be carried out in the following sec-

(15) R. Guidelli, *J. Phys. Chem.*, **74**, 95 (1970).

tion. Here we simply note that at the low concentrations of Tl^{3+} for which the cathodic curve on prereduced platinum maintains a constant half-wave potential (see Figure 4), the influence of the specific adsorption of Tl^{3+} and Tl^{+} may be considered to be negligible. An examination of the cathodic curve at these low concentrations may give some useful information about the mechanism of the electroreduction of Tl^{3+} to Tl^{+}. Although the anodic curve on smooth preoxidized platinum is affected by adsorption of both reactant and product up the lowest accessible concentrations of Tl^{+}, we can state, again prior to further discussion, that its shape is not appreciably altered by such an adsorption. Hence the plot of log $[\bar{\imath}_a/(\bar{\imath}_{a,d} - \bar{\imath}_a)]$ *vs.* E may be usefully employed in order to draw some conclusions about the mechanism of the electrooxidation of Tl^{+} to Tl^{3+}.

The most plausible mechanisms by which the overall electrode process $Tl^{3+} + 2e \rightleftharpoons Tl^{+}$ may proceed are

Mechanism a

$$Tl^{3+} + 2e \rightleftharpoons Tl^{+} \qquad (1)$$

Mechanism b

$$\begin{cases} Tl^{3+} + e \rightleftharpoons Tl^{2+} & (2) \\ Tl^{2+} + e \rightleftharpoons Tl^{+} & (3) \end{cases}$$

Mechanism c

$$\begin{cases} Tl^{3+} + e \longrightarrow Tl^{2+} \\ 2Tl^{2+} \longrightarrow Tl^{3+} + Tl^{+} \end{cases} \left.\begin{matrix} (2) \\ (4) \end{matrix}\right\} \text{toward reduction}$$

$$\begin{cases} Tl^{+} \longrightarrow Tl^{2+} + e \\ 2Tl^{2+} \longrightarrow Tl^{3+} + Tl^{+} \end{cases} \left.\begin{matrix} (3) \\ (4) \end{matrix}\right\} \text{toward oxidation}$$

Mechanism a predicts the simultaneous uptake of two electrons by Tl^{3+} and therefore is rather improbable. Mechanism c predicts a second-order homogeneous disproportionation of Tl^{2+} into Tl^{3+} and Tl^{+}. Whether the overall electrode reaction $Tl^{3+} + 2e \rightleftharpoons Tl^{+}$ proceeds through mechanism a, b, or else through mechanism c in which the charge-transfer step is regarded as the rate-determining one, the plot of log $[\bar{\imath}/(\bar{\imath}_d - \bar{\imath})]$ *vs.* E, as obtained from the cathodic curve as well as from the anodic one, is expected to be linear (see ref 16 and eq 18 in the present paper). The slope of such a plot should be equal to $-(\alpha_{o\rightarrow r}F)/2.3RT$ for the cathodic curve and to $+(\alpha_{r\rightarrow o}F)/2.3RT$ for the anodic one, where the charge-transfer coefficients $\alpha_{o\rightarrow r}$ and $\alpha_{r\rightarrow o}$ are given by

$$\alpha_{o\rightarrow r} = \frac{n_{o\rightarrow r}}{\nu_{o\rightarrow r}} + n'_{o\rightarrow r}\beta_{o\rightarrow r}$$

$$\alpha_{r\rightarrow o} = \frac{n_{r\rightarrow o}}{\nu_{r\rightarrow o}} + n'_{r\rightarrow o}\beta_{r\rightarrow o} \qquad (5)$$

In eq 5 the subscripts o→r and r→o indicate the direction in which the overall electrode process $Tl^{3+} + 2e \rightleftharpoons Tl^{+}$ proceeds; n is the number of electrons preceding the rate-determining stage, n' is the number of electrons involved in the rate-determining stage, and ν and β are the stoichiometric number and the symmetry factor for such a stage. Table I summarizes the values of n, n', ν, and α both in the direction toward oxidation and in that toward reduction for the various mechanisms, under the reasonable assumption that the β value is close to 0.5. The experimental plots of log $[\bar{\imath}/(\bar{\imath}_d - \bar{\imath})]$ *vs.* E are linear both for the cathodic and for anodic curves. The values of $\alpha_{o\rightarrow r}$ and $\alpha_{r\rightarrow o}$ as obtained from these plots are, respectively, equal to 0.45 and 0.54. We must therefore conclude that the rate-determining step in the electroreduction of Tl^{3+} to Tl^{+} is expressed by eq 2 whereas the rate-determining step in the electrooxidation of Tl^{+} to Tl^{3+} is expressed by eq 3. From the table it is manifest that it is impossible to establish whether the step following the charge-transfer step (2) in the electroreduction process (or the charge-transfer step (3) in the electrooxidation process) is represented by the disproportionation of Tl^{2+} as predicted by mechanism c or by a further elementary charge-transfer step, as predicted by mechanism b.

Table I

Mechanism	Toward reduction $n_{o\rightarrow r}$	$n'_{o\rightarrow r}$	$\nu_{o\rightarrow r}$	$\alpha_{o\rightarrow r}$	Toward oxidation $n_{r\rightarrow o}$	$n'_{r\rightarrow o}$	$\nu_{r\rightarrow o}$	$\alpha_{r\rightarrow o}$
a	0	2	1	~1	0	2	1	~1
b [the r.d.s. is expressed by eq 2]	0	1	1	~0.5	1	1	1	~1.5
b [the r.d.s. is expressed by eq 3]	1	1	1	~1.5	0	1	1	~0.5
c (the charge-transfer step is the rate determining one)	0	1	1	~0.5	0	1	1	~0.5

Similar conclusions were drawn by Vetter and Thiemke[1] in sulfuric acid, notwithstanding the fact that they do not take mechanism c into account. It should be noted that these authors do not base their conclusions on the values of $\alpha_{o\rightarrow r}$ and $\alpha_{r\rightarrow o}$, but rather on the observation that the value of the exchange current density for the process $Tl^{3+} + 2e \rightleftharpoons Tl^{+}$, as obtained by extrapolating the cathodic Tafel line to the equilibrium potential, is appreciably different from, and in fact, less than the value of the exchange current density as obtained from the anodic Tafel line. Since it is quite probable that even in sulfuric acid the cathodic curve develops on an oxide-free electrode and the anodic curve on an oxide-covered electrode, the difference between the two values for the exchange current density, as observed by Vetter and Thiemke, could be

simply attributed to this phenomenon and consequently it does not represent a valuable criterion for the determination of the mechanism of the electrode process under study. Completely different conclusions were drawn by Catherino and Jordan,[2] according to whom the experimental behavior of the voltammetric curves of Tl^{3+} and Tl^{+} in 1 M $HClO_4$ confirms "in a conclusive way" the validity of mechanism c. The above authors base their conclusions on the observation that the formal potential of the Tl^{3+}/Tl^{+} couple falls at a point along the rising portion of the anodic curve rather than in the zero-current region included between the anodic and cathodic curves. As a matter of fact this experimental observation was confirmed neither by us nor by the various other authors who worked on this subject. Quite probably the data of Catherino and Jordan were distorted by the presence in the solution of traces of chloride ion, as was observed by James.[3] On the other hand, the phenomenological treatment of mechanism c reported by Catherino and Jordan is not correct. In fact the net current I is considered to be the resultant of a cathodic component I_+, due to the unidirectional reduction of Tl^{3+} to Tl^{2+} (eq 40, ref 2) and of an anodic component I_-, due to the unidirectional oxidation of Tl^{+} to Tl^{2+} (eq 41, ref 2), without accounting for the fate of the Tl^{2+} ions produced irreversibly by these two component currents. In fact the steady-state condition for the concentration of Tl^{2+} ions, expressed by eq 42 of ref 2, is not at all employed in the derivation of the final expression for the current–potential characteristic (eq 43 of ref 2) employed by Catherino and Jordan.

Influence of the Adsorption of Tl^{+} and Tl^{3+} upon the Voltammetric Curves of these Species. After having drawn some conclusions about the mechanism of the electrode process $Tl^{3+} + 2e \rightleftharpoons Tl^{+}$, let us consider the influence of the specific adsorption both of Tl^{3+} and of Tl^{+} upon such a process. In ref 15 one of us derived an approximate expression of the current–potential characteristic for the general process $O + ne \rightleftharpoons R$, in which both O and R are specifically adsorbed according to Langmuirian isotherms. In the present case the current–potential characteristic for the cathodic curve is derivable from the simple equations (*cf.* eq 27 of ref 15)

$$\frac{\bar{i}_c}{2F} = l(C_3^* - \bar{C}_3) = l(\bar{C}_1 - C_1^*) \tag{6}$$

and

$$\frac{\bar{i}_c}{2F} = \frac{Ak^\circ_{o\rightarrow r}\bar{C}_3\vartheta^{-\alpha_{o\rightarrow r}}}{1 + K_{3,r}\bar{C}_3 + K_{1,r}\bar{C}_1} \tag{7}$$

provided the electroreduction is totally irreversible. Analogously, the current–potential characteristic for the anodic curve is given by the equations

$$\frac{\bar{i}_a}{2F} = l(\bar{C}_1 - C_1^*) = l(C_3^* - \bar{C}_3) \tag{8}$$

and

$$\frac{\bar{i}_a}{2F} = -\frac{Ak^\circ_{r\rightarrow o}\bar{C}_1\vartheta^{\alpha_{r\rightarrow o}}}{1 + K_{3,o}\bar{C}_3 + K_{1,o}\bar{C}_1} \tag{9}$$

provided the electrooxidation is totally irreversible. In eq 6–9 $\bar{C}_3$ and $\bar{C}_1$ are the volume concentrations of Tl^{3+} and Tl^{+} at the electrode surface, whereas $K_{3,r}$, $K_{1,r}$ and $K_{3,o}$, $K_{1,o}$ are the corresponding adsorption coefficients on a "prereduced" and a "preoxidized" electrode, respectively. The parameter ϑ is defined by the equation

$$\vartheta = \exp\left[\frac{F}{RT}(E - E_o)\right] \tag{10}$$

where E_o is an arbitrary reference potential; $\alpha_{o\rightarrow r}$ and $\alpha_{r\rightarrow o}$ are the charge-transfer coefficients relative to the electrode process proceeding toward reduction and oxidation, respectively, and are defined in eq 5; $k^\circ_{o\rightarrow r}$ and $k^\circ_{r\rightarrow o}$ are the rate constants of step 2 and step 3, respectively, and are referred to potential E_o; A is the geometric area of the electrode; l is a parameter which depends on the mode of mass transport of the species Tl^{3+} and Tl^{+} toward the electrode. For spherical diffusion we have

$$l = A\left(\frac{2D^{1/2}}{\pi^{1/2}t_1^{1/2}} + \frac{D}{r_o}\right) \tag{11}$$

where D is the diffusion coefficient, considered to be equal for the species Tl^{3+} and Tl^{+}, t_1 is the period of electrolysis, and r_o is the radius of the stationary spherical electrode. In writing eq 6–9 it has been assumed that the surface concentration of the unstable intermediate Tl^{2+} is negligible with respect to those of Tl^{+} and Tl^{3+} at all potentials investigated. In view of eq 6 the cathodic mean diffusion limiting current, $\bar{i}_{c,d}$, for which the condition $\bar{C}_3 = 0$ holds, is given by

$$\bar{i}_{c,d} = 2FlC_3^* \tag{12}$$

Analogously the anodic mean diffusion limiting current, $\bar{i}_{a,d}$, for which the condition $\bar{C}_1 = 0$ holds, is given by

$$\bar{i}_{a,d} = -2FlC_1^* \tag{13}$$

Upon suitably combining eq 6, 7, 10, and 12 we immediately obtain the following $\bar{i}_c - E$ characteristic

$$E = E_o - \frac{RT}{\alpha_{o\rightarrow r}F}\ln \times \frac{\bar{i}_c\left[\frac{\bar{i}_c}{F}(K_{1,r} - K_{3,r}) + 2l(1 + K_{3,r}C_3^* + K_{1,r}C_1^*)\right]}{2Ak^\circ_{o\rightarrow r}(\bar{i}_{c,d} - \bar{i}_c)} \tag{14}$$

Analogously, from eq 8, 9, 10, and 13 the following relation between the anodic mean current $\bar{i}_a$ and the potential E is obtained

$$E = E_o + \frac{RT}{\alpha_{r\rightarrow o}F} \ln \times \frac{\bar{i}_a\left[\frac{\bar{i}_a}{F}(K_{1,o} - K_{3,o}) + 2l(1 + K_{3,o}C_3^* + K_{1,o}C_1^*)\right]}{2Ak^\circ_{r\rightarrow o}(\bar{i}_{a,d} - \bar{i}_a)} \quad (15)$$

The degree of accuracy of the approximate eq 14 and 15 is satisfactory, as was shown by comparing the $\bar{i}$–E characteristics derived from these equations with those obtained through a rigorous numerical procedure.[16,17] In the case of validity of the inequality

$$K_{3,r}C_3^* + K_{1,r}C_1^* \ll 1 \quad (16)$$

we also have

$$\frac{\bar{i}_c|K_{1,r} - K_{3,r}|}{2Fl} < \frac{\bar{i}_{c,d}|K_{1,r} - K_{3,r}|}{2Fl} =$$

$$C_3^*|K_{1,r} - K_{3,r}| \ll 1 \quad (17)$$

and consequently eq 14 for the cathodic curve simplifies as follows

$$E = E_o - \frac{RT}{\alpha_{o\rightarrow r}F} \ln \frac{l}{Ak^\circ_{o\rightarrow r}} - \frac{RT}{\alpha_{o\rightarrow r}F} \ln \frac{\bar{i}_c}{\bar{i}_{c,d} - \bar{i}_c} \quad (18)$$

This equation is the well-known current–potential characteristic for a totally irreversible cathodic curve uncomplicated by adsorption phenomena. We have previously seen that eq 18 is actually verified on smooth prereduced platinum for values of log $C_3^* \leq -3.5$ and that from the experimental value of $\Delta E/\Delta \log [\bar{i}_c/(\bar{i}_{c,d} - \bar{i}_c)] = -130$ mV the value 0.45 is obtained for the charge-transfer coefficient $\alpha_{o\rightarrow r}$.

As log C_3^* is increased above -3.5 the unequalities 16 and 17 are no longer valid and the specific adsorption of Tl^{3+} and Tl^+ starts to affect the shape and the position of the theoretical cathodic characteristic through the occurrence of two phenomena, namely: (a) a shift of $E_{1/2,c}$ toward less positive values according to the equation

$$E_{1/2,c} = E_o - \frac{RT}{\alpha_{r\rightarrow o}F} \ln \frac{l}{Ak^\circ_{o\rightarrow r}} - \frac{RT}{\alpha_{o\rightarrow r}F} \ln \times \left[1 + \frac{K_{1,r} + K_{3,r}}{2}C_3^* + K_{1,r}C_1^*\right] \quad (19)$$

which is immediately obtained from eq 14 upon setting $\bar{i}_c = \bar{i}_{c,d}/2 = FlC_3^*$; (b) a gradual change in the slope of the cathodic curve according to the equation

$$E_{1/4,c} - E_{3/4,c} = \frac{RT}{\alpha_{o\rightarrow r}F} \ln 9 + \frac{RT}{\alpha_{o\rightarrow r}F} \ln \times \frac{1 + K_{1,r}C_1^* + \left(\frac{K_{3,r}}{4} + \frac{3}{4}K_{1,r}\right)C_3^*}{1 + K_{1,r}C_1^* + \left(\frac{3}{4}K_{3,r} + \frac{K_{1,r}}{4}\right)C_3^*} \quad (20)$$

which is easily derivable from eq 14 by setting alternatively $\bar{i}_c = 3\bar{i}_{c,d}/4$ and $\bar{i}_c = \bar{i}_{c,d}/4$. Both preceding theoretical predictions have been verified experimentally. The shift of $E_{1/2,c}$ with an increase in log C_3^* is shown in Figure 4, in which the circles express experimental values and the solid curve expresses the theoretical behavior. The fitting of the theoretical and the experimental $E_{1/2,c}$ – log C_3^* curves has been realized quite simply by plotting the function

$$E_{1/2,c} = a - \frac{2.3RT}{\alpha_{o\rightarrow r}F} \log (1 + x) \quad (21)$$

against log x; in the expression (21) $\alpha_{o\rightarrow r}$ is given the experimental value 0.45 whereas $a \equiv E_o - RT/\alpha_{o\rightarrow r}F \ln l/(Ak^\circ_{o\rightarrow r})$ is given the experimental value of the half-wave potential of the cathodic curve at the low thallic ion concentrations at which adsorption is not felt. We then slide this plot over an experimental $E_{1/2,c}$ *vs.* log C_3^* plot characterized by a log C_3^* scale unit identical with that of log x, until we obtain the best overlap. Under these conditions the intersection point $P \equiv (E_{1/2,c} = a, x = 1)$ between the two straight lines $E_{1/2,c} = a$ and $E_{1/2,c} = a - 2.3RT/\alpha_{o\rightarrow r}F \log x$ (the broken lines a and b in Figure 4), which express the two asymptotic behaviors of $E_{1/2,c} = f(x)$ for low and high values of x, respectively, is such that its projection on the log C_3^* axis equals

$$\log C_3^{*\prime} = \log \frac{2}{K_{3,r} + K_{1,r}} \quad (22)$$

Equation 22 is immediately obtained by comparing equations 19 and 21, in which equations C_1^* is set equal to zero and x equal to 1. From Figure 4 it appears that $C_3^{*\prime} = 1.4 \times 10^{-3}$ M, so that $K_{1,r} + K_{3,r} = 1.4 \times 10^3$ l./mol. Since the addition of an excess of Tl^+ to a solution of Tl^{3+} does not appreciably alter either the form or the position of the cathodic curve, then we must conclude in view of eq 19 that $K_{1,r}$ is much less than $K_{3,r}$ and consequently that the adsorptivity of Tl^{3+} is much greater than that of Tl^+. Hence in practice on smooth prereduced platinum $K_{3,r}$ equals 1.4×10^3 l./mol. The change in the slope of the cathodic curve with an increase in C_3^*, predicted by eq 20, is also verified experimentally, as appears from Figure 6. In this figure the circles denote the experimental cathodic voltammograms relative to three different concentrations of Tl^{3+}, whereas the solid curves express the corresponding theoretical characteristics as derived from eq 12 and 14 upon setting $\alpha_{o\rightarrow r} = 0.45$, $E_o - RT/(\alpha_{o\rightarrow r}F) \ln l/(Ak^\circ_{o\rightarrow r}) = 0.79$ V, $K_{3,r} = 1.4 \times 10^3$ l./mol, $K_{1,r} = 0$ and $l/A = 1.73 \times 10^{-3}$ cm/sec. This latter value has been obtained from eq 11 upon noting that under the present experimental conditions we have $r_o = 0.1$ cm,

(16) J. Heyrovsky and J. Kuta, "Principles of Polarography," Academic Press, New York, N. Y., 1966, pp 208–217.

(17) R. Guidelli, *Electroanal. Chem.*, **33**, 303 (1971).

$t_1 = 3.7$ sec, and $D \cong 8 \times 10^{-6}$ cm²/sec. If we neglect $K_{1,r}$ with respect to $K_{3,r}$, then from eq 20 it follows that for $C_3^* = 10^{-2}$ M and $K_{3,r} = 1.4 \times 10^3$ l./mol the quantity $E_{1/4,c} - E_{3/4,c}$ equals 76 mV. This theoretical value is in good agreement with the experimental value of 72 mV.

From eq 13 and 15 it immediately follows that the half-wave potential $E_{1/2,a}$ for the anodic curve is given by the equation

$$E_{1/2,a} = E_o + \frac{RT}{\alpha_{r\to o}F} \ln \frac{l}{Ak^\circ_{r\to o}} + \frac{RT}{\alpha_{r\to o}F} \ln \times \left[1 + K_{3,o}C_3^* + \frac{K_{1,o} + K_{3,o}}{2} C_1^*\right] \quad (23)$$

In practice the half-wave potential $E_{1/2,a}$ of the anodic curve given by Tl^+ solutions of progressively increasing concentrations on smooth preoxidized platinum already shifts toward more positive values at the lowest experimentally accessible concentrations (see curve a in Figure 7), so that the $E_{1/2,a}$ *vs.* log C_1^* plot already attains a limiting slope of 110 mV for $C_1^* > 10^{-5}$ M. In light of eq 23 this limiting slope equals $2.3RT/\alpha_{r\to o}F$, so that $\alpha_{r\to o} = 0.54$. The experimental plot of $E_{1/2,a}$ *vs.* log C_1^*, denoted by circles, shows a slight curvature for log $C_1^* < 10^{-5}$ M; the theoretical plot of $E_{1/2,a}$ against log C_1^* is expressed by the solid curve a. The fitting of the theoretical $E_{1/2,a}$ *vs.* log C_1^* plot to the experimental one has been realized as usual by plotting the function $E_{1/2,a} \equiv b + 2.3RT/\alpha_{r\to o}F \log (1 + x)$, in which $\alpha_{r\to o}$ is set equal to 0.54 and b is given an arbitrary value, against x. Upon overlapping in the best way this latter plot on an experimental $E_{1/2,a}$ *vs.* log C_1^* plot having the same scale units as the $E_{1/2,a} = E_{1/2,a}(x)$ plot both on the abscisses and on the ordinates, it is possible to attribute the value 1.24 V to the parameter b, which expresses the half-wave potential $E_{1/2,a}$ in the absence of adsorption phenomena. The intercept of the two dashed lines 1 and 2 of Figure 7, which express the two asymptotic behaviors of $E_{1/2,a} = E_{1/2,a}(x)$, is such that its projection, log $C_1^{*\prime}$, on the log C_1^*-axis yields

$$C_1^{*\prime} = \frac{2}{K_{3,o} + K_{1,o}} = 2.4 \times 10^{-6}\ M \quad (24)$$

Some properties of the anodic curve of Tl^+ on smooth preoxidized platinum indicate that the adsorptivities of Tl^+ and Tl^{3+} are comparable on this type of electrode. Thus the experimental plot of log $[\bar{i}_a/(\bar{i}_{a,d} - \bar{i}_a)]$ *vs.* E is linear at all the concentrations investigated and, apart from a progressive shift toward more positive potentials with an increase in C_1^*, its reciprocal slope $\Delta E/\Delta \log [\bar{i}_a/(\bar{i}_{a,d} - \bar{i}_a)]$ remains equal to 105 mV. This behavior can be justified by the assumption that $K_{1,o} \cong K_{3,o}$. In fact in this case the equation for the anodic characteristic [eq 15] assumes the form

$$E = E_o + \frac{RT}{\alpha_{r\to o}F} \ln \frac{l(1 + K_{3,o}C_3^* + K_{1,o}C_1^*)}{Ak^\circ_{r\to o}} + \frac{RT}{\alpha_{r\to o}F} \ln \frac{\bar{i}_a}{\bar{i}_{a,d} - \bar{i}_a} \quad (25)$$

which predicts the linearity of the E *vs.* log $[\bar{i}_a/(\bar{i}_{a,d} - \bar{i}_a)]$ plot. According to eq 25 the slope of this plot equals $2.3RT/\alpha_{r\to o}F$. The $\alpha_{r\to o}$ value derived from the slope of the log $[\bar{i}_a/(\bar{i}_{a,d} - \bar{i}_a)]$ *vs.* E plot ($\alpha_{r\to o} = 0.54$) coincides with the value obtained independently from the slope of the $E_{1/2,a}$ *vs.* log C_1^* plot. The substantial validity of eq 25 explains why in the preceding section we were in a condition to correctly use the slope of the experimental log $[\bar{i}_a/(\bar{i}_{a,d} - \bar{i}_a)]$ *vs.* E plot for the computation of $\alpha_{r\to o}$ without having to worry about adsorption phenomena. The most direct evidence that the values of $K_{3,o}$ and $K_{1,o}$ are comparable is furnished by the experimental observation that the addition to a given solution of Tl^+ ions of a comparable quantity of Tl^{3+} ions causes an appreciable shift of the anodic curve toward more positive potentials. In view of eq 23 the difference $\Delta E_{1/2,a}$ between the half-wave potentials of the anodic curves furnished respectively by a Tl^+ solution of concentration C_1^* and by a solution containing Tl^+ of concentration C_1^* and Tl^{3+} of concentration C_3^* is given by

$$\Delta E_{1/2,a} = \frac{2.3RT}{\alpha_{r\to o}F} \log \left[1 + \frac{2}{1 + K_{1,o}/K_{3,o}} \frac{C_3^*}{C_1^*}\right] \quad (26)$$

provided the inequality $K_{3,o}C_3^* + [(K_{3,o} + K_{1,o})/2] \cdot C_1^* \gg 1$ holds. In practice this inequality is satisfactorily valid for $C_3^* > 10^{-5}$ M. For $C_3^* = C_1^* = 10^{-4}$ M and $K_{1,o} = K_{3,o}$, eq 26 yields a $\Delta E_{1/2,a}$ value equal to 32 mV. The experimental value of $\Delta E_{1/2,a}$ is about 30 mV, thus confirming the approximate equality of $K_{1,o}$ and $K_{3,o}$. In view of eq 24 we therefore have: $K_{1,o} \cong K_{3,o} \cong 4 \times 10^5$ l./mol. It should be noted that on account of the scarse accuracy with which the $C_1^{*\prime}$ value is determined (see curve a of Figure 7), only the order of magnitude values of $K_{1,o}$ and $K_{3,o}$ is certain.

The anodic curves on variously platinized preoxidized platinum yield linear plots of log $[\bar{i}_a/(\bar{i}_{a,d} - \bar{i}_a)]$ against E with reciprocal slopes of about 110 mV, just as on smooth platinum. Furthermore, for all roughness factors investigated, the plot of $E_{1/2,a}$ *vs.* log C_1^* is linear, with a slope identical with that encountered on smooth platinum (see curves b, c, and d of Figure 7). The change $\Delta E_{1/2,a}$ in the half-wave potential of the anodic curve following the addition of a given amount of Tl^{3+} to a given solution of Tl^+ is practically the same both on smooth and on variously platinized platinum. In view of eq 26 it follows that the ratio $K_{1,o}/K_{3,o}$ is practically independent of the roughness factor ρ.

It is of interest to determine the dependence of the rate constant $k^\circ_{o\to r}$ of eq 9 upon ρ. The rate constant $k^\circ_{r\to o}$ is defined by the equation (see ref 15)

$$k^\circ_{r\to o} = k^\circ \Gamma_m K_{1,o} \quad (27)$$

where Γ_m is the maximum surface concentration of Tl^+ in mol/cm² and the parameter k° is a proportionality constant relating the current i_a/A per unit of the geometric area to the surface concentration Γ_1 of Tl^+

$$\frac{i_a}{A} = -2Fk^\circ \vartheta^{\alpha_{r\to o}} \Gamma_1 \quad (28)$$

Taking into account the procedure employed for the determination of the roughness factor ρ, it is reasonable to assume that Γ_m is proportional to ρ. It is of interest to ascertain whether k° depends on ρ or not. In fact, if k° is independent of ρ, then the increase of $k^\circ_{r\to o}$ with ρ is exclusively determined by an increase in Γ_m, and hence in the number of the adsorption sites available for the charge-transfer process. Conversely, if k° depends on ρ, then we must conclude that platinization causes the adsorption sites not only to increase in number but also to change their nature, at least as far as their influence on the charge-transfer step is concerned.

In view of eq 23 and 27, the half-wave potential $E_{1/2,a}$ of the anodic curve furnished by a Tl^+ solution of a given concentration $C_1^* > 10^{-5}$ M not containing Tl^{3+} can be expressed under the form

$$E_{1/2,a} = E_o + \frac{RT}{\alpha_{r\to o}F} \ln \frac{l}{A\Gamma_m} - \frac{RT}{\alpha_{r\to o}F} \ln k^\circ + \frac{RT}{\alpha_{r\to o}F} \ln \left[\left(1 + \frac{K_{3,o}}{K_{1,o}} \right) \frac{C_1^*}{2} \right]$$

In writing the above equation we have considered that for $C_1^* > 10^{-5}$ M the inequality $(K_{1,o} + K_{3,o})C_1^*/2 \gg 1$ is experimentally satisfied. Since $K_{3,o}/K_{1,o}$ is experimentally independent of ρ, a plot of $E_{1/2,a}$ against $-\log \rho \equiv -\log \Gamma_m +$ constant should exhibit a slope

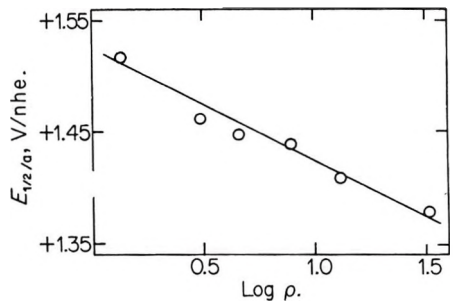

Figure 8. Plot of the half-wave potential, $E_{1/2,a}$, for the anodic curve of 10^{-3} M Tl^+ in 1 M $HClO_4$ on differently platinized platinum electrodes against the common logarithm of the roughness factor, log ρ.

$2.3RT/(\alpha_{r\to o}F) = 110$ mV if k° is also independent of ρ. This is actually verified in practice, as shown in Figure 8. We must therefore conclude that the change in the adsorption sites following platinization is of a quantitative rather than of a qualitative nature. The above conclusions may probably be extended to several other electrode processes taking place on platinized platinum.

In the polarographic literature[18-21] many redox systems are known which yield irreversible waves shifting toward increasing overpotentials with an increase in the reactant concentration. Consequently the method for the determination of the entity of adsorption of electroactive substances herein applied to the Tl^{3+}/Tl^+ system and based on a quantitative analysis of such a shift is amenable to several other useful applications.

(18) B. Nygård, *Ark. Kemi*, **20**, 163 (1962).

(19) M. Fedoronko and H. Berg, *Z. Phys. Chem. (Leipzig)*, **220**, 120 (1962).

(20) M. Fedoronko and H. Berg, *Chem. Zvesti*, **16**, 28 (1962).

(21) S. G. Mairanovskii and Ya. P. Stradyn', *Izv. Akad. Nauk SSSR, Otd. Khim. Nauk*, **12**, 2239 (1961).

Competitive Electron-Scavenging Experiments in the Radiolysis of Hydrocarbons. Kinetics of the Reactions of Secondary Ions[1]

by Pierre P. Infelta and Robert H. Schuler*

Radiation Research Laboratories, Center for Special Studies and Department of Chemistry, Mellon Institute of Science, Carnegie-Mellon University, Pittsburgh, Pennsylvania 15213 *(Received November 5, 1971)*

Publication costs assisted by Carnegie-Mellon University and the U. S. Atomic Energy Commission

A detailed kinetic treatment of the effect of secondary electron transfer reactions in the irradiation of hydrocarbon solutions containing two electron scavengers is given. It is shown that the possible extent of secondary reactions is limited by the short lifetime of most of the geminate ion pairs. Expressions are developed to describe the concentration dependence of product formation in two solute systems, and these expressions are applied to competitive studies using CH_3Br or CH_3Cl as indicator solutes. Results are presented on binary systems containing SF_6, N_2O, or CO_2 from which the reactivities of these solutes toward electrons are obtained. In competition between CH_3Cl and each of these solutes the methyl radical yield is found to be lower than expected, presumably as the result of the removal of metastable CH_3Cl^- radical anions by electron transfer processes. Analysis of the results indicates that the lifetime of this anion is $\sim 3 \times 10^{-8}$ sec. Methyl bromide behaves very nearly ideally in competition with both SF_6 and N_2O as a result of a low transfer rate and/or rapid autodissociation of the radical anion. In competition with CO_2, however, spuriously high methyl radical yields are observed. Because of this, considerable caution is indicated in the interpretation of results from competitive studies with methyl bromide.

In many cases[2-10] it has been found possible to describe the concentration dependence for ionic processes which occur in the radiolysis of liquid hydrocarbon solutions in terms of a function of the type

$$G(\mathrm{P})_S = \left[G_{fi} + G_{gi}\frac{\sqrt{\alpha[\mathrm{S}]}}{1+\sqrt{\alpha[\mathrm{S}]}}\right]\epsilon \qquad \text{(I)}$$

In eq I $G(\mathrm{P})_S$ is the yield of product P produced with an efficiency ϵ as a result of ionic reactions which occur with the solute at concentration [S]. G_{fi} and G_{gi} are, respectively, the yields of free and geminate pairs of ions and α is a constant which describes the competition between scavenging of one of the ions and recombination of the geminate pairs (see Rzad, *et al.*,[11] for a detailed description of the physical and kinetic significance of G_{fi}, G_{gi}, and α). In certain cases, where the parameters of eq I can be evaluated directly from measurements of $G(\mathrm{P})_S$, it is possible to predict the effects of solutes on other processes. Thus in cyclohexane, measurements of the methyl radical yields from methyl bromide solutions have allowed a prediction of the way in which the hydrogen[12] and cyclohexyl radical[13] yields are influenced by the addition of methyl bromide. With a knowledge of the relative values of α the effects of various other electron-scavenging solutes can also be predicted. In fact, since eq I appears to hold for both electron and positive ion scavengers,[4] the effects of even these two different types of solutes can be interrelated.[4,12,13]

Values for the parameter α are not always available from direct measurements on the formation of product from the various solutes so that it is desirable to explore the possibility of using competitive methods to determine appropriate values of α. The present studies were carried out in an attempt to determine α for SF_6, N_2O, and CO_2 by examining the influence of these solutes on the methyl radical yield from methyl bromide or chloride solutions. Competitive studies of ionic processes have, in fact, been carried out previously by a number of investigators,[14-16] but quantitative treatment of the data was difficult until the recent development of an algebraic description of the scavenging

(1) Supported in part by the U. S. Atomic Energy Commission.

(2) J. M. Warman, K.-D. Asmus, and R. H. Schuler, *J. Phys. Chem.*, **73**, 931 (1969).

(3) J. M. Warman and S. J. Rzad, *J. Chem. Phys.*, **49**, 2861 (1968); *ibid.*, **52**, 485 (1970).

(4) S. J. Rzad, R. H. Schuler, and A. Hummel, *ibid.*, **51**, 1369 (1969).

(5) G. Bakale and H. A. Gillis, *J. Phys. Chem.*, **73**, 2178 (1969).

(6) R. R. Hentz and W. V. Sherman, *ibid.*, **73**, 2676 (1969).

(7) R. R. Hentz and H. P. Lehmann, *ibid.*, **73**, 4283 (1969).

(8) N. H. Sagert and T. A. Reid, *Can. J. Chem.*, **48**, 2429 (1970).

(9) T. Kimua, K. Fueki, and Z. Kuri, *Bull. Chem. Soc. Jap.*, **43**, 3090 (1970).

(10) K.-D. Asmus, *Int. J. Radiat. Phys. Chem.*, **3**, 419 (1971).

(11) S. J. Rzad, P. P. Infelta, J. M. Warman, and R. H. Schuler, *J. Chem. Phys.*, **52**, 3971 (1970).

(12) K.-D. Asmus, J. M. Warman, and R. H. Schuler, *J. Phys. Chem.*, **74**, 246 (1970).

(13) K. M. Bansal and R. H. Schuler, *ibid.*, **74**, 3924 (1970).

(14) W. V. Sherman, *J. Chem. Soc. A*, 599 (1966).

(15) R. J. Hagemann and H. A. Schwarz, *J. Phys. Chem.*, **71**, 2694 (1967).

(16) L. A. Rajbenbach, *J. Amer. Chem. Soc.*, **88**, 4275 (1966).

process. A detailed treatment is now possible and the initial study in which eq I was proposed[2] also included a test of the validity of a competitive approach. There is reason to believe from this previous study[2] that in certain cases secondary ionic reactions interfere with simple interpretation of the results from two solute systems. The present results similarly indicate that such competitive experiments should be used with considerable discretion in any attempt to determine the electron-scavenging coefficient for a particular solute.

Experimental Section

In general the approach used here is to examine the reduction in the yield of product from an indicator solute produced by the addition of a second solute. In an idealized system where complicating secondary reactions do not occur, this reduction should be directly interpretable in terms of reaction of the electrons with the second solute.[2] In all cases cyclohexane was used as the solvent, and methyl bromide and methyl chloride were used at concentrations of 0.01–0.3 M as the indicator solutes. The yields of methyl radicals produced by irradiation with doses $\sim 3 \times 10^{17}$ eV/cm^3 were determined by trapping them with radioiodine present at a concentration of $\sim 10^{-3}$ M and separating the resultant radiomethyl iodide gas chromatographically. The product methyl iodide concentrations were $\sim 10^{-5}$ M. The experimental procedures used were identical with those described previously.[2] The gaseous solutes were measured volumetrically and added to the outgassed solutions of radioiodine on a vacuum line. After sealing, the sample tubes had a vapor space of $<10\%$ so that very little of the added solute was present in the vapor phase. All studies were carried out at room temperature.

The equations derived in this type of study are frequently very complicated algebraic expressions which cannot be put into a form in which the parameters can be evaluated directly. The best approach seems to be to evaluate the expressions in the form of the experimental results, *i.e.*, G *vs.* solute concentration, and make a direct comparison with experiment. This was conveniently done, and the effects of the parameters were examined in detail by plotting concentration dependences with a Hewlett-Packard 9100 calculator-plotter. For purposes of plotting the results, the measurements were made at concentrations of the indicator solute near the nominal values indicated in the figures and slight corrections for any departures made by multiplying the observed yields by the ratio of the yields calculated from eq XIII at the nominal and real concentrations. This correction was insensitive to the choice of parameters and never more than a few per cent.

The radiomethyl iodide fraction usually contained $\sim$10,000 counts so that the inherent error in this type of measurement is of the order of 1%. The reproducibility was only slightly poorer than this, and the root-mean-square deviation of the G values between the measured yields and those calculated from eq I was $\sim$0.04 or 2–3%.[2] Similar agreement should be expected for proper treatment of the data from multisolute systems.

Kinetic Considerations of Ion Scavenging in Two Solute Systems

It was previously indicated[2] that from eq I it is expected when two solutes S_1 and S_2 are present in a hydrocarbon system the total yield of scavenging should be given by

$$G(P_1)_{S_2} + G(P_2)_{S_1} = G_{fi} + G_{gi}\frac{\sqrt{\alpha_1[S_1] + \alpha_2[S_2]}}{1 + \sqrt{\alpha_1[S_1] + \alpha_2[S_2]}} \quad \text{(II)}$$

In eq II $G(P_1)_{S_2}$ and $G(P_2)_{S_1}$ are the yields of products from S_1 and S_2 (each assumed to be produced with unit efficiency) as affected by the presence of the other solute. This expression allows one to take into account the increased fraction of geminate ions which are scavenged when a second solute is added to a given system. If no secondary reactions occur, the partial yield from S_1 should be given by

$$G(P_1)_{S_1} = \frac{\alpha_1[S_1]}{\alpha_1[S_1] + \alpha_2[S_2]} \times \left[G_{fi} + G_{gi}\frac{\sqrt{\alpha_1[S_1] + \alpha_2[S_2]}}{1 + \sqrt{\alpha_1[S_1] + \alpha_2[S_2]}}\right] \quad \text{(III)}$$

and similarly for $G(P_2)_{S_1}$ by $\alpha_2[S_2]/(\alpha_1[S_1] + \alpha_2[S_2])$ times the total yield.

Equation I has not, as yet, been derived from first principles but merely represents a very good empirical correlation of the experimental data, a correlation which is accurate to within the experimental errors involved in the measurements. There is, at the moment, no basis to believe that eq I is exact and similarly eq II and III and the other equations derived here are very probably only close approximations to the real situation. It should be noted, however, that the form of the scavenging dependence carries through the various transformations involved in the integrations discussed below and is reflected in the final expressions. The fact that one is using an empirical expression to describe the results in no way invalidates the qualitative aspects of the conclusions, and the quantitative aspects should be accurate to the extent that eq I is accurate. In practice all of the yields calculated here are based on $G_{fi} = 0.12$, $G_{gi} = 3.80$, $\epsilon = 1$, α values for CH_3Cl and CH_3Br of 5.41 and 16.2 M^{-1}, respectively,[2] and appropriate values for the other parameters as described below.

Equation III was originally written on the assumption that the reactivities $\alpha_1[S_1]$ of the individual com-

ponents are additive. Detailed considerations of eq I show that α_1 must indeed be proportional to the rate constant for reaction of the electrons with the individual components[11] so that this assumption is, in fact, required by the model and eq III is a direct consequence of eq I. While the result is obvious, it is useful to carry out a rigorous derivation of eq III since it provides a model for the more complex situations involving secondary reactions.

The partition of the free ion yield between the two reactants can, of course, be treated readily by standard kinetic methods and gives the term involving G_{fi} in eq III. For the contribution of the scavenging of the geminate ions we will consider the scheme

$$RH \rightsquigarrow [RH^+ + e^-] \quad (1)$$

$$[RH^+ + e^-] \xrightarrow{\lambda} RH \quad (2)$$

$$e^- + S_1 \xrightarrow{k_1} S_1^- \longrightarrow P_1 \quad (3)$$

$$e^- + S_2 \xrightarrow{k_2} S_2^- \longrightarrow P_2 \quad (4)$$

where the brackets indicate that if scavenging does not interfere, recombination of the initial electron-positive ion pair will occur. In this scheme products P_1 and P_2 can be produced either by autodissociation of the source anions or as a result of the charge neutralization process. At this point the detailed mechanism is unimportant, and it matters only that products P_1 and P_2 ultimately are produced with unit efficiency as a result of electron scavenging by the respective solutes.

For an electron that has a lifetime t, the probability that reaction will occur with solute S_1 in the absence of other solutes is obtained by integrating the normalized rate of reaction at time t' over the electron's lifetime, *i.e.*, $\int_0^t k_1[S_1]e^{-k_1[S_1]t'}dt' = 1 - e^{-k_1[S_1]t}$. When a second solute S_2 is added, the rate of reaction at time t' is modified by the probability $e^{-k_2[S_2]t'}$ that it will have escaped reaction with the additional solute. In this case

$$\int_0^t k_1[S_1]e^{-k_1[S_1]t'}e^{-k_2[S_2]t'}dt' = \frac{k_1[S_1]}{k_1[S_1] + k_2[S_2]}(1 - e^{-(k_1[S_1]+k_2[S_2])t})$$

The fraction of the electrons which react with S_1 in the presence of S_2 is obtained by integrating this probability over the lifetime distribution of the electrons.

$$F(P_1)_{S_2} = \frac{k_1[S_1]}{k_1[S_1] + k_2[S_2]} \times \int_0^\infty f_e(t)_0(1 - e^{-(k_1[S_1]+k_2[S_2])t})dt \quad (IV)$$

The appropriate lifetime distribution function $f_e(t)_0$ is that for electrons in the hydrocarbon containing no scavengers. Since $\int_0^\infty f_e(t)_0 = 1$, eq IV becomes

$$F(P_1)_{S_2} = \frac{k_1[S_1]}{k_1[S_1] + k_2[S_2]} \times \left[1 - \int_0^\infty f_e(t)_0 e^{-(k_1[S_1]+k_2[S_2])t}dt\right] \quad (V)$$

The integral in eq V is a Laplace transform which can be evaluated from the form of the observed concentration dependence for scavenging, *i.e.*

$$\int_0^\infty f_e(t)_0 e^{-k[S]t}dt = \frac{1}{1 + \sqrt{\frac{k}{\lambda}}[S]} \quad (VI)$$

where λ is a frequency characteristic of the ion-recombination process (see ref 11). In the present case the coefficient of t in eq VI is $k_1[S_1] + k_2[S_2]$ so that the fractional reaction is given by

$$F(P_1)_{S_2} = \frac{k_1[S_1]}{k_1[S_1] + k_2[S_2]} \times \left[1 - \frac{1}{1 + \sqrt{\frac{1}{\lambda}}(k_1[S_1] + k_2[S_2])}\right] \quad (VII)$$

If we now substitute $\alpha_i = k_i/\lambda$, then eq VII reduces to eq III. It should be noted that since the form of the integral of eq VI is known from the observed scavenging dependence, it has not been necessary to give an explicit expression for $f_e(t)_0$ nor to evaluate λ.

In principle, if eq III holds, the parameter α_2 can be determined from a measurement of the yield of product P_1 from the two solute system. The applicability of eq II and III was tested in the previous study[2] for the solute pairs CH_3Br–C_2H_5Br and CH_3Cl–C_2H_5Br where both products P_1 and P_2 (methyl and ethyl radicals, respectively) were measurable. In this case the competitive situation is completely definable in terms of parameters independently measured in the single solute systems. In both of these cases the total yields were found to be described very well by eq II. In the case of the CH_3Br–C_2H_5Br system the individual yields of methyl and ethyl radicals were also described quite reasonably by eq III although the methyl yields tended to be slightly lower and the ethyl yields slightly higher than expected, particularly at the higher solute concentrations. In the case of CH_3Cl–C_2H_5Br a very significant departure in this same direction occurred. As was pointed out previously,[2] the measured values of $(G(C_2H_5)/[C_2H_5Br])/(G(CH_3)/[CH_3Cl])$ (which should be equal to $\alpha_{C_2H_5Br}/\alpha_{CH_3Cl}$) are all higher than the ratio of 1.45 expected from the results on the individual solutes. The values of this ratio are, in fact, not constant so that no one set of the α parameters can explain all of the data and reactions over and above those in-

cluded in scheme 1–4 must be important. Effectively the ethyl bromide appears to be reacting with more than its share of the electrons. It is difficult to see how the low yields of methyl radicals can result from some process other than a removal by chemical reaction of the intermediate radical anions produced in reaction 3. It appears, therefore, that electron capture by the CH_3Cl does not occur dissociatively and that as a result the CH_3Cl^- can undergo electron transfer to the C_2H_5Br. Such a scheme then requires that the methyl radicals which are observed be produced by a delayed autodissociation process or upon neutralization. The fact that the methyl yields are low and that the ethyl radical yields are correspondingly high is in accord with the suggested electron transfer from the chloride to the bromide. The methyl radical yields, of course, cannot be low if electron capture occurs dissociatively and secondary reaction occurs at some later time.

Kinetics of Secondary Electron Exchange Reactions. Various different complicating situations involving secondary reactions can arise. We will treat here the case qualitatively indicated above where the anion S_1^- is stable and transfers an electron to S_2 so that a decrease in the yield of product P_1 and a corresponding increase in the yield of P_2 results. Equation 3 of the above scheme is replaced by (3a)

$$e^- + S_1 \longrightarrow S_1^- \qquad (3a)$$

and reaction 5

$$S_1^- + S_2 \xrightarrow{k_e} S_1 + S_2^- \longrightarrow S_1 + P_2 \qquad (5)$$

will then compete with the charge neutralization step 3b

$$S_1^- + RH^+ \longrightarrow P_1 \qquad (3b)$$

Such a scheme conserves the total amount of product, and eq II remains valid.

As in the previous treatment[11] we will consider electrons which would have lifetime t in the absence of scavenger but react with solute S_1 at time t' to produce an anion which has a mobility less than that of the electron. Effectively when capture occurs the residual lifetime of the geminate pair $(t - t')$ will be extended as a result of the reduction in the mobility of the negative entity (see ref 11). The negative ion, S_1^-, if it is stable, will exist for a period $(t - t')r_D$ where r_D is the ratio of the sum of the mobilities (or diffusion coefficients) of the two ions before and after electron capture. In the following treatment the factor r_D is assumed to be constant for all times of capture and for all anions. During the period $(t - t')r_D$ the probability that reaction 5 will occur is $1 - e^{-k_e[S_2](t-t')r_D}$. The fraction of the electrons of lifetime t which are scavenged by S_1 but ultimately produce P_2 rather than P_1 is given by integrating the product of this probability and the normalized scavenging rate as modified by the presence of S_2 up to time t, *i.e.*

$$\int_0^t (1 - e^{-k_e[S_2](t-t')r_D}) k_1[S_1] e^{-k_1[S_1]t'} e^{-k_2[S_2]t'} dt' =$$

$$1 - e^{-k_1[S_1]t} + \frac{k_1[S_1]}{k_1[S_1] + k_2[S_2] - k_e[S_2]r_D} \times$$

$$(e^{-k_1[S_1]t} - e^{-k_e[S_2]r_D t}) \qquad \text{(VIII)}$$

The fraction given by eq VIII can then be integrated over the lifetime distribution for all the electrons, $f_e(t)_0$, in much the same way as was done above, to give the fractional contribution to P_2 as

$$F_{exch}(P_2)_{S_1} = \frac{\sqrt{k_1[S_1] + k_2[S_2]}}{\sqrt{k_1[S_1] + k_2[S_2] + \sqrt{\lambda}}} \times$$

$$\frac{k_1[S_1]}{k_1[S_1]1 - k_2[S_2]} \left(1 - \frac{k_1[S_1]}{k_1[S_1] + k_2[S_2] - k_e[S_2]r_D}\right) +$$

$$\frac{k_1[S_1]}{k_1[S_1] + k_2[S_2] - k_e[S_2]r_D} \cdot \frac{\sqrt{k_e[S_2]r_D}}{\sqrt{k_e[S_2]r_D} + \sqrt{\lambda}} \qquad \text{(IX)}$$

We will now define an exchange parameter $\beta_e = (r_D/\lambda)k_e$, multiply (IX) by G_{gi}, and subtract this contribution from eq III. Since the anions are assumed to be stable, those produced from the free ions will always undergo reaction 5 and the free ion component must also be subtracted. The resultant yield is

$$G(P_1)_{S_2} = \frac{\alpha_1[S_1]}{\alpha_1[S_1] + \alpha_2[S_2]} G_{gi} \frac{\sqrt{\alpha_1[S_1] + \alpha_2[S_2]}}{1 + \sqrt{\alpha_1[S_1] + \alpha_2[S_2]}} \times$$

$$\frac{\alpha_1[S_1] + \alpha_2[S_2]}{\alpha_1[S_1] + \alpha_2[S_2] - \beta_e[S_2]} \left(1 - \frac{\sqrt{\beta_e[S_2]}}{1 + \sqrt{\beta_e[S_2]}} \times \right.$$

$$\left. \frac{1 + \sqrt{\alpha_1[S_1] + \alpha_2[S_2]}}{\sqrt{\alpha_1[S_1] + \alpha_2[S_2]}}\right) \qquad \text{(X)}$$

It is seen that when exchange is very slow the last two factors in eq X approach unity. This equation is not applicable to the case where $\beta = 0$ since it neglects the free ion component.

The applicability of eq X to the methyl radical yields from the CH_3Cl–C_2H_5Br system is tested in Figure 1. This system is particularly good for such a test because of the significant departures from ideality previously noted and because, as mentioned above, values for all of the parameters except β_e are known from direct measurements on the individual solutes.[2] It is seen in Figure 1 that at a CH_3Cl concentration of 0.1 M the predicted methyl radical yield is quite dependent on the choice of β_e and that, in fact, for no value of β_e does the calculated curve fit the experimental data exactly. From the results at high C_2H_5Br concentrations β_e must have a value of at least 0.5 M^{-1}. Such a value, however, predicts a slightly more rapid decrease in the $CH_3\cdot$ yield at low concentrations of added C_2H_5Br than is observed. It is obvious from this that some complication in addition to reaction 5 must be important.

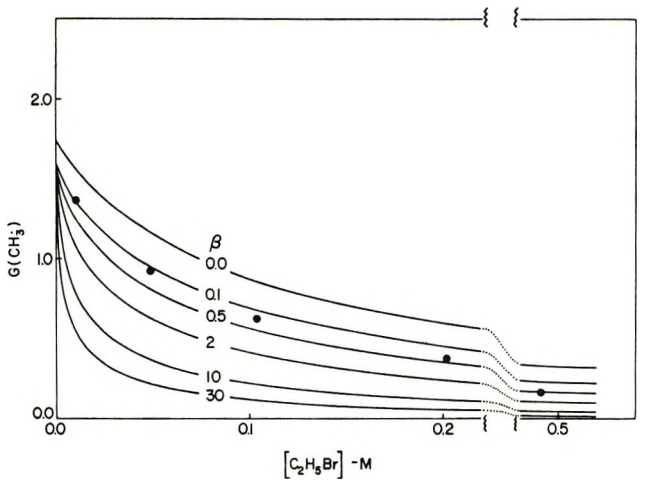

Figure 1. Effect of C_2H_5Br on the $CH_3\cdot$ yield from 0.1 M CH_3Cl solutions. Data are taken from ref 2 and the curves are calculated from eq X for the indicated values of β_e. The uppermost curve represents the ideal case where secondary reactions are unimportant. The approximate lower limit to the yields expected, if reaction 5 interferes with the production of $CH_3\cdot$ radicals at a diffusion-controlled rate, is in the region between the curves for $\beta = 2$ and 10 M^{-1}.

Equation X was derivcd on the assumption that the radical anion S_1^- is stable and exists until either exchange or charge neutralization occurs. However, at low concentrations of ethyl bromide, where the period required for the transfer reaction is relatively long, the experimental data indicate that this latter reaction does not take place. The simplest explanation of such an effect is the presence of a first-order decay of the anion which occurs parallel to the competing reactions 3b and 5.

$$S_1^- \xrightarrow{1/\tau} P_1 + X^- \qquad (6)$$

Kinetic Treatment of Anion Decay. In describing the kinetics involved in reactions 1–6 it is helpful to keep in mind the time coordinates indicated in Figure 2. We will consider an electron created at time 0 that has a lifetime t in the hydrocarbon. If this electron reacts at time t' the resultant anion will live for a time $(t - t')r_D$ provided neither decay nor secondary reaction has occurred. If we multiply the probability that decay has not occurred at time t'', *i.e.*, $e^{-t''/\tau}$, by the rate per initial ion pair of the exchange reaction, $k_e[S_2]e^{-k_e[S_2]t''}$, and integrate over the lifetime of the secondary ion we obtain the fraction which undergoes reaction 5. Integrating the product of this fraction and the rate of scavenging by S_1 as modified by the presence of S_2 over the lifetime t gives the fraction which is captured by S_1 but subsequently exchanges with S_2. Finally if we sum over the entire distribution of electron lifetimes, we obtain the total increment which should be observed experimentally. The above can be summarized by the expression

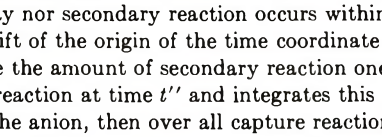

Figure 2. The reaction time coordinate. Electrons which have a lifetime t react with scavenger at time t'. The secondary anions formed will then live for a time $(t - t')r_D$ provided neither decay nor secondary reaction occurs within this period. Note the shift of the origin of the time coordinate of the anion. To calculate the amount of secondary reaction one considers the rate of reaction at time t'' and integrates this first over the lifetime of the anion, then over all capture reactions that have occurred up to time t and finally over the lifetime distribution of the electrons (see eq XI).

$$F_{exch}(P_2)_{S_1} = \int_0^\infty f_e(t)_0 dt \int_0^t k_1[S_1]e^{-k_1[S_1]t'}e^{-k_2[S_2]t'}dt' \times \int_0^{(t-t')r_D} e^{-t''/\tau}k_e[S_2]e^{-k_e[S_2]t''}dt'' \qquad (XI)$$

Equation XI is an exact description of the consequences of scheme 1–6 regardless of the explicit form of $f_e(t)_0$. It assumes only that r_D is a constant so that the second integration can be carried out and that all reactions involving the solutes can properly be described in terms of pseudo-first-order kinetics. The integrations can be readily carried out as indicated above for the more simple cases since the various integrals involved all reduce to Laplace transformations of the form of eq VI. Introducing the parameter $\delta_i = (r_D/\lambda)(1/\tau_i)$ (δ is dimensionless since λ has the dimension of frequency) the fractional exchange of the geminate component is given by

$$F_{exch}(P_2)_{S_1} = \frac{\beta_e[S_2]}{\beta_e[S_2] + \delta_1} \frac{\sqrt{\alpha_1[S_1] + \alpha_2[S_2]}}{1 + \sqrt{\alpha_1[S_1] + \alpha_2[S_2]}} \times \frac{\alpha_1[S_1]}{\alpha_1[S_1] + \alpha_2[S_2]}\left(1 - \frac{\alpha_1[S_1] + \alpha_2[S_2]}{\alpha_1[S_1] + \alpha_2[S_2] - (\beta_e[S_2] + \delta_1)}\right) + \frac{\alpha_1[S_1]}{\alpha_1[S_1] + \alpha_2[S_2] - (\beta_e[S_2] + \delta_1)} \frac{\sqrt{\beta_e[S_2] + \delta_1}}{1 + \sqrt{\beta_e[S_2] + \delta_1}} \qquad (XII)$$

The fraction of the free ions which undergoes reaction 5 is given by considering the competition between reactions 5 and 6 and is $(\alpha_1[S_1]/(\alpha_1[S_1] + \alpha_2[S_2]))(\beta_e[S_2]/(\beta_e[S_2] + \delta_1))$. Subtracting these exchange components from eq III, the complete expression for the yield becomes

$$G(P_1)_{S_2} = \frac{\alpha_1[S_1]}{\alpha_1[S_1] + \alpha_2[S_2]}\left[\left(1 - \frac{\beta_e[S_2]}{\beta_e[S_2] + \delta_1}\right)G_{fi} + G_{gi}\frac{\sqrt{\alpha_1[S_1] + \alpha_2[S_2]}}{1 + \sqrt{\alpha_1[S_1] + \alpha_2[S_2]}} \cdot Q\right] \qquad (XIII)$$

where Q is a correction factor to the geminate component of the ideal case given by

$$Q = 1 - \frac{\beta_e[S_2]}{\beta_e[S_2] + \delta_1} \times \left[1 - \frac{\alpha_1[S_1] + \alpha_2[S_2]}{\alpha_1[S_1] + \alpha_2[S_2] - (\beta_e[S_2] + \delta_1)} \times \left(1 - \frac{\sqrt{\beta_e[S_2] + \delta_1}}{1 + \sqrt{\beta_e[S_2] + \delta_1}} \times \frac{1 + \sqrt{\alpha_1[S_1] + \alpha_2[S_2]}}{\sqrt{\alpha_1[S_1] + \alpha_2[S_2]}}\right)\right] \quad \text{(XIIIa)}$$

It is seen that if either β_e is small (*i.e.*, exchange is very slow) or if δ_1 is large (*i.e.*, the radical anion dissociates very rapidly to produce P_1), then Q approaches unity and eq XIII approaches eq III. Only if τ is long and $\beta_e[S_2]$ significant with respect to both $\alpha_1[S_1]$ and $\alpha_2[S_2]$ does exchange become important. In the limit where τ is very long, *i.e.*, $\delta \rightarrow 0$, eq XIII reduces to eq X, as of course it must.

The CH_3Cl–C_2H_5Br System. The methyl chloride–ethyl bromide system appears to be relatively simple in that the total radical yield from the solute obeys eq II very well.[2] It seems likely that the difference in the electron affinities of the chloride and bromide will be sufficiently great that electron transfer will occur in only one direction. As indicated above qualitatively, the net transfer is in the direction of the bromide. If this is so, then eq XIII should be able to describe the experimental results. It is somewhat unfortunate that one must choose values for two parameters, but the choice is made palatable by the fact that δ_1 is relatively unimportant at high values of $[S_2]$. This fact permits a reasonable evaluation of β_e which in turn allows one to choose an appropriate value of δ_1 to describe the yields at lower concentrations. The lifetime parameter δ_1 is important only for nonzero values of β_e and for any given value of β_e can only increase the yield of P_1 over that calculated from eq X. From Figure 1 it is seen that β_e must have a value of at least 0.5 M^{-1} in order to explain the low methyl radical yields observed at the highest C_2H_5Br concentrations. Since the effect of the terms involving β_e in eq XIII is reduced when the secondary ions undergo some decay ($\delta > 0$), the actual value of β_e must be at least slightly higher than 0.5 M^{-1}. A value of $\delta_1 \sim 0.03$ is required to explain the data at low concentrations of S_2 and with this β_e is estimated to be 0.6 M^{-1}. Somewhat higher values of β_e are compatible with the data if the increased transfer rate is compensated for by an increased decay rate. For example, the data are predicted reasonably well for $\beta_e = 1\ M^{-1}$ if δ_1 is increased to 0.1. Values of β_e and δ_1 higher than these predict excessively high yields at the lower concentrations of CH_3Cl.

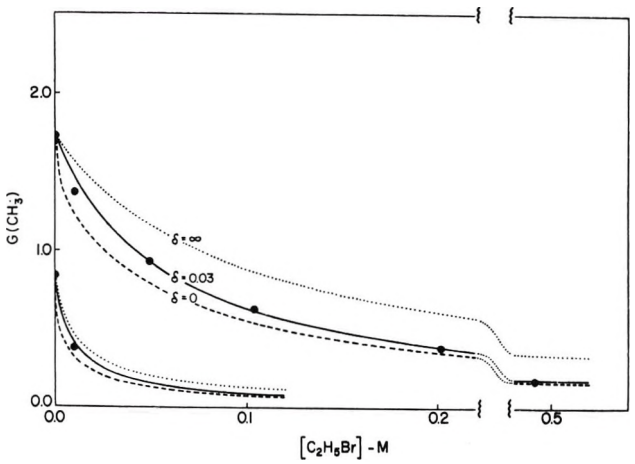

Figure 3. Effect of C_2H_5Br on the $CH_3\cdot$ yield from 0.1 and 0.01 M CH_3Cl solutions taking into account both autodissociation of the chloride and electron exchange from the chloride to the bromide. The solid curves are calculated from eq XIII with $\beta_e = 0.6\ M^{-1}$ and $\delta_1 = 0.03$. Curves for $\beta_e = 0.6\ M^{-1}$, $\delta_1 = 0$, and $\beta_e = 0$ (or $\delta_1 = \infty$) are given by the dashed and dotted curves, respectively. It is seen that when the lifetime of the anion is limited by decay, this decay has very little effect on the calculated yields at high C_2H_5Br concentrations.

Plots of eq XIII calculated with $\beta_e = 0.6\ M^{-1}$ and $\delta_1 = 0.03$ are given by the solid curves in Figure 3 for CH_3Cl concentrations of 0.1 and 0.01 M. All of the experimentally observed values previously reported[2] are compared with the calculated values in Table I. The data require a scheme of reactions at least as complex as that written above (reactions 1–6). Such a scheme seems reasonable and while there is, of course, no guarantee that the actual system is not more complex than this, it is seen that eq XIII does describe the data very well.

Table I: Methyl Radical Yields from Methyl Chloride–Ethyl Bromide Solutions in Cyclohexane

$[CH_3Cl]$	$[C_2H_5Br]$	$G(CH_3)_{obsd}$[a]	$G(CH_3)_{calcd}$[b]	$\left(\frac{\alpha_{C_2H_5Br}}{\alpha_{CH_3Cl}}\right)_{calcd}$[c]
0.203	0.101	1.00	0.99	1.45
0.201	0.202	0.68	0.66	1.40
0.107	0.0103	1.40	1.49	1.72
0.100	0.049	0.93	0.93	1.49
0.102	0.104	0.63	0.63	1.46
0.103	0.202	0.38	0.40	1.50
0.103	0.491	0.17	0.18	1.56
0.0485	0.103	0.34	0.36	1.60
0.0209	0.103	0.18	0.17	1.31
0.0098	0.0100	0.38	0.40	1.50

[a] From ref 2. [b] Calculated from eq XIII with $\alpha_{CH_3Cl} = 5.41\ M^{-1}$, $\alpha_{C_2H_5Br} = 7.82$, $\beta_e = 0.6\ M^{-1}$, $\delta_{CH_3Cl} = 0.03$. The sum of the methyl and ethyl radical yields is given by eq II with a root-mean-square deviation of 2.8% between the calculated and observed results. [c] Calculated from eq XV with parameters as above (see text). Average is 1.50 ± 0.11. The ratio from the direct measurements on the scavenging dependences is 7.82/5.41 = 1.45.

The equation previously given[2] to take into account the secondary reactions in this system (arrived at by analogy before one had the benefit of the detailed mathematics presented here)

$$G(P_1) = \frac{\alpha_1[S_2]}{\alpha_1[S_1] + \alpha_2[S_2]} \times \left(G_{fi} + G_{gi}\frac{\sqrt{\alpha_1[S_1] + \alpha_2[S_2]}}{1 + \sqrt{\alpha_1[S_1] + \alpha_2[S_2]}}\right) \times \left(\frac{1}{1 + \sqrt{\beta[S_2]}}\right) \quad \text{(XIV)}$$

is somewhat similar to the limiting approximation of eq XIII when $\beta_e[S_2] + \delta \ll \alpha_1[S_1] + \alpha_2[S_2]$. It is seen that eq XIII has an additional term $(1 + \sqrt{\alpha_1[S_1] + \alpha_2[S_2]})/\sqrt{\alpha_1[S_1] + \alpha_2[S_2]}$ which magnifies the effect of the exchange so that the present value of β_e is somewhat less than given previously. The other conclusions based on eq XIV are modified only slightly by eq XIII. As long as $\beta_e \ll \alpha_2$ the correction factor Q given by eq XIIIa will be only slightly dependent on $[S_1]$. This fact is borne out experimentally since, as was previously noted, the four experiments at 0.1 M C_2H_5Br all give observed methyl radical yields which are ~72% of those calculated from eq III. (For 0.1 M C_2H_5Br the calculated value of Q varies from 0.72 at 0.0209 M CH_3Cl to 0.75 at 0.203 M CH_3Cl and averages to 0.73). One can show from eq II and XIII that

$$\frac{\alpha_1}{\alpha_2} \simeq \frac{G(P_2)_{S_1}}{G(P_1)_{S_2}} \cdot \frac{[S_1]}{[S_2]} \cdot \frac{Q}{1 + \frac{\alpha_1[S_1]}{\alpha_2[S_2]}(1 - Q)} \quad \text{(XV)}$$

In the ideal case $Q = 1$ and the final factor on the right side of equation XV also becomes unity. It is, of course, attractive to attempt to determine the relative rates from measurement of the product ratio since certain of the experimental uncertainties cancel. It is seen, however, that the correction factor for exchange can be considerable and can introduce errors of a factor of 2 or even larger. For the data of Table I the last factor in eq XV varies from 0.87 to 0.51. While the α parameters enter into this correction, the factor itself is not sensitive to these parameters so that the relative reactivities can be evaluated reasonably well from the measurement of the yields from both components. Values of α_2/α_1 calculated in this way are given in the final column of Table I and are seen to be considerably more constant than the ratios $(G(P_2)_{S_1}/G(P_1)_{S_2})([S_1]/[S_2])$ (see ref 2). The average, 1.50, agrees with the ratio of the parameters determined on the individual solutes and provides some measure of the internal consistency of the above arguments.

Significance of the Magnitude of β_e and δ. From the definition of β_e the rate constant k_e for the electron exchange reaction is equal to $(\lambda/r_D)\beta_e$. It has previously been shown that a good measure of λ/r_D can be obtained from direct observations on the recombination of anions with their geminate partners in pulse experiments.[11] The decay of diphenylide anion observed in cyclohexane solution on the 10^{-8} to 10^{-7} sec time scale by Thomas, *et al.*,[17] can be interpreted in terms of a value of $\sim 1.3 \times 10^9$ sec^{-1} for λ/r_D.[11,18] The parameter λ depends only on the solvent and r_D on the mobility of the anion formed in the capture reaction. The mobilities of most small anions are similar so that we should be able to combine this value of λ/r_D with the β_e of 0.6 M^{-1} given above to obtain a rate constant of 8×10^8 M^{-1} sec^{-1} for electron transfer from CH_3Cl^- to C_2H_5Br. Such a rate constant is similar to that for transfer from diphenylide anion to phenanthrene (6×10^8 M^{-1} sec^{-1})[19] and a factor of ~5 less than the maximum expected for a diffusion-controlled reaction between moderate size molecular entities. In general β_e can be somewhat larger than observed in the CH_3Cl–C_2H_5Br system. Arai, Grev, and Dorfman[19] have, for example, reported electron transfer rate constants between aromatic solutes in the range of 0.3 to 6×10^9 M^{-1} sec^{-1}. The latter corresponds to $\beta_e = 5$ M^{-1}, a value which would appear to be a reasonable upper limit for this parameter. Because of the relatively short lifetime of most of the geminate pairs, there is a very strong restriction on the amount of secondary ionic reaction which can occur. This point is very important in treating systems such as nitrous oxide, as will be commented on separately.[20]

At concentrations of $S_1 \sim 0.1$ M the difference between the yields calculated from eq III and X become significant only for values of β_e in excess of 0.01 M^{-1}. For smaller values the differences are of the order of the experimental errors. It can be said, therefore, that electron exchange reactions which occur with rate constants $\sim 10^7$ M^{-1} sec^{-1} or less will have little effect on the chemistry. They are sufficiently unimportant, except at the highest solute concentrations, that the results can be reasonably interpreted in terms of eq III. This conclusion is, of course, as it must be since the lifetime of most of the anions is insufficient to allow the secondary reactions to compete (90% of the anions have lifetimes less than 10^{-7} sec).[11]

The above comments apply only if the anion involved has a lifetime toward dissociation sufficiently long that significant decay does not occur within the period required for geminate recombination. From the definition of δ, the lifetime τ is $(r_D/\lambda)(1/\delta)$. From the value of 0.03 given above for δ_{CH_3Cl} in the CH_3Cl–C_2H_5Br system, the lifetime of the methyl chloride

(17) J. K. Thomas, K. Johnson, T. Klippert, and R. Lowers, *J. Chem. Phys.*, **50**, 5034 (1969).

(18) S. J. Rzad, P. P. Infelta, J. M. Warman, and R. H. Schuler, *ibid.*, **50**, 5034 (1969).

(19) S. Arai, D. A. Grev, and L. M. Dorfman, *ibid.*, **46**, 2572 (1967).

(20) P. P. Infelta and R. H. Schuler, to be published.

anion in the liquid state can be estimated to be $\sim 3 \times 10^{-8}$ sec. It is known from gas phase results that methyl chloride does not capture electrons readily (the second-order capture rate constant for CH_3Cl has been measured to be seven orders of magnitude less than that for SF_6).[21] In spite of this, capture appears to occur readily in solution.

It is seen in Figure 3 that anion decay can reduce the effect of the exchange reaction at low concentrations of S_2 but has relatively little effect at high concentrations. This result is particularly important for CH_3Cl at concentrations ~ 0.01 M or less where exchange is of relatively minor significance, and one can reasonably readily estimate values for α_2 even with approximate values of β_e. One can proceed iteratively and estimate the latter at high concentrations of both solutes. This fact is made use of below in the CH_3Cl–N_2O and CH_3Cl–CO_2 systems.

For anion lifetimes less than 10^{-10} sec ($\delta > 3$) the curves of eq XIII approach those calculated from eq III. As far as the secondary chemistry is concerned the initial capture can be regarded as having occurred dissociatively. As will be remarked on next, the experiments with CH_3Br appear to approach this limit. In this situation it is not possible to determine the value of the exchange coefficient β_e nor even to distinguish between the two cases where the rate constant for the exchange reaction is low or the period for autodissociation of the anion is short. Finally we would note that the value of δ should be a property for each given solute. This fact is tested below, as far as is possible, in examining the results of CH_3Cl in competition with the various second solutes.

The CH_3Br–C_2H_5Br System. Data on the methyl bromide–ethyl bromide system were previously reported,[2] and it was shown that the individual yields are predicted reasonably well by eq III (as shown by the dotted curves in Figure 4) although at the highest concentrations there is a slight bias in favor of low methyl and high ethyl radical yields. There seems to be no question but that the lifetime of the methyl bromide anion and/or the net rate constant for its exchange reactions are very low in this system. If exchange is assumed to be completely unimportant, then the data can be fitted very well if the ratio $\alpha_{C_2H_5Br}/\alpha_{CH_3Br}$ is increased by about 15%. The effect of exchange is not very large, and it is clearly difficult to say that exchange definitely occurs in this system, but all the results are internally somewhat more consistent if one assumes that a net transfer does occur in the direction of reaction 5. The bias toward low observed methyl radical yields seems very likely to be real, and if so it can be explained only by a nonzero lifetime of the methyl bromide radical anion. From the departure of the data from the dotted curve at 0.1 M CH_3Br one can estimate the CH_3Br^- lifetime as 1×10^{-9} sec if β_e is taken as 0.6 M^{-1}. However, β_e may very well be somewhat smaller.

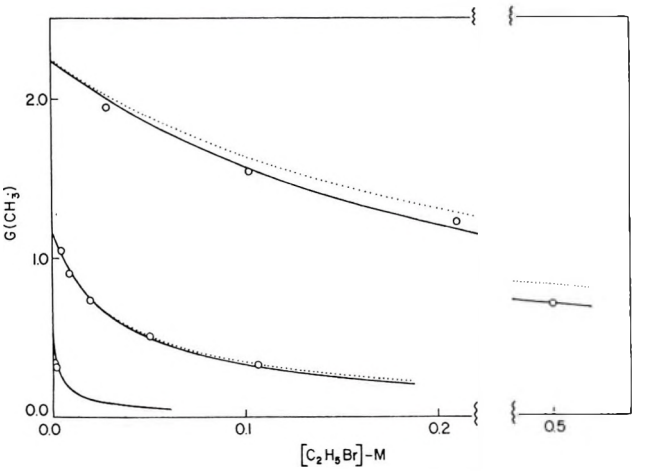

Figure 4. Effect of C_2H_5Br on the $CH_3\cdot$ yield from CH_3Br solutions. Upper curve 0.1 M CH_3Br, central curve 0.01 M CH_3Br, and lower curve 0.001 M CH_3Br. Dotted curves are for ideal case calculated from eq III. Solid curves calculated calculated from eq XIII with $\beta_e = 0.3$ M^{-1} and $\delta = 0.3$. It is seen that with these parameters electron exchange is of negligible significance at 10^{-2} M CH_3Br and below.

A lifetime of 2.5×10^{-9} sec would be obtained if β_e is taken as 0.3 M^{-1} (the solid curve of Figure 3). This lifetime would seem to be a reasonable upper limit to that for CH_3Br^-. Unfortunately, however, it is not possible to distinguish between the various situations or even the complete lack of exchange as indicated above. For the moment we can only suggest that values of $\beta_e = 0.3$ M^{-1} and $\delta = 0.3$ be used with eq XIII to correlate the data as is done by the curves of Figure 4. It is seen in this figure that any effect of exchange is of only trivial importance at the lower concentrations. This latter fact is used in treating the data from the mixed solutes CH_3Br–SF_6 and CH_3Br–N_2O.

Determination of α for SF_6, CO_2, and N_2O

Up to this point we have described the model and illustrated the kinetics with data previously reported on the CH_3Cl–C_2H_5Br and CH_3Br–C_2H_5Br systems. We will report here new data on the binary systems of SF_6, CO_2, and N_2O with both CH_3Br and CH_3Cl in cyclohexane solution at room temperature. These studies were carried out with a view toward determining α for SF_6, CO_2, and N_2O, but it is obvious that the complicating effects indicated above must be considered in detail. In fact, except for the CH_3Br–SF_6 and CH_3Br–N_2O systems, even the first inspection shows that the data cannot be fitted by eq III with a singular value of α so that complications are unquestionably present. In general it was expected that the CH_3Cl systems would be complicated by exchange reactions and that CH_3Br might be the better indicator solute. This expectation seems to be borne out in the case of SF_6 and N_2O. However the results with CO_2 show that

(21) K. M. Bansal and R. W. Fessenden, private communication.

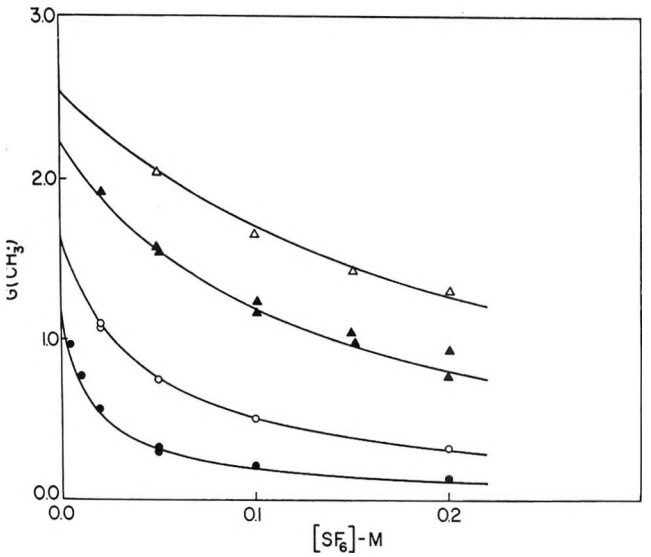

Figure 5. Effect of SF_6 on $CH_3\cdot$ yields from CH_3Br solutions. CH_3Br concentrations are (△) 0.2, (▲) 0.1, (○) 0.03, and (●) 0.01 M. Curves are calculated from eq XIII with $\alpha_{SF_6} = 17\ M^{-1}$, $\beta_e = 0.3\ M^{-1}$, and $\delta_{CH_3Br} = 0.3$.

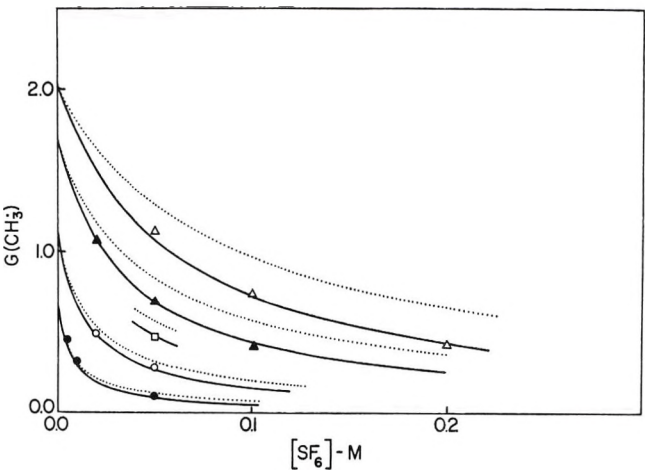

Figure 6. Effect of SF_6 on the $CH_3\cdot$ yields from CH_2Cl solutions. CH_3Cl concentrations are (△) 0.2, (▲) 0.1, (□) 0.06, (○) 0.03, and (●) 0.01 M. Dotted curves are for ideal case (eq III) with $\alpha_{SF_6} = 17\ M^{-1}$. Solid curves include electron transfer and decay according to eq XIII ($\beta_e = 0.5\ M^{-1}$, $\delta = 0.03$).

econdary reactions involving transfer *to* CH_3Br can be mportant and result in an excessively high methyl adical yield. The high observed yields, if their source s not recognized, might be misinterpreted in terms of a ow value for α_{CO_2}. Methyl chloride presumably has a ow electron affinity so that electron transfer does not ormally occur to this solute. Also it is relatively inert oward radical attack. One concludes, therefore, that CH_3Cl is the better indicator solute provided the trans- er reaction can be taken into account. In all cases, studies must be carried out at both high and low solute concentrations in order to define the possible extent of the complications.

CH_3Br–SF_6. Of the six systems studied in detail the CH_3Br–SF_6 system seems to be the closest to an ideal one. Data are given in Figure 5 for the effect of SF_6 on the $CH_3\cdot$ yield at four CH_3Br concentrations. The data of this figure can be fitted very reasonably by eq III if a value of α_{SF_6} of 18 M^{-1} is assumed. It may be, however, that the methyl radical yield is decreased slightly by secondary processes and, as in the CH_3Br–C_2H_5Br system, it would be better to use eq XIII together with a value of δ_{CH_3Br} of 0.3 as given above. With a value of δ as high as this the choice of β_e is not critical. Taking β_e as 0.3 M^{-1} the results at 10^{-2} M should not be significantly affected by the exchange process (see Figure 4), and one can use the data at this concentration to determine α_{SF_6}. A value of 17 M^{-1} is indicated. The remaining data can then be fitted by the solid curves of Figure 5 with no further adjustments of the parameters. The possible range for α_{SF_6} is certainly quite limited, and one has a fair degree of confidence that the correct value is very close to the 17 M^{-1} given here. The decrease in the hydrogen yield produced by the addition of SF_6 to cyclohexane was previously explained[12] in terms of $\alpha_{SF_6} = 17.8\ M^{-1}$, but the present study provides a more critical evaluation of this parameter. The fact that the methyl radical yields decrease as expected at the highest SF_6 concentrations is a very strong indication that neither electron exchange nor other spurious secondary chemical processes (*e.g.*, H-atom attack) contribute significantly to the observed methyl radical yield.

CH_3Cl–SF_6. Similar results for the effect of SF_6 on the methyl radical yield from CH_3Cl are reported in Figure 6. If α_{SF_6} were completely unknown, we could first consider the data at 0.01 M and then proceed iteratively as indicated above. A value of ~17 M^{-1} would be obtained. One, however, knows α_{SF_6} from the above so that the yields expected from eq III (the dotted curves in Figure 6) can be readily calculated. The observed yields are lower than calculated, and it appears that considerable exchange from the methyl chloride anion to SF_6 must occur. The reaction scheme must be qualitatively similar to that used for the CH_3Cl–C_2H_5Br system and eq XIII should apply. We know δ_{CH_3Cl} from the analysis of the CH_3Cl–C_2H_5Br data so it remains only to choose a value for β_e to calculate the expected dependence. This value can be determined from one of the measurements at a high concentration of both CH_3Br and SF_6 with the results at all lower concentrations then being completely determined. Excellent agreement with the remaining yields is obtained with $\beta_e = 0.5\ M^{-1}$ (and $\alpha_2 = 17\ M^{-1}$, $\delta = 0.03$) as is shown by the solid curves of Figure 6. It is, of course, gratifying that the data for this system can be fitted so well with a reasonable value for the one remaining adjustable parameter.

CH_3Cl–N_2O. Nitrous oxide is a substance which has received a considerable amount of attention in electron-scavenging experiments. In 1964, the large nitrogen

yields observed in the irradiation of N_2O solutions in hydrocarbons again drew attention to the importance of electron scavenging.[22] However, the nitrogen yields observed are very much higher than the yields for scavenging by alkyl halides at comparable solute concentrations and do not appear to be a proper measure of the electron-scavenging process. In spite of considerable controversy on the subject, it now appears that the processes producing nitrogen are complicated by side effects which very probably involve secondary ionic reactions.[23,24] It is important to have a measure of α_{N_2O} so that estimates of the initial yield can be made. In the present study measurements have been made against both CH_3Br and CH_3Cl as the indicator solutes but, because of the possibility of complications in the case of the bromide as is indicated below, the results with the chloride should be considered first.

Data on CH_3Cl–N_2O mixed solutes are presented in Table II. Qualitatively it is seen that addition of N_2O reduces the CH_3 yield from CH_3Cl in much the same way as the above samples. Taking $\delta_{CH_3Cl} = 0.03$ and iteratively fitting the other two parameters one finds $\alpha_{N_2O} = 10\ M^{-1}$ and $\beta_e = 0.6\ M^{-1}$. The agreement with the yields calculated on the basis of eq XIII is seen to be quite good, and as far as one can tell the applicable scheme is very similar to that with both C_2H_5Br and SF_6.

Table II: Methyl Radical Yields from CH_3Cl–N_2O Solutions in Cyclohexane

$[CH_3Cl]$	$[N_2O]$	$G(CH_3)_0$[a]	$G(CH_3)_{obsd}$	$G(CH_3)_{calcd}$[b]
0.266	0.033	2.19	1.64	1.61
0.266	0.064		1.24	1.30
0.268	0.098		1.04	1.08
0.266	0.130		0.92	0.93
0.100	0.100	1.73	0.59	0.57
0.101	0.200		0.35	0.34
0.027	0.025	1.17	0.54	0.50
0.022	0.016	1.09	0.60	0.55
0.010	0.005	0.84	0.53	0.52

[a] Yield in the absence of N_2O. [b] Yield calculated from eq XIII with $\alpha_{N_2O} = 10\ M^{-1}$, $\beta = 0.6\ M^{-1}$, and $\delta = 0.03$.

CH_3Br–N_2O. One suspects that this system might prove to be abnormal in that both neutral and ionic products from electron capture by the nitrous oxide might attack the methyl bromide to give additional methyl radicals. It is known, for example, that the cyclohexyl radical yield from N_2O solutions is abnormally high.[13] In fact this system appears to be very well behaved in that, as is seen in Figure 7, high concentrations of N_2O reduce the CH_3 yield in the way expected if α is taken as 10 M^{-1} (as determined above). Even at high CH_3Br concentrations there is no evidence of any large spurious methyl radical yield and the data

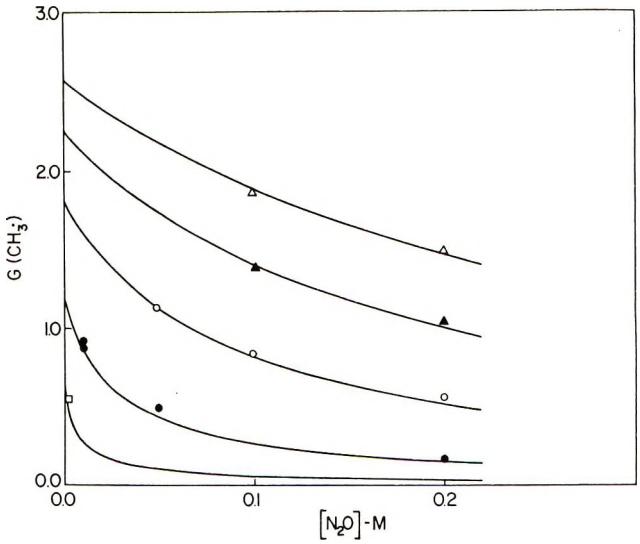

Figure 7. Effect of N_2O on the $CH_3\cdot$ yields from CH_3Br solutions. CH_3Br concentrations are (△) 0.2, (▲) 0.1, (○) 0.04, (●) 0.01, and (□) 0.002 M. Curves are calculated from eq XIII with $\alpha_{N_2O} = 10\ M^{-1}$, $\beta_e = 0.5\ M^{-1}$, and $\delta = 0.3$. The fact that the yields decrease as expected indicates that spurious secondary reactions do not result in $CH_3\cdot$ formation.

can be fitted very well by eq XIII with $\alpha_{N_2O} = 10\ M^{-1}$, $\beta_e = 0.5\ M^{-1}$, and $\delta_{CH_3Br} = 0.3$ (Figure 7). The amount of exchange appears to be somewhat greater than that which occurs for the case of CH_3Br–C_2H_5Br. A lower value for β_e would require a slightly higher value for α_{N_2O} in order to explain the data at 0.1 and 0.2 M N_2O. If one were to consider only data on this system, a lower limit of 9 M^{-1} for α_{N_2O} would be estimated but even very small corrections for CH_3 radical production from secondary reactions involving the N_2O will increase this value considerably.

CH_3Cl–CO_2. It is seen in Figure 8 that the CH_3Cl–CO_2 system qualitatively follows the format of the other three systems containing CH_3Cl and treatment of the data appears to be fairly straightforward. Again α_{CO_2} can be evaluated from the reduction observed at 0.01 M CH_3Cl. A value of 13 M^{-1} is indicated. With δ_{CH_3Cl} taken as 0.03 an exchange parameter $\sim$0.25 M^{-1} is required to describe the data at 0.2 M CH_3Cl. With all the parameters determined by the above arguments the remaining data are described very well by eq XIII as is seen in the figure.

CH_3Br–CO_2. The data for the CH_3Br–CO_2 system presented in Figure 9 make it immediately obvious that complications outside those considered above are present. The dotted (lowermost) curves in the figure illustrate the dependences expected if no secondary

(22) G. Scholes and M. Simic, *Nature (London)*, **202**, 895 (1964).

(23) The importance of secondary reactions was first pointed out by Sato and coworkers [S. Sato, R. Yugeta, K. Shinsaka, and T. Terao, *Bull. Chem. Soc. Jap.*, **39**, 156 (1966)]. See also ref 24 for comments on the subject.

(24) J. M. Warman, K.-D. Asmus, and R. H. Schuler, *Advan. Chem. Ser.*, **No. 82**, 25 (1968).

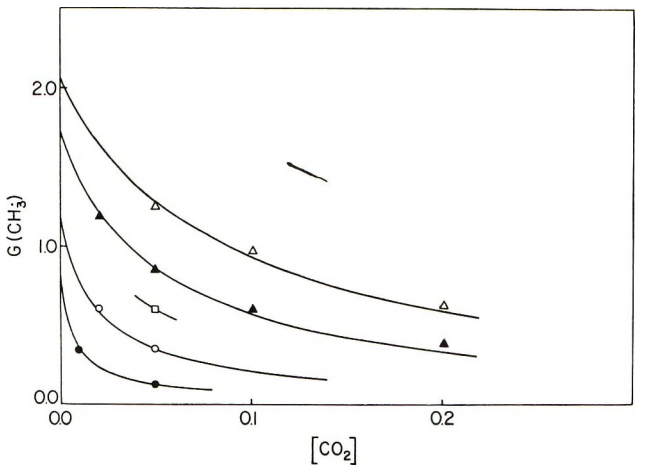

Figure 8. Effect of CO_2 on $CH_3\cdot$ yields from CH_3Cl solutions. CH_3Cl concentrations are (△) 0.2, (▲) 0.1, (□) 0.06, (○) 0.03, and (●) 0.01 M. Curves are calculated from eq XIII with $\alpha_{CO_2} = 13\ M^{-1}$, $\beta_e = 0.25\ M^{-1}$, and $\delta_{CH_3Cl} = 0.03$.

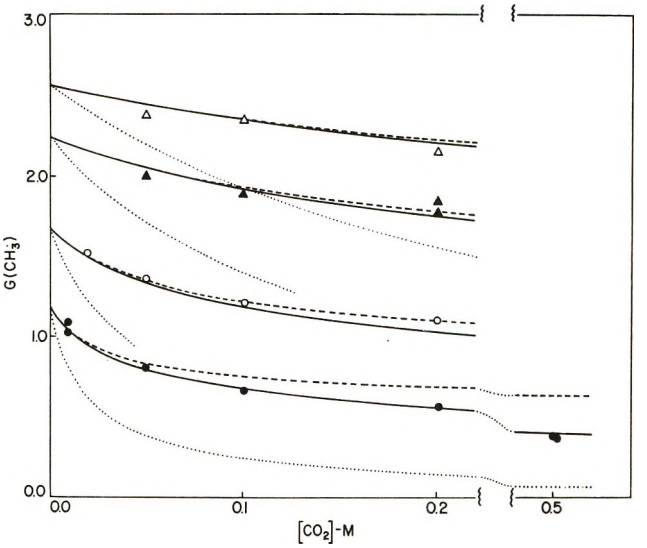

Figure 9. Effect of CO_2 on the $CH_3\cdot$ yields from CH_3Br solutions. CH_3Br concentrations are (△) 0.2, (▲) 0.1, (○) 0.03, and (●) 0.01 M. Dotted curves are calculated for the ideal case with no secondary reaction. It is seen that in all cases the experimentally observed yields are considerably higher. The data at the highest concentration require a β_e of at least 2.0 M^{-1} in eq XVI to explain the observed increase above the ideal but the dashed curves calculated on this assumption (and $\delta = 0$) are then excessively high at the lower concentrations. The solid curves are calculated on the assumption that CO_2 quenches the transfer reaction, *i.e.*, $\delta_2 = 0.05[CO_2]$.

reactions occur (eq III with $\alpha = 13\ M^{-1}$ as given by the above interpretation of the data from the CH_3Cl–CO_2 system). It is seen that, in general for this system, the $CH_3\cdot$ yields observed are considerably higher than predicted. For example, the yield from a solution 0.01 M in CH_3Br and 0.5 M in CO_2 is *ca.* five times that predicted by eq III. This situation contrasts with the other systems discussed above where the observed yields are lower than expected from simple competitive considerations. Spurious reactions which produce $CH_3\cdot$ radicals over and above the yield expected from the direct reactions of the electrons with the bromide are apparently of considerable importance. Such reactions could conceivably involve a reactive neutral intermediate produced from the CO_2. However, an explanation of the results at 0.1 M CH_3Br would require that about 50% of the electrons which react with CO_2 produce a product which attacks the CH_3Br and ultimately produces $CH_3\cdot$. The yields observed at the lower CH_3Br concentrations should then be considerably higher and increase with CO_2 concentration. It is not apparent that a model of this sort can satisfactorily explain the observed dependences.

Another possible explanation is that the anion produced in the capture by CO_2 transfers an electron to the CH_3Br in a secondary ionic process. This would result in an increased $CH_3\cdot$ yield which is quite parallel to the excess $C_2H_5\cdot$ yield produced in the CH_3Cl–C_2H_5Br system.[2] Such an explanation requires a consideration of the competition between the transfer process, recombination of the CO_2^- with its positive ion partner and other possible reactions of secondary or tertiary anions. The concentration dependence expected is embodied in an equation of the type of XI with, however, an appropriate interchange of subscripts. The fraction of geminate pairs which react with the CO_2 and subsequently transfer an electron to CH_3Br will be given by an equation similar to eq XII. Adding the increase in yield expected from transfer to eq III the total yield can be put in a form similar to eq XIII, *i.e.*

$$G(P_1)_{S_2} = \frac{\alpha_1[S_1]}{\alpha_1[S_1] + \alpha_2[S_2]} \times \left[\left(1 + \frac{\alpha_2[S_2]}{\alpha_1[S_1]}\frac{\beta_e[S_1]}{\beta_e[S_1] + \delta_2}\right)G_{fi} + G_{gi}\frac{\sqrt{\alpha_1[S_1] + \alpha_2[S_2]}}{1 + \sqrt{\alpha_1[S_1] + \alpha_2[S_2]}}Q'\right] \quad \text{(XVI)}$$

$$Q' = 1 + \frac{\beta_e[S_1]}{\beta_e[S_1] + \delta_2}\cdot\frac{\alpha_2[S_2]}{\alpha_1[S_1]} \times \left[1 - \frac{\alpha_1[S_1] + \alpha_2[S_2]}{\alpha_1[S_1] + \alpha_2[S_2] - (\beta_e[S_1] + \delta_2)} \times \left(1 - \frac{\sqrt{\beta_e[S_1] + \delta_2}}{1 + \sqrt{\beta_e[S_1] + \delta_2}} \times \frac{1 + \sqrt{\alpha_1[S_1] + \alpha_2[S_2]}}{\sqrt{\alpha_1[S_1] + \alpha_2[S_2]}}\right)\right] \quad \text{(XVIa)}$$

Equation XVI, in fact, describes the $C_2H_5\cdot$ yield from the CH_3Cl–C_2H_5Br system with the parameters β_e and δ_2 determined by the measurements on $G(CH_3)$. If only exchange and recombination are important in the

present case (*i.e.*, $\delta = 0$), then the data at the highest CH_3Br concentrations require that β_e be $\sim 2\ M^{-1}$ which in turn gives the dashed (uppermost) curves in Figure 9. With an upper limit of $5\ M^{-1}$ for β_e the lifetime of the anions must be at least 4×10^{-9} sec ($\delta < 0.2$) in order for exchange to produce the large effect noted at 0.1 and 0.2 M CH_3Br. This model predicts yields considerably higher than observed at low CH_3Br concentrations so that if it is at all correct some additional process must limit the lifetime of the CO_2^- anions. One can introduce into the model an exponential decrease of CO_2^- with time which results either from a spontaneous decay or more likely from a pseudo-first-order reaction with the solvent. In this case δ_2 will be a constant and independent of the CO_2 concentration. A value of $\delta_2 = 0.025$ is required to reproduce the yield observed at 0.01 M CH_3Br and 0.5 M CO_2, but such a value predicts considerably less $CH_3\cdot$ than is observed at lower CO_2 concentrations. The results of the experiments at 0.01 M in both CH_3Br and CO_2 are ~ 0.2 units above those predicted for the absence of secondary reaction which indicates that δ cannot be larger than 0.001 (*i.e.*, that the inherent period for disappearance of CO_2^- is greater than 10^{-6} sec).

The only internally consistent model which has been found to reproduce the observed results is one involving quenching of the secondary reactions by CO_2 itself. In this case the period τ is given by the reciprocal of the pseudo-first-order quenching constant $k_q[CO_2]$. Equation XVI can readily be adapted by replacing δ_2 by $\beta_q[CO]_2$ where $\beta_q = k_q r_D/\lambda$. It is seen in Figure 9 that the data can be fitted by such a treatment if β_q is taken as $0.05\ M^{-1}$. This value is an order of magnitude less than the exchange and corresponds to a self-quenching rate constant of $6 \times 10^7\ M^{-1}\ sec^{-1}$ which is of reasonable magnitude. In spite of the excellent agreement between the calculated and observed yields such an explanation is not very satisfying since it is not evident what reactions can be responsible for the required quenching. The data, in any event, do seem to require that in some manner CO_2 inhibits the secondary reactions responsible for $CH_3\cdot$ production.

Summary of the Reaction Parameters

The reaction parameters for the various systems studied above are summarized in Table III. In general except for electron exchange of the type indicated by reaction 5, chemical complications in these competitive experiments will result in an excess yield of methyl radicals which could possibly be interpreted in terms of a low value of α. As a result, the values of α should generally be regarded as lower limits, but they are believed to be accurate to $\sim 20\%$ or better. If the methyl halide anion does not decay rapidly, it is possible that the methyl radical yields may be low but it is shown here that the problem is of minimal importance at concentrations of the indicator solute of $\sim 10^{-2}\ M$ or below and can be taken into account reasonably well. The results certainly indicate that the radical products produced from electron capture by SF_6 and N_2O do not attack either of the methyl halides to any significant extent. This fact is perhaps somewhat surprising in view of the high cyclohexyl radical yields observed[13] in both of these cases. Apparently the fragments produced from the SF_6 or N_2O react very rapidly with the solvent and are removed from further reaction.

Table III: Summary of the Reaction Parameters

	Values of α					
	Direct[b]	Hydrogen[c] depression	Competitive experiments CH_3Cl	Competitive experiments CH_3Br[d]	β_e[a]	δ
CH_3Cl	5.4	5	...	...	...	~ 0.03[e]
CH_3Br	16.2	16	...	...	...	>0.3[f]
C_2H_5Br	7.8	~ 16	8	~ 8	0.6	...[g]
SF_6	...	18	17	≥ 17	0.5	...[g]
N_2O	~ 10[h]	16	10	≥ 9	0.6	...[g]
CO_2	...	8	13	...[i]	0.25	<0.001

[a] Transfer coefficient from CH_3Cl to second solute. [b] From ref 2. [c] From ref 12. [d] Determined assuming $\beta_e = 0.3\ M^{-1}$ ($0.5\ M^{-1}$ for N_2O) and $\delta = 0.3$. Values $\sim 10\%$ higher are obtained if it is assumed that exchange is completely unimportant. [e] A common value of δ_{CH_3Cl} of 0.03 satisfies the results observed in competition experiments with C_2H_5Br, SF_6, N_2O, and CO_2. [f] Corresponds to β_e of $0.3\ M^{-1}$ for electron exchange from CH_3Br^- to second solute. [g] Decay not manifest in the present experiments. [h] Rough estimate from concentration dependence of N_2 formation. [i] Not determinable because of secondary complexities.

In treating the data the parameters β_e and δ are not independent in that an increase in β_e can be compensated for by increasing δ, *i.e.*, a high rate of reaction is compensated for by a short lifetime. Thus in the CH_3Cl–C_2H_5Br system the calculated curves for $\beta_e = 0.5\ M^{-1}$, $\delta = 0.02$; $\beta_e = 0.6\ M^{-1}$, $\delta = 0.03$; and $\beta_e = 0.7\ M^{-1}$, $\delta = 0.04$ are essentially identical. Certain limits are, however, imposed by the data. A value of β_e smaller than $0.5\ M^{-1}$ is insufficient to explain the observed reduction at high C_2H_5Br concentrations (see Figure 1). A value greater than $1\ M^{-1}$ requires $\delta > 0.1$ and predicts less curvature to the concentration plot than is observed at low concentrations. If we accept the value of 0.03 for δ then the values for the parameter β_e for electron transfer from CH_3Cl^- to the other solutes depend on the values taken for α but appear to be accurate to $\sim 50\%$. Given that the values of both α and δ are correctly chosen, β_e cannot be varied significantly. For the case of CH_3Cl, δ and the lifetime of the anion appear to be correct to within a factor of 2. It is particularly noted that for this solute the data from all four second solutes examined can be satisfied with a common value of 0.03. In the case of methyl bromide, the value of δ_{CH_3Br} depends on whether

or not the exchange reaction has an appreciable rate and the value obtained can be varied by an order of magnitude in either direction if it is accompanied by an appropriate change in the exchange parameter β_e. In this case the conclusion on ionic lifetime can only be regarded as an approximate upper limit.

The values of α from the competitive experiments are compared in the table with values estimated from the decrease in hydrogen yield.[12] As indicated previously[12] the interpretation of the effect of solutes on $G(H_2)$ in terms of α is subject to considerable uncertainty and all of the present values are well within this uncertainty. An estimate of $\alpha_{N_2O} \sim 10\ M^{-1}$ can be given from the measurement of nitrogen production if it is assumed that each electron produces approximately two molecules of nitrogen. A value of $\sim 100\ M^{-1}$ would be required if only one molecule of nitrogen were produced and such a value is obviously excessively high. Comparison of nitrogen yields from N_2O solutions with the present results requires a detailed consideration of the secondary ionic processes in that system and will be treated separately.[20]

One should also comment on the high reactivity of CO_2 toward electrons indicated by the present experiments. As with CH_3Cl this result contrasts with gas phase studies where the rate of electron attachment is at least nine orders of magnitude less than that for SF_6.[21] The high rate in hydrocarbon solutions is corroborated by the large effect of CO_2 on $G(H_2)$ noted by a number of observers.[12,25,26] The rates of reaction of a particular solute towards electrons in the liquid hydrocarbon bears no resemblance to that found in the gas phase although it seems likely that substances which react rapidly with electrons in the gas will also do so in solution.

Some General Comments

Perhaps the most important aspect of the present contribution is the demonstration that various complicating situations, where secondary ionic reactions compete with the recombination of geminate pairs, can be treated analytically and in detail. Given a particular reaction scheme the existence of a distribution function for geminate pair lifetimes makes it possible to develop algebraic expressions to describe the dependence of yields on solute concentrations. These expressions, while frequently very complicated, can be readily evaluated and *must* describe the experimental results quite closely if the proposed scheme is complete. One, of course, can never be sure that the actual scheme is not more complex than assumed, but certain limitations on possible complications are imposed by the short lifetime of the majority of the geminate pairs.

A number of examples have been presented here in which the results appear to correspond to the scheme assumed. One scheme (reactions 1, 2, 3a–6) is common to all but one example, and this scheme is sufficiently simple (with reasonable values for the reaction parameters) that it is very probably close to a complete description. The exception (CH_3Br–CO_2) can be treated if it is assumed that CO_2^- reacts competitively with CO_2 as well as with its geminate partner and with methyl bromide. This assumption is at the moment *ad hoc* and far from satisfying.

The various examples treated illustrate the extent to which complicating secondary reactions can invalidate simple interpretation of competitive experiments. At this point there can be no question but that complications exist. Any use of the competitive approach to determine values of the reactivity parameter α must involve experiments over a sufficiently extensive range of solute concentrations that it is possible to understand the complicating effects in at least some detail. In certain cases where secondary reactions dissociate the indicator solute (*e.g.*, CH_3Br–CO_2) it is impossible to determine the value of α_{S_2} except within broad limits. These cases are manifest by an excess yield of product from the indicator at high relative concentrations of the solute under study. In other cases the limiting situations approach each other under certain circumstances and often quite reasonable estimates of the reactivity parameter can be made. This comment is particularly true for the studies where methyl chloride was used as the indicator solute since as yet in no case has spurious decomposition of the methyl chloride been noted. Electron transfer from the chloride to the second solute is a problem at high concentrations but of only minor importance at low concentrations ($\sim 0.01\ M$ and lower). One benefits here from the fact that an estimate can be made of the maximum effect that can possibly be attributed to transfer (see Figure 3). Ideally one wishes to have as an indicator solute a compound which undergoes rapid dissociation to a measurable product upon electron capture and with which spurious reactions do not occur or at least do not give the same product. Methyl bromide appears to fulfill this requirement in three of the four cases examined, but the existence of the fourth case argues for due caution in examining unknown situations.

Acknowledgment. The authors wish to thank Dr. Stefan J. Rzad very sincerely for bringing to their attention an error involving the limits of integration of eq XI in a manuscript version of the present work and for his other comments during the course of these studies.

(25) N. H. Sagert, *Can. J. Chem.*, **46**, 95 (1968).

(26) S. Sato, T. Terao, M. Kono, and S. Shida, *Bull. Chem. Soc. Jap.*, **40**, 1818 (1967).

Transient Electrons in Pulse-Irradiated Crystalline Water and Deuterium Oxide Ice

by G. Nilsson,* H. Christensen,

AB Atomenergi, Studsvik, Nyköping, Sweden

P. Pagsberg, and S. O. Nielsen

Danish AEC Research Establishment, Risö, Roskilde, Denmark *(Received August 24, 1971)*

Publication costs assisted by The Swedish Atomic Research Council

Crystalline samples of H_2O and D_2O ice were irradiated with electron pulses from a Linac and the optical absorption spectrum of the transient electron was recorded at different temperatures from -5 to $-190°$. At $-10°$ the position of the absorption peaks in the two matrices are at 682 (1.82 ± 0.01 eV) and 668 nm (1.86 ± 0.01 eV), respectively. The peak energy continuously increases as the temperature becomes lower, and at about $-130°$ constant values of 1.90 and 1.94 eV are reached. The electron decay could be accounted for by a second-order reaction between the electron and a species present in a concentration greater than its own. This second species is very probably the proton, and the proton excess was found to increase as the temperature decreases. The rate constants for the reaction in H_2O and D_2O ice at $-10°$ are (1.95 ± 0.06) × 10^{11} and (0.42 ± 0.04) × 10^{11} M^{-1} sec^{-1}, respectively, and the activation energies are 4.5 ± 1.0 and 6.8 ± 1.0 kcal/mol. The yield of electrons (G) decreases rapidly from 0.95 at $-5°$ to 0.05 at $-50°$. Our interpretation of the kinetics gives a reasonable explanation to this fact.

Introduction

The localized excess electron in the solid aqueous phase was first observed as a long-lived species in irradiated hydroxide–water glasses at 77°K.[1,2] In this matrix the electron is characterized by an esr singlet and an optical absorption band in the visible part of the spectrum.[3] The trap is supposed to be a hydroxide anion vacancy,[4] and the degree of structural disorder of the matrix was found to be of great importance for the trapping.[5-8]

Crystalline ice, on the other hand, would be expected to have a low concentration of defects suitable as electron traps and, since self-trapping as in liquid water would not be feasible due to the long dielectric relaxation time, it was at first believed that the electron could not be localized in this matrix. In spite of this the optical absorption spectrum of a transient electron was observed by pulse radiolysis of crystalline ice at temperatures not far from its melting point.[9,10] The absorption spectrum of this new species closely resembles that of the solvated electron in liquid water (e_{aq}^-). The yield is, however, less and the lifetime is shorter. The lifetime increases with decreasing temperature and the yield decreases rapidly.[11,12] At 77°K, at which the electron is stable, the yield (G) is only 2×10^{-4}.[13,14]

In the present investigation the study of the localized electron in crystalline ice has been extended to lower temperatures ($-190°$) and to D_2O ice. The temperature shift of the absorption peak has been recorded in both H_2O and D_2O ice. The temperature variation of the yield has also been studied, and the kinetics could be accounted for by a much simpler reaction scheme (with only one type of electrons) than that given

(1) D. Schulte-Frohlinde and K. Eiben, *Z. Naturforsch. A*, **17**, 445 (1962).

(2) J. Jortner and B. Sharf, *J. Chem. Phys.*, **37**, 2506 (1962).

(3) See, for example, the review articles by (a) L. Kevan in "Radiation Chemistry of Aqueous Systems," 19th L. Farkas Memorial Symposium, Hebrew University, Jerusalem, Dec 27–29 1967, G. Stein, Ed., Weizmann Science Press of Israel, Jerusalem, 1968, p 21; (b) D. Schulte-Frohlinde and K. Vacek in "Current Topics in Radiation Research," Vol. 5, M. Ebert and A. Howard, Ed., North-Holland Publishing Co., Amsterdam, 1969, p 39; (c) J. K. Thomas in "Advances in Radiation Chemistry," Vol. 1, M. Burton and J. L. Magee, Ed., Wiley-Interscience, New York, N. Y., 1969, p 103.

(4) M. J. Blandamer, L. Shields, and M. C. R. Symons, *Nature*, **199**, 902 (1963), and *J. Chem. Soc.*, 4352 (1964).

(5) T. Henriksen, *Radiat. Res.*, **23**, 63 (1964).

(6) K. Eiben and D. Schulte-Frohlinde, *Z. Phys. Chem. (Frankfurt am Main)*, **45**, 20 (1965).

(7) D. Schulte-Frohlinde in "Radiation Research," Third International Congress of Radiation Research, Cortina d'Ampezzo, June–July, 1966, G. Silini, Ed., North-Holland Publishing Co., Amsterdam, 1967, p 251.

(8) H. Barzynski and D. Schulte-Frohlinde, *Z. Naturforsch. A*, **22**, 2131 (1967).

(9) V. N. Shubin, V. I. Zhigunov, V. I. Zolotarevsky, and P. I. Dolin, *Nature*, **212**, 1002 (1966), and *Dokl. Akad. Nauk SSSR*, **174**, 416 (1967).

(10) G. Nilsson, H. C. Christensen, J. Fenger, P. Pagsberg, and S. O. Nielsen, Abstracts, Eight International Free Radical Symposium Novosibirsk USSR, 1967.

(11) G. Nilsson, H. C. Christensen, J. Fenger, P. Pagsberg, and S. O. Nielsen, *Advan. Chem. Ser.*, **No. 81**, 71 (1968).

(12) I. A. Taub and K. Eiben, *J. Chem. Phys.*, **49**, 2499 (1968).

(13) K. Eiben and I. A. Taub, *Nature*, **216**, 782 (1967).

(14) O. F. Khodzhaev, B. G. Ershov, and A. K. Pikaev. *Izv. Akad. Nauk SSSR, Ser. Khim.*, 246 (1968).

by Taub and Eiben.[12] In addition our interpretation of the kinetics gives a reasonable explanation to the rapid decrease in the yield when the temperature decreases.

Experimental Section

Large blocks of transparent ice were grown in a quartz tube from triply distilled H_2O or D_2O (D_2O 99.98%), which was degassed by shaking and evacuation. The degassing procedure included saturation of the water three times at a pressure of 1 atm with hydrogen or helium gas that had passed a liquid nitrogen cooled trap. The quartz tube, surrounded by a thermally controlled jacket and filled with the gas to 1 atm pressure, was then placed in a refrigerator, maintained at $-20°$, and the currents in the four heating coils of the jacket were adjusted in such a way that the freezing started at the water surface, proceeded down the tube axis and stopped about 20 mm from the bottom of the tube. Ice blocks, 70 mm long and 30 mm in diameter, were obtained in about 4 days. Examination of the blocks with polarized light showed that they generally consisted of a few large crystals oriented in different directions.

The blocks were stored at $-20°$ for several days, and before each run a 30-mm long sample was cut out from the middle section of a block with a hot platinum wire. The sample was heated to $-5°$, and its end faces were made plane with a smooth warm aluminum plate and polished with a filter paper. The sample was then quickly transferred to the cryostat, cooled to the desired temperature, and irradiated.

The cryostat loaded with an ice sample is shown in Figure 1. Cooling is achieved by a pulsed stream of liquid nitrogen, and an evacuated window cylinder and an electrically heated wire (not shown) are used to avoid frosting of the front window. Within the temperature range 0 to $-190°$ the temperature was regulated with a precision of $\pm 0.5°$ as measured by a small thermocouple in direct contact with the sample surface. This simple method of cryostating also proved useful for growing single crystals of organic compounds at subambient temperatures. The method for temperature regulation is therefore described elsewhere.[15]

The optical detection system is fully described elsewhere[16] and comprises the following principal optical and electronic components: an Osram XBO, 450-W high-pressure xenon lamp, a Zeiss MM12 double quartz prism monochromator, a dc-coupled EMI 9558 Q photomultiplier tube, and two Tektronix 555 double beam oscilloscopes equipped with Type W plug-in units.

Three of the oscilloscope beams were used to record the time profile of the transient in three different time scales. The fourth beam was used to record the time profile of the electron pulse, as monitored by the current induced in a coil surrounding the electron beam.

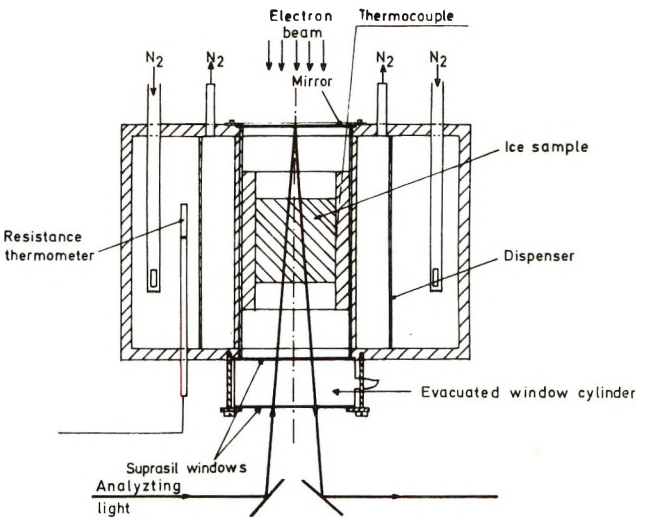

Figure 1. The cryostat and the light passage. The evacuated window cylinder and an electrically heated wire (not shown) are used to avoid frosting of the front window.

The oscilloscope traces were recorded on Type 3000 Polaroid film, enlarged four times and analyzed. The overall time constant of the detection channel was 80 nsec.

The cryostat was irradiated from the mirror end with single electron pulses from a Varian V-7700 linear accelerator equipped with a single-pulse trigger generator.[17] The peak current of the pulse was 250 mA, and the average energy was 11 MeV. The pulse length could be varied from 0.25 to 4 μsec.

The absolute dose was obtained from the recorded absorption trace of the hexacyanoferrate(III) ions ($\epsilon_{420\ nm} = 1000\ M^{-1}\ cm^{-1}$)[18] produced by the electron pulse in a polystyrene cell, replacing the ice sample, which was filled with N_2O-saturated, 1 mM hexacyanoferrate(II) solution. The cell had thin polystyrene windows and the same length as the ice sample. For relative dosimetry we utilized the time profiles of the electron pulses as recorded on the oscilloscope screen. The mean dose rate in the half of the sample facing the evacuated window cylinder was 20% less than the mean dose rate in the rear half. This inhomogeneity in dose rate along the sample axis was accounted for.

Results and Discussion

1. Spectra. The transient optical absorption spectrum of crystalline ice recorded after a single electron pulse is very similar, both in shape and position, to that caused by the solvated electron in liquid water. On this basis the absorption has been assigned to a localized excess electron e_s^-, in structure almost identical with

(15) T. Dahlgren, T. Gillbro, G. Nilsson, and A. Lund, *J. Sci. Instrum.*, **4**, 61 (1971).

(16) H. C. Christensen, G. Nilsson, P. Pagsberg, and S. O. Nielsen, *Rev. Sci. Instrum.*, **40**, 786 (1969).

(17) J. Fenger, *Nucl. Instrum. Methods*, **74**, 95 (1969).

(18) J. Rabani and M. S. Matheson, *J. Phys. Chem.*, **70**, 761 (1966).

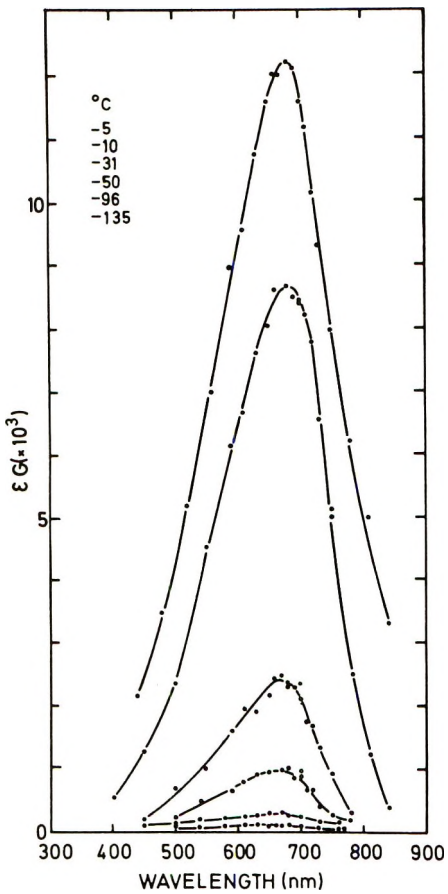

Figure 2. Absorption spectra of the electron in H_2O ice (ϵ, extinction coefficient). The temperatures are given in order of decreasing peak heights; dose 6×10^{17} eV/g; pulse length 2.6 μsec.

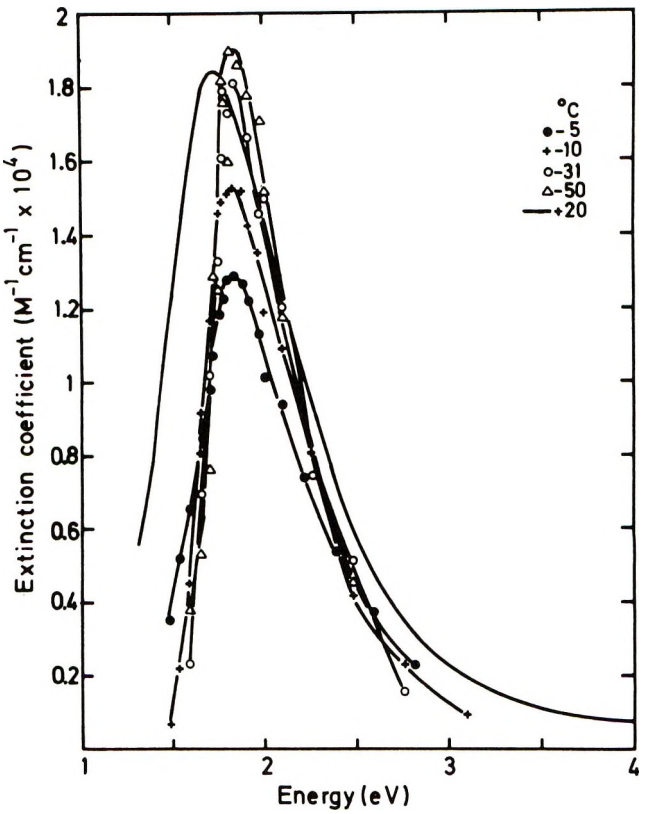

Figure 3. Absorption spectra of the electron in H_2O ice and the absorption spectrum of the solvated electron in liquid water.[22] The spectra for the electron in ice are calculated using an oscillator strength of 0.33.

e_{aq}^-.[9-12, 19] The spectra of the excess electron in H_2O ice recorded at different temperatures in the range -5 to $-135°$ are shown in Figure 2. All the spectra are broad bands with a single maximum and no structure. The peak height decreases with decreasing temperature, and the shapes of the spectra in general agree with those reported by Shubin, *et al.*,[9] and by Taub and Eiben.[12]

For electrons in the hydroxide–water glasses at 77°K the extinction coefficient, ϵ, is known, since the electron concentration can be measured by esr spectroscopy. A "best" value of $2.0 \times 10^4\ M^{-1}\ cm^{-1}$ for ϵ_{max}, differing very little from the value for water ($\epsilon_{max} = 1.85 \times 10^4\ M^{-1}\ cm^{-1}$),[20] has been reported.[21] For the transient electron in crystalline ice, on the other hand, the extinction coefficient is unknown. Its value can, however, be estimated if we presuppose a temperature-independent oscillator strength, f. The value of ϵ_{max} as calculated from the optical density is then found to increase very slowly with decreasing temperature below $-50°$, and by taking $f = 0.33$ the curve could be extrapolated to $\epsilon_{max} = 2.0 \times 10^4\ M^{-1}\ cm^{-1}$ at 77°K. We thus obtain a value of the oscillator strength for the electron in H_2O ice which is smaller than that for the electron in water ($f = 0.71$).[22] This is in agreement with the calculations of Fueki, *et al.*[23] It may also be pointed out that the treatment of f as temperature independent (as it is for F centers in alkali halides) is a reasonable approximation supported by the form of the theoretical expression for this quantity.[24]

By taking $f = 0.33$ the spectra shown in Figure 3 are obtained, which are thus based on a temperature-independent oscillator strength, and the value of ϵ_{max} for alkaline ice at 77°K. From this figure, which also shows the e_{aq}^- spectrum,[22] we conclude that the electron absorbs in the same spectral range in ice and water. The absorption peak is, however, shifted to a higher energy in ice and the half-width of the peak is smaller in the solid phase. All bands shown have a comparatively sharp low energy edge and a tail on the high energy side.

(19) B. G. Ershov and A. K. Pikaev, *Advan. Chem. Ser.*, **No. 81**, 1 (1968).

(20) E. M. Fielden and E. J. Hart, *Radiat. Res.*, **32**, 564 (1967).

(21) H. Hase and L. Kevan, *J. Chem. Phys.*, **54**, 908 (1971).

(22) E. J. Hart and M. Anbar, "The Hydrated Electron," Wiley-Interscience, New York, N. Y., 1970, p 40.

(23) K. Fueki, D.-F. Feng, and L. Kevan, *J. Phys. Chem.*, **74**, 1976 (1970).

(24) J. Jortner, S. A. Rice, and E. G. Wilson, "Solutions Metal-ammoniac. Colleque Weyl, Lille (1963)," G. Lepoutre and M. J. Sienko, Ed., W. A. Benjamin, New York, N. Y., 1964, p 245.

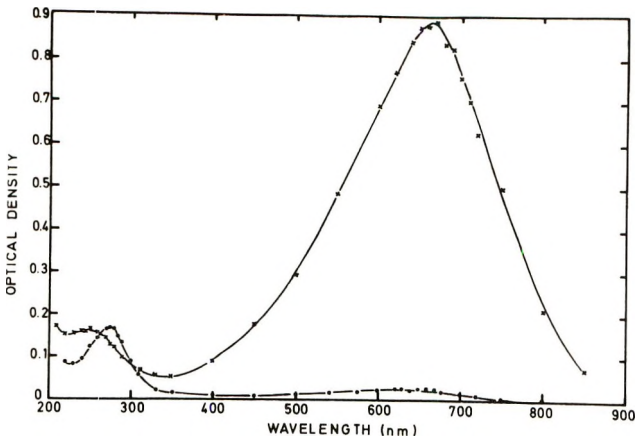

Figure 4. Absorption spectrum of the electron (broad peaks), the OD radical (275 nm) and the DO_2 radical (250 nm) at $-6°$ (×) and at $-101°$ (●); dose, 1.2×10^{18} eV/g; pulse length 3.0 μsec.

Raising the temperature broadens the band in ice (the half-width increases from 0.52 eV at $-50°$ to 0.70 eV at $-5°$) and shifts λ_{max} to longer wavelengths, which are properties common to the F center, e_{aq}^-, and $e_{NH_3}^-$.

The absorption of irradiated D_2O ice is very similar to that of H_2O ice. Overall spectra obtained at -6 and $-101°$ are shown in Figure 4. The broad absorption band is due to the electron. The absorption below 300 nm very much resembles that found by Taub and Eiben at -98 and $-14°$ in H_2O ice.[12] In accordance with these authors assignment of the 280-nm peak to the OH radical and the 230-nm peak to the HO_2 radical, we assign the 275-nm peak to the OD radical and the 250-nm peak to the DO_2 radical.

Figure 5 shows the absorption spectrum of the electron in D_2O ice at different temperatures from -6 to $-190°$. As seen from the figure the peak height at first decreases with decreasing temperature as in H_2O ice. Below $-100°$, however, it increases again (see also Figure 8). In the same way as in H_2O ice the band maximum is shifted to higher energy with decreasing temperature. At the same temperature, however, the absorption maximum is at a shorter wavelength in D_2O ice than in H_2O ice, which is clearly shown in Figure 6 for $-5°$, where the energy difference between the maxima is 0.04 eV.

All points in the spectra shown refer to minimum light transmission as read from the oscilloscope traces and the values of ϵG are corrected for the decay during the electron pulse. No displacement of the absorption peak during the lifetime of the transient was detected in the temperature range -10 to $-40°$; *i.e.*, the full trapping energy was developed within 0.25 μsec after the electron pulse.

2. The Temperature Shift of the Absorption Peak. The shift of the band maximum with temperature is shown in Figure 7. To avoid arbitrariness in the determination of λ_{max}, the midpoints of a number of horizontal lines cutting an absorption curve were connected, and the intersection between this line and the curve was taken as the maximum point. The errors indicated are estimated ones. The figure includes results of Gottschall and Hart for e_{aq}^- in liquid H_2O,[25] of Brown, *et al.*,[26] and Schindewolf, *et al.*,[27] for e_{aq}^- in liquid D_2O, and of Taub and Eiben for the trapped electron in H_2O ice.[12] As seen from the figure, the shift of the band maximum is nowhere a linear function of the temperature, as it is for e_{aq}^- in liquid water[25] and as it was reported by Taub and Eiben to be also for ice.[12] Instead the energy reaches a constant value at about $-130°$. The positions of the band maxima at the plateau are 1.90 eV for H_2O ice and 1.94 eV for D_2O ice. At $-10°$ the values are 1.82 ± 0.01 and 1.86 ± 0.01 eV, respectively. The energy difference is 0.04 eV throughout the whole temperature range, which can be compared with a difference of 0.05 eV for the liquids[27] and 0.12 eV for the 10 *M* alkaline–water glasses at 77°K.[6] At 0° the curve for the liquid phase fits smoothly to the curve

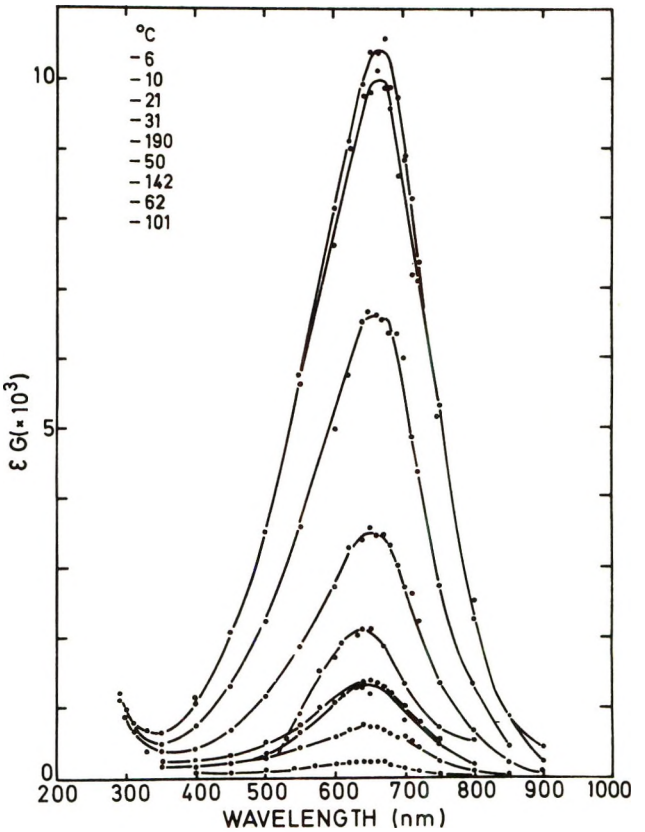

Figure 5. Absorption spectra of the electron in D_2O ice (ϵ, extinction coefficient). The temperatures are given in order of decreasing peak heights; dose $(1.1–1.2) \times 10^{18}$ eV/g; pulse length 2.7 to 3.0 μsec.

(25) W. C. Gottschall and E. J. Hart, *J. Phys. Chem.*, **71**, 2102 (1967).

(26) D. M. Brown, F. S. Dainton, J. P. Keene, and D. C. Walker, *Proc. Chem. Soc.*, 266 (1964).

(27) U. Schindewolf and R. Olinger, *Ber. Bunsenges. Phys. Chem.*, **72**, 1066 (1968).

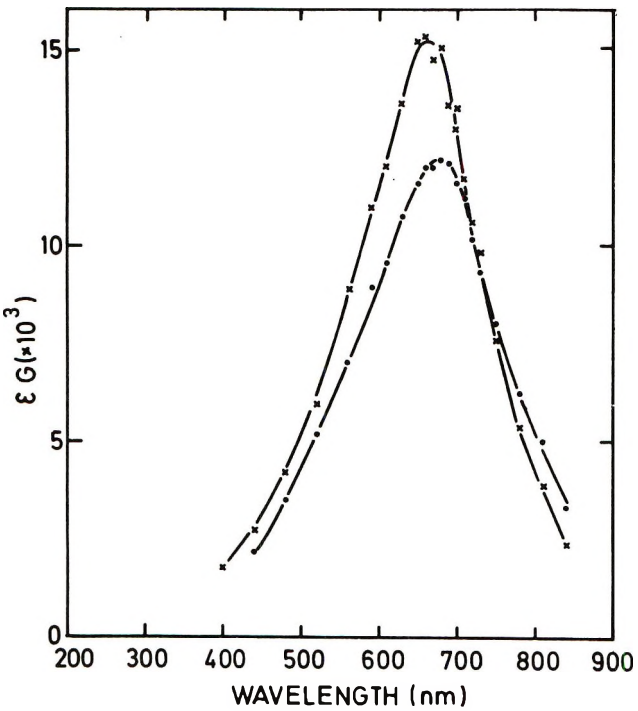

Figure 6. Absorption spectra of the electron in H_2O (●) and D_2O ice (×) at −5°; dose 6 × 10^{17} eV/g; pulse length 2.7 μsec.

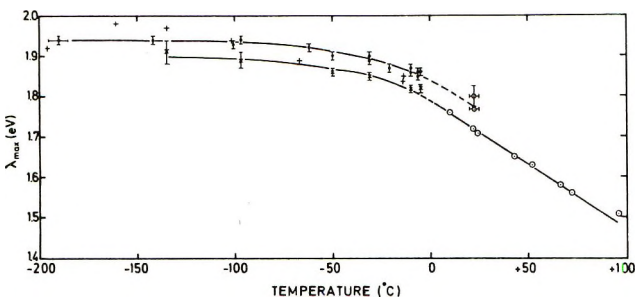

Figure 7. Temperature shift of the maximum of the absorption band of the electron in H_2O (✱) and D_2O ice (✱). The figure includes results of Gottschall and Hart for e_{aq}^- in liquid H_2O[25] (⊙), of Brown, *et al.*,[26] (⊢⊙⊣) and of Schindewolt, *et al.*,[27] (⊢○⊣) for e_{aq}^- in liquid D_2O and of Taub and Eiben[12] (+) for electrons in H_2O ice.

for the solid phase. The absence of a discontinuity at that point is a strong indication that the trapping mechanism is essentially the same in the two phases. It may also be pointed out that the temperature shift of λ_{max} as pictured in Figure 7 resembles very much the temperature shift of the optical absorption band of the F center. For both, λ_{max} reaches a limiting value at low temperatures.[28]

3. Yield and Kinetics. The product $\epsilon_{max}G$ (Figure 8) decreases with decreasing temperature, at first very fast, between −50 and −100° considerably slower, and finally it increases in D_2O ice at temperatures below −100°. The increase is due to a population of short-lived electrons which are not observed at the higher

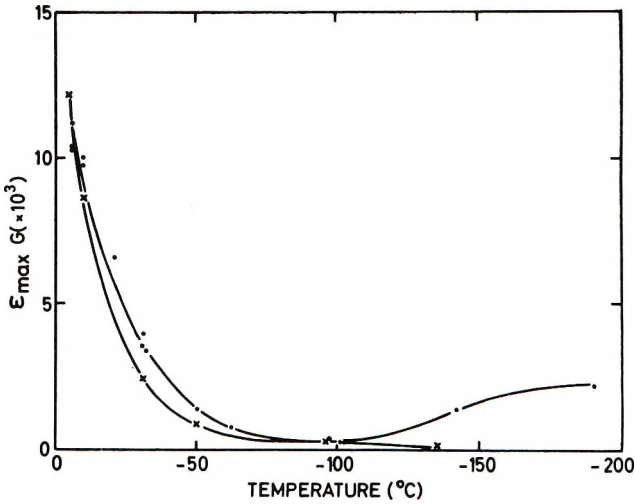

Figure 8. Temperature variation of the product of the extinction coefficient ϵ_{max} and G for the electron in H_2O (×) and D_2O ice (●).

temperatures. A similar increase would probably have been found also for H_2O ice if the measurements had been extended to still lower temperatures. This is corroborated by the fact that below −100° the decay becomes faster in H_2O ice. The slightly higher value of $\epsilon_{max}G$ for D_2O ice is in accordance with the behavior of e_{aq}^- in the liquid phases where there is an increase in both G (11%) and ϵ_{max} (28%) when passing from light to heavy water.[29]

On the basis of ϵ_{max} from Figure 3 the temperature variation of G for H_2O ice has been calculated. The results are shown in Table I. The large variation of G with temperature is remarkable since the yield in liquid water is almost independent of the temperature between +4 and +90°.[25]

Table I: The Temperature Variation of G for Localized Excess Electrons in H_2O Ice

Temp, °C	$\epsilon_{max}G$, M^{-1} cm^{-1} e_s^-/100 eV (× 10^3)	ϵ_{max}, M^{-1} cm^{-1} (× 10^4)	G, e_s^-/100 eV
−5	12.21	1.29	0.95
−10	8.66	1.53	0.57
−31	2.40	1.83	0.13
−50	0.91	1.90	0.05
−96	0.30	1.94[a]	0.02
−135	0.11	1.96[a]	0.01

[a] Extrapolated values.

The kinetic behavior of the electron in the temperature range −5 to −50° is characterized by increasing half-life with decreasing temperature (about ten times) and a longer half-life in D_2O ice than in H_2O ice (about

(28) J. J. Markham, *Solid State Phys.*, Suppl. 8, 1 (1966).
(29) E. M. Fielden and E. J. Hart, *Radiat. Res.*, **33**, 426 (1968).

two times). The kinetics can neither be fitted to a first- nor to a simpler second-order plot, and it is not a composite first-order decay, for if the optical density is divided by the dose the resulting curves are not superimposable. The decay and the yield are furthermore not affected by the total dose given to the sample. Most samples were therefore pulsed repeatedly.

At present there is no general agreement regarding the reaction order of the electron in crystalline ice. Taub and Eiben[12] characterized the kinetics as predominantly simple second order above $-14°$ and as first order in the temperature range -40 to $-70°$. To account for the change in rate law with temperature they postulate an equilibrium between immobile and mobile electrons and a reaction scheme where the immobile electrons react with mobile protons, giving rise to a second-order decay, and the mobile electrons react with OH and other radiation-produced species and give rise to a pseudo-first-order decay. Since there is a temperature-dependent competition between the two decay modes, the overall decay changes from mainly second order at $-14°$ to mainly first order at $-70°$. On the other hand, Pernikova, *et al.*,[30] studied the initial decay rate of the electron after the pulse and concluded that the kinetics could be accounted for by the parallel occurrence of a true monomolecular process and a sum of bimolecular reactions.

To gain some information about the kinetics from our data, different kinetic models were fitted to sets of decay curves obtained by varying the pulse length only. The fits were performed by a computer, and each experimental point (optical density) was weighted according to the relative standard deviation assigned to it. The dose inhomogeneity along the sample axis was taken into account by dividing the sample into two halves having a dose rate ratio of 1:0.8. The dose rate was also corrected, as it changed a little with the pulse length. The goodness of the fit as given by the standard deviation $\pm [\Sigma\Delta^2/(n - s)]^{1/2}$, where Δ is the difference between the experimental and computed values for each point, n the number of points, and s the number of parameters, was then used to select the best model for the electron decay.

Examination of our data showed that two decay curves for the electron have the characteristic feature of crossing each other if the decays start at different electron concentrations at the end of the electron pulse. This behavior is most simply explained by general second-order kinetics, the electron reacting with a species present in a concentration greater than its own. The reaction partner is very probably the proton and one plausible explanation to the electron deficiency may be that some electrons form dimers as they do in the hydroxide–water glasses[31] and probably also in water.[32-34] This would show up as an electron deficiency since the dimers, absorbing in the near-infrared part of the spectrum, are not defected by us. However, when testing a model with dimers, it was found that the rate constant for the reaction of the dimers with protons was almost zero, and the standard deviation of the rate constant was very large. The precision of the fit would thus not be less if the rate constant for the dimer reaction was put equal to zero. This was indeed the fact and the remaining equations

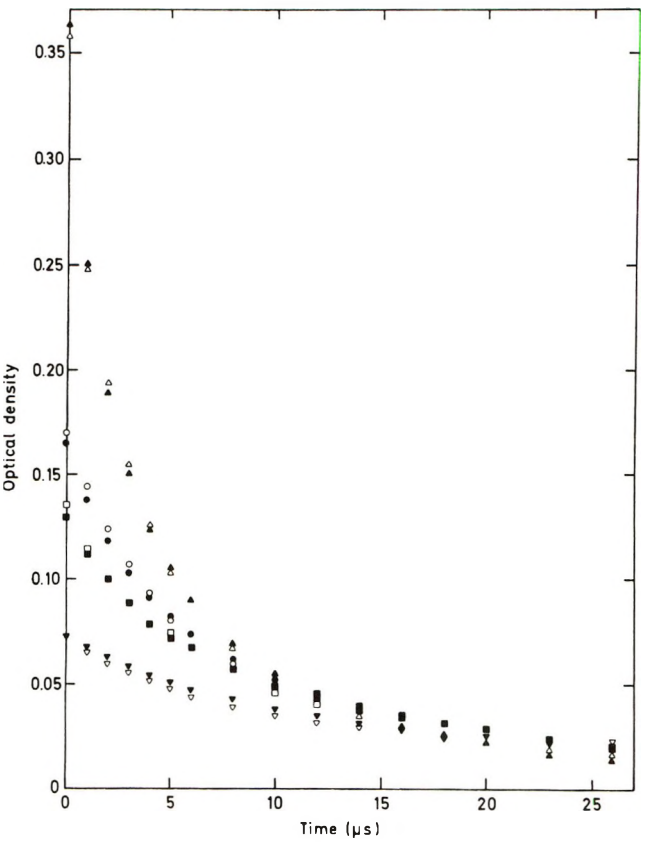

Figure 9. The fit of experimental data to the general second-order decay at $-10°$ for excess electrons in H_2O ice: unfilled symbols, experimental points; filled symbols, computed points. Pulse lengths: 1.79 (△,▲); 0.77 (○, ●); 0.68 (□, ■) and 0.42 μsec (▽, ▼).

$$de_s^-/dt = PG_{e_s^-} - ke_s^-H^+ \quad (1)$$

$$dH^+/dt = PG_{H^+} - ke_s^-H^+ \quad (2)$$

where P is the dose rate, G the yield, k (μ sec^{-1}) the rate constant, and e_s^- and H^+ are the optical densities of, respectively, localized electrons and protons, describe the kinetics very well, as can be seen from Figure 9. The computed curves cross each other and $G_{e_s^-}/G_{H^+}$, which is <1, decreases with the temperature (Figure 10).

(30) T. E. Pernikova, S. A. Kabakchi, V. N. Shubin, and P. I. Dolin, *Radiat. Effects*, **5**, 133 (1970).

(31) L. Kevan, D. R. Renneke, and R. J. Friauf, *Solid State Commun.*, **6**, 469 (1968).

(32) N. Basco, G. A. Kenney, and D. C. Walker, *Chem. Commun.*, **16**, 917 (1969).

(33) K. Fueki, *J. Chem. Phys.*, **50**, 5381 (1969).

(34) G. Czapski and E. Peled, *Chem. Commun.*, **20**, 1303 (1970).

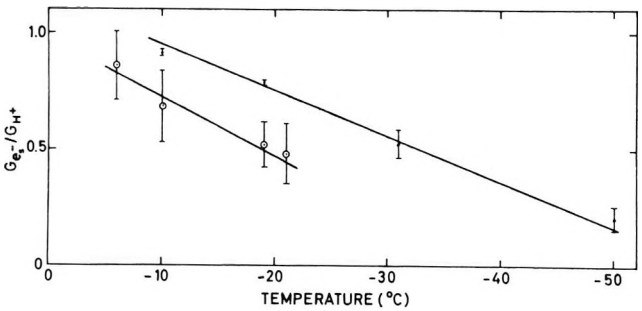

Figure 10. The computed temperature variation of G_e^-/G_{H^+} in H_2O (●) and D_2O ice (○).

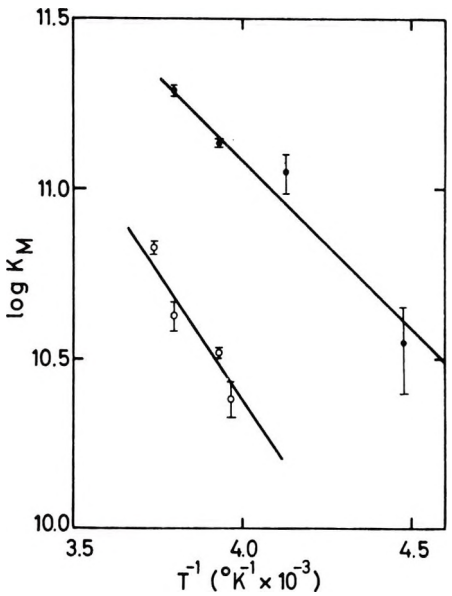

Figure 11. Arrhenius plots for the electron decay between −5 and −50° in H_2O (●) and D_2O ice (○).

The computed values of $G_{e_s^-}/G_{H^+}$ and k with their standard deviations are shown in Table II. The rate constants k_M (M^{-1} sec^{-1}) in Table II are for H_2O ice based on the extinction coefficients of Figure 3. For the optical absorption of the electron in D_2O ice ϵ_{max} was supposed to be higher by 28%.[29] The extinction coefficients and the activation energies E, which were obtained from Figure 11, are all given in Table II.

For −10° the model of Taub and Eiben (I) and Pernikova, *et al.* (II), fit our experimental decay curves with almost the same precision as the general second-order decay (III). The standard deviations of the rate constants of I at −10° and of II at −50° are, however, considerably larger than for III. If models I and III are compared, it is evident that the change of rate law with temperature, which in II is explained by a temperature-dependent competition between two decay modes, is inherent in the general second-order decay, since $G_{e_s^-}/G_{H^+}$ decreases with the temperature. The kinetics therefore looks like simple second order at high temperatures and becomes pseudo-first order at low temperatures, all in accordance with Taub and Eiben's observations.[12] The concept of equilibrium between two types of electrons, as proposed by Taub and Eiben,[12] is not required if the apparent rate law depends on the $G_{e_s^-}/G_{H^+}$ ratio in a general second-order decay.

Table II: The Computed Results of the General Second-Order Kinetics[a]

Sample	Temp, °C	$G_{e_s^-}/G_{H^+}$	k, μsec^{-1}	ϵ_{max}, M^{-1} cm^{-1} (× 10^4)	k_M, M^{-1} sec^{-1} (× 10^{11})	E, kcal/mol
H_2O ice	−10	0.913 ± 0.012	2.12 ± 0.06	1.53	1.95 ± 0.06	4.5 ± 1.0
	−19	0.784 ± 0.007	1.34 ± 0.02	1.70	1.37 ± 0.02	
	−31	0.512 ± 0.060	1.03 ± 0.15	1.83	1.13 ± 0.16	
	−50	0.190 ± 0.049	0.31 ± 0.09	1.90	0.35 ± 0.10	
D_2O ice	−6	0.860 ± 0.149	0.63 ± 0.03	1.76	0.67 ± 0.03	6.8 ± 1.0
	−10	0.680 ± 0.156	0.36 ± 0.03	1.96	0.42 ± 0.04	
	−19	0.515 ± 0.100	0.25 ± 0.01	2.18	0.33 ± 0.01	
	−21	0.475 ± 0.133	0.18 ± 0.02	2.20	0.24 ± 0.03	

[a] The standard deviation of the activation energy, E, is estimated. All other standard deviations are computed.

The decay of the electron in crystalline ice can apparently be accounted for in different ways. The simplest way is, however, by the general second-order kinetics (III), a model containing only two parameters, the rate constant and the $G_{e_s^-}/G_{H^+}$ ratio. Since the missing fraction of electronic charge, $(G_{H^+} - G_{e_s^-})/G_{H^+}$, increases with decreasing temperature, this model also provides us with an explanation of the remarkably rapid drop of the yield as the temperature decreases (Table I).

The fact that the two simple equations (1 and 2) account for the decay must imply that either the missing electrons are trapped as dielectrons or they are trapped in some other way; they do not react with the protons in either case. The OH radicals must therefore be of minor importance as electron traps, since the rate constant for the $H^+ + OH^-$ reaction is very large. It seems most likely that the missing electrons are to be found in shallow (unrelaxed) traps in the matrix. The presence of shallow traps near the conduction band has in fact been observed in irradiated alkaline ice.[35]

The rate constant for the $e_s^- + H^+$ reaction in O_2H ice at −10° based on $f = 0.33$ (1.95×10^{11} M^{-1} sec^{-1}, Table I) is greater than the rate constant for the same reaction in the liquid phase (2.06×10^{10} M^{-1} sec^{-1}),[36]

(35) I. Eisele and L. Kevan, *J. Chem. Phys.*, **53**, 1867 (1970).
(36) J. P. Keene, *Radiat. Res.*, **22**, 1 (1964).

which, on the other hand, is somewhat less than the diffusion-limited rate[37] as calculated from the Debye equation.[38]

Considering the high value of the rate constant one would expect that the $e_s^- + H^+$ reaction is diffusion controlled in ice. The reaction rate would then be determined by the proton mobility (which according to recent measurements is almost the same in water and ice[39,40]) since the electron mobility is so small compared to the proton mobility that it can be neglected. The activation energy measured by us for the $e_s^- + H^+$ reaction is, however, 4.5 ± 1.0 kcal/mol (Table II), while the activation energy for the proton mobility in ice is close to zero[41] and there is even some evidence that the mobility increases with decreasing temperature.[39] In view of this fact the reaction cannot be diffusion controlled but may instead take place in two steps

$$H^+ + e_s^- \rightleftarrows (H^+e_s^-) \xrightarrow{k_1} H \qquad (3)$$

where the electron in the intermediate complex $(H^+e_s^-)$ has the same optical absorption characteristics as e_s^-.

The first step of reaction 3 is fast and limited only by the proton mobility. This step can be represented by a diffusion-controlled equilibrium with equilibrium constant K as given by Fuoss.[42] The second step is slow and rate determining and can be represented by a first-order rate constant k_1. The experimental overall rate constant k_0 is then given by.

$$k_0 = k_1K = k_1\frac{4\pi N\sigma^3}{3000} \exp(-U(\sigma)/RT) \qquad (4)$$

where N is Avogadro's number, σ the reaction distance, R the gas constant, T the absolute temperature, and $U(\sigma)$ the potential energy of interaction. The potential is coulombic, and the interaction energy is therefore given by $U(\sigma) = -e^2/\epsilon_{eff}\sigma$, where e is the electronic charge and ϵ_{eff} the effective dielectric constant. The simplest explanation of the slow second step is that the proton is immobilized by two negative Bjerrum faults (L defects)[43] when it comes close to the electron site. The concentration of L defects is certainly high in this region due to the alignment of the water dipoles, and the immobilized proton cannot start diffusing again (or the electron cannot tunnel to the proton site) until a D defect arrives and annihilates one of the L defects attached to it. The time it has to wait is given by the dielectric relaxation time, τ. The first-order rate constant can therefore be replaced by $\tau^{-1} = A^{-1} \exp(-B/RT)$[44] and the overall rate constant becomes

$$k_0 = \frac{4\pi N\sigma^3}{3000A} \exp[(e^2/\epsilon_{eff}\sigma - B)/RT] \qquad (5)$$

where according to Table I, $k_0 = 1.95 \times 10^{11}\ M^{-1}\ sec^{-1}$ and $(e^2/\epsilon_{eff}\sigma - B) = -4.5$ kcal/mol. By substituting experimental values of A (5.3×10^{-16} sec)[44] and B (14.2 ± 0.2 kcal/mol)[45] we obtain $\sigma = 6.1$ Å and $\epsilon_{eff} = 5.6$. For $f = 0.71$ we have instead $k_M = k_0 = 4.18 \times 10^{11}\ M^{-1}\ sec^{-1}$, and a repeated calculation gives $\sigma = 7.8$ Å and $\epsilon_{eff} = 4.4$. The values of the reaction distances are plausible, and the values of the effective dielectric constants can be compared with that calculated from the Onsager–Dupuis equation[43]

$$(\epsilon_{eff})^{-1} = (z_iz_je^2)^{-1}[(z_ie + \varphi_iq) \times (z_je + \varphi_jq)/\epsilon_\infty + \varphi_i\varphi_jq^2/(\epsilon_0 - \epsilon_\infty)] \qquad (6)$$

where ϵ_0 and ϵ_∞ are the static and high frequency dielectric constants, respectively, z_i and z_j the ion valences and φ_i and φ_j the number of Bjerrum faults of charge q attached to each ion. The proton is always screened by one L defect[43] of effective mean charge $0.53e$.[46] We therefore take $\varphi_{H^+}q = -0.53e$ and for the effective mean charge of the electron $(-e + \varphi_{e_s^-}q)$ the full charge may be taken. Then with $\epsilon_0 = 95$ and $\epsilon_\infty = 3.1$ the value of ϵ_{eff} becomes 6.6. Accordingly the two-step treatment of the $e_s^- + H^+$ reaction in H_2O ice gives plausible values of both the reaction distance and the effective dielectric constant.

As already pointed out the decrease of the yield with decreasing temperature, as shown by Table I, is remarkable since it does not agree with the theory for the motion of thermalized electrons in polar media. This motion is governed simultaneously by diffusion and coulomb attraction to the positive charge. Some electrons are therefore recaptured by the positive charge, and some escape charge neutralization. Onsager[47] showed that in the case of a nonpolar gas the escape probability for ions is simply given by the reciprocal of the Bolzmann factor with respect to the initial potential energy or

$$p = \exp(-e^2/\epsilon_ir_0\kappa T) \qquad (7)$$

where r_0 is the initial distance between the ions, ϵ_i a dielectric constant, and κ the Bolzmann constant. The escape probability for ions in condensed polar

(37) M. S. Matheson, *Advan. Chem. Ser.*, **No. 50**, 45 (1965).

(38) P. Debye, *Trans. Electrochem. Soc.*, **82**, 265 (1942).

(39) B. Bullemer, H. Engelhardt and N. Riehl in "Physics of Ice," International Symposium, Munich, Sept 9–14, 1968, N. Riehl, B. Bullemer, and H. Engelhardt, Ed., Plenum Publishing Co., New York, N. Y., 1969, p 416.

(40) M. A. Maidique, A. von Hippel, and W. B. Westphal, *J. Chem. Phys.*, **54**, 150 (1971).

(41) M. Eigen, L. De Maeyer, and H.-Ch. Spatz, *Ber. Bunsenges. Phys. Chem.*, **68**, 19 (1964).

(42) R. M. Fuoss, *J. Amer. Chem. Soc.*, **80**, 5059 (1958).

(43) L. Onsager and M. Dupuis, Electrolytes, International Symposium Trieste 1959, Proceedings, Pergamon Press, Oxford, 1962, p 27.

(44) R. P. Auty and R. H. Cole, *J. Chem. Phys.*, **20**, 1309 (1952).

(45) R. Ruepp and M. Käss in "Physics of Ice," International Symposium Munich, Sept 9–14, 1968, N. Riehl, B. Bullemer, and H. Engelhardt, Ed., Plenum Publishing Co., New York, N. Y., 1969, p 555.

(46) C. Jaccard, *Phys. Kondens. Mater.*, **3**, 99 (1964).

(47) L. Onsager, *Phys. Rev.*, **54**, 554 (1938).

media was calculated by Mozumder,[48] and he arrived at an expression which for very long and very short dielectric relaxation times reduces to the simple Onsager formula.

Since the yield of escaped electrons may reasonably be identified with their radiation chemical yield, Mozumder[48] calcuated the thermalization length of electrons in water by matching the computed escape probability with G/G_i, where G is the experimental radiolytic yield of solvated electrons (G value) and G_i the ionization yield. By taking $G_i = 5$ the thermalization length was found to increase from 19.5 Å at 100° to 35 Å at 0°. This is to be expected since at the lower temperature the electrons have to lose more energy to become thermalized and the travel distance must be longer.

For ice we get a quite different result. In this case the relaxation time is very long and Mozumder's equation reduces to the Onsager formula. Taking $\epsilon_i = \epsilon_\infty = 3.1$, $G_i = 5$, and G from Table I the thermalization length in H_2O ice decreases from 94 Å at −10° to 52 Å at −50°. A similar result was found by Mozumder[48] when using yields reported by Taub and Eiben.[12] The reason for this unexpected behavior is that for ice the radiolytic yield cannot simply be identified with the yield of escaped electrons. The general second-order kinetics has shown that the observed electrons are only a fraction of the total escaped electronic charge, and this fraction steadily decreases as the temperature becomes lower (Figure 10). The yield of escaped electrons which is the quantity to be used in eq 7, therefore, decreases less quickly than the radiation chemical yield as given by Table I. If we take this into account and recalculate r_0 from the yield of escaped electrons, *i.e.*, from $G \times G_{H^+}/G_{e_s^-}$, where $G_{H^+}/G_{e_s^-}$ is taken from Figure 10, the thermalization length decreases from 96 Å at −10° to 90 Å at −50°. Taking into consideration that the precision of $G_{H^+}/G_{e_s^-}$ is not so good, the result, despite the absence of increase of r_0, is reasonable and the kinetics thus provides us with an explanation for the rapid decrease of the G value when the temperature decreases.

Acknowledgments. The authors wish to thank the operator staff of the accelerator at Risö for skillful assistance, Mr. T. Dahlgren for valuable help in preparing the ice samples, and Mr. C. Lissing for programming the computer. We also gratefully acknowledge the financial support of The Swedish Atomic Research Council.

(48) A. Mozumder, *J. Chem. Phys.*, **50**, 3153 (1969).

Electron Spin Resonance of X-Irradiated Heptanal Trapped in a Single Crystal of Perhydrotriphenylene[1a]

by Zofia Ciecierska-Tworek,[1b] G. Bruce Birrell,[1c] and O. Hayes Griffith*

Institute of Molecular Biology and Department of Chemistry, University of Oregon, Eugene, Oregon 97403
(Received October 28, 1971)

Publication costs assisted by the National Science Foundation

Free radicals trapped in X-irradiated heptanal oriented in a single crystal of perhydrotriphenylene were investigated using electron spin resonance techniques. An analysis of the data indicates the presence of two free radicals: a short-lived radical, $CH_3(CH_2)_4\dot{C}HCHO$, and a stable semidione radical, $CH_3(CH_2)_5\dot{C}OHCO(CH_2)_5CH_3$. All spectra are well resolved and agree with computer-simulated spectra. A table of proton coupling constants and g values is given.

I. Introduction

Interest in radiation-produced free radicals in organic molecules has led to numerous studies of aliphatic acids[2,3] and esters,[4] ketones,[5] and alcohols.[6,7] However, progress on aliphatic aldehydes has been limited to frozen glasses of short-chain aldehydes including formaldehyde[8,9] and acetaldehyde.[10,11] However, because the aldehyde molecules are randomly oriented in these rigid glasses, esr spectra of the resulting radicals

(1) (a) This work was supported by the National Science Foundation under Grant No. GP-16341; (b) Fulbright-Hays Exchange Scholar; (c) NIH Postdoctoral Fellow (Fellowship No. 5 FO3-CA42789-02) from the National Cancer Institute.

(2) J. R. Morton, *Chem. Rev.*, **64**, 453 (1964).

Table I: Hyperfine Coupling Constants and g Values for Heptanal Radicals Trapped in Perhydrotriphenylene Inclusion Crystals[a]

Radical	Coupling constants and g values[b]	
Short-lived radical	(1) $a_z^H = 28.0 \pm 0.3$ G (2) $a_z^H = 19.0 \pm 0.3$ G $g_z = 2.0045 \pm 0.0002$	(1) $a_{xy}^H = 14.5 \pm 0.3$ G (2) $a_{xy}^H = 18.0 \pm 0.3$ G $g_{xy} = 2.0042 \pm 0.0002$
Stable radical	(4) $a_z^H = 9.5 \pm 0.4$ G $g_z = 2.0046 \pm 0.0002$	(1) $a_{xy}^H = 2.9 \pm 0.1$ G (2) $a_{xy}^H = 9.7 \pm 0.1$ G (2) $a_{xy}^H = 9.9 \pm 0.1$ G $g_{xy} = 2.0042 \pm 0.0002$

[a] The numbers in parentheses represent the number of protons with a given coupling constant. z and xy indicate the crystal orientation with respect to the magnetic field. [b] Relative to DPPH ($g = 2.0036$).

are necessarily poorly resolved, making an accurate assignment difficult. To date no studies of aldehyde radicals in an oriented matrix have been reported. The purpose of this paper is to report a study of radicals from X-irradiated heptanal, $CH_3(CH_2)_5CHO$, trapped in a single crystal of *trans-anti-trans-anti-trans*-perhydrotriphenylene (PHTP). It has been shown by Farina, Allegra, and Natta[12] that PHTP is capable of forming inclusion compounds with a large variety of guest molecules. Long-chain hydrocarbon molecules, trapped in the tubular cavities of the hexagonal PHTP crystals, are oriented with the long molecular axis of the guest molecule parallel to the crystalline needle axis. PHTP is a suitable host for the otherwise transient free radicals because all trapped molecules are magnetically equivalent.[13] Radical lifetimes vary but are generally several minutes to several days at room temperature.

II. Experimental Section

Single crystals of the heptanal–PHTP inclusion compound were prepared in the following way: 30–35 mg of PHTP (synthesized according to the method of Farina[14]) was dissolved in 1 ml of freshly distilled heptanal (Aldrich) in a tightly stoppered vial. The resulting solution was then cooled from 313 to 281°K over a period of 2 days in a 600-ml Dewar containing 400 ml of water. The z axis was defined to lie along the needle axis of the hexagonal crystal and the xy plane was chosen to be perpendicular to the z axis. Crystals were irradiated for 2 hr with a GE XRD-5 tungsten target X-ray tube operated at 40 kV and 20 mA. Spectra were recorded on a Varian E-3 esr spectrometer. Spectral simulations were performed on a Varian 620/i computer.

III. Results and Discussion

A. The Hydrogen Abstraction Radical. When heptanal–PHTP inclusion crystals were irradiated at 77°K, resulting esr spectra indicated the presence of one prominent short-lived radical. Less intense spectral lines belonging to other radicals were also present. The room temperature esr spectrum of the short-lived radical recorded with the magnetic field perpendicular to the crystalline z axis is shown in Figure 1a; Figure 1b is the computer simulation. The esr spectra of the short-lived radical result from two large isotropic proton coupling constants and one anisotropic proton coupling constant. Coupling constants and g values for this radical recorded at the major crystalline orientations are indicated in Table I.

An estimate of the isotropic component, a_0^α, of the anisotropic α-proton coupling constant can be obtained from the relation[4]

$$a_0^\alpha = (1/3)(2a_{xy}^\alpha + a_z^\alpha) \quad (1)$$

where a_{xy}^α and a_z^α are the values of the α-proton coupling constant measured with the magnetic field direction in the xy plane and parallel to the z axis, respectively. Using eq 1 and the data of Table I, $a_0^\alpha = 19.0$ G. Similarly the isotropic g value, g_0, can be obtained from the relationship[4]

$$g_0 = (1/3)(2g_{xy} + g_z) \quad (2)$$

Employing eq 2 and the data of Table I, $g_0 = 2.0043$.

These coupling constant data clearly suggest a radical having a large π-electron spin density on the α-carbon atom. The most logical choices are the radicals $R\dot{C}HOH$ or $R\dot{C}HCOR'$. However, the values of a_0^α and g_0 are substantially higher than would be expected

(3) D. Kivelson and C. Thomson, *Ann. Rev. Phys. Chem.*, **15**, 197 (1964).
(4) O. H. Griffith, *J. Chem. Phys.*, **41**, 1093 (1964).
(5) O. H. Griffith, *ibid.*, **42**, 2644 (1965).
(6) P. J. Sullivan and W. S. Koski, *J. Amer. Chem. Soc.*, **85**, 384 (1963).
(7) G. B. Birrell and O. H. Griffith, *J. Phys. Chem.*, **75**, 3489 (1971).
(8) J. A. Brivati, N. Keen, and M. C. R. Symons, *J. Chem. Soc.*, 237 (1962).
(9) F. J. Adrian, E. L. Cochran, and V. A. Bowers, *J. Chem. Phys.*, **36**, 1661 (1962).
(10) C. Chachaty and R. Marx, *J. Chim. Phys.* **58**, 787 (1961).
(11) V. I. Smirnova, G. S. Zhuravleva, K. G. Yanova, and D. N. Shigorin, *Zh. Fiz. Khim.*, **38**, 742 (1964).
(12) M. Farina, G. Allegra, and G. Natta, *J. Amer. Chem. Soc.*, **86**, 516 (1964).
(13) O. H. Griffith, *Proc. Nat. Acad. Sci. U. S.*, **54**, 1296 (1965).
(14) M. Farina, *Tetrahedron Lett.*, **30**, 2097 (1963).

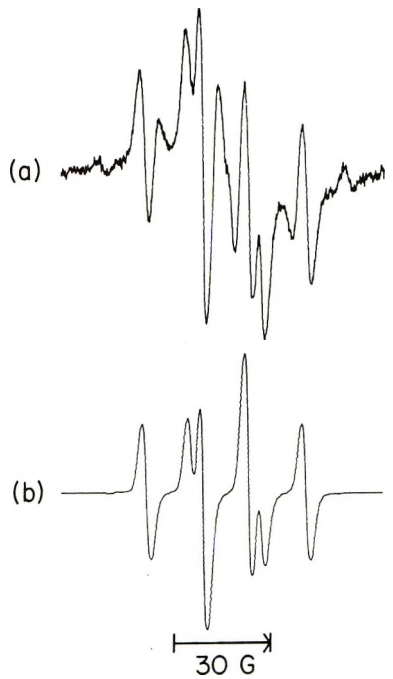

Figure 1. Experimental (a) and computer simulated (b) esr spectra of the short-lived radical from an X-irradiated heptanal–perhydrotriphenylene inclusion crystal. The experimental spectrum was recorded at room temperature with the magnetic field perpendicular to the crystalline z axis. Coupling constants used in the simulation were a^H = 18.0 G (two protons) and a^H = 14.5 G (one proton).

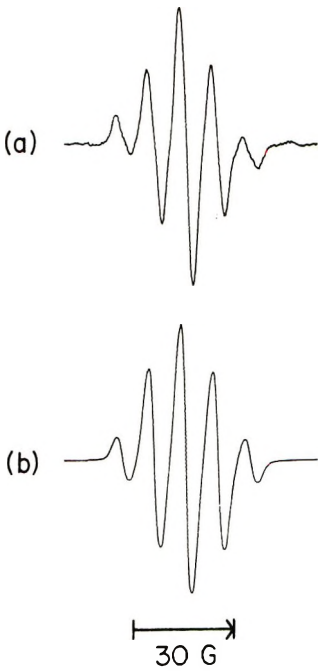

Figure 2. Experimental (a) and simulated (b) esr spectra of the stable free radical from an X-irradiated heptanal–perhydrotriphenylene inclusion crystal. The experimental spectrum was recorded at room temperature with the magnetic field parallel to the crystalline z axis. The simulation was performed on a Varian 620/i computer using the coupling constants of Table I.

from an alcohol radical, RĊHOH. For example, Zeldes and Livingston[15] observed a free radical formed in the solution photolysis of acetaldehyde which they identified as $CH_3\dot{C}HOH$ with a_0^α = 15.22 G, a_0^β = 22.11 G, and g_0 = 2.0032. Similarly, Dixon and Norman[16] examined the free radical produced by the reaction of ethanol with ·OH in acidic solutions of $TiCl_3$–H_2O_2 and found that the $CH_3\dot{C}HOH$ radical was formed with a_0^α = 15.0 G and a_0^β = 22.0 G. In addition, Birrell and Griffith[7] studied the radicals formed in X-irradiated long-chain alcohols trapped in single crystals of urea and reported the predominant species to be RĊHOH, with a_0^α = 14.4 G, a_0^β = 20.8 G, and g_0 = 2.0031.

The data of Table I, however, are reminiscent of the a_0^α of 18.5 G and g_0 of 2.0041 obtained for a variety of aliphatic ketone radicals, RĊHCOR′, in X-irradiated urea inclusion compounds,[5] which are derived from the parent hydrocarbon by abstraction of a hydrogen atom from the carbon adjacent to the carbonyl group. Based on these similarities in a_0^α and g_0, we conclude that the short-lived radical formed by X-irradiating heptanal at 77°K is

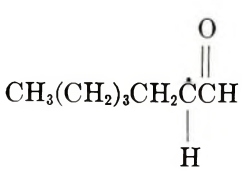

A similar radical, $\dot{C}H_2CHO$, was observed by Livingston and Zeldes[17] during the solution photolysis of ethylene glycol. The coupling constants reported by Livingston and Zeldes were a_0^H = 19.2 G, a_0^H = 18.7 G, and a_0^H = 0.5 G; g_0 = 2.0046. A small splitting of the order of 0.5 G would be effectively obscured in the 2–3-G line width of the heptanal spectra.

B. The Semidione Radical. At room temperature, spectral lines belonging to the short-lived radical from heptanal–PHTP rapidly disappeared, leaving the esr spectrum of a second radical,[18] as shown in Figures 2 and 3. Figures 2a and 3a are experimental spectra recorded at room temperature with the magnetic field along the crystalline z axis and in the xy plane, respectively; Figures 2b and 3b are the respective simulations. The spectra result from four isotropic and nearly equivalent proton coupling constants (of 9.5–10 G), which are further split by one small (~3 G) proton coupling constant when the magnetic field is in the crystalline xy plane. The second radical was stable for several weeks at room temperature. Similar spectra

(15) H. Zeldes and R. Livingston, *J. Chem. Phys.*, **47**, 1465 (1967).

(16) W. T. Dixon and R. O. C. Norman, *J. Chem. Soc.*, 3119 (1963).

(17) R. Livingston and H. Zeldes, *J. Amer. Chem. Soc.*, **88**, 4333 (1966).

(18) Although it is possible that the short-lived radical is the precursor of the second radical, it was not possible to verify this in the present study. Both of these radicals, of course, are relatively stable and are not necessarily the initially formed species.

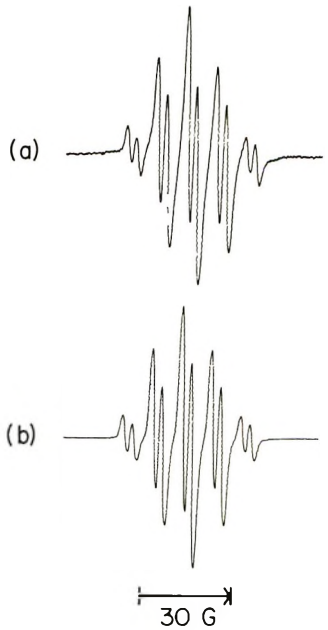

Figure 3. Experimental (a) and simulated (b) esr spectra of the stable free radical from an X-irradiated heptanal–perhydrotriphenylene inclusion crystal. The experimental spectrum was recorded at room temperature with the magnetic field in the crystalline *xy* plane. The simulation was performed on a Varian 620/i computer using the data of Table I.

were obtained from X-irradiated butyraldehyde–PHTP inclusion crystals and also by subjecting a fresh (non-irradiated) butyraldehyde–PHTP inclusion crystal to uv light from a PEK 110-W mercury lamp for 12 hr. Coupling constants and g values for the second radical observed in heptanal–PHTP recorded at the principal crystalline orientations are indicated in Table I.

The essential features of the spectra are the relatively small coupling constants, suggesting a delocalized spin distribution. This can best be explained by the formation of a bimolecular reaction product of the type $RCH_2\dot{C}OHCOCH_2R$ where R is $(CH_2)_4CH_3$. For example, a hybrid of the structures

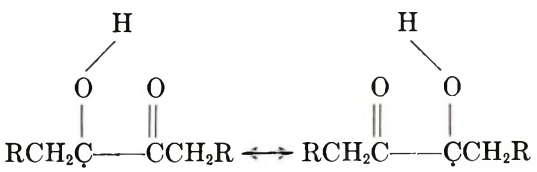

accounts for the esr data. Another explanation would be rapid proton exchange between two radicals of the type

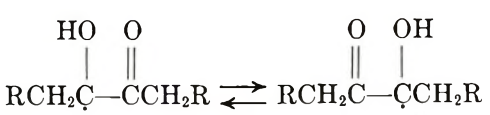

The available data, including a limited low temperature study, do not distinguish between these two possibilities.

An INDO[19] calculation was performed on the free-radical geometry

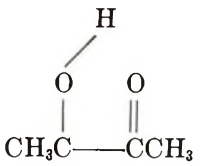

using as bond lengths R_{C-H} = 1.08 Å, R_{C-O} = 1.32 Å, R_{C-C} = 1.46 Å, and R_{O-H} = 1.82 Å and bond angles ∠HCH = 109.5°, ∠CCO = 120°, and ∠COH = 100°. For this calculation we assumed a dihedral angle of 60°, between the axis of the 2p orbital with unpaired spin density and the projection of the C–H_β bond onto a plane perpendicular to the C–C bond. (A dihedral angle of 60° is not unusual for molecules trapped in PHTP inclusion crystals.[20]) As calculated by the INDO method, the two out-of-plane methyl proton coupling constants are 7.3 G, in reasonably good agreement with the experimental results.

In a related study Norman and Pritchett[21] obtained a_{CH_3} = 8.3 G (six protons) and g_0 = 2.0044 for the radical formed in the one electron reduction of biacetyl, $CH_3COCOCH_3$, at pH = 0.5 using the $TiCl_3$–H_2O_2 system. Norman and Pritchett[21] concluded that their spectra were due to the monoprotonated semidione radical. This free radical evidently exists in the tautomeric forms

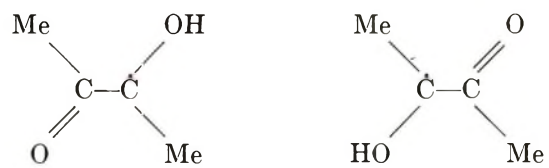

with the rate of interconversion of the tautomers varying with pH. Rates of interconversion were postulated to be rapid at pH 0.5 (resulting in the two sets of methyl proton coupling constants being equivalent) and diminishing as the pH was raised (with a resulting non-equivalence of the two sets of methyl proton coupling constants). Differences in coupling constants were also noted for the cis–trans isomers of these tautomers.[21] It is interesting to note that in the photolysis of acetaldehyde in *tert*-butyl alcohol,[15] the acetoin radical, $CH_3\dot{C}OHCOCH_3$, with $a_{CH_3}^{H}$ of 13.57 G (three protons), $a_{CH_3}^{H}$ of 2.44 G (three protons), and a^H of 1.97 G (one proton) was the only species identified. In this case, therefore, rapid proton exchange did not occur.

(19) J. A. Pople, D. L. Beveridge, and P. A. Dobash, *J. Amer. Chem. Soc.*, **90**, 4201 (1968); a copy of this program (program 141) was obtained from the Quantum Chemistry Program Exchange, Indiana University, 1969.

(20) G. B. Birrell, A. A. Lai, and O. H. Griffith, *J. Chem. Phys.*, **54**, 1630 (1971).

(21) R. O. C. Norman and R. J. Pritchett, *J. Chem. Soc. B*, 3119 (1967).

These solution studies, then, are consistent with the single crystal results of this paper and serve to point out the remarkable variety of conditions under which the semidione radical can be observed.

Ion Pairing in Alkali Metal Durosemiquinone Solutions

by Robert D. Allendoerfer* and Richard J. Papez

Department of Chemistry, State University of New York at Buffalo, Buffalo, New York 14214
(Received September 29, 1971)

Publication costs assisted by the Petroleum Research Fund

The esr spectra of Li^+, Na^+, K^+, Rb^+, Cs^+, and $TNBA^+$ durosemiquinone in DME solution are reported and precise values of the g values and hyperfine splitting constants given. An equilibrium between a contact ion pair and the free ion is observed for Na, K, Rb, and Cs, and the thermodynamic parameters characterizing this equilibrium are measured. These data are combined with the known rates of intramolecular ion exchange for the tight ion pairs to give a more complete description of the mechanism of ion exchange.

Introduction

Since the first electron spin resonance experiment with a *p*-benzosemiquinone radical,[1] dozens of papers have appeared describing the details of the esr spectra obtained. From these compounds, two effects have been of particular interest: first, the tendency of these ions to show an alternation in line width in their spectra, caused by rapid exchange of the counterion between positions adjacent to the one of the two carbonyl groups; and second, the formation of various types of ion pairs, which give rise to hyperfine couplings with the counterion and distortions of the symmetry of the semiquinone ion. These effects are particularly pronounced in ethereal solutions. Our study is restricted to 1,2-dimethoxyethane (DME) solution in an effort to reduce the problem to feasible proportions. The semiquinone ions have been studied in this solvent by several groups, principally those of Symons,[2] Warhurst,[3] Gough,[4] and Das[5] and their coworkers. These references and those contained therein, while not intended to be complete, should provide an adequate introduction to this complex field.

While numerous papers have been written about durosemiquinone and related compounds, they have not received the detailed analysis accorded the alkali metal naphthalenide system with respect to the nature of the ion pairs formed in solution, probably because the semiquinone esr spectra are much more complex. The simultaneous observation of contact ion pairs, solvent-separated ion pairs, and free ions was first reported by Hirota[6] for the sodium naphthalenide system and has since been studied by several workers. Recently, precise determinations of the kinetic and thermodynamic parameters involved have been made by Szwarc, *et al.*, for the naphthalene ion pair equilibria,[7] and the temperature and solvent dependences of the g and various hyperfine coupling values have been determined by Dodson and Reddoch[8] and by Fraenkel, *et al.*[9]

In this paper, we have applied the precise techniques used above to the durosemiquinone ion ($DSQ\cdot^-$) in DME solution to determine the thermodynamic parameters for the various equilibria involved and also tried to correlate the trends in g and hyperfine coupling values with current concepts of the nature of the ion pairs in these solutions.

Experimental Section

The alkali metal durosemiquinone ion pairs were prepared using the standard *in vacuo* reduction technique[10]

(1) B. Venkataramen and G. K. Fraenkel, *J. Amer. Chem. Soc.*, **77**, 2707 (1955).

(2) J. Oakes and M. C. R. Symons, *Trans. Faraday Soc.*, **66**, 10 (1970).

(3) D. H. Chen, E. Warhurst, and A. M. Wilde, *ibid.*, **63**, 2561 (1967).

(4) (a) P. S. Gill and T. E. Gough, *ibid.*, **64**, 1997 (1968); (b) T. E. Gough and P. R. Hindle, *Can. J. Chem.*, **49**, 2412 (1971).

(5) M. P. Khakhar, B. S. Prabhananda, and M. R. Das, *J. Amer. Chem. Soc.*, **89**, 3100 (1967).

(6) N. Hirota, *J. Phys. Chem.*, **71**, 139 (1967).

(7) K. Höfelmann, J. Jagur-Grodzinski, and M. Szwarc, *J. Amer. Chem. Soc.*, **91**, 4645 (1969).

(8) C. L. Dodson and A. H. Reddoch, *J. Chem. Phys.*, **48**, 3226 (1968).

(9) W. G. Williams, R. J. Pritchett, and G. K. Fraenkel, *ibid.*, **52**, 5584 (1970).

(10) D. E. Paul, D. Lipkin, and S. I. Weissman, *J. Amer. Chem. Soc.*, **78**, 116 (1956).

in 1,2-dimethoxyethane solution. Duroquinone was obtained from the Aldrich Chemical Company, Inc., and sublimed (mp 112°) before use. The sodium, rubidium, and cesium metal mirrors were obtained by decomposition of the appropriate metal azide, obtained from Matheson Coleman and Bell, Inc., under vacuum. The metal thus obtained was then distilled to remove any organic products of the decomposition. The metal azides were used as the source of the alkali metal not only for convenience and safety, but also to provide a mirror free from contamination by other alkali metals. The azides are much easier to purify than the metals themselves. Freshly cut potassium metal was simply introduced into the apparatus and distilled under vacuum. Lithium wire was cleaned in ethanol and introduced rapidly into the apparatus, where it was allowed to react without further purification. To avoid contamination of the sodium and potassium ion pairs with K^+ and Na^+ ions leached from the Pyrex apparatus used in the distillation, the apparatus was soaked in cleaning solution prepared with sodium or potassium dichromate in the hope of removing the undesired surface ions by ion exchange. Using these procedures, we have not observed any effects such as those described by Tuttle, *et al.*,[11] which can be ascribed to the presence of cationic impurities. The "electrolytic" durosemiquinone ion was produced by two electrode *in situ* electrolysis using tetra-*n*-butylammonium perchlorate as supporting electrolyte.

The esr spectra were obtained on a Varian V-4502 epr spectrometer equipped with the V-4540 temperature controller. Temperatures were measured with a Cu–constantan thermocouple. For intensity comparisons, the required double integration of the spectra was accomplished by digitizing the spectra with a Digital Equipment Corp. PDP-8 computer and performing the numerical integration on the CDC-6400, where drift and base line corrections were more readily programmed into the calculation. The g values were measured using a Magnion G-502 gaussmeter and a Hewlett-Packard 4245L frequency counter equipped with a 5255A frequency converter to measure the microwave frequency. The measurements were made by adjusting the magnetic field until it was stationary at the first-derivative zero of the appropriate esr line and then adjusting the gaussmeter nmr frequency until the first-derivative nmr signal was nulled. Then, the radio and microwave frequencies (ν_p and ν_e) were read as rapidly as possible. Several gaussmeter probe positions were used for each measurement to assess the Z magnetic field gradient and the appropriate correction applied. The g values were calculated from the equation $g = \kappa\nu_e/\nu_p$,[12] using $\kappa = 3.041893 \times 10^{-3}$.[13] Using this technique, we can readily reproduce several of the g values reported by Segal, *et al.*,[12] to within 5 ppm. The second-order shift correction for durosemiquinone has been neglected, since it is only 1 ppm.[12] The endor spectra were obtained by modifying the V-4502 epr spectrometer as we have described previously.[14]

Results

The results of our esr measurements on the alkali metal durosemiquinone ion pairs are given in Table I. The data are presented for −75° only, since the g shifts do not vary with temperature within our experimental error, and the temperature dependence of the metal couplings, a^M, and the difference in proton couplings between the two types of methyl groups, $a_2^H - a_1^H$, have been reported previously.[2,4,5] In general, the coupling constant difference $a_2^H - a_1^H$ increases with increasing temperature, as does the absolute value of the metal coupling, which indicates tighter association between the ions as the dielectric constant of the solvent decreases.

Table I

Cation	g shift[a] ± 10 ppm	$a_2^H - a_1^H$ [a] ± 0.01 G	a^M [a] ± 0.01 G
Li^+	1303	1.76	
Na^+	1323	1.27	0.19
K^+	1404	0.98	
Rb^+	1363	0.82[d]	0.36[b]
			0.11[c]
Cs^+	1316	0.76[d]	0.26
$TNBA^+$	1289	>0	
Free ion[e]	1452	0	

[a] Temperature = −75°, solvent DME. [b] ^{87}Rb. [c] ^{85}Rb. [d] ±0.05 G. [e] From K^+ solution.

The g shifts are reported in somewhat unusual units, parts per million (ppm), because we feel the data are more easily understood when presented as shifts rather than as a list of very similar absolute g values. Previous authors have presented g shifts in units of gauss[4a] and more accurately as simply the difference between the observed g value and that of the free electron.[9] We feel g values of organic molecules should be presented in a manner analogous to the chemical shift in nmr, and hence we have defined our g shift as

$$g \text{ shift} = \left(\frac{g_{obsd} - 2.0023192}{2.0023192}\right)10^6$$

We originally prepared the durosemiquinone ion electrolytically to obtain a g value for the free ion. However, careful analysis of the spectra obtained as a function of temperature indicates an alternating line

(11) P. Graceffa and T. R. Tuttle, Jr., *J. Chem. Phys.*, **50**, 1908 (1969).

(12) B. G. Segal, M. K. Kaplan, and G. K. Fraenkel, *ibid.*, **43**, 4191 (1965).

(13) R. Allendoerfer, *ibid.*, **55**, 3615 (1971).

(14) R. Allendoerfer and D. Eustace, *J. Phys. Chem.*, **75**, 2765 (1971).

width, which we interpret as being caused by time-dependent motion of the tetra-*n*-butylammonium cation ($TNBA^+$) associated with the durosemiquinone anion, ($DSQ\cdot^-$). Therefore, this ion pair should be classed with the others in the table, and one can say that its g value is not that of the free ion. Owing to the higher viscosity of DME when it is 0.5 M in tetra-*n*-butylammonium perchlorate, and because of the greater bulk of the $TNBA^+$–$DSQ\cdot^-$ ion pair, the rotational correlation time for this molecule is much longer than for the others in the series; consequently, the line widths are much broader as the solvent approaches its freezing point. This makes it impossible to accurately determine the value of $\tau(a_2^H - a_1^H)^2$, where τ is the intramolecular ion-exchange correlation time. Thus, this result indicates only that $a_2^H - a_1^H > 0$. It is tempting to correlate the g shift and value of $a_2^H - a_1^H$, thus allowing one to make an estimate of $a_2^H - a_1^H$ for the $TNBA^+$ ion. However, the ionic strength of the DME solution of the $TNBA^+$–$DSQ\cdot^-$ ion pair is nearly 500 times that of the other ion pairs because of the supporting electrolyte present, so the solvent effects on the g values are not comparable and the $TNBA^+$ g value may not really belong in the table at all.

As will be shown below, all the ion pairs except Li^+–$DSQ\cdot^-$ are in equilibrium with their free ions; thus, the g shift for the free durosemiquinone ion can readily be measured from dilute solutions of these ion pairs. The Na, Rb, and Cs nuclei all have nuclear spins which are odd multiples of $^1/_2$, so the esr spectra of their DSQ ion pairs have no central line; unfortunately, the g shift difference between the free ion and the ion pair is approximately $a^M/2$ in every case, so that the central line of the free ion is almost directly superimposed on the first low-field line of ion pair and thus its position cannot be accurately determined. For the K^+ ion, because of its smaller magnetic moment, the metal coupling is too small to observe. Thus, the free-ion spectrum in this system is free of the overlapping lines mentioned above and the g value is readily measured. Since this free-ion spectrum obtained by endor-induced esr[15] shows no evidence of an alternating line width effect even at −78°, we believe that the spin density distribution is the static one of a symmetrically solvated ion corresponding to $a_2^H - a_1^H \equiv 0$. The average proton coupling $(a_1^H + a_2^H)/2$ is 1.92 ± 0.01 G for all the ions in Table I, which shows that, within the limits of error of this measurement, the total spin density on the methyl-bound ring carbons is independent of the cation.

All of the ion-pair spectra with the exception of that of lithium exhibit marked, temperature-dependent, variations in line width. These variations are readily interpreted by assuming that the cation migrates rapidly between two equivalent sites, one near each carbonyl group.[16] The corresponding time-dependent perturbation of the $DSQ\cdot^-$ spin distribution (caused by the polarizing effect of the cation) gives rise to an out-of-phase modulation of the hyperfine couplings of the two pairs of magnetically equivalent methyl groups. This effect, often called the alternating-line-width effect,[17] can be used to analyze the experimentally observed line-width variations for all the ion-pair spectra observed.

Gough and Hindle[4b] have recently made a detailed study of this effect for durosemiquinone ions in DME and measured the correlation time for this intramolecular ion exchange as a function of temperature. The pertinent kinetic parameters describing this exchange given by these authors[4b] are summarized in Table II.

Table II[a]

Cation	$\Delta H^{\ddagger}$, kcal	$\Delta G^{\ddagger}$, kcal	$\Delta S^{\ddagger}$, eu
Li^+			
Na^+	3.17	6.83	−18.3
K^+	4.65	5.88	−6.2
Rb^+			
Cs^+	4.06	5.18	−6.1

[a] Data taken from ref 4b for DME solutions of $DSQ\cdot^-$ ion pairs at 200°K.

These data, along with similar data obtained in our laboratory, including those for the Rb^+ ion, have been used to simulate the esr spectra of these rapidly exchanging pairs using a modification of the computer program suggested by Bolton.[17] Once the ion-exchange data are properly interpreted, the experimental spectra can be compared with the calculated ion-pair spectra to look for other species such as solvent-separated ion pairs or free ions. For all the metal ions except lithium, there is a second species present in increasing abundance as the temperature is lowered. This second species is generally considered to be the free durosemiquinone ion.[2,3,15] For reasons which will be discussed below, the metal ion systems with the most negative enthalpy of dissociation to the second species exhibit, at low temperature, a clear esr spectrum of this second species. Figure 1 shows the Cs^+ spectrum at −60°. At this temperature, the ion-pair spectrum consists of seven groups of sharp lines split by 3.84 G, with each group split into eight components of equal intensity by the Cs^+ ion with nuclear spin of $^7/_2$. Only the central five groups are intense enough to observe under high-resolution conditions. The six missing groups are broadened beyond detection by the alternating-line-width effect. Superimposed on this

(15) R. Allendoerfer and R. Papez, *J. Amer. Chem. Soc.*, **92**, 6971 (1970).

(16) T. A. Claxton, J. Oakes, and M. C. R. Symons, *Nature (London)*, **216**, 914 (1967).

(17) P. D. Sullivan and J. R. Bolton, *Advan. Magn. Resonance*, **4**, 39 (1970).

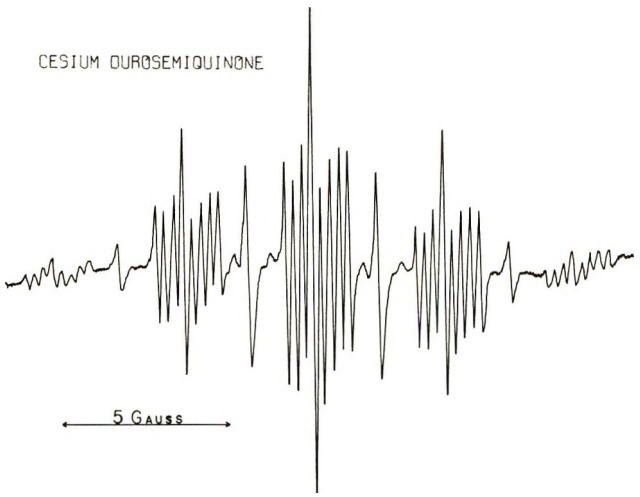

Figure 1. The esr spectrum of cesium durosemiquinone in equilibrium with the free durosemiquinone ion.

spectrum can clearly be seen the central nine components of the symmetrical 13-line spectrum of the free ion, with hyperfine splitting constant 1.92 G. The spectra for the other ions are not as easily interpreted, because the free-ion spectrum is not relatively as abundant at the temperature where the alternating line width is most important, but it can readily be observed in very dilute samples. We also have performed endor-induced esr experiments[15] on each of the ion pairs and satisfied ourselves that the distortion of the esr spectrum is, in every case, due only to the presence of the symmetrical 13-line spectrum of the free ion. While the endor-induced esr experiment gives a more aesthetically pleasing separation of the spectra, it is not suitable for measuring the relative abundance of the two species because the intensity of the endor enhancement depends in a complicated way on the electron and nuclear relaxation times, which, as the line widths in the esr spectra indicated, are not the same for the two species.

In order to measure the relative abundance of the free ion and ion pair, it was necessary to select the sets of least overlapped esr lines, compute their statistical weight, and measure their relative line widths and then their relative peak-to-peak heights. If we assume that the second species arises from the chemical reaction $MDSQ\cdot \rightleftarrows M^+ + DSQ\cdot^-$, then, in addition to the relative concentration of MDSQ· and $DSQ\cdot^-$, we must know the total radical concentration to compute the equilibrium constant for the reaction. This was found by comparison of the intensity of the overmodulated spectra to that of spectra obtained under the same conditions from known concentrations of the galvinoxyl radical. The thermodynamic parameters derived from studying the temperature dependence of this equilibrium are given in Table III. The ΔH data are more precise than those for ΔG, not only because the total radical concentration need not be known for ΔH, but also because the ratio of the line widths of the two species enters into the calculation of the equilibrium constant to the fourth power, and this is the major source of error in the calculation of the equilibrium constant. Inasmuch as this ratio is independent of temperature, it cancels out in a plot of log K *vs.* $1/T$. The uncertainty given for the ΔH values is the least-squares error in the slope of this plot, while that for ΔG includes our estimate of the precision of the double integration and relative line width measurement.

Table III

Cation	$\Delta H \pm 0.5$ kcal	$\Delta G_{298} \pm 1$ kcal	$\Delta S \pm 5$ eu
Li^+			
Na^+	−2.7	8.6	−38
K^+	−3.5	11.4	−50
Rb^+	−5.5	8.8	−48
Cs^+	−7.5	8.9	−55

Discussion

Before any interpretation of the data given above can be presented, the identities of the chemical species involved must be established. Because of the magnitude of the alkali metal couplings, the species referred to above as an ion pair is generally thought to be a contact ion pair with no solvent molecules separating the ions. The only exception is the lithium ion, for which no metal coupling is observed at any temperature. The sign and magnitude of alkali metal couplings are known to vary markedly as the position of the alkali metal changes with respect to the organic anion, even to the extent of changing sign as a function of temperature for a single system.[18] Thus, it is possible that the lithium ion pair is a contact ion pair in which the lithium ion lies at the point of zero coupling. It seems unlikely that this would be the case over the entire temperature range studied but the ion does distort the symmetry of the $DSQ\cdot^-$ ion more than any of the others, and no effects of ion exchange are observed. Thus, this ion pair must be tight as opposed to labile, but the possibility of a solvent-separated ion pair remains. The symmetrical 13-line esr spectrum with intensities following the binomial distribution expected for 12 equivalent protons does not uniquely define the nature of the second species in these solutions. A solvent-separated ion pair in which the cation exchanges ends of the anion rapidly with respect to $a_2^H - a_1^H$ would give the same spectrum as a free ion, where no correlation with a specific cation exists. Since all three species have been observed simultaneously for sodium naphthalenide systems by Hirota,[6] it is important to distinquish between the two possibilities here. In an attempt to prove that the species observed is a solvent-separated ion pair, we first attempted to measure the g value for

(18) B. M. P. Hendricks, G. W. Canters, C. Corvaja, J. W. M. deBoer, and E. deBoer, *Mol. Phys.*, **20**, 193 (1971).

the second species of each of the alkali metals, but, as discussed above, these measurements could not be made with sufficient precision to establish any trends. Second, we examined the line shape of the esr signal of the second species obtained with cesium as the counterion to look for possible hidden metal splittings as suggested by Jones, *et al.*[19] The lines are broader in the wings than a pure Lorentzian line, but this effect can be reproduced in the calculated spectra either by including a small unresolved metal coupling or by including the effect of the strong but very broad ion-pair signal which is always superimposed on the esr signal of the second species. Endor-induced esr spectra[15] for the cesium system show no hint of metal couplings on the spectrum of the second species, although metal couplings are observed in endor-induced esr spectra of ion pairs just as in esr. Thus, we believe the latter interpretation of the line-shape data is correct. Positive, and we feel compelling, evidence that the second species is indeed a free ion was obtained by studying the concentration dependence of the ratio of free ion to ion pair for the potassium system. If the equilibrium is a simple dissociation of an ion pair to two free ions

$$\mathrm{KDSQ}\cdot \rightleftharpoons \mathrm{K}^+ + \mathrm{DSQ}\cdot^- \qquad (1)$$

then the equilibrium constant is given by $K = r^2c/(r + 1)$, where r is the ratio $[\mathrm{DSQ}\cdot^-]/[\mathrm{KDSQ}\cdot]$ and c is the total radical concentration. If the equilibrium involves contact and solvent-separated ion pairs

$$\mathrm{KDSQ}\cdot + n\mathrm{DME} \rightleftharpoons \mathrm{K}^+(\mathrm{DME})_n\mathrm{DSQ}\cdot^- \qquad (2)$$

then in the limit of infinite dilution, $K = r$, the ratio of the two species. By varying c over the range 10^{-3} to 10^{-6} M, we have obtained a quantitative fit to eq 1. Thus, the only important species and equilibria involved are those given in Figure 2, the contact-ion-pair exchange equilibrium $A_1 \rightleftarrows A_2$ and the tight-ion–free-ion equilibrium $A \rightleftarrows B$.

The polarization of the $\mathrm{DSQ}\cdot^-$ spin density, as indicated by $a_2^{\mathrm{H}} - a_1^{\mathrm{H}}$, decreases smoothly through the series Li, Na, K, Rb, Cs, as one would predict considering the electronegativity of the metals, but we find the increasingly negative enthalpy of dissociation somewhat surprising. The enthalpy can be divided into two important terms, first the heat of solution of the ions created and second the enthalpy associated with breaking the ionic bond in the ion pair. The heat of solution is expected to depend on temperature as the dielectric constant of the solvent changes. Thus, linear plots of log K *vs.* $1/T$ are not expected unless this effect on ΔH is linear with temperature or negligible. Our plots are linear, but we are unable to distinguish between the two possibilities mentioned. Thus, the absolute values of our overall enthalpies pertain to a system of uncertain definition, but the differences among ions in the same solvent should be meaningful, since, at worst, the dielectric constant effect can only change

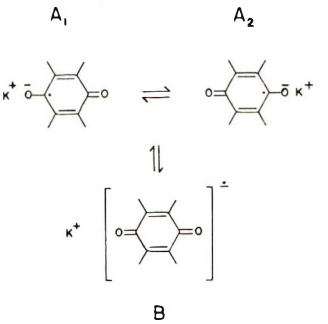

Figure 2. Species and equilibria present in DME solutions of potassium durosemiquinone.

the intercept of the plot. We expect the apparent heat of solution to be decreasingly negative as we go down the series,[20] so the enthalpy of bond breaking must be decreasingly positive. That is, the ion which polarizes $\mathrm{DSQ}\cdot^-$ spin density most successfully also forms the strongest bond. The large and uniformly negative entropy of dissociation has been observed many times previously and is indicative of the highly ordered solvation of metal ions in glymes.[21]

The g shifts first increase and then decrease as we go down the series. The increase is thought to arise from two sources. First, the total oxygen spin density should increase, thereby increasing the effects of electron spin–orbit coupling with the oxygen orbitals as the spin density distribution becomes more uniform and the strength of the ionic bond decreases. Second, strong polarization of the electrons in the carbonyl bond will inhibit their orbital motion, thus decreasing the spin–orbit coupling contribution to the g shift to the largest extent for the most polarized ion. These considerations predict a smooth increase in the g shift from the 1303 of the most polarized Li^+–$\mathrm{DSQ}\cdot^-$ to the 1452 of the symmetrical free ion. Fraenkel, *et al.*,[9] observed decreasing g shifts for naphthalenide ion pairs in the series K^+, Rb^+, Cs^+, which they ascribed to spin–orbit coupling with the orbitals on the metal ion. The electron spin–orbit coupling constant increases dramatically in this series,[9] so it is also reasonable to ascribe the decrease observed for the $\mathrm{DSQ}\cdot^-$ ion as one goes from K^+ to Rb^+ to Cs^+ to this effect.

Some insight into the mechanism of the intramolecular cation migration can be achieved by comparison of the thermodynamic data for ion dissociation given in Table III with the kinetic data for the ion exchange given in Table II. We have shown that the enthalpy change for breaking the ionic bond correlates well with the polarizing ability of the cation as measured by $a_2^{\mathrm{H}} - a_1^{\mathrm{H}}$. Similarly, Gough and Hindle[4b] found a

(19) M. T. Jones, M. Komarynsky, and R. D. Rataiczak, *J. Phys. Chem.*, **75**, 2769 (1971).

(20) M. Szwarc, *Science*, **170**, 23 (1970).

(21) L. L. Chan, K. H. Wong, and J. Smid, *J. Amer. Chem. Soc.*, **92**, 1955 (1970).

good correlation between $\Delta G^{\ddagger}$ for the ion exchange and $a_2^H - a_1^H$. Thus, one can infer that there is a similarity between the energetics of the processes involved in promotion to the activated complex and complete dissociation. For K, Rb, and Cs, the intramolecular ion migration apparently takes place entirely within the solvent shell, as indicated by the following argument. The free energies of activation for these three systems are substantially less than the free energies of dissociation given in Table III, which would indicate that the transition state cannot entirely resemble separated ions. Moreover, the calculated small negative entropies of activation indicate that the transition state is only slightly more solvated than the contact ion pair and, accordingly, only slightly more ionic. For Na^+–$DSQ\cdot^-$, on the other hand, the entropy of activation is substantially more negative, nearly one-half the value for complete dissociation. The free energy of activation also approaches the free energy of dissociation, so the transition state for the ion exchange more nearly resembles the dissociated ions. The Li^+–$DSQ\cdot^-$ ion pair has not been observed to undergo this type of ion exchange. However, Gough and Hindle[4b] extrapolated their $\Delta G^{\ddagger}$ data on the basis of the values for $a_2^H - a_1^H$, to give an estimate of 14 kcal/mol as the free energy of activation for this exchange with the Li^+ ion. This is substantially greater than any of our values for the free energy of dissociation. Thus, it seems likely that the trend toward increasingly ionic transition states should continue as the size of the cation decreases.

Acknowledgment. The authors wish to thank Professor R. J. Kurland for many helpful discussions and to acknowledge the support of this research by the Petroleum Research Fund, administered by the American Chemical Society.

Ultraviolet Spectra of Single and Double Molecules of Gaseous Bromine

by Walter Y. Wen and Richard M. Noyes*

Department of Chemistry, University of Oregon, Eugene, Oregon 97403 *(Received October 15, 1971)*

Publication costs assisted by the National Science Foundation

The absorption spectrum of bromine vapor between 220 and 290 nm has been measured at 30°. Deviation from the Beer–Lambert law has been interpreted in terms of the formation of double molecules of Br_2, and the relative contributions of single and double molecules of Br_2 to the observed absorption have been assigned.

At wavelengths longer than 300 nm, light absorption by bromine vapor obeys Beer's law, and the spectrum has been well characterized.[1] At shorter wavelengths, a band centered at about 210 nm deviates strongly from Beer's law. Passchier, Christian, and Gregory[1] and also Ogryzlo and Sanctuary[2] have attributed some of this absorption to Br_4 molecules.

Reported absorbance data that recognize Beer's law deviations[1,2] do not cover the region between 230 and 300 nm. In connection with a kinetic study of the reaction between Cl_2 and HBr,[3] we had occasion to measure the concentration dependence of light absorption in this region.

Measurements were made with a Beckman DU spectrophotometer on a quartz cell with 9.8-cm optical path thermostated to 30° by a water jacket. Mallinckrodt analytical grade bromine was dried over P_2O_5 at liquid nitrogen temperature and admitted to the evacuated cell. Final pressure was measured to better than 1 mm with a Pace Wiancko PIA-20 psia pressure transducer connected to a transducer indicator that had been calibrated against a mercury manometer. Concentrations (in the range 0.002–0.009 M) were computed by assuming the ideal gas law. Although the apparatus was designed primarily for kinetic measurements,[3] it was satisfactory for the spectral measurements.

The apparent extinction coefficients (defined as $A/s[Br_2]_t$, where A is the absorbance, s is the cell length in centimeters, and $[Br_2]_t$ is the total concentration of bromine in moles/liter) are plotted against concentration in Figure 1 and show the deviations from Beer's law at the shorter wavelengths. If these deviations are due to equilibrium 1, then the total absorbance can be described by eq 2, where ϵ_2 and ϵ_4 are the molar

(1) A. A. Passchier, J. D. Christian, and N. W. Gregory, *J. Phys. Chem.*, **71**, 937 (1967), and references cited therein.

(2) E. A. Ogryzlo and B. C. Sanctuary, *ibid.*, **69**, 4422 (1965).

(3) W. Y. Wen, Ph.D. Thesis, University of Oregon, 1971.

$$2Br_2 \rightleftharpoons Br_4 \quad (1)$$

$$A = \epsilon_2 s[Br_2] + \epsilon_4 s K_p RT[Br_2]^2 \quad (2)$$

extinction coefficients of Br_2 and Br_4 molecules, respectively, K_p is the equilibrium constant for reaction 1 in reciprocal atmospheres, RT is in liter atmospheres per mole, and $[Br_2]$ is the true concentration of bromine molecules. If the extent of association is sufficiently small, no significant error is introduced by substituting $[Br_2]_t$ for $[Br_2]$ in eq 2.

The results of our measurements are presented in Table I and compared with previously reported values where possible. Values of ϵ_2 tend to be somewhat smaller than those reported by Aickin and Bayliss,[4] even if allowance is made for their failure to recognize Beer's law deviations, and the values of $K_p\epsilon_4$ extend the wavelength range reported by Passchier, Christian, and Gregory.[1]

Table I: Calculated Extinction Coefficients for Br_2 and Br_4

Wavelength, nm	ϵ_2, l./(mol cm) Reported		This work, 30°	$K_p\epsilon_4$, l./(mol cm atm) Reported	This work, 30°
220	2.6[a]	3.33[b]	2.84 ± 0.13	25.0[a]	21.0 ± 0.1
225	2.8[a]	3.23[b]	2.93 ± 0.09	14.3[a]	12.2 ± 0.6
230	2.6[a]	3.30[b]	2.66 ± 0.05	8.15[a]	7.6 ± 0.4
235		2.85[b]	2.80 ± 0.06		2.7 ± 0.4
240		2.60[b]	2.22 ± 0.04		2.5 ± 0.3
245		2.10[b]	1.96 ± 0.04		1.3 ± 0.3
250		1.69[b]	1.59 ± 0.04		1.0 ± 0.3
255		1.36[b]	1.00 ± 0.04		1.2 ± 0.3
260		1.08[b]	0.92 ± 0.05		0.3 ± 0.3
265		0.88[b]	0.54 ± 0.04		0.8 ± 0.3
270		0.65[b]	0.28 ± 0.06		0.8 ± 0.4
275		0.48[b]	0.24 ± 0.04		0.4 ± 0.3
280		0.46[b]	0.24 ± 0.05		
285		0.35[b]	0.14 ± 0.04		0.1 ± 0.3
290		0.39[b]	0.12 ± 0.05		0.2 ± 0.3

[a] 25° data of ref 1. [b] Room-temperature interpolated data of ref 4, not corrected for concentration dependence of apparent extinction coefficients.

Any evaluation of ϵ_4 requires an independent evaluation of K_p. Results of gas density measurements are ambiguous. Lasater, Colley, and Anderson[5] interpreted deviations from the ideal gas law by means of van der Waals' equation without any assumptions

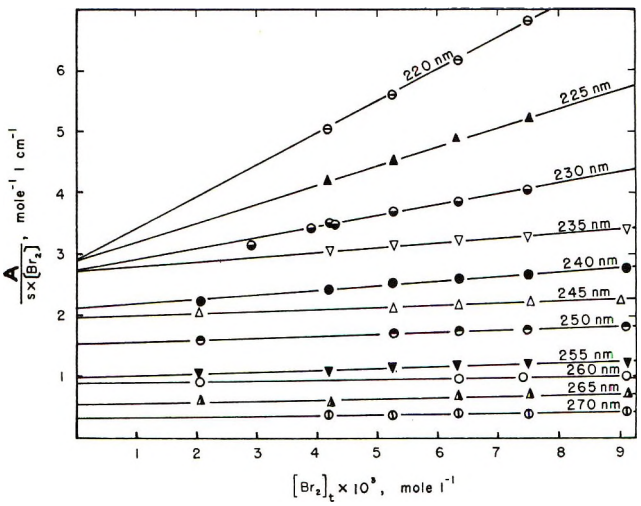

Figure 1. Plots of the apparent extinction coefficients against $[Br_2]_t$.

about chemical equilibria, but Kokovin[6] interpreted his data by eq 3. Such an interpretation implies $\Delta H°$

$$\log K_p = (576/T) - 3.28 \quad (3)$$

$= -2.6$ kcal/mol for reaction 1, in good agreement with the temperature dependence of $K_p\epsilon_4$ observed by Passchier, Christian, and Gregory[1] at short wavelengths. However, such an evaluation of K_p assumes that all deviations from ideal gas behavior are due to association forming specific double molecules and that long-range intermolecular forces do not affect those deviations. Because there is considerable uncertainty in the value of any K_p calculated by means of such assumptions, the data in Table I have been reported in terms of $K_p\epsilon_4$ without any attempt to evaluate ϵ_4. However, the K_p of 0.043 atm^{-1} at 30° implied by the Kokovin[6] data indicates that even saturated bromine vapor would have only about 1% Br_4 molecules and fully justifies the substitution of $[Br_2]_t$ for $[Br_2]$ in eq 2.

Acknowledgment. This research was supported at different times by the U. S. Army Research Office and by the National Science Foundation.

(4) R. G. Aickin and N. S. Bayliss, *Trans. Faraday Soc.*, **34**, 1371 (1938).

(5) J. A. Lasater, S. D. Colley, and R. C. Anderson, *J. Amer. Chem. Soc.*, **72**, 1845 (1950).

(6) G. A. Kokovin, *Zh. Neorg. Khim.*, **10**, 287 (1965); *Russ. J. Inorg. Chem.*, **10**, 150 (1965).

A Raman Spectroscopic Investigation of the Magnesium Nitrate–Water System

by Mordechai Peleg

Department of Inorganic and Analytical Chemistry, The Hebrew University of Jerusalem, Jerusalem, Israel
(Received August 31, 1971)

Publication costs borne completely by The Journal of Physical Chemistry

The magnesium nitrate–water system has been examined by Raman spectroscopy covering the entire range from highly dilute solution to the anhydrous molten salt mixture ($Mg(NO_3)_2$–$NaNO_3$). The results indicate that the above system can be divided into five approximate regions. At high dilutions both ions are completely hydrated, the nitrate ion being perturbed by the water molecules. As the water content is lowered, the polarization power of the magnesium begins to affect the nitrate ion, but no contact ion pairing occurs until the water content is reduced below 6 moles of water per mole of salt. Below this region both contact ion pairs and solvent-separated species are in equilibrium. At melt concentrations of $Mg(NO_3)_2 \cdot 2.4H_2O$ and $Mg(NO_3)_2 \cdot 2.0H_2O$, a specific rearrangement occurs producing Raman bands that are not present at either of the higher water contents or in the anhydrous melt. A perturbed quasilattice structure is suggested for this region. Evidence is also presented indicating that molten $(Mg(NO_3)_2 \cdot 6H_2O$ behaves as a hydrated melt.

Introduction

Raman spectroscopy is being increasingly used to investigate ionic association and solvation in solution,[1-3] especially in aqueous metal nitrate systems,[4] since the vibrational modes of the polyatomic ion are sensitive to their environment and can be used as an indicator of interionic interactions.

An isolated and unperturbed NO_3^- ion would have D_{3h} symmetry and give rise to only four vibrational frequencies, corresponding to the species A_1' (R) + A_2'' (ir) + 2E′ (R, ir), where R and ir indicate Raman and infrared activity, respectively. Lowering of the NO_3^- ion symmetry by loss of the equivalence of the three oxygen atoms, to produce C_{2v} or C_s symmetry, is expected to lead to loss of degeneracy from both of the E′ modes whether the nitrate acts as unidentate[5] or bidentate[6] ligand. However, it has been noted that the anticipated splitting of the ν_4(E′) mode does not occur unless contact ion pairs are present in the solution, while the ν_3(E′) band appears as a doublet even in very dilute aqueous solutions. This splitting is attributed to perturbation of the nitrate ion by water molecules.[4,7]

Angell[8] has proposed that fused hydrated salts such as calcium nitrate tetrahydrate and magnesium chloride hexahydrate might be treated as molten salts with large cations, with the water bound up to the cation. The proposal of a hydrated cation has been further substantiated by such studies as transport properties[9,10] and volumetric properties[11] in $Ca(NO_3)_2 \cdot 4H_2O$ and in its mixtures with KNO_3 and by spectrophotometric studies of Ni(II) in aqueous magnesium chloride solutions.[12] Ellis and Hester,[13] however, have shown that the anion in a hydrate melt significantly affects the pmr chemical shift, interpreting this to support displacement equilibria of the type considered in a quasilattice model, with anion displacement of water molecules from the metal ion inner coordination spheres. Further, Raman and infrared spectral studies of concentrated aqueous calcium nitrate solutions[14,15] and cadmium nitrate solutions[16] have been interpreted in terms of the formation of contact ion pairs such as $CaNO_3^+$ and $CdNO_3^+$. As stated by Braunstein,[17] contact ion pairs might not be inconsistent in molten tetrahydrates (accompanied by some distortion of the coordination shell) with Angell's[8] proposal of a large hydrated cation, but it is more difficult to reconcile with hexahydrated cations.

The present report presents results on the $Mg(NO_3)_2$–H_2O system covering almost the entire concentration range from dilute solutions to ultraconcentrated aqueous solutions (2 mol of water to 1 mol of $Mg(NO_3)_2$) in order to investigate whether a hexahydrate melt also

(1) G. J. Janz, *J. Electronal. Chem.*, **29**, 107 (1971).

(2) R. E. Hester, *Annu. Rept. Progr. Chem.*, **66A**, 79 (1969).

(3) D. E. Irish in "Ionic Interaction: Dilute Solutions to Molten Salts," S. Petrucci, Ed., Academic Press, New York, N. Y., 1971, Chapter 9.

(4) D. E. Irish, A. R. Davis, and R. A. Plane, *J. Chem. Phys.*, **50**, 2262 (1969).

(5) H. Brintzinger and R. E. Hester, *Inorg. Chem.*, **5**, 980 (1966).

(6) R. E. Hester and W. E. L. Grossman, *ibid.*, **5**, 1308 (1966).

(7) A. R. Davis, J. W. Macklin, and R. A. Plane, *J. Chem. Phys.*, **50**, 1478 (1969).

(8) C. A. Angell, *J. Electrochem. Soc.*, **112**, 1224 (1965).

(9) C. T. Moynihan, *J. Phys. Chem.*, **70**, 3399 (1966).

(10) J. Braunstein, L. Orr, A. R. Alvarez-Fumes, and H. Braunstein, *J. Electroanal. Chem.*, **15**, 337 (1967).

(11) J. Braunstein, L. Orr, and W. Macdonald, *J. Chem. Eng. Data*, **12**, 415 (1967).

(12) C. A. Angell and D. M. Gruen, *J. Amer. Chem. Soc.*, **88**, 5192 (1966).

(13) V. S. Ellis and R. E. Hester, *J. Chem. Soc. A*, 607 (1969).

(14) R. E. Hester and R. A. Plane, *J. Chem. Phys.*, **40**, 411 (1964).

(15) D. E. Irish and G. E. Walrafen, *ibid.*, **46**, 378 (1967).

(16) A. R. Davis and R. A. Plane, *Inorg. Chem.*, **7**, 2565 (1968).

(17) J. Braunstein in ref 3, Chapter 4.

Table I: Nitrate Frequencies Observed in the Raman Spectra of the $Mg(NO_3)_2$–H_2O System[a]

R_{H_2O}	Frequency, cm^{-1}										Temp, °C
77	363		717		1048.5		1348	1400	1619	1658	90
42	356		716		1048.5		1348	1400	1640	1661	90
20	354	715		719	1047.5		1338	1407	1644	1657	90
13	348	712		720	1047.5		1332	1409	1644	1656	100
9.5	334	711		722	1048.5		1342	1428	1639	1652	100
6	344	711		725	1049		1347	1445	1644	1652	100
5.1	332	719		728	1049.5		1341	1445	1651	1641	100
4.2	322	717		746	1053		1337	1451	1650	1640	100
3.4	322	717		751	1053		1334	1461		1634	100
2.9	322 (vw)	717		751	1052		1341	1468		1634	120
2.4		717		754	1034	1060	1328	1486		1634	120
2.0		717		755	1038	1066	1333	1493		1634	120
$Mg(NO_3)_2$/ $NaNO_3$											
1/1.35		713		757	812	1051	1330	1485		1620	200
Assignment (C_{2v})	Mg–OH_2 (A) Symstr	$\nu_8(B_1)$		$\nu_3(A_1)$	$\nu_6(B_2)$	$\nu_2(A_1)$	$\nu_1(A_1)$	$\nu_4(B_1)$	δ(HOH)	$2\nu_2$	
	p	dp		p		p	p	dp	dp	p	
	sh	msp		msp		sp	b	b	m	m	

[a] p = polarized, dp = depolarized, sh = shoulder, m = medium, sp = sharp, b = broad, vw = very weak.

shows contact ion pairs, and also to study the structure of concentrated solutions containing $Mg(NO_3)_2$.

Experimental Section

Baker Analyzed reagent grade $Mg(NO_3)_2 \cdot 6H_2O$ was used as the starting material without any further purification. The water content of the starting material was ascertained to be $6H_2O$ by heating the hexahydrate under vacuum at 120° for several hours until constant weight was attained. Samples containing more than 6 moles of water per mole of salt were prepared by adding water to the hexahydrate, while samples containing less than 6 moles of water were prepared by removing controlled amounts of water from the hydrated salt by careful heating and then weighing to measure the amount of water vaporized. All samples were filtered under pressure through a glass frit directly into the Raman sample tube. The solutions were heated in a simple tube furnace to the desired temperature.

The laser Raman apparatus employed in the investigations is that described by Claassen, *et al.*,[18] and included the following commercial units: a Spex 1400 II double monochromator, a Spectra-Physics 125 He–Ne laser, a Spex cryostat fitted with an ITT FW 130-S-20 photomultiplier detector, a Victoreen 1001 dc amplifier, and a Texas Instruments recorder. Further details are included in the cited reference. The positions of the Raman bands were calibrated with reference to the neon lines. The concentrations recorded in this paper are given as mole ratios, R, moles of H_2O per mole of $Mg(NO_3)_2$.

Most of the spectra were run at a temperature of 100° except for the very dilute solutions, where a temperature of 90° was chosen (owing to the high vapor pressure of the water), and for the most concentrated solutions (120°). Experiments have shown that over a limited temperature range the positions of the spectral line do not change.

Results

The results are recorded in Table I for the entire spectrum range covered. Also included for comparison are our preliminary results for the $Mg(NO_3)_2$–$NaNO_3$ mixture (at a ratio of 1 mol of $Mg(NO_3)_2$ to 1.35 mol of $NaNO_3$). The Raman band positions are believed to be correct to within ± 0.5 cm^{-1} for the sharp Raman bands and within ± 1 cm^{-1} for the broader bands. Where overlapping or superimposed Raman bands existed or were believed to exist, a computer technique was used to analyze the bands for the best fit to the Gaussian function. As pointed out by Irish, *et al.*,[19] and observed in our own present results, discretion and considerable physical knowledge of the system must be applied in such analyses lest nonexistent lines be invoked.

As observed from Table I, the frequency of the *ca.* 1050-cm^{-1} Raman band is quite concentration dependent (Figure 1). Another interesting fact is the sudden appearance of two bands around 1050 cm^{-1} for R equal to 2.4 and 2 (Figure 2). A value of 1048.5 $\pm$ 0.5 cm^{-1} obtained in the most dilute solution (R = 77) is in good agreement with the value of 1049 $\pm$ 0.5 cm^{-1} reported by Irish and Davis[20] for dilute alkali

(18) H. H. Claassen, H. Selig, and J. Shamir, *Appl. Spectrosc.*, **23**, 8 (1969).

(19) D. E. Irish and H. Chen, *ibid.*, **25**, 1 (1971).

(20) D. E. Irish and A. R. Davis, *Can. J. Chem.*, **46**, 943 (1968).

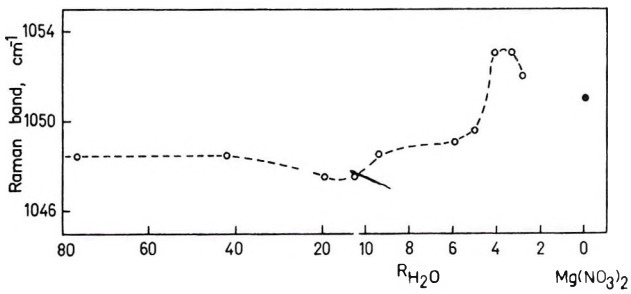

Figure 1. The variation of the Raman band position at *ca.* 1050 cm^{-1} with the mole ratio concentration R_{H_2O} of magnesium nitrate: (O) $Mg(NO_3)_2$–H_2O, (●) $Mg(NO_3)_2$–$NaNO_3$ (ratio 1/1.35).

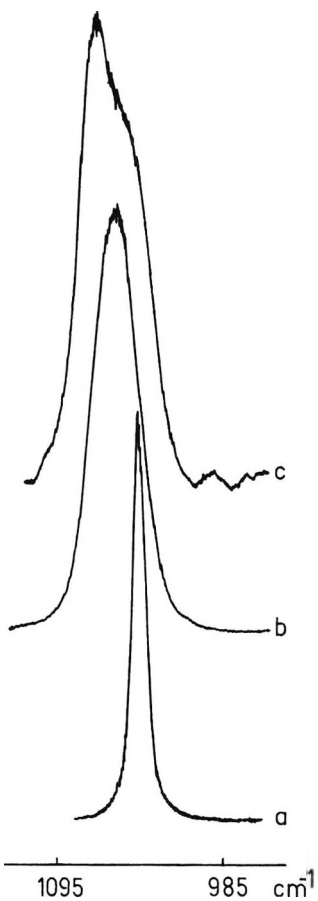

Figure 2. Raman spectra of $Mg(NO_3)_2$ at various mole ratio concentrations in the *ca.* 1050-cm^{-1} region: (a) R_{H_2O} = 42, (b) R_{H_2O} = 2.9, (c) R_{H_2O} = 2.4.

nitrate solutions. On decreasing the water content, it appears as if the Raman band frequency slowly decreases to a minimum value of 1047.5 cm^{-1} at R = 20 and 13. Between R = 6 and 4.2, there is a sharp increase to a value of 1053 cm^{-1} and then once more a slight decrease which appears to approach the value for the pure dry salt mixture (*cf.* alkali metal nitrate solutions).[20]

The frequencies of the 700–750-cm^{-1} Raman bands are markedly concentration dependent, as observed in Figures 3 and 4. It is observed that at high dilu-

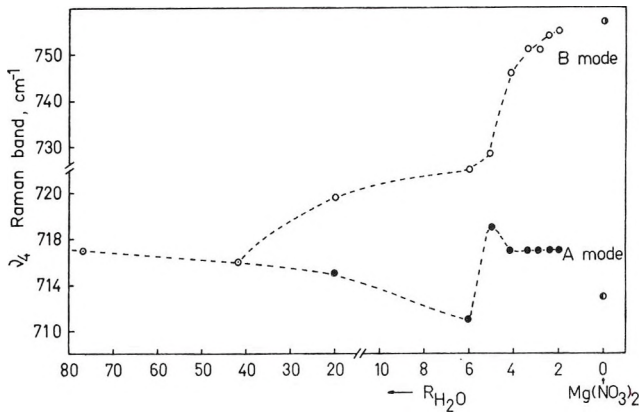

Figure 3. The variation of Raman band positions in the 700–750-cm^{-1} region with the mole ratio concentration of magnesium nitrate: (⊙, O, ●) $Mg(NO_3)_2$–H_2O, (◐) $Mg(NO_3)_2NaNO_3$ (ratio 1/1.35).

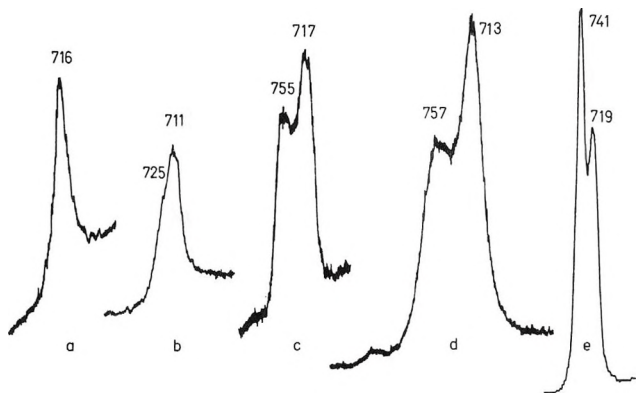

Figure 4. Raman spectra of $Mg(NO_3)_2$ at various mole ratio concentrations in the 700–750-cm^{-1} region: (a) R_{H_2O} = 42, (b) R_{H_2O} = 6, (c) R_{H_2O} = 2, (d) $Mg(NO_3)_2$–$NaNO_3$ (ratio 1/1.35), (e) $Ca(NO_3)_2 \cdot 4H_2O$.

tion only one frequency is noted (Figure 4a), and it is only at R = 6 that the appearance of a slight shoulder on the high-frequency side of the band is visually noted (Figure 4b). This splitting of the Raman band becomes increasingly apparent as the water content decreases (Figure 4c,d). However, by applying computer techniques it was possible to resolve the 700–750-cm^{-1} band into two separate bands even for solutions where R = 20, as shown in Table I.

The unresolved two main peaks in the 1300–1500-cm^{-1} region are listed in Table I. The variation of the two Raman band positions and their change of band shape with concentration are shown in Figures 5 and 6.

As the water content is reduced, it is noted that the spectra become more complex and there appear to be three or four lines in the 1300–1500-cm^{-1} region (Figure 6). This region was examined by a computer technique, and it was observed that for almost all concentrations it was possible to fit three and/or four bands to the observed Raman spectra. The results obtained therefore had to be treated with great care lest nonexis-

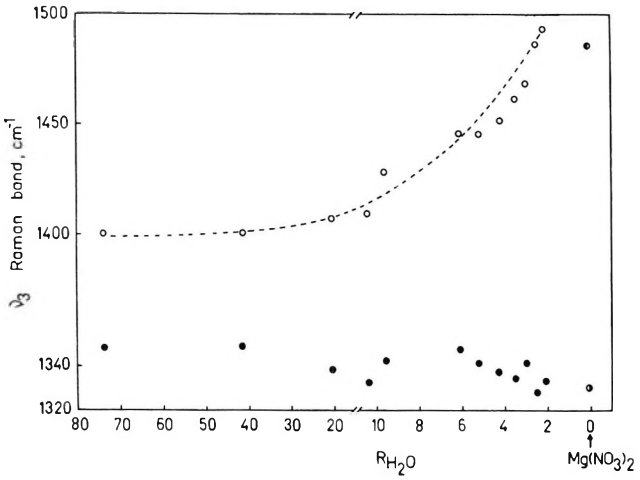

Figure 5. The variation of Raman band positions in the 1300–1500-cm^{-1} region with the mole ratio concentration of magnesium nitrate: (○) $Mg(NO_3)_2$–H_2O, B mode; (●) $Mg(NO_3)_2$–H_2O, A mode: (◐, ◑) $Mg(NO_3)_2$–$NaNO_3$ (ratio 1/1.35), B and A modes.

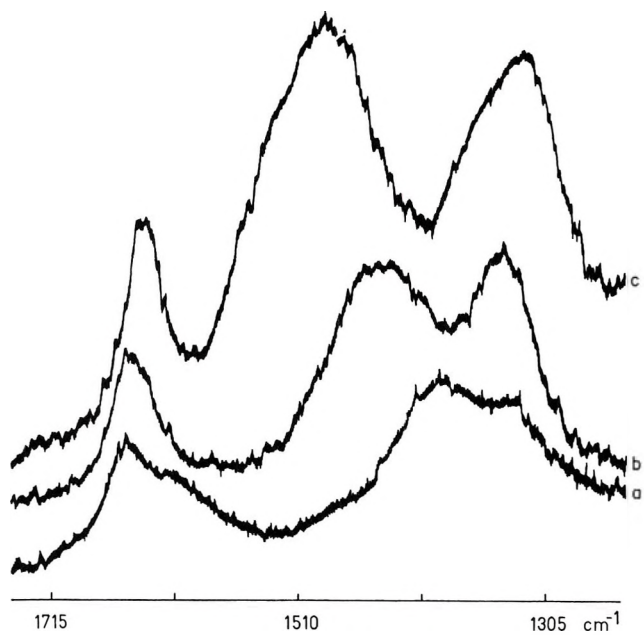

Figure 6. Raman spectra of $Mg(NO_3)_2$ at various mole ratio concentrations in the 1300–1700-cm^{-1} region: (a) R_{H_2O} = 42, (b) R_{H_2O} = 6, (c) R_{H_2O} = 2.

tent lines be invoked. For all concentrations greater than and including R = 5.1, it seems best to treat as only two lines. Below this concentration the following bands, as indicated in Table II, can be tentatively postulated.

The 1600–1700-cm^{-1} band can be separated for higher water content into two bands (Figure 6a,b), one which is polarized and whose relative intensity increases with respect to the other band (depolarized) as the water content decreases. At values of R equal to or less than 3.4, only one band is noted in this region. The polarized band is assigned to the $2\nu_2$ frequency, while

Table II: Nitrate Frequences in the 1300–1500-cm^{-1} Region

R_{H_2O}	Frequency, cm^{-1}						
6.0		1347	1445				
5.1		1341	1445				
4.2		1342	1444			1330	1454
3.4		1369	1443			1331	1484
2.9		1368	1462			1330	1492
2.4	1377			1469	1320		1512
2.0	1342			1490	1313		1555
0.0						1330	1485

the depolarized is the water deformation (or bending) mode. The $2\nu_2$ band shows a steady decrease in frequency with decreasing water content, reaching a steady value of 1634 cm^{-1} as compared to 1620 cm^{-1} for the anhydrous molten salt mixture, and a value of 813 cm^{-1} for the fundamental ν_2 band.

Only one Raman band was observed in the 200–400-cm^{-1} region, and this was a polarized line which decreased in frequency on decreasing water content. Hester and Plane[21] have attributed peaks in this region to metal–water–oxygen symmetric stretching modes consistent with the formation of hexacoordinated aqua complexes. It is surprising to see a discrepancy between our results for the ν_{Mg-OH_2} stretching frequency and those of Hester and Plane,[21] who quote a value of 370 cm^{-1} for a near-saturated solution at room temperature. Our value for a near-saturated solution (R = 20) at 100° is 354 cm^{-1}. Experiments carried out at room temperature on the dilute solutions showed that the low-frequency line ν_{Mg-OH_2} hardly changed with temperature. However, the difficulty of assigning exact band positions which appear as shoulders on the exciting line may account for the above difference. While it is difficult to compare intensities in the present results, it was possible to observe that the intensity of this low-frequency line decreased as the water content was lowered below R = 6.0 and completely disappeared below R = 2.9. No band was observed in the *ca.* 250-cm^{-1} region even for the molten salt mixture, indicating that the metal–oxygen interaction is primarily electrostatic.

Discussion

From a study of the work of Brintzinger and Hester,[5] we believe it is possible to explain the changes in band position with changing water content. These authors calculated the fundamental frequencies in an NO_3^- anion and frequency shifts caused by both M–O bond formation and polarization in a complex with C_{2v} symmetry. From examination of Figure 1 of ref 5, the following conclusions can be drawn. For the ν_1 frequency, polarization effects will cause a decrease of the ν_1 frequency while metal binding effects will give

(21) R. E. Hester and R. A. Plane, *Inorg. Chem.*, 3, 768 (1964).

rise to the opposite effect—increase of the symmetric stretching frequency value. Polarization effects will cause a splitting of the degenerate ν_4 frequency into A and B modes, the B mode increasing with increasing polarization and the A mode decreasing. Metal binding will only affect the A mode, causing an increase in stretching frequency, while the B mode will be unaffected.

According to Brintzinger and Hester,[5] it is noted that the metal-binding effects hardly affect the A and B modes of the ν_3 frequency, and it is only the polarization effects that cause the variation in the A and B mode Raman band position. In the $Mg(NO_3)_2$–H_2O system, it may be assumed that as long as the mole ratio of water is larger or equal to six, then the Mg^{2+} cation will be completely hydrated and the nitrate ion cannot be in contact with the cation and will therefore feel only polarization effects. However, once there are fewer than six molecules of water to each magnesium ion, contact ion pairing is possible and the anion will be influenced by both polarization and metal-binding effects.

Thus, one would expect a sudden increase of the ν_1 stretching frequency for the $Mg(NO_3)_2$–H_2O system once R is less than six. Similarly, for the ν_4 frequency, the A mode would be expected to show a sudden increase once there are fewer than 6 moles of water per mole of salt, while the B mode would be unaffected. On the other hand, the A and B modes of the ν_3 frequency would not be expected to show any sudden changes once there is insufficient water to form a complete hydration sheath around the magnesium ion. The above effects are indeed observed.

At $R = 77$ and 42, the nitrate ion is completely unaffected by the cation, as shown by the agreement of our ν_1 frequency value with that obtained by Irish and Davis[20] for dilute alkali nitrate solution. It is possible that there is a slight decrease in ν_1, at $R = 20$ (although this is uncertain owing to the error in measuring the frequencies), suggesting that even through about two layers of water molecules the high polarization ability of the magnesium ($z/r = 3.03$) is being felt. The sudden increase in band position from 1049.5 to 1053 cm^{-1} for the frequency that occurs between $R = 5.1$ and 4.2 is explainable by the fact that the nitrate ion can now form direct contact ion pairs and the metal-binding effects more than overcome the polarization effects. On further decrease of water content, the ν_1 band position decreases slightly, indicating that the polarization effects continue to increase as the remaining water is removed.

In the 720–750-cm^{-1} region (ν_4), it is observed that at high dilution only one frequency is noted (polarization too weak to affect the ν_4 band); however, at $R = 20$ a split of 4 cm^{-1} is observed, which increases to 14 cm^{-1} at $R = 6$. The higher frequency can be attributed to the B mode, which increases with decreasing water content (increase of polarization due to smaller separation between cation and anion), and the lower frequency to the A mode.

With fewer than 6 mol of water per mol of salt, while the B mode frequency continues to increase monotonously, the A mode moves from 711 cm^{-1} at $R = 6$ to 719 cm^{-1} at $R = 5.1$. This is consistent with the fact that below $R = 6$ metal binding comes into play, causing an increase in the A mode but leaving the B mode unaffected. On further lowering of the water content, the B mode continues to increase, reaching a value almost equal to that in the $Mg(NO_3)_2$–$NaNO_3$ mixture. The A mode, on the other hand, drops slightly and remains constant at 717 cm^{-1} from $R = 4.2$ to $R = 2.0$, indicating that the increasing polarization effect is balancing out the opposing metal-binding effects.

Irish, *et al.*,[4] have suggested that the loss of degeneracy from ν_4 be taken as an indication of contact ion pair formation. In the present case it is obviously not so, since ν_4 looses its degeneracy before contact ion pairing occurs. Apparently, in most cases where contact ion pairing does not occur, the polarization effect is too weak to noticeably affect the ν_4 frequency. However, the polarization of the magnesium cation is sufficient to cause loss of degeneracy. Even then, only by applying computer techniques could the lines be resolved. However, once contact ion pairing does occur, the polarization and metal-binding effects are large enough to cause noticeable splitting of the ν_4 frequency.

From the previously mentioned work of Brintzinger and Hester,[5] the sudden appearance of metal-binding effects at $R < 6$ should not be expected to affect the A and B modes of the ν_3 frequency. This is in fact observed, the B mode showing a monotonous increase with decreasing water content, while the A mode also decreases, albeit in not so regular a manner. Both modes approach almost the values obtained for the molten salt mixtures. It is not to be expected that the changes will be regular, since it is obvious, as observed in Figure 6, that there are more than two bands present in the 1300–1500-cm^{-1} region, especially in the higher concentration region. It should be noted that while it might be expected that the changes in frequency of both the A and B mode should be of similar magnitude,[5] this is not so. The B mode shifts by 85 cm^{-1}, while the A mode decreases by only 18 cm^{-1}. The nitrate ion is unidentate in all cases, since the lower frequency band is polarized, whereas the higher frequency line is depolarized.[5,6]

As has been observed previously, Irish and Davis[20] assigned the splitting of the $\nu_3(E')$ mode for even very dilute solutions of aqueous alkali nitrates as being due to perturbation of the NO_3^- ion by water molecules. The perturbation of the dilute-solution nitrate spectrum, which has been ascribed to hydration, has been

verified by comparison with ir studies of chloroform and methanol solutions of tetraphenylarsonium nitrate.[7] Davis, *et al.*, further suggested that the splitting is a direct result of hydrogen bonding of water to nitrate rather than a perturbation imposed by specific water structure. Irish and Davis[20] observed a split of 56 cm^{-1} for all the aqueous alkali metal nitrates studied at 25°. At room temperature, we also obtained a splitting of 56 cm^{-1} for magnesium nitrate solutions at $R = 77$ and 42, suggesting also that the nitrate is completely hydrated and that the splitting of the $\nu_3(E')$ nitrate mode is not a function of the cation present at very high water contents. The separation of the two bands at 90° decreases to 52 cm^{-1}, indicating a slight weakening of the hydration at 90°.

As the water content is reduced to $R = 20$, the splitting of the $\nu_3(E')$ mode increases, indicating once more that the nitrate ion is feeling the polarization effect of the cation even through about two layers of water molecules. It may be correct to assume that the $\nu_3(E')$ mode of the nitrate ion is affected now both by the hydration effects of the water and the polarization effects of the magnesium cation. Hester and Krishnan[22] have shown that the magnitude of splitting of the $\nu_3(E')$ mode for some molten divalent metal nitrates can be correlated with the polarization power (z/r) of the cation. If we assume that at $R = 6$ the magnesium cation is completely hydrated and acts as a large cation, as suggested by Angell,[8] this will give a value of z/r for the $Mg(H_2O)_6^{2+}$ cation of 0.58. The split separation of the two bands in the 1300–1500-cm^{-1} region for the hexahydrated melt is 98 cm^{-1}. On subtracting the hydration effect split of 52 cm^{-1} (assuming it remains constant as the water content is decreased), then the split due to the polarization effects will be 46 cm^{-1}, which fits quite well the correlation graph of Hester and Krishnan[22] (see Figure 7).

It is obvious by examining Table I that the nitrate ion experiences a strong change in environment as the water content is varied below $R = 6$. It is possible, however, to separate the changes into four separate regions, $R = 6.0$–5.1, 4.2–2.9, 2.3 and 2.0, and 0, or the anhydrous molten salt mixture. On reducing the water content from 6 to 5 mol per mole of magnesium, the bands remain essentially the same with only a small increase in separation due to the increase of the polarization effects. However, from $R = 4.2$ to $R = 2.9$ it is possible to separate the bands into four distinct bands. Two of the bands can be assigned to the nitrate–magnesium contact ion pair as in the molten salt (*ca.* 1330- and *ca.* 1490-cm^{-1} lines), especially for the $R = 3.4$ and 2.9 concentrations. The other two lines may be assigned to the nitrate ion which is not in contact with the magnesium. While at $R = 4.2$ and 3.4 the *ca.* 1444-cm^{-1} line remains almost in the same position as for the $R = 5.1$ concentration, the other lower frequency line increases suddenly from 1341 ($R = 5.1$) to 1372 ($R = 4.2$) and then remains almost constant. The decrease in the band separation at $R = 4.2$ may be assigned to a decrease or complete removal of the previously noted hydration effect of the water, which caused a 52-cm^{-1} split in the ν_3 band at high dilutions. Thus, this region can be described as a region where part of the nitrate ions are in contact with the magnesium ion, as for the molten salt, while the remaining nitrate ions are peventod by the water molecules from completely approaching the cation.

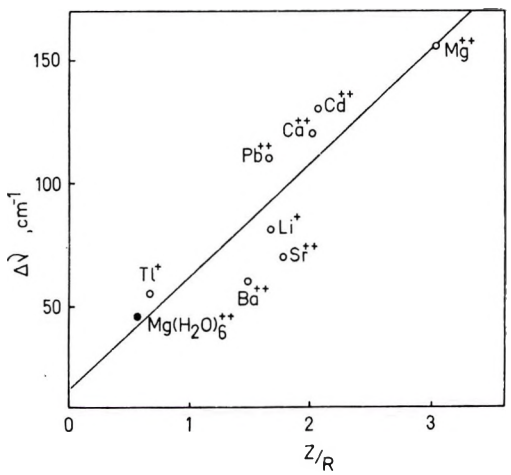

Figure 7. Plot of ionic potential z/r against the frequency difference in the 1300–1500-cm^{-1} region for various divalent molten nitrates (Figure 5a, ref 22). Also included are results for Li^+ and Tl^+ [S. C. Wait, Jr., A. T. Ward, and G. J. Janz, *J. Chem. Phys.*, **45**, 133 (1966)] and present result for $Mg(H_2O)_6^{2+}$.

For the two solutions $Mg(NO_3)_2 \cdot 2.4H_2O$ and $Mg(NO_3)_2 \cdot 2.0H_2O$, it is obvious that there is a sudden change of environment for the nitrate ion, new bands appearing for both these concentrations, similar to the effect observed in the *ca.* 1050-cm^{-1} region, but not observed in the 700–750-cm^{-1} region. Surprisingly, bands corresponding to the anhydrous melt (1330 and 1485 cm^{-1}) are absent, suggesting that at these two concentrations a special type of orientation is occurring around the nitrate ion. On removing all water, the anhydrous mixture $Mg(NO_3)_2$–$NaNO_3$ (1/1.35 mole ratio) shows only two bands corresponding to the cation ion pair with a separation of 155. Hester and Krishnan[22] also reported a difference between the two lines in this region of 155 cm^{-1}, although the absolute positions were different (1320 and 1475 cm^{-1}).

It appears, therefore, that below $R = 6.0$ a portion of the magnesium ions remain hexacoordinated to the water molecules and the remaining cations are hydrated with fewer than six water molecules. However, once a concentration of fewer than three water molecules per molecule of salt is reached, it appears that it is no longer possible for part of the cations to be hexa-

(22) R. E. Hester and K. Krishnan, *J. Chem. Phys.*, **47**, 1747 (1967).

hydrated and in equilibrium with fewer hydrated cations, and a sudden change of configuration occurs, as also observed by the changes in position of the other Raman bands at the $R = 2.4$ and 2.0 concentrations.

The sudden appearance at very low water content ($R = 2.4$ and 2.0) of two lines in the 1050-cm^{-1} region is worthy of note. Neither of these two lines appears at frequencies similar to those of solutions of higher water content or the anhydrous melt.

Splitting of the *ca.* 1050-cm^{-1} band in a manner similar to the present case has been reported, however, by Hester and Krishnan[23] in their study of the vibrational spectra of some glasses of alkali nitrates with group IIa and IIb metal nitrates and with zinc chloride and water. We have recently noted a similar effect in molten $Mg(NO_3)_2$–$NaNO_3$ and $Mg(NO_3)_2$–KNO_3. Hester and Krishnan[23] interpreted their results by postulating the existence in the glasses of definite magnesium nitrate complexes distribututed in a matrix whose structure is essentially that of the simple alkali nitrate melts. However, in the absence of a second cation in the $Mg(NO_3)_2$–H_2O system, it must be assumed that both the frequencies are attributable to the nitrate ion affected by the magnesium cation.

Irish, *et al.*,[24] in a recent paper have suggested quasilattice features for highly concentrated lithium nitrate solutions. They suggested from a comparison of the results for concentrated aqueous solutions, hydrated and anhydrous solids, and also the results for molten lithium nitrate, that in the melt there may exist two sites for the nitrate anion. One or more nitrate ions may contact the lithium in the plane of the nitrate (layering) and other nitrates above and below these layers. Similarly, in the present system, the $Mg(NO_3)_2 \cdot 2.4H_2O$ and $Mg(NO_3)_2 \cdot 2H_2O$ melts may possess a perturbed lattice structure of the two-site model suggested by Irish.[24] Apparently the two remaining water molecules are in contact with the magnesium cation, producing two nonequivalent sites for the nitrate anion. This behavior is supported by the frequencies observed in the 1300–1500-cm^{-1} region for the above two solutions.

General Interpretation. The structure of the $Mg(NO_3)_2$–H_2O system can be divided into five approximate concentration ranges, but sharp changes are not implied. The first stage is the very dilute range ($R > 20$), where the nitrate ion and the magnesium ion are completely hydrated and the nitrate is not at all affected by the cation present but is hydrated by the water molecules. In the second region ($R = 20$–6), the magnesium and nitrate ions remain hydrated, but now the nitrate ion is feeling the increasing effect of the polarization power of the cation in addition to the hydration effects. It is further suggested that the magnesium cation is hexahydrated and behaves like a large cation, as suggested by Angell,[8] and behaves as an aqueous melt.

Apparently, the fact that the magnesium is hexahydrated allows it to behave as a unique large cation without any contact ion pairing until the water content is reduced to less than 6 moles per mole of magnesium nitrate. This is in contrast to salts such as $Ca(NO_3)_2 \cdot 4H_2O$ and $Cd(NO_3)_2 \cdot 4H_2O$, which melt retaining their water and show contact ion pairs even at high water concentration.[14,16,25] Thus, while a salt such as $Ca(NO_3)_2 \cdot 4H_2O$ melts retaining its water molecules, coordination factors still allow contact ion pairs, as suggested by Braunstein.[17] Recent crystallographic work[26] on calcium nitrate tetrahydrate has shown that the solid consists of centrosymmetric $Ca_2(NO_3)_4 \cdot 8H_2O$ units with oxygen atoms both of the nitrate ions and water dipoles in contact with the calcium cation. Irish, *et al.*, note also[27] that the nitrate ion does not come into contact with the magnesium ion until the water ratio decreases below 6:1, when the appearance of a band at *ca.* 750 cm^{-1} indicates contact ion pairing, agreeing with the present results.

In the third region ($R = 5.1$–2.9) there is insufficient water to form complete hydration sheaths around all the cations. The removal of water now results in contact ion pairs, but there probably also exists in the solution hexahydrated cation in equilibrium with the contact ion pairs

$$Mg(H_2O)_6^{2+} \underset{H_2O}{\overset{NO_3^-}{\rightleftharpoons}} Mg^{2+}(NO_3^-)_x(H_2O)_{6-x}$$

($x = 1$ or 2), with the equilibrium being pushed more to the right as the water is removed. In the fourth region ($R = 2.4$–2.0), a structural rearrangement appears to occur. With the limited information available, it is difficult to postulate exactly what is occurring here. Apparently, some type of quasilattice or glass-type rearrangement has taken place (both concentrations, however, crystallize out on cooling), which provides two different sites for the nitrate anion around the cation. Or maybe the nitrate ions and water molecules are forming some type of quasilattice and trapping the magnesium inside. More careful work is being carried out on these extremely concentrated solutions and will be reported in the near future. The final stage is arrived at by completely removing all the water to produce a quasilattice molten salt with contact ion pairs.

(23) R. E. Hester and K. Krishnan, *J. Chem. Soc. A*, 1955 (1968).

(24) D. E. Irish, D. L. Nelson, and M. H. Brooker, *J. Chem. Phys.*, **54**, 654 (1971).

(25) See also the Raman spectra for molten $Ca(NO_3)_2 \cdot 4H_2O$ at 50° (Figure 4) in the 700–750-cm^{-1} region. Note the relative intensity of the higher frequency to lower frequency line and the separation between them as compared to that for $Mg(NO_3)_2 \cdot 6H_2O$.

(26) A. Leclaire and J. C. Monier, *C. R. Acad. Sci., Ser. C*, **271**, 1555 (1970).

(27) D. E. Irish, G. Chang, and D. L. Nelson, *Inorg. Chem.*, **9**, 425 (1970).

Solid State Spectra and Conductivities of the Potassium Salts of Anthracene

by P. C. Li, J. Paul Devlin,*

Department of Chemistry, Oklahoma State University, Stillwater, Oklahoma 74074

and H. A. Pohl

Department of Physics, Oklahoma State University, Stillwater, Oklahoma 74074 *(Received October 29, 1971)*

Publication costs assisted by the National Science Foundation

Crossed molecular beam vapor cocondensation techniques have been used to prepare thin films of the potassium salts of anthracene in a form well suited to both infrared and Raman sampling. Three distinct stoichiometric salts, as contrasted to solid solutions of potassium in anthracene, are apparently produced by variation of the metal–anthracene ratio. Though the existence of distinct salt crystals is strongly suggested by the observation of three sets of characteristic infrared and Raman bands, an identification of the salts as KA_2, KA, and K_2A remains tentative. The vibrational data represent the best available empirical evidence of the effect of electron transfer on the bond strengths in anthracene but are of marginal value barring transformation into force constants. Resistivities and electronic absorption spectra have also been measured for selected samples. Resistivity values, which roughly match those reported by Ubbelohde, decreased somewhat with increasing metal to organic deposition ratios. The anthracene skeletal symmetric stretching mode gave a strong resonance Raman effect with 5145-Å (green) excitation of the K_2A salt.

Introduction

The polycyclic hydrocarbon anions, typified by the mono- and dinegative ions of anthracene, are of interest as possible reaction intermediates, as subjects for the testing of chemical bonding theories and because their solid state salts may be characterized by unusual electrical properties. Thus, Hoijtink, *et al.*, have argued that one-electron LCAO MO methods apply more quantitatively to the mono- and dinegative ions than to the corresponding neutral arenes[1] and have compared theoretical predictions with liquid solution transition energies.[2] The radical anion esr spectra have long been of interest[3] primarily as information regarding charge densities and the association with cations in solutions. However, solid state studies have been almost completely restricted to the work by Ubbelohde, *et al.*, on dielectric and conductivity properties of bulk solids with alkali metal donors.[4] The bulk solids were not characterized by either X-ray or spectroscopic methods but were apparently viewed as solid solutions of alkali metals in the crystalline arenes.

Although the bond order changes that accompany electron transfer to various arenes have been estimated theoretically,[1] no direct experimental measure of the differences in bonding between the arene anions and the parent hydrocarbons has been reported. In particular, neither solution nor solid state vibrational spectra are available. Solid state fluorescent spectra for alkali metal–anthracene salts of unknown composition have been described,[5] but electronic spectra for stoichiometric solid salts are apparently missing from the literature.

A basically spectroscopic study of the potassium salts of anthracene is reported here as part of a more general study to obtain solid state vibrational and electronic spectra for stoichiometric salts of arene anions. Such data will allow ready identification of these salts in the future and, also, permit the determination of empirical force constants for certain arene anions and, thus, a comparison with theoretical predictions of bond order changes relative to the neutral arenes. Finally, resistivities determined by the four-point probe method[6] on thin salt films will be compared with values reported by Ubbelohde for related bulk samples.[4]

Experimental Section

The potassium salts of anthracene have been prepared by cocondensation of the metal with the organic from molecular beams which cross at the surface of a substrate having properties appropriate for the anticipated measurement. The techniques are an extension of those originally developed for infrared sampling of thin films of the alkali metal salts of tetracyanoethyl-

(1) P. Balk, S. DeBruijn, and G. J. Hoijtink, *Recl. Trav. Chim. Pays-Bas*, **76**, 813 (1957).

(2) K. H. J. Buschow, J. Dieleman, and G. J. Hoijtink, *J. Chem. Phys.*, **42**, 1993 (1965).

(3) D. Lipkin, D. E. Paul, J. Townsend, and S. I. Weissman, *J. Amer. Chem. Soc.*, **78**, 119 (1956).

(4) See, for example (a) J. P. V. Gracey and A. R. Ubbelohde, *J. Chem. Soc.*, 4089 (1955); and (b) G. C. Martin, N. D. Parkyns, and A. R. Ubbelohde, *ibid.*, 4958 (1961).

(5) V. V. Slobodyanik and A. N. Faidysk, *Opt. Spektrosk.*, **26**, 138 (1969).

(6) L. B. Valdes, *Proc. I.R.E.*, **41**, 420 (1954).

ene.[7] The molecular beams originated from Knudsen cells containing the liquid metal (~200°) and crystalline anthracene (~120°). The Knudsen cells were mounted within the vacuum shroud of a low-temperature cell (resembling those commonly employed in matrix isolation spectroscopy)[8] and directed towards the cryotip which supported appropriate substrates for absorption, Raman scattering, and conductivity measurements. Deposition was thus simultaneously onto a central CsBr optical plate, an aluminum wedge for Raman sampling by the single reflection technique,[9a] and a gold striped fused quartz plate for conductivity measurements. The ratio of metal to organic in the condensate was controlled by varying the Knudsen cell temperatures.

Originally depositions were made at ~100°K (substrate temperature), but the occlusion of unreacted potassium or anthracene aggregates, though a source of some unusual spectroscopic effects, tended to confuse both the spectroscopic and conductivity results. Consequently, the technique has evolved wherein the thin films are prepared at 25° but subsequently cooled to liquid N_2 temperatures for most measurements. The reduced temperatures kinetically stabilized the deposits which detectably deteriorate in a few hours at 25°, even in a 10^{-5} Torr vacuum. Since the anthracene is volatile at 25°, the warmer temperatures guarded against deposition of pure anthracene in anthracene-rich deposits while the potassium was sufficiently mobile at 25° to ensure the absence of metal aggregates in a 2:1 (metal-rich) deposit. The warmer substrate temperatures did necessitate that more extreme precautions be taken to eliminate surface moisture, since, at 25°, such moisture is highly reactive towards the anthracene salts.

The deposits were transparent, brightly colored (yellow-green through blue) films a few microns thick as required for measurement of the infrared spectra. Raman spectra were also easily obtained, although sample fluorescence (probably from tetracene impurity in most cases) often dictated a choice of the laser excitation wavelength of 5145 Å rather than 4880 Å. The sample film thicknesses, optimized for measurement of vibrational spectra, were, in general, too great for observation of details in the electronic absorption spectra though qualitative data have been obtained.

Infrared data were recorded from 600 to 4000 cm^{-1} on a Beckman IR-7 spectrometer, while the Raman and visible absorption measurements were with a Jarrell-Ash 25-100 dual monochromator fitted with an ITT FW-130 PM tube and photon-counting gear. Raman spectra were excited with a Coherent Radiation Model 52 argon ion laser using both the 4880 (blue) and 5145 Å (green) lines. The electronic spectra were determined in a single beam mode with a tungsten lamp source and using the Jarrell-Ash system, rather than a conventional uv–visible instrument, as dictated by the size and geometry of our sampling system. Resistivities were deduced from voltage and current measurements from the thin films on a fused quartz substrate using a four-point probe.[6] Current measurements were with a Keithley Model 417 picoammeter while voltages were followed using a Philbrick/Nexus millivoltmeter.

Results and Discussion

A. Vibrational Spectra. Both the vibrational and electronic spectra of the codeposits clearly suggest that the anthracene molecule can assume three distinctly different forms in the potassium–anthracene solid films. Each form has a unique vibrational spectrum that differs significantly from that of pure anthracene and, thus, suggests that considerable ionic character is involved in the metal–organic interaction in each case.[9b] Based on the approximate K/A ratios that produce the films in which the various unique spectra are dominant, it is suggested that the different anthracene forms correspond to (a) two anthracene molecules with one associated potassium atom (KA_2), (b) one anthracene molecule per associated potassium atom (KA), and (c) one anthracene molecule per two associated potassium atoms (K_2A).

Although it has been possible to obtain KA and K_2A in nearly pure form, this alone does not completely confirm that stoichiometric salt crystals of regular structure are the dominant solid forms. It is still conceivable that the solids are basically solutions of continuously variable composition with irregular structures in which KA_2, KA, and K_2A units occur with a frequency dictated by the metal–organic ratio deposited. However, it is our judgment that the uniqueness and sharp quality of the three sets of vibrational spectral features are indicative of the formation of three regular stoichiometric salts, KA_2, KA, and K_2A, with the potassium assuming a cationic form in each case. Tentatively, and as a basis for discussing the various experimental

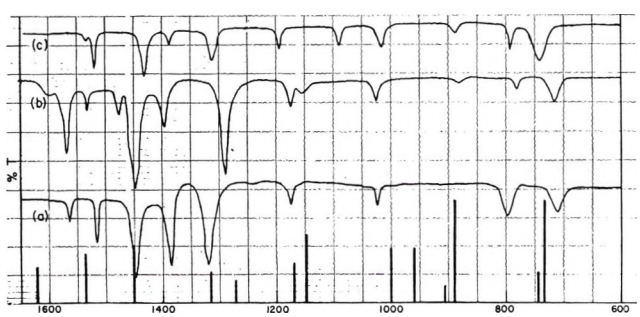

Figure 1. Infrared spectra for anthracene (bar graph) and the potassium salts of anthracene: (a) KA_2, (b) KA, and (c) K_2A.

(7) J. Stanley, D. Smith, B. Latimer, and J. P. Devlin, *J. Phys. Chem.*, **70**, 2011 (1966).

(8) See, for example, L. Andrews, *J. Chem. Phys.*, **54**, 4935 (1971).

(9) (a) I. Levin, *Spectrochim. Acta, Part A*, **25**, 1157 (1969); (b) Y. Matsunaga, *J. Chem. Phys.*, **42**, 1982 (1965).

results, we have assumed that three salts are formed: yellow-green KA_2, green KA, and green-blue K_2A.

The infrared spectra for the three salts and the Raman spectra for K_2A and KA, along with the spectra for pure anthracene, are presented in Figures 1 and 2. The Raman spectra are untouched, while the infrared curves are composites of measurements from several different deposits. No Raman spectrum for KA_2 is shown although a few band frequencies are listed in Table I. This reflects the instability of this salt, particularly in the laser beam, which prevented its preparation in a form approaching the pure state.

Table I: Frequencies (cm^{-1}) of Raman bands of Anthracene, KA_2, KA, and K_2A[a]

Anthracene[b]	KA_2	KA	K_2A
			2715
1632		1598	1542
1555		1538	1470
1481	1471	1442	1390
1403		1395	1357
		1293	1315
1261	1260	1260	
1188		1180	1160
1165	1155	1152	
1009	1025	1022	1017
956[c]		950	
904[c]	~900	880	
		835	
754	738	735	722
655		642	650(?)
602		605	595
525			480
395		370	390
290[b]		305	210(?)

[a] For relative intensities see Figure 2. [b] N. Abasbegovic, N. Vukotic, and L. Colombo, *J. Chem. Phys.*, **41**, 2575 (1964). [c] M. Suzuki, T. Yokoyama, and M. Ito, *Spectrochim. Acta, Part A*, **24**, 1091 (1968).

The untouched Raman curves of Figure 2 are evidence of the near purity of certain of the K_2A and KA films. It should be emphasized, however, that the preparation procedures only guarantee that the "K_2A" deposits are richer in K than the "KA" deposits but do not require that the actual metal to organic ratios be 2:1 and 1:1, respectively. In other words, despite the control of such parameters as temperature and orifice size, the relative densities of the molecular beams from the potassium and anthracene Knudsen cells have not been established with sufficient accuracy. What is known is that the bands in Figure 2a (or 2b) go with a single compound judging from their constant relative intensities over the range of deposition ratios in which they are detectable. The stability of the mono- and dinegative anthracene anions in solution[2] favor the KA and K_2A choice for the stable salts.

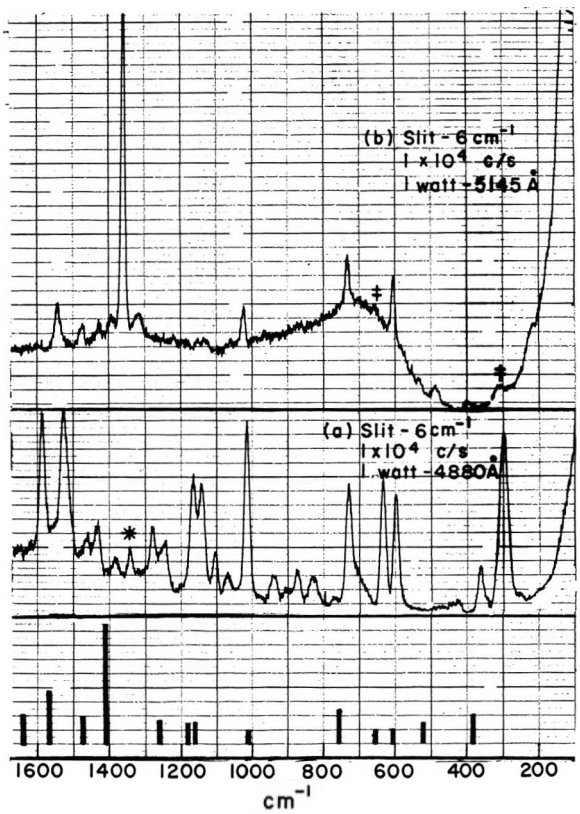

Figure 2. Raman spectrum of anthracene (bar graph) and the potassium salts of anthracene: (a) KA and (b) K_2A. The asterisk denotes KA_2 impurity in KA, and the daggers denote KA impurity in KA_2.

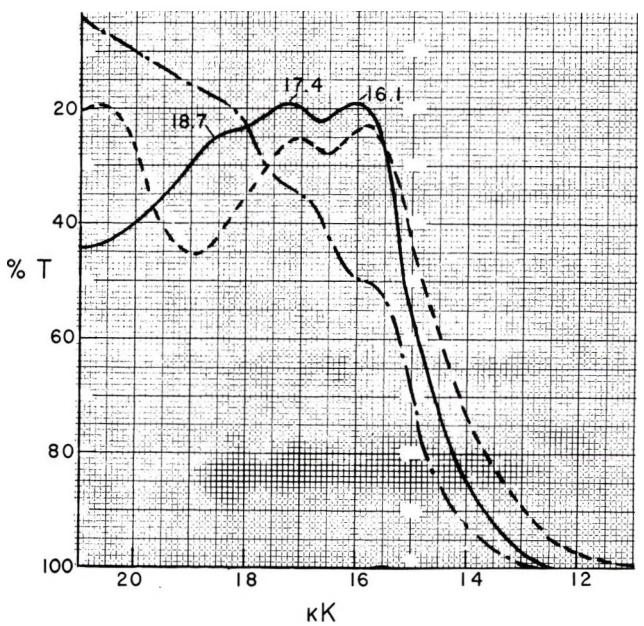

Figure 3. Electronic absorption spectra for the potassium salts of anthracene in the 12–21-kK frequency range: —·—, KA_2; - - -, KA; —, K_2A.

The vibrational data for the three salts are tabulated in Tables I and II with an attempt made to follow the frequency variation of some modes through the series

$A \rightarrow K_2A$. It is expected that a force constant analysis will establish more clearly the trends in bond order changes for this series and eventually permit reliable assignments of the vibrational data to molecular normal modes. Until such empirical force constants have been determined (from a study now in progress) the precise significance of the individual frequency shifts will remain obscure. It can be noted, however, that theory predicts that certain bonds will be strengthened while others are weakened as a result of one and two electron transfer to anthracene.[1] Thus, although the transferred electron(s) has a net antibonding quality, an orderly decrease in the fundamental frequencies is not expected. In fact, irregularities are apparent in the behavior of certain modal frequencies in Tables I and II (*e.g.*, the anthracene mode at 1009 cm^{-1} increases to 1022 cm^{-1} in KA but then decreases to 1017 cm^{-1} in K_2A). The lack of a completely regular pattern makes a force constant analysis an imperative step in any quantitative consideration of bonding effects.

Table II: Frequencies (cm^{-1}) for Infrared Bands of Anthracene, KA_2, KA, and K_2A[a]

Anthracene[b]	KA_2	KA	K_2A
3049	...	3030	3010
3022	...	2990	2960
		1600	
1620	1564	1567	1533
		1530	
1533	1515	1475	1519
1448	1448	1445	1431
1398	1383	1395	1387
1316	1320	1288	1312
1269	...	...	...
1169 / 1150	1173	1175	1194 / 1155
			1090
999	1023	1025	1016
956	...	...	...
886	...	882	888
743	798	782	793
737 / 727	710	715	740

[a] For relative intensities see Figure 1. [b] From S. Califano, *J. Chem. Phys.*, **36**, 903 (1962).

B. Electronic Absorption Spectra. Qualitatively useful visible absorption spectra for the anthracene salts are presented in Figure 3 for the frequency range 12 to 21 kK, the region where new bands are known to appear in the solution spectra of these anions. The electronic spectra are of particular interest for comparison with solution spectra reported for the mono- and dianions associated with various cations.[2] The visible spectra were also of interest in this study because resonance Raman effects have been detected (see next section) that suggest absorption patterns requiring substantiation.

The salt spectra resemble those of the corresponding solvated anion. Thus, K_2A has a structured absorption band centered near 18 kK as does the dianion in association with the potassium cation in solution.[2] The comparison for the KA salt with the mononegative anion spectrum shows a greater difference, but the red shift relative to K_2A is in the direction of the ~14-kK band peak reported for the mononegative anion associated with Na^+ in solution.[2] The absorption curve for the KA_2 solid, like most of the data for this extremely unstable compound, may be less reliable. The KA_2 spectrum, however, is markedly different than for the other salts with no obvious band maxima in the 12 to 21 kK range, a fact consistent with the yellow-green color.

The K_2A absorption band system near 18 kK has components spaced by ~1300 cm^{-1} with maxima at 16.1, 17.4, and 18.7 kK. The spacing of maxima is reminiscent of that of ~1400 cm^{-1} in the familiar absorption and fluorescence spectra of pure anthracene[10] and suggests that the same vibrational mode, a symmetric ring-stretching mode, is involved in the dianion absorption process.

C. K_2A Resonance Raman Effect. The colored quality of the salts and the nature of the Raman sampling procedure favored observation of the resonance Raman phenomenon.[11] In particular, the visible absorption spectrum for the K_2A salt (Figure 3) indicates that the 18.7-kK component is absorbing at the 19.4-kK frequency of the argon laser green line. Further, the thin film character of the samples minimized the probability of reabsorption of resonantly scattered light. Thus, not surprisingly, the K_2A Raman active mode at 1357 cm^{-1} gave a strong Resonance Raman effect with green line (5145 Å) excitation. This mode displayed a normal intensity with blue (4880 Å) excitation, but appeared with a factor of 5 greater intensity than any other K_2A Raman feature when the 5145 Å line was used. It is possible that other modes displayed less pronounced resonance scattering, but only the intensity of the K_2A feature at 1357 cm^{-1} varied in a striking manner with change of excitation frequency. The resonant character of the scattering was further evidenced by a significant overtone intensity (2715 cm^{-1}).

As was noted above, the K_2A electronic absorption (~18 kK) was characterized by components spaced by ~1300 cm^{-1}. This observation is undoubtedly relevant to the resonant scattering noted for the 1357 cm^{-1} mode since it is known that the resonance effect is most pronounced when the excitation frequency is matched to a vibronic absorption feature involving the vibrational mode in question.[11] In other words, the resonant scattering at 1357 cm^{-1} is consistent with the as-

(10) See, for example, B. J. Mulder, *J. Phys. Chem. Solids*, 29, 182 (1968).

(11) J. Behringer in "Raman Spectroscopy," H. Szymanski, Ed., Plenum Press, New York, N. Y., 1967.

signment of the structure on the electronic absorption band as the result of vibronic transitions involving the anthracene ring symmetric stretching mode. Of course, the $\sim$1300-cm^{-1} value would be characteristic of the mode for the electronic excited state.

D. Conductivity Results. Ubbelohde, *et al.*, have described rather extensive studies of the electrical characteristics of the alkali metal–anthracene crystals prepared from solution. They conclude that the conductivity increases significantly as the metal to anthracene ratio is increased, but that resistivities remain quite high—in the 10^8 to 10^{10} ohm-cm range at 20°. Though our thin film spectroscopic results seem to contradict their view of the solids as solutions of metal atoms in anthracene with a continuously variable composition, the new data support their contention that electron transfer occurs from the metal atoms to anthracene. Further, our resistivity data, obtained by the four-point probe method, are reasonably compatible with the published values from the bulk samples. Thus, the resistivity was observed to decrease roughly two decades as the metal to anthracene ratio was varied from 1:2 to 2:1. However, the measured thin film resistivities were significantly lower than those reported for bulk samples of comparable composition, the range extending from 10^6 to 10^8 ohm-cm at $\sim$100°K. Our data do not warrant a more quantitative presentation at this time.

Acknowledgments. This research was supported by the National Science Foundation under Grant GP-24256, the Paint Research Institute, and the Oklahoma State University Research Foundation.

Photoelectron Spectra of CH_3SH, $(CH_3)_2S$, C_6H_5SH, and $C_6H_5CH_2SH$; the Bonding between Sulfur and Carbon

by D. C. Frost, F. G. Herring, A. Katrib, C. A. McDowell,* and R. A. N. McLean

Department of Chemistry, University of British Columbia, Vancouver 8, British Columbia, Canada
(Received November 17, 1971)

Publication costs assisted by The National Research Council of Canada

The first ionization potential in the photoelectron spectra of CH_3SH (9.42 eV) and $(CH_3)_2S$ (8.65 eV) as in H_2S (10.47 eV) corresponds to ionization of a lone-pair electron, and, although there is a small π interaction in the C–S bond, the inductive effect is thought to cause the considerable shift to lower energy. In contrast to these molecules and α-toluenethiol (first I.P., 9.25 eV) the sulfur lone pair in thiophenol exhibits a considerable amount of π interaction with the adjacent benzene ring. The higher I.P.'s of CH_3SH and $(CH_3)_2S$ have been assigned, and it is shown that ionization occurs more readily from σ orbitals situated mainly in the C–S bond than the S–H bond.

Introduction

Photoelectron spectroscopic studies have been carried out previously on divalent sulfur compounds.[1,2] In particular the PE spectrum of hydrogen sulfide is the subject of intensive research.[2] The present study reports the effect on the PE spectrum of successive replacement of the hydrogen atoms in H_2S by alkyl and phenyl groups.

Divalent sulfur is generally thought to participate in bonding *via* two σ bonds involving mainly two of the three 3p orbitals on the sulfur atom leaving the 3s orbital and the remaining 3p orbital to accommodate the four nonbonding electrons. The possibility of the sulfur 3d electrons playing a role in the bonding is discussed in section D later in this paper. The formally "3s nonbonding pair" is much more tightly held by the sulfur atom than the "3p nonbonding pair" and is directly involved in molecular bonding. The replacement of hydrogen atoms in H_2S by electron-donating groups leads to a destabilization of these electron pairs, which is reflected in the ionization potentials of these molecules. The first ionization potentials of a number

(1) W. R. Cullen, D. C. Frost, and D. A. Vroom, *Inorg. Chem.*, **8**, 1803 (1969).

(2) (a) J. Delwiche and P. Natalis, *Chem. Phys. Lett.*, **5**, 564 (1970); (b) D. W. Turner, C. Baker, A. D. Baker, and C. R. Brundle, "Molecular Photoelectron Spectroscopy," Wiley, New York, N. Y., 1970, Chapter 4; (c) D. C. Frost, A. Katrib, C. A. McDowell, and R. A. N. McLean, *Int. J. Mass Spectrom. Ion Phys.*, **7**, 485 (1971).

Table I: Vertical Ionization Potentials of Methylmercaptan and Dimethyl Sulfide (eV)

Methylmercaptan			Dimethyl sulfide			
CNDO/2	Experimental	Orbital type	CNDO/2	Experimental		Orbital[b] type
8.4	9.42	n(S3p) a''	7.7	8.68[a]	8.65	n(S3p) b_1
10.8	12.0	σ(S–C) a'	11.4	10.96	11.2	σ(S–C) a_1
14.5	13.9	σ(S–H) a'	11.5	12.16	12.6	σ(S–C) b_2
17.1	15.0	$\sigma(CH_3)$ a''	15.1	13.68	14.2	$\sigma(CH_3)$ b_2
17.3	15.5	$\sigma(CH_3)$ a''	16.1		14.8	$\sigma(CH_3)$ a_2
21.4	~20.0	n(S,3s) a'	17.5		15.4	$\sigma(CH_3)$ b_1
			18.4		15.7	$\sigma(CH_3)$ a_1
			20.3		19.7	~n(S,3s) a_1

[a] From ref 1 (adiabatic I.P.'s). [b] Assuming C_{2v} symmetry.

of divalent sulfur compounds earlier obtained by other methods[3] illustrate this effect, *e.g.*, CH_3SH (9.44 eV), C_2H_5SH (9.285 eV), $C_2H_5CH_2SH$ (9.195 eV), CH_3SCH_3 (8.685 eV), $C_2H_5SCH_3$ (8.55 eV), and $C_2H_5SC_2H_5$ (8.43 eV). Obviously the larger the alkyl group, the greater will be the destabilization and the lower the ionization potentials.

We wish to report here the high-resolution 584-Å photoelectron spectra of methyl mercaptan, dimethyl sulfide, thiophenol, and α-toluenethiol together with CNDO/2 calculations which are used to aid the interpretation in the absence of more rigorous calculations.

Experimental Section

The photoelectron spectrometer used in this work will be fully described elsewhere.[4] The energy source is the helium I 584-Å (21.22 eV) resonance line. Calibration of the spectra was accomplished by inclusion of small amounts of argon as an internal standard. The sample pressure in the instrument was about 10^{-5} Torr.

The materials for the study were obtained from Matheson Co. Ltd. (CH_3SH) and K & K Laboratories, Inc. ($(CH_3)_2S$, C_6H_5SH and $C_6H_5CH_2SH$). There were no obvious impurity lines observed in the spectra.

In the following discussion Koopman's theorem is assumed to hold. The vertical ionization potentials and results of CNDO/2 calculations for CH_3SH and $(CH_3)_2S$ are listed in Table I.

Results and Discussion

A. "Nonbonding" Electrons. It is to be expected, as in H_2S, that the first electron removed from molecules of the type RSH or R_2S will come from the "3p lone-pair" orbital unless one of the groups R possesses energy levels of its own near the energy of the sulfur 3p orbital. This situation occurs in thiophenol and α-toluenethiol where the benzene ring I.P.'s lie at about the same energy as the sulfur lone-pair I.P.

The PE band produced on ionization of a nonbonding electron is characteristically sharp reflecting the negligible change in the Franck–Condon envelope between the neutral species and the ion. Consequently the lone-pair I.P.'s in CH_3SH and $(CH_3)_2S$ are readily identifiable, as can be seen from Figure 1, at 9.42 and 8.65 eV, respectively, compared to 10.47 eV for H_2S. These compare well with earlier values.[3,5] Therefore, as expected, the sulfur lone pair has become progressively destabilized. The CNDO/2 calculations[6] we have carried out predict the separation of the lone-pair ionization of these compounds (H_2S, 9.4; CH_3SH, 8.4; $(CH_3)_2S$, 7.7 eV) well, although after the usual 4-eV scale has been employed the predicted I.P.'s are about 1 eV too low. The results of the calculation indicate that the methyl group orbitals destabilize the sulfur 3p

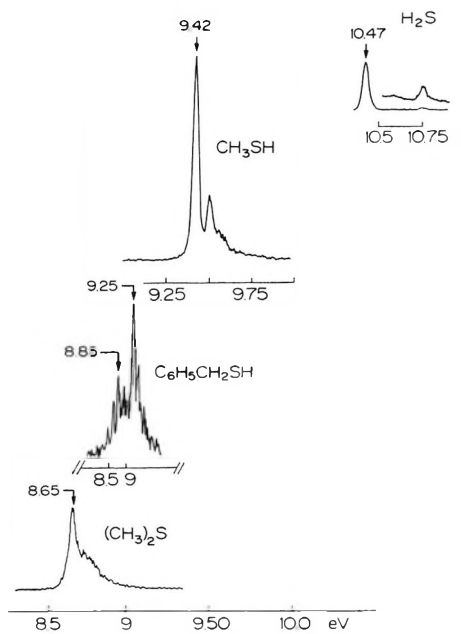

Figure 1. First I.P.'s of H_2S, CH_3SH, $C_6H_5CH_2SH$, and $(CH_3)_2S$ observed in their photoelectron spectra obtained using the He 584-Å resonance radiation.

(3) K. Watanabe, T. Nakayama, and J. Mottl, *J. Quant. Spectrosc. Radiat. Transfer*, 2, 369 (1962).

(4) D. C. Frost, A. Katrib, and C. A. McDowell, to be published.

(5) G. Herzberg, "Electronic Spectra of Polyatomic Molecules," Van Nostrand, Princeton, N. J., 1967.

(6) J. A. Pople and D. L. Beveridge, "Approximate Molecular Orbital Theory," McGraw-Hill, New York, N. Y., 1970.

orbital and produce an increasingly S–C π-antibonding molecular orbital.

The vibrational spacing evident in the photoelectron spectra should give some indication of this antibonding character. For CH_3SH, the vibrational spacings are 680 ± 40 and 1250 ± 80 cm^{-1}. The first obviously corresponds to the C–S stretching vibration, which is expected to be excited if there is any interaction between the sulfur $p\pi$ orbital and a carbon p orbital. As the C–S stretching frequency is 704 cm^{-1} [5] in the neutral species, it is impossible to say whether the highest orbital is bonding or antibonding with respect to the carbon–sulfur bond, but whichever it is the interaction is apparently fairly small. The 1250-cm^{-1} vibration almost certainly corresponds to the symmetrical deformation of the CH_3 group (reduced from 1335 cm^{-1} in the neutral species) in line with the slight amount of CH_3 σ-bonding character in the mainly lone-pair orbital. It would be useful to compare the vibrational structure on the first PES band of CH_3SH with that of the alkyl halides. The best molecule for such a comparison would be CH_3I where the spin-orbit coupling is large enough to produce two components well enough separated such that their mutual interaction is small. Also as far as interaction of the "lone pair" with other orbitals is concerned, it is best to compare sulfur and iodine, since CH_3I has its first I.P. at $\simeq$9.50 eV.[7] In CH_3I the principal vibration excited is ν_2, the symmetric deformation (1290,[2] 1260,[8] or 1225 cm^{-1} [7]). The C–I stretching vibration is also evident,[7,8] though it is not well resolved in the former study, and the symmetric CH-stretching vibration has been observed[7] as well. In CH_3I there is similar slight reduction in the C–I stretching frequency on ionizing, indicating a slightly π-bonding interaction in the C–I bond. It seems therefore that if anything the slight reduction for CH_3SH may just be significant despite the error limit and that in contrast to the calculation there is a very small amount of π-bonding character in the C–I bond. However as a whole the sulfur lone pair is destabilized compared to that of H_2S by interaction with the methyl group, mainly by σ donation.

The substitution of another H atom by a CH_3 group does not have as large an effect on the I.P., but the vibrational frequency is now somewhat greater for the ion (750 ± 60 cm^{-1}) than in the neutral species (685 cm^{-1}).[9] The lone pair must be very slightly antibonding with respect to the two carbon atoms which must be bonding with respect to each other. This was also shown in the CNDO/2 calculations. It seems that the large shift of the first I.P. to lower energy in $(CH_3)_2S$ and CH_3SH compared to H_2S is due principally to a large σ-inductive effect raising the coulomb energy of the sulfur 3p orbitals, and to a much lesser extent, to π interaction between sulfur and carbon orbitals.

The π interaction of a sulfur lone pair with methyl groups is relatively small. However, we shall now see that the opposite is the case when sulfur is attached to a phenyl group. This can best be seen by comparing the PE spectra of benzenethiol (PhSH) and toluenethiol ($PhCH_2SH$). In benzene the lowest I.P. due to ionization from the π e_{1g} orbital is at 9.25 eV[10] and in monosubstituted benzenes (C_{2v} or lower symmetry) this is split into two orbitals, one having a π interaction with the substituent (b_1 in C_{2v}) and one non- (or less) interacting (a_2 in C_{2v}). The separation between these two levels is greatest with substituents with polarizable lone pairs and least for a substituent with no lone pairs.[11] Toluene is of this latter type and the PE band exhibits only a slight broadening and a shift to lower energy compared to benzene.[11,12] Replacement of one of the H atoms of the CH_3 group by the SH group produces no remarkable changes in the PE spectrum except for the superposition of a new sharp peak (at 9.25 eV) with at least one other vibrational component (spacing $\sim$1220 cm^{-1}). The first vertical I.P. is 8.85 eV (*cf.* 8.81 eV in toluene). It can be seen in this case that the sulfur lone pair has an almost negligible effect on the orbitals of the benzene ring. The inverse is also true, as besides the sharp band, $PhCH_2SH$ has its sulfur lone-pair I.P. at 9.25 eV (Figure 1) compared with that of CH_3CH_2SH at 9.285 eV.[3] The vibrational spacing of 1220 ± 50 cm^{-1} probably corresponds to the wagging motion of the CH_2 group at $\sim$1400 cm^{-1}, as there will be some interaction between the sulfur lone pair and the CH_2 orbitals.

In contrast to α-toluenethiol, the replacement of one H atom in benzene by a SH group has an enormous effect. Below 11 eV instead of the one I.P., there are three at vertical I.P.'s 8.28, 9.38, and 10.65 eV, respectively (Figure 2). The 9.38-eV band obviously corresponds to the noninteracting benzene ring orbital. The separation between the other two I.P.'s (2.37 eV) shows the size of the interaction between the sulfur lone pair (originally at $\sim$9.4 eV) and the π ("B_1") orbital of the benzene ring (originally at 9.38 eV). Iodobenzene also shows a large interaction, but the separation between the two b_1 I.P.'s is only 1.78 eV and the lowest I.P. is at 8.67 eV.[11] This latter is also mainly π (C_6H_5) as the a_2 π (C_6H_5) is still at 9.38 eV and the b_2 π (I) is at 9.64 eV. The 8.28-eV I.P. of PhSH is slightly narrower than the 10.65-eV band and because the 0 →

(7) J. L. Ragle, I. A. Stenhouse, D. C. Frost, and C. A. McDowell, *J. Chem. Phys.*, **53**, 178 (1970).

(8) A. W. Potts, H. J. Lempka, D. G. Streets, and W. C. Price, *Phil. Trans. Roy. Soc. London, Ser. A*, **268**, 59 (1970).

(9) G. Herzberg, "Electronic Spectra of Polyatomic Molecules," Van Nostrand, Princeton, N. Y., 1967, p 652.

(10) I. D. Clark and D. C. Frost, *J. Amer. Chem. Soc.*, **89**, 244 (1967).

(11) (a) D. W. Turner, C. Baker, A. D. Baker, and C. R. Brundle, "Molecular Photoelectron Spectroscopy," Wiley, New York, N. Y., 1970, Chapter 11; (b) A. D. Baker, D. P. May, and D. W. Turner, *J. Chem. Soc. B*, 22 (1968).

(12) A. Cornford, D. C. Frost, and R. A. N. McLean, unpublished results.

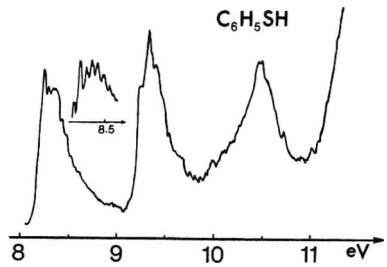

Figure 2. The photoelectron spectrum of C_6H_5SH obtained using the He 584-Å resonance radiation.

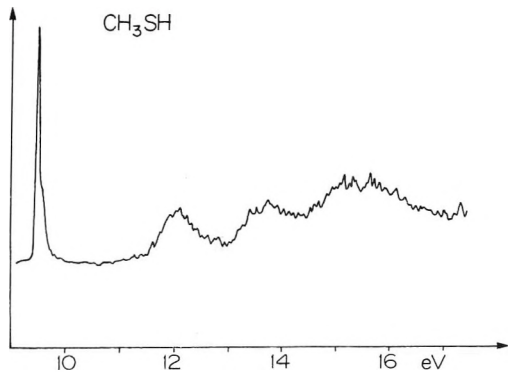

Figure 3. The photoelectron spectrum of CH_3SH obtained using the He 584-Å resonance radiation.

0 transition is the vertical one, we believe the corresponding orbital to have more sulfur lone-pair character. The vibrational structure on the band consists of a progression of eight peaks separated by ~400 cm^{-1}, which probably corresponds to the substituent-sensitive ring breathing mode at 412 cm^{-1} in the neutral thiophenol.[13]

CNDO/2 calculations carried out on α-toluenethiol assuming the $C(H_2)$–S–H plane to be perpendicular to the ring predict the second ionization potential to be associated with the removal of an electron from the sulfur lone-pair orbital. This lone-pair orbital is almost completely noninteracting as regards the benzene ring. Slight deviations in this configuration are predicted to cause little change in the ionization potential. However, if the $C(H_2)$–S–H plane coincides with the plane of the benzene ring and becomes the origin of the lowest I.P. comparison of the calculations and photoelectron spectra indicates that the former configuration is preferable. In the case of thiophenol the calculations show that the first I.P. arises from an orbital which is formed mainly from the sulfur lone pair with a considerable amount of benzene ring character, which is in agreement with the interpretation of the PE spectrum suggested above.

B. Sulfur–Carbon and Sulfur–Hydrogen σ-Bonding Electrons. For methanethiol and dimethyl sulfide, the second and third ionization potentials (see Figures 3 and 4) should correspond to ionization from mainly the C–S–H and C–S–C bonding regions, respectively. In CH_3SH the second and third I.P.'s are at 12.01 and 13.9 eV, neither band having any resolvable vibrational structure (the lack of structure in the second band is probably due to a dissociation to CH_3S^+ at 11.2 ± 0.5 eV).[14] By comparison with H_2S and $(CH_3)_2S$ it should be possible to decide which orbital has more S–H character and which more S–C character. In H_2S the S–H bonding orbitals are at −13.4 (a_1) and −15.2 eV (b_2), and in $(CH_3)_2S$ we assign the C–S bonding orbitals I.P.'s as 11.2 (a_1) and 12.6 eV (b_2). Thus, by taking the average of these two it seems that the 12.0-eV band arises from an orbital with more S–C character and the 13.9-eV band from an orbital with more S–H character. The CNDO/2 calculations show an almost equal amount of each with the second I.P. MO having most of its density on the sulfur and the third on carbon and the unique hydrogen, hence the usual[15] overestimation of the separation between them. Methyl iodide (which we have compared with methanethiol above as regards the lone pairs) has its C–I σ-bonding I.P. at 12.50 eV, which is again fairly close to the mainly C–S σ-bonding I.P. at 12.0 eV.

C. Other Bands of Methanethiol and Dimethyl Sulfide. As in the alkyl halides[7,8,16] the higher energy I.P.'s below 21.22 eV can be assigned as from mainly CH_3-bonding orbitals. Around 15 eV in the alkyl halides there is a band with a Jahn–Teller contour assigned as ionization from the e (CH_3) bonding orbital.[8,16] In methanethiol there is a broad band of intensity twice that of the 12.0- and 13.9-eV bands with twin maxima at 15.0 and 15.5 eV which is almost the same as occurs in the PE spectrum of CH_3Br. It could almost be considered that the CH_3 group is only observing the SH group as a single atom, and certainly the CNDO/2 calculations indicate this as the two low-energy bonding CH_3 I.P.'s are almost degenerate at 17.11 and 17.27 eV. The other CH_3-bonding orbital which appears to be almost all C(2s) produces a very diffuse band in the alkyl halides PE spectra at ~20 eV, and the same thing is observed in the case of methanethiol.

For dimethyl sulfide four low-energy CH_3-bonding orbitals are expected and in the broad band from 13.50 to 16.4 eV four components can be isolated. The CNDO/2 calculations indicate a much larger than observed range for these CH_3 orbitals and probably over-

(13) D. W. Scott, J. P. McCullough, W. N. Hubbard, J. F. Messerly, I. A. Hossenlopp, F. R. Frow, and G. Waddington, *J. Amer. Chem. Soc.*, **78**, 5463 (1956).

(14) W. E. W. Ruska and J. L. Franklin, *Int. J. Mass Spectrom. Ion Phys.*, **3**, 221 (1969).

(15) We have generally found that CNDO/2 calculations tend to overestimate the interaction between symmetry related orbitals of similar energies. This can lead to errors in the assignment of PE spectra, but with consideration of this complication this can be eliminated at least in small molecules.

(16) D. W. Turner, C. Baker, A. D. Baker, and C. R. Brundle, "Molecular Photoelectron Spectroscopy," Wiley, New York, N. Y., Chapter 8.

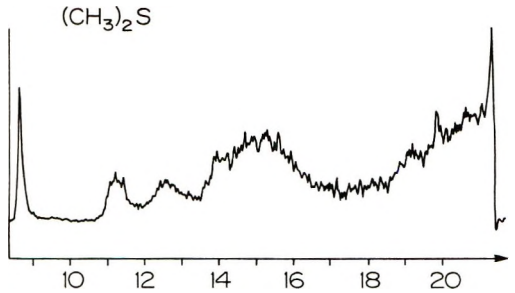

Figure 4. The photoelectron spectrum of $(CH_3)_2S$ obtained using the He 584-Å resonance radiation.

estimate the interaction between orbitals on the two CH_3 groups.

D. Sulfur 3d-Orbital Participation. There has been considerable discussion on the involvement of 3d orbitals in the bonding of bivalent sulfur compounds.[17-19] It is possible to make deductions about d-orbital participation in the normal valence states of second row elements from the PE spectral data,[20] although there may be other interactions which produce the same effects. We believe some of our results are pertinent in this regard.

Goodman and Taft[21] explained the decrease in the intensity of the $^1L_b \leftarrow {}^1A$ transition in going from thiophenol to *p*-methylthiophenol in their substituent interference experiments in terms of a strong interaction between the π orbitals of the benzene ring and sulfur 3d orbitals. However, remeasurement of the spectra by Di Lomardo and Zauli[22] indicated that there was a slight increase in intensity from thiophenol to *p*-methylthiophenol. They inferred that there is little involvement of the sulfur 3d orbitals and that the only perturbation of the benzene ring π orbitals is *via* $S(3p\pi)$–$C(2p\pi)$ bonding. This latter interaction has been considered fully above, but we also have evidence to support Di Lomardo and Zauli's conclusion. Again assuming C_{2v} symmetry for thiophenol, it is possible for the "a_2" benzene ring π orbital to interact with the sulfur d_{xy} orbital and the "b_1" benzene π orbital to interact with the sulfur d_{xz} orbital. In the first case the overlap will be very small as the constituent orbitals involve nonadjacent atoms, and, as expected the "a_2" π orbital occurs at almost exactly the same energy (± 0.1 eV) as in PhOH, $PhNH_2$, $PhCH_3$, $PhSiH_3$, and many other monosubstituted benzenes. The real test of sulfur d-orbital interaction is in the "b_1" π orbitals with I.P.'s at 8.28 and 10.65 eV, respectively, which, as mentioned above, must have almost equal amounts of benzene π and sulfur lone-pair character. If the unperturbed benzene ring b_1 orbital I.P. were at the average of these two I.P.'s *i.e.*, 9.46 eV, the stabilization compared to the a_2 orbital would be negligible. It could be explained by the expected greater inductive effect of the sulfur atom on the b_1 orbital. As both levels would be almost at the same energy if they were unperturbed $\sim$9.40 eV, it is difficult to find any other method of measuring the interaction. We believe that this indicates if there is any stabilization of the b_1 π orbitals by the use of sulfur 3d orbitals, it is very small and has little effect on the orbital energies. The main effect on the orbital energies is the interaction between the sulfur $3p\pi$ orbital and the benzene π orbital.

Acknowledgments. We are grateful for generous financial support from the National Research Council of Canada. One of us (R. A. N. M.) thanks the University of British Columbia for a Killam Fellowship.

(17) D. R. Williams and L. T. Komtik, *J. Chem. Soc. B*, 312 (1971), and references therein.

(18) M. J. S. Dewar and N. Trinajstic, *J. Amer. Chem. Soc.*, **92**, 1453 (1970).

(19) D. P. Santry and G. A. Segal, *J. Chem. Phys.*, **47**, 158 (1967); D. P. Craig and T. Thirunamachandran, *ibid.*, **45**, 4183 (1965); E. A. C. Lucken, *J. Chem. Soc. A*, 991 (1966); E. A. C. Lucken, *Theor. Chim. Acta*, **1**, 397 (1963); I. H. Hillier and V. R. Saunders, *Chem. Commun.*, 1183 (1970).

(20) D. C. Frost, F. G. Herring, A. Katrib, R. A. N. McLean, J. E. Drake, and N. P. C. Westwood, *Chem. Phys. Lett.*, **10**, 347 (1971); *Can. J. Chem.*, **49**, 4033 (1971).

(21) L. Goodman and R. W. Taft, *J. Amer. Chem. Soc.*, **87**, 4385 (1965).

(22) G. Di Lomardo and C. Zauli, *J. Chem. Soc. A*, 1305 (1969).

Ionic–Covalent Interactions and Glass Formation in Molten Acetates: Cobalt(II) as a Spectroscopic Probe

by M. D. Ingram,* G. G. Lewis, and J. A. Duffy

Department of Chemistry, University of Aberdeen, Old Aberdeen, Scotland *(Received August 2, 1971)*

Publication costs borne completely by The Journal of Physical Chemistry

The structural chemistry of a wide range of glass-forming molten acetates has been examined using cobalt(II) as a spectroscopic probe. In several systems containing lead acetate, *e.g.*, $Pb(OAc)_2$–KOAc, cobalt(II) undergoes an octahedral–tetrahedral transition which is analogous to similar phenomena previously reported in chloride melts and borate glasses. On this basis, it is possible to distinguish between the covalent (polymeric) structure of lead acetate glass and the more ionic character of other acetate glasses. Measurements of the glass transition temperature, T_g, indicate that the LiOAc–NaOAc glasses fall into the same pattern of behavior as the ionic nitrate glasses, but that appreciable deviations occur for the lead(II) containing glasses. Molten acetates provide an interesting system for testing current theories of mass transport in molten salts.

Introduction

In recent years, it has been discovered that a wide range of fused salts, other than silicates, borates, and phosphates, can be quenched to form glasses.[1–5] These systems have received attention for two reasons. First, it is possible to test the various structural theories of glass formation for both polymeric and ionic glasses.[6] Second, since the glass transition can be regarded as the true low-temperature limit of the liquid state,[7] transport measurements in these supercooled melts can be very informative. These two aspects of glass–melt behavior are clearly related, and if a satisfactory treatment of transport behavior in molten salts is to be achieved, then something must be known about glass structure. This point is illustrated by the variation in the T_g/T_0 ratio with glass structure. The glass-forming nitrate melts have been the subject of extensive study,[6a] and it is found that the experimental glass transition temperature, T_g, is only a little higher than the ideal glass transition temperature, T_0 (calculated from transport and thermodynamic measurements). Typically, for the KNO_3–$Ca(NO_3)_2$ (62:38) glass $T_g/T_0 = 1.05$, and this has been correlated with the typically *ionic* structure of melt and glass. In contrast, in the polymeric borate and silicate systems T_g/T_0 ratios are 1.5 or greater. It is apparent, therefore, that in the discussion of these glass–melt systems, the nature of the ionic–covalent interactions among the constituent particles is important and can influence strongly both the liquid state transport properties and the glass transformation phenomena. For this reason, systems in which changes in ionicity can be brought about by straightforward composition changes (*e.g.*, $ZnCl_2$ + KCl) are of special interest and have recently received some attention.[6b,8]

The glass-forming molten acetates can also provide a bridge between essentially polymeric and ionic systems, and evidence for this is discussed in this paper. Thus, Bartholomew, *et al.*,[5d] have shown that there exists a wide range of glass compositions, and these embrace cations of widely different chemistries. This range includes (i) single-component systems, *e.g.*, LiOAc or $Pb(OAc)_2$; and (ii) various mixtures, *e.g.*, KOAc–$Ca(OAc)_2$ and KOAc–$Pb(OAc)_2$. Of particular interest are the two-component systems based on lead acetate, since it is possible that major changes in glass structure with composition can be detected spectroscopically. The spectra of transition metal ions can provide such insight into the structure of glasses.[6b,9] In this investigation cobalt(II) is used as a spectroscopic probe to distinguish different types of acetate glass. On the basis of the structural models proposed, a comparison is made between the acetate and nitrate glasses and further work in the acetate system is suggested.

(1) (a) A. P. Rostkowskii, *Zh. Obshch. Khim.*, **62**, 2055 (1939); (b) E. Thilo, C. Wieker, and W. Wieker, *Silikat Tech.*, **15**, 109 (1964).

(2) I. Schulz, *Naturwissenschaften*, **14**, 536 (1957).

(3) (a) T. Förland and W. A. Weyl, *J. Amer. Ceram. Soc.*, **33**, 186 (1950); (b) M. D. Ingram, J. A. Duffy, and S. M. Forbes, *J. Appl. Electrochem.*, **1**, 53 (1971).

(4) C. A. Angell, *J. Amer. Ceram. Soc.*, **48**, 540 (1965).

(5) (a) A. Lehrman and P. Skell, *J. Amer. Chem. Soc.*, **61**, 3340 (1939); (b) J. A. Duffy and M. D. Ingram, *J. Amer. Ceram. Soc.*, **52**, 224 (1969); (c) R. F. Bartholomew and H. J. Holland, *ibid.*, **52**, 402 (1969); (d) R. F. Bartholomew and S. S. Lewek, *ibid.*, **53**, 445 (1970).

(6) (a) C. A. Angell, *ibid.*, **51**, 117 (1968); (b) C. A. Angell and J. Wong, *J. Chem. Phys.*, **53**, 2053 (1970).

(7) C. A. Angell and C. T. Moynihan in "Molten Salts, Characterization and Analysis," G. Mamantov, Ed., Marcel Dekker, New York, N. Y., 1969, pp 315–376.

(8) (a) J. R. Moyer, J. C. Evans, and G. Y.-S. Lo, *J. Electrochem. Soc.*, **113**, 158 (1966); (b) C. A. Angell and D. M. Gruen, *J. Phys. Chem.*, **70**, 1601 (1966); (c) C. A. Angell and D. M. Gruen, *J. Inorg. Nucl. Chem.*, **29**, 2243 (1967).

(9) (a) J. A. Duffy and M. D. Ingram, *J. Chem. Soc. A*, 398 (1969); (b) M. D. Ingram and J. A. Duffy, *J. Amer. Ceram. Soc.*, **53**, 317 (1970).

Experimental Section

Materials. Both reagent grade and AnalaR chemicals were used after drying *in vacuo* at 100° and without further purification. The purity and dryness of the solids were checked by determination of the melting point and the values obtained (LiOAc, 285°; KOAc, 304°; $Pb(OAc)_2$, 203°) were found to be in good agreement with published values.[10]

Glass Preparation. In the $Pb(OAc)_2$–KOAc and $Pb(OAc)_2$–LiOAc systems, glasses were prepared containing up to 60% KOAc and 67% LiOAc, respectively, and it was also possible to prepare a pure LiOAc glass. To confirm that the "glasses" were not supercooled liquids, experiments performed with a Dupont 900 differential thermal analyzer confirmed the occurrence of a glass transition above room temperature in each case. The values of the glass transition temperature, T_g, were reproducible to ±2° for different glasses of the same composition.

Care is required in preparing glasses suitable for spectroscopic study. First, decomposition occurs if the glass-forming mixture is allowed to overheat, and second, some of the glasses are hygroscopic. Several techniques were tried, but it was found that these difficulties could be minimized by preparing the glasses inside Pyrex test tubes using gentle heating from a cool Bunsen flame. In general, it was found most convenient to prepare an intimate mixture of the components before melting. For one composition, $Pb(OAc)_2$–KOAc (3:2 mole ratio), a melt was not obtained from the above procedure, and it appeared that potassium acetate crystals were catalyzing the decomposition of the lead acetate. Successful melting was achieved by keeping the components in separate layers and allowing potassium acetate to dissolve directly into the lead acetate melt. The glasses were stored in a desiccator.

Spectroscopic Study. Spectra were recorded on a Unicam SP 700C spectrophotometer. Owing to the number of spectra which were required, and because of the limited life of optical cells when used for quenching acetate melts, the spectrophotometer was adapted so that it would record spectra of glasses in 12 × 75 mm Pyrex or silica test tubes.

Glass densities (required for the calculation of molarities) were measured with a Beckman Air Comparison pycnometer.

Results and Discussion

A. Spectroscopic Measurements. Spectrophotometric data for cobalt(II) in glasses in the $Pb(OAc)_2$–KOAc, $Pb(OAc)_2$–LiOAc, and $Pb(OAc)_2$–NaOAc systems are included in Table I. For each glass composition, four spectra were obtained with varying concentrations of cobalt(II), and the average extinction coefficients were calculated. In a previous study[9a] it was noted that when cobalt(II) acetate was used low values for the extinction coefficient were obtained (probably due to a decomposition reaction), and so in this investigation cobalt(II) was added as $CoCl_2 \cdot 6H_2O$. Check experiments revealed that identical spectra were obtained with addition of anhydrous $CoCl_2$, $CoSO_4 \cdot 7H_2O$,

Table I

Glass composition (mole ratio)	Density, kg l.$^{-1}$	ν_{max}, kK	ϵ_{max}[a]
	$Pb(OAc)_2$–KOAc system		
1:0	3.22	7.2	8
		18.4	35
3:1	3.00	7.2	15
		17.8	85
		18.8 sh	
3:2	2.70	7.6	21
		17.6	155
		18.8 sh	
1:1	2.60	7.6	30
		17.6	255
		18.8 sh	
2:3	2.36	7.8	36
		17.6	300
		18.8 sh	
	$Pb(OAc)_2$–LiOAc system		
1:1	2.69	7.2	9
		17.8	55
		18.6 sh	
1:2	2.19	7.2	11
		17.8	80
		18.6 sh	
0:1	1.25	7.5	15
		17.8	125
		19.0 sh	
	$Pb(OAc)_2$–NaOAc system		
1:1	2.50	7.4	22
		17.6	185
		18.8 sh	
	$Ca(OAc)_2$–KOAc system		
2:3	1.57	7.2	30
		17.6	180
		18.8 sh	
	LiOAc–NaOAc system[b]		
4:3	1.40	7.2	30
		17.6	180
		18.6 sh	
	$[Co(CF_3CO_2)_4]^{2-}$ in acetonitrile[c]		
		7.1	30
		17.4	180
		18.8	

[a] The values of ϵ_{max} were reproducible to ±5%, but an apparent dependence of absorbance on experimental variables including the quench rate makes the absolute accuracy difficult to assess. [b] See ref 9a. [c] See ref 11.

(10) (a) A. Lehrman and E. Leiper, *J. Amer. Chem. Soc.*, **60**, 142 (1938); (b) E. J. Pochtakova, *Russ. J. Inorg. Chem.*, **10**, 1268 (1965); (c) M. Braghetti, D. Leonesi, and P. Franzosini, *Ric. Sci.*, **38**, 116 (1968).

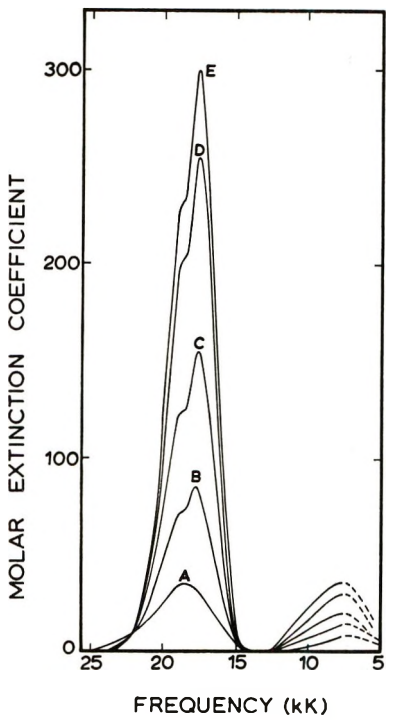

Figure 1. Spectra of cobalt(II) in lead acetate–potassium acetate glasses. Percentages of potassium acetate are as follows: A, 0%; B, 25%; C, 40%; D, 50%; E, 60%. Note: 1 kK = 1000 cm^{-1}.

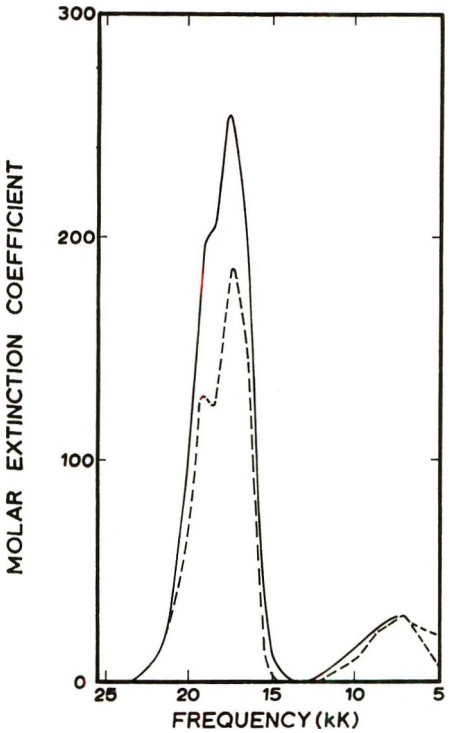

Figure 2. Spectra of "acetato"–cobalt(II) complexes. Spectrum - - - - is for $[Ph_4As]_2[Co(CF_3COO)_4]$ in MeCN; spectrum —— is for cobalt(II) in $Pb(OAc)_2$–KOAc (1:1) glass.

and $Co(NO_3)_2 \cdot 6H_2O$, and so interference from the trace anion can be discounted.

Lead Acetate–Potassium Acetate System. Figure 1 shows the spectrum of cobalt(II) in lead acetate glass, and the changes brought about by a progressive increase in the potassium acetate content. (Below 7.5 kK the spectra are shown as dashed lines because of regions of nontransparency in the glasses.)

Curve A is the spectrum in pure lead acetate glass and may be tentatively assigned to an octahedral environment. However, the spectrum differs from that of cobalt(II) in glacial acetic acid (previously assigned to octahedral coordination).[9a] For example, in the visible region the absorption maximum is at 18.4 kK instead of at 19.1 kK, and the extinction coefficient is 35 instead of 17. This pattern of data is very similar to that found in changing from sulfuric acid to a sulfate glass.[9b] It seems reasonable to advance here a similar explanation, namely that in the glass some of the acetate ions in the coordination sphere of the cobalt(II) are acting as chelating ligands.

Curves B to E show the growth of bands corresponding to a new cobalt(II) species with tetrahedral symmetry as potassium acetate is added. The spectrum of this species (*e.g.*, curve D) is nearly superposable with that of cobalt(II) in the LiOAc–NaOAc glass,[9a] and also with that of the complex anion $[Co(CF_3COO)_4]^{2-}$ (see Figure 2),[11] and it seems reasonable to infer the presence of the species $[Co(OAc)_4]^{2-}$ in the glass. Over the range of compositions studied, the molar extinction coefficients of both spectral bands continued to increase with added potassium acetate, and so it is not possible to say when conversion into the $[Co(OAc)_4]^{2-}$ complex ion is complete. However, since the extinction coefficients in the glasses D and E (Figure 1) are in fact greater than the corresponding values for the $[Co(CF_3COO^-)_4]^{2-}$ complex in acetonitrile, it seems reasonable to conclude that in the "high-alkali" acetate glasses, conversion into the $[Co(OAc)_4]^{2-}$ complex is substantial. The difference caused by replacing CF_3COO^- by CH_3COO^- is difficult to assess, but it is noteworthy that the spectrum of cobalt(II) in CF_3COOH is little different from that in CH_3COOH.[9a]

Lead Acetate–Lithium Acetate System. Figure 3 shows the spectrum of cobalt(II) in lead acetate glass and the corresponding changes brought about by addition of lithium acetate. The changes are very similar to those induced by the addition of potassium acetate, but the spectrum assigned to the $[Co(OAc)_4]^{2-}$ species grows more slowly.

Comparison of Lead Acetate–Alkali Metal Acetate Systems. It is possible to compare the extent of formation of the complex $[Co(OAc)_4]^{2-}$ in different glasses by comparing the molar extinction coefficients of the band maxima at 17.6 kK. For three glasses, $Pb(OAc)_2$–LiOAc, $Pb(OAc)_2$–NaOAc, $Pb(OAc)_2$–KOAc (each in 1:1 mole ratio), the extinction coefficients

(11) J. G. Bergman and F. A. Cotton, *Inorg. Chem.*, 5, 1420 (1966).

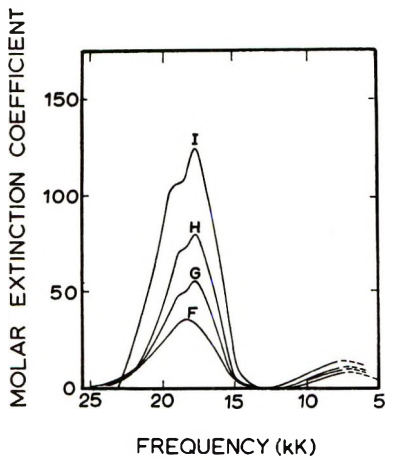

Figure 3. Spectra of cobalt(II) is lead acetate–lithium acetate glass. Percentages of lithium acetate are as follows: F, 0%; G, 50%; H, 67%; and I, 100%.

have values of 55, 185, and 255, respectively. The order of effectiveness of the alkali metal acetates in producing the $[Co(OAc)_4]^{2-}$ complex is thus lithium < sodium < potassium.

B. Ionic–Covalent Interactions. It is apparent that acetate glasses can provide two distinct types of environment for the Co^{2+} cation. In pure lead acetate glass, cobalt(II) occupies approximately octahedral sites whereas in other acetate glasses, the $[Co(OAc)_4]^{2-}$ complex anion is present to an extent which depends on glass composition (see Table I). In the $Pb(OAc)_2$–KOAc system, a well-defined octahedral–tetrahedral change is observed, and this can be represented schematically by the equation

$$\underset{\text{(octahedral sites)}\ Pb(OAc)_2\ \text{glass}}{Co^{2+}} \xrightarrow{KOAc} \underset{\text{(tetrahedral sites)}\ KOAc\text{–}Pb(OAc)_2\ \text{glasses}}{[Co(OAc)_4]^{2-}}$$

The spectra do not indicate whether this change occurs *via* a two-species equilibrium or a continuous distortion mechanism.

The significance of this coordination change is evident, if reference is made to analogous changes found in chloride melts[12] and borate glasses.[13] These may be summarized as

$$\underset{\text{(octahedral sites)}\ Al_2Cl_6\ \text{melt}}{Co^{2+}} \xrightarrow{KCl} \underset{\text{(tetrahedral complex)}\ KCl\text{–}AlCl_3\ (>1:1)\ \text{melt}}{[CoCl_4]^{2-}}$$

$$\underset{\text{(octahedral chromophore)}\ B_2O_3\ \text{glass}}{Co^{2+}} \xrightarrow{K_2O} \underset{\text{(tetrahedral chromophore)}\ K_2O\text{–}B_2O_3\ (3:7)\ \text{glass}}{[CoO_4]^{6-}}$$

In both cases, cobalt(II) changes from octahedral to tetrahedral coordination as the *ionicity* of the glass or melt increases, and indeed this effect seems to be quite general for transition metal ions in oxidation state +2.[14]

It can be concluded, therefore, that there is appreciable covalent bonding in lead acetate glass and that its structure differs qualitatively from the ionic structure present in the other acetate glasses. In short, the failure to detect the $[Co(OAc)_4]^{2-}$ species in lead acetate glass indicates the absence of "free" acetate ions.

The covalent nature of lead acetate glass is in accordance with the observed tendency towards glass formation, since in a single-component melt it is difficult to understand the suppression of crystallization processes unless polymeric species are present. The presence of such polymeric species is not surprising in view of the known power of acetate to act as a bridging ligand,[15] and the "polymers" must be polynuclear $[Pb(OAc)_2]_n$ complexes. These polynuclear species might be either chains or three-dimensional networks, but in view of the low T_g value, it is tempting to draw an analogy with vitreous boric oxide and to postulate a random network containing a high proportion of ring systems.[16] The increase in *ionicity* on addition of KOAc (and to a lesser extent NaOAc and LiOAc) to $Pb(OAc)_2$ glass can thus be understood in terms of the breakup of $[Pb(OAc)_2]_n$ groups and the concurrent formation of discrete complexes, possibly $[Pb(OAc)_3]^-$ or $[Pb(OAc)_4]^{2-}$.

With reference to the spectrum of cobalt(II) in pure lithium acetate glass, it is apparent from the band maximum at 17.6 kK that the $[Co(OAc)_4]^{2-}$ species is present but the low molar absorbance is evidence either for distortion of the complex or presence of octahedrally coordinated cobalt(II) (which has low absorbance). There is probably some polymeric character in lithium acetate glass, but there is less covalency than in the lead acetate glass.

It is instructive also to make a comparison between glasses containing lead(II) and calcium(II). The extinction coefficient of the band maximum at 17.6 kK is higher in a $Pb(OAc)_2$–KOAc glass than in the corresponding $Ca(OAc)_2$–KOAc glass; for 2:3 mole ratio glasses, the values are 300 and 180, respectively. This observation is interesting, since it might be taken as indicating greater ionicity in glasses containing lead(II) as compared with calcium(II). However, as mentioned above, in the "high-alkali" lead(II) glasses the stoichiometry permits the formation of $[Pb(OAc)_3]^-$ and $[Pb(OAc)_4]^{2-}$ complexes, and these are likely to be both more stable and more covalent than the corre-

(12) H. A. Oye and D. M. Gruen, *J. Inorg. Chem.*, **4**, 1173 (1965).

(13) (a) M. A. Aglan and H. Moore, *J. Soc. Glass. Technol.*, **39**, 351T (1955); (b) B. F. Dzhurinskii, *Izv. Akad. Nauk SSSR, Neorgan., Mater.*, **1**, 272 (1965); (c) A. Paul and R. W. Douglas, *Phys. Chem. Glasses*, **9**, 21 (1968).

(14) (a) T. Bates in "Modern Aspects of the Vitreous State," Vol. 2, J. D. Mackenzie, Ed., Butterworth, London, 1962, pp 145–254; (b) W. E. Smith, J. Brynestad, and G. P. Smith, *J. Amer. Chem. Soc.*, **89**, 5983 (1967).

(15) (a) C. Oldham in "Progress in Inorganic Chemistry," Vol. 10, F. A. Cotton, Ed., Wiley, New York, N. Y., 1968, pp 223–258; (b) R. W. Brandon and D. V. Claridge, *Chem. Commun.*, 677 (1968).

(16) J. Krogh Moe, *J. Non-Cryst. Solids*, **1**, 269 (1968).

sponding Ca^{2+} containing species. In short, the polarizing power of the Pb^{2+} ion is effectively screened by complex formation, and the remaining acetate ions in the glass are essentially free to coordinate with the Co^{2+} probe cation. In contrast, the interaction between Ca^{2+} and (OAc^-) ions is less specific; moreover, the coordination number of Ca^{2+} may be higher than that of Pb^{2+} and so all the acetate ions in the glass may be modified to some extent. It is to be expected therefore that the long-range coulombic forces, which are largely responsible for the cohesive energy of the glass, will be less in $Pb(OAc)_2$–KOAc than in corresponding $Ca(OAc)_2$–KOAc systems.

C. Glass Transition Temperatures. Values of T_g for a wide range of acetate glasses are listed in Table II, together with comparable data obtained by Bartholomew.[17] It is apparent that the present T_g values are some 12–15° higher than those previously reported. The data appear to be reliable since the melting points of LiOAc and $Pb(OAc)_2$ recorded on the D.T.A. trace agreed satisfactorily with directly determined values (as is also true for Bartholomew's data). Furthermore, the same heating rate (10°/min) has been used in both investigations. The discrepancy in T_g values appears, therefore, to be genuine and may arise from a difference in the technique of sample preparation. In the present experiments, the glasses were melted in the D.T.A. capillaries and quenched *in situ*, whereas Bartholomew used powdered samples,[17b] and thus some annealing could have occurred.

Table II

Glass composition	T_g, °C	T_g, °K	Cation potential $\frac{\Sigma N_i z_i}{r_i}$
	LiOAc–NaOAc system		
1:0	134 (121[a])	407 (394[a])	1.68
	113	386	1.63
3:1	92	365	1.52
2:1	84	357	1.47
4:3	77 (62[a])	350 (335)[a]	1.41
	$Ca(OAc)_2$–KOAc system		
1:1	110	383	1.39
2:3	100	373	1.26
1:2	100 (87[a])	373 (360[a])	1.17
	LiOAc–$Pb(OAc)_2$ system		
1:0	134	407	1.68
2:1	53	326	1.63
1:1	50	323	1.57
0:1	44	317	1.52
	$Pb(OAc)_2$–KOAc system		
1:0	44	317	1.52
3:1	42	315	1.33
1:1	53.5	326.5	1.14
2:3	48	321	1.06

[a] See ref 16a.

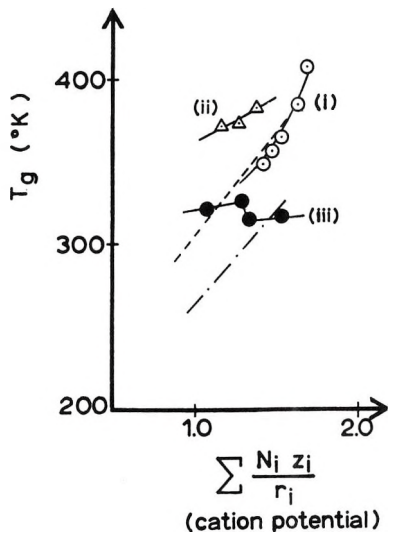

Figure 4. Composition dependence of T_g in acetate and nitrate glasses. Selected acetate systems: (i) ○, LiOAc–NaOAc; (ii) △, $Ca(OAc)_2$–KOAc; (iii) ●, $Pb(OAc)_2$–KOAc. Nitrate systems: ----, $Ca(NO_3)_2$–KNO_3; -·-·-, $Cd(NO_3)_2$–$TlNO_3$.

To display the general pattern of data, selected values of T_g are plotted (in Figure 4) *vs.* the mean cationic potential of the glass, $\Sigma N_i z_i / r_i$, where the symbols have their usual meaning.[18] For comparison, straight-line plots of data for the KNO_3–$Ca(NO_3)_2$ and $TlNO_3$–$Cd(NO_3)_2$ systems taken from Figure 6, ref 7, are included in the diagram. The acetate systems differ somewhat in behavior, and it is convenient to consider briefly each in turn.

LiOAc–NaOAc System. The T_g values, curve i, increase almost linearly with cationic potential and lie close to the linear extrapolation of the data from the KNO_3–$Ca(NO_3)_2$ system. This seems to indicate the presence of simple ionic species in these acetate glasses.

KOAc–$Ca(OAc)_2$ System. T_g values in this system, curve ii, are higher than T_g values of corresponding glasses in the KNO_3–$Ca(NO_3)_2$ system. No satisfactory explanation for this can be advanced, but it may be related to more efficient packing geometries in the acetate glasses.

KOAc–$Pb(OAc)_2$ System. The behavior of this system, curve iii, is noteworthy in two respects: (i) The T_g values do not increase uniformly with increasing cation strength but exhibit a slight maximum at the equimolar composition; and (ii) T_g values are in general noticeably lower than for the corresponding $Ca(OAc)_2$–KOAc glasses.

Both these effects can be explained in terms of the structural model for acetate glasses developed in the

(17) (a) R. F. Bartholomew, *J. Phys. Chem.*, **74**, 2507 (1970); (b) R. F. Bartholomew, private communication.

(18) C. A. Angell, *J. Phys. Chem.*, **68**, 1917 (1964).

preceding section. Thus, if lead acetate glass consists partly of ring structures, the cohesive force will be low and T_g will be low. Addition of alkali acetate leads to production of discrete charged complexes, *e.g.*, $[Pb(OAc)_3]^-$, and the resulting enhancement of ionic interactions causes the observed maximum in the T_g curve. Further addition of alkali acetate produces only a minor effect. (See also ref 7, pp 366, 367.) However, even in the "high-alkali" acetate glasses, covalent bonding *within* the $[Pb(OAc)_3]^-$ and $[Pb(OAc)_4]^{2-}$ complexes leads to partial neutralization of the charges on the Pb^{2+} and $(OAc)^-$ ions, and the cationic potential of the glass is therefore less than the value expected from $\Sigma N_i z_i / r_i$. The present authors understand this "charge neutralization" effect to be a very general phenomenon in glasses and molten salts; this point will be discussed in future papers.

It is also possible that the lower T_g values in the Pb(II) containing acetate glasses and in the $TlNO_3$–$Cd(NO_3)_2$ glasses may be related to the high atomic weights of the constituent atoms. Thus Angell[7] has suggested that the glass transition temperature is equivalent (or nearly equivalent) to the Debye temperature in amorphous systems, and therefore an inverse square root dependence on effective masses is to be predicted. However, more recently Schnaus, *et al.*,[19] have demonstrated for a series of glasses (As_2O_3, As_2S_3, As_2Se_3, $As_2Se_{1.5}Te_{1.5}$) that θ_D shows the expected mass dependence but T_g does not. On balance, it seems more satisfactory to correlate apparently "low" T_g values with charge neutralization effects.

D. General Conclusions. It has been established that acetate glasses vary considerably in ionic–covalent character. Whereas the pure lead acetate system is appreciably covalent, at the other extreme the mixed lithium acetate–sodium acetate glasses are essentially ionic and are closely related to the nitrate glasses. When the problem of chemical instability in acetate melts is overcome,[20] these systems will offer promising opportunities for examining changes in transport behavior which accompany major structural changes in the liquid state.

Acknowledgments. We thank the Science Research Council for a maintenance grant to one of us (G. G. L.). We are indebted also to Professor C. A. Angell for helpful discussions of the glass transformation phenomena.

(19) U. E. Schnaus, C. T. Moynihan, R. W. Gammon, and P. B. Macedo, *Phys. Chem. Glasses*, 11, 213 (1970).

(20) F. J. Hazlewood, E. Rhodes, and A. R. Ubbelohde, *Trans. Faraday Soc.*, 62, 2101 (1966).

Anion Exchange in Aqueous–Organic Solvent Mixtures. II[1a]

by C. H. Jensen,[1b] A. Partridge,[1c] T. Kenjo,[1d] J. Bucher, and R. M. Diamond*

Lawrence Berkeley Laboratory, University of California, Berkeley, California 94720 *(Received September 29, 1971)*

Publication costs assisted by the Lawrence Berkeley Laboratory

The uptake by Bio-Rad AGl-X4 anion resin of LiCl and of solvent from isopropyl alcohol–water solutions has been measured. As with dioxane–water solutions, the resin selectively absorbs water. The values of the distribution ratios, D, for tracer ReO_4^-, I^-, Br^-, and F^- with macro Cl^- concentrations was determined as a function of alcohol mole fraction, as was also D *vs.* acetone mole fraction for tracer ReO_4^-, Br^-, and F^-. The distribution ratios for the larger anions decreased with increasing solvent mole fraction, while those for F^- increased. For reasons discussed in the text this is expected to be a general phenomenon. The behavior of complex anions is also indicated.

Introduction

A previous paper has discussed the anion-exchange selectivity shown by (organic) ion-exchange resins with water–dioxane solutions.[2] Experimentally, the selectivity dropped markedly with an increase in dioxane content, so that by 50% mole fraction dioxane, the ratio of the distribution coefficients of I^- to F^- was only ~4, instead of the ~100 in water alone. That paper pointed out, as is generally recognized, that water is a much better solvating agent for anions than is dioxane,

(1) (a) Work supported under the auspices of the U. S. Atomic Energy Commission; (b) Summer visitor, 1967, NSF College Teachers Research Participation Program; permanent address: Cabrillo College, Aptos, Calif.; (c) Summer visitor, 1970, Undergraduate Research Participation Program; (d) Present address: The Research Institute for Iron, Steel and other Metals, Tohoku University, Ooarai-machi, Ibaragi-Ken, Japan.

for a number of reasons.[3-5] Thus, anions would compete to follow the distribution of water between the resin and external phases, and the smaller, more basic anion, which stands to gain the most in solvation energy, would win and push the other larger, less basic anion into the dioxane-rich phase. Since it was also found that the resin phase took up water in preference to dioxane, this means that the smaller anions, which strongly favor the external phase with dilute aqueous solutions, should prefer that phase less and less as the proportion of dioxane increases. This is just what was observed.

But if this idea has validity, it would be interesting to compare the behavior of the same anions and resin when using mixtures of water and a hydroxylic solvent, such as an alcohol. Certainly a less marked decrease in selectivity with increasing organic-solvent mole fraction should be expected than was the case with dioxane, for the alcohol molecule can hydrogen-bond to an anion and so offer it better solvation, though still not as complete as with water. Isopropyl alcohol was chosen for this study.

Experimental Section

Reagents. The anion-exchange resin used was the same Bio-Rad AGl-X4, 100-200 mesh, employed in the previous study.[2] Its capacity and water uptake were 4.04 mequiv and 1.73 g, respectively, per gram of dry Cl^--form resin. The isopropyl alcohol used was Matheson Coleman and Bell, spectral grade, and the acetone was Baker and Adamson, reagent grade. The LiCl was Baker and Adamson, reagent grade; a saturated solution was made, filtered, diluted, and analyzed with standard $AgNO_3$ using dichlorofluorescein as indicator. The $^{82}Br^-$ and $^{186}ReO_4^-$ tracers were prepared by neutron irradiation of LiBr and $KReO_4$ at the Vallecitos Reactor. The $^{18}F^-$ tracer was prepared by the $^{16}O(\alpha,d)^{18}F$ reaction on conductivity water at the Lawrence Berkeley Laboratory 88-in. cyclotron. The ^{59}Fe tracer was purchased from New England Nuclear Corp. as Fe^{III} in dilute HCl.

Procedure. The uptake by the resin of isopropyl alcohol and water from solutions of varying composition was determined in the same manner as previously,[2] using the index of refraction of the solutions to determine their composition.

The ion invasion of the resin by 0.010 *M* LiCl in the solutions of different alcohol mole fraction was studied in the same manner as previously,[2] including making a correction for liquid adhering to the outside of the resin beads by using an equal volume of glass beads of 170-230 mesh.

The distribution measurements were made by batch experiments as before,[2] except that 60-ml glass-stoppered bottles were used. The value of the distribution ratio, *D*, is given by

$$D = \frac{[\overline{X^-}]}{[X^-]} = \frac{[(\text{counts/min})_{\text{initial}} - (\text{counts/min})_{\text{equil}}][\text{volume of solution}]}{(\text{counts/min})_{\text{equil}} \times [\text{g of dry } Cl^-\text{-form resin}]} \quad (1)$$

Results and Discussion

Solvent Uptake. It can be seen in Figure 1 that above an external-phase mole fraction of ~0.07 isopropyl alcohol, this strong-base resin in the Cl^- form preferentially takes up water into the resin. In the very dilute alcohol region, isopropyl alcohol is somewhat preferentially absorbed. Both of these results are in agreement with earlier studies on alcohol uptake by other investigators.[6,7] At this time it is hard to give a detailed explanation for this behavior, but we believe the following description is essentially correct.

The dominating feature of the solvent uptake from aqueous solutions of dioxane and of isopropyl, *n*-propyl, ethyl, and to a smaller extent, methyl alcohols is the preferential absorption of water by the strong-base resin. Since it requires more work to place charges in the aqueous-organic mixture (of lowered bulk dielectric

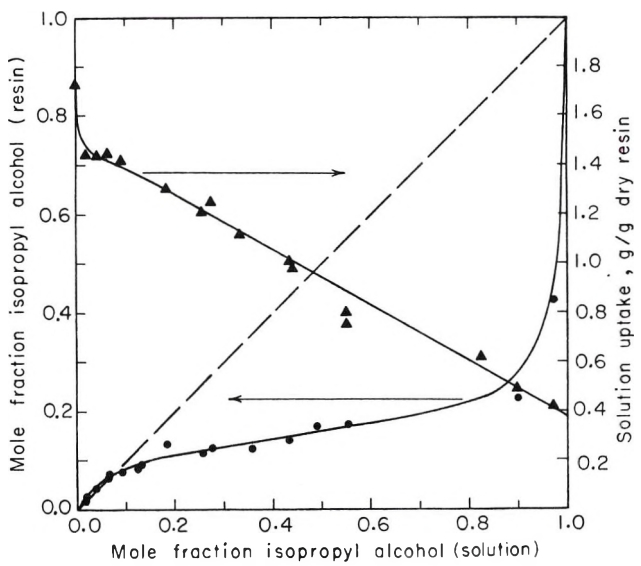

Figure 1. The isopropyl alcohol mole fraction in the resin (left-hand ordinate scale) and total uptake of solution, g/g of dry resin, (right-hand scale) *vs.* the isopropyl alcohol mole fraction in the equilibrium solution. The resin is Bio-Rad AGl-X4 in Cl^- form.

(2) C. H. Jensen and R. M. Diamond, *J. Phys. Chem.*, **75**, 79 (1971).

(3) (a) E. Price, "Solvation of Electrolytes and Solvation Equilibria," in "The Chemistry of Non-Aqueous Solvents," Vol. I, J. J. Lagowski, Ed., Academic Press, New York, N. Y., 1966; (b) E. Grunwald, G. Baughman, and G. Kohnstam, *J. Amer. Chem. Soc.*, **82**, 5801 (1960).

(4) A. J. Parker, *Quart. Rev., Chem. Soc.*, **16**, 163 (1962).

(5) D. Feakins and D. J. Turner, *J. Chem. Soc.*, 4986 (1965).

(6) Y. Marcus and J. Naveh, *J. Phys. Chem.*, **73**, 591 (1969).

(7) H. Rückert and O. Samuelson, *Acta Chem. Scand.*, **11**, 303 (1957).

constant) than in the original aqueous system, there is an increase in the electrostatic free energy of the system when water molecules are replaced by the organic molecules. Upon addition of solvent, the resin phase will suffer a much larger electrostatic free-energy increase than the external phase, because it has a high concentration of charge while the external solution is usually dilute, or may not have any electrolyte present at all. Water and the organic diluent distribute in such a way as to minimize this increase in free energy for the whole system, and clearly, this can best be done if the solvent that can provide the best electrostatic solvation moves preferentially into the resin phase. Molecules with the largest bond dipole moments and with the smallest size, so as to furnish the largest number of moments per unit volume, will provide the maximum of such solvation to the resin-phase ions. In comparison to most of the usual polar organic solvents, water, with a dipole moment of 1.85 D[8] and a small molar volume (18 ml), is by far the best solvating agent. So with increasing organic-diluent mole fraction, the resin phase preferentially takes up water rather than diluent, thus minimizing the electrostatic free energy of the concentrated resin phase and of the system as a whole.

It should also be noted that the free energy of short-range chemical solvation ordinarily leads to the same conclusions. Water molecules usually provide anions with the best hydrogen-bonded first-shell coordination; small highly charged anions obtain additional solvation by means of additional shells of oriented water molecules. Since the concentration of counteranions is greater in the resin phase than in the dilute external solution, we would expect (from chemical solvation) a preferential uptake of water in the resin phase, the degree of uptake depending on the type of counterion. Therefore we might anticipate (1) the smaller Cl^- to require more water in the Cl^--form resin than ClO_4^- in the ClO_4^--form resin; (2) F^-- or OH^-- or polyvalent anion-form resins (those greatly in need of hydration) to be very selective in water uptake; and (3) resins containing large singly charged anions such as $AuBr_4^-$ to be much less selective, or even to prefer polar organic solvents with large dipole moments. The first expectation has been observed,[6,7] the second has been substantiated by work with OH^--form[9] and SO_4^{2-}-form[7] resins, and the third has yet to be tested.

It remains to explain the behavior at very low alcohol mole fraction, where the resin shows a small preference for the alcohol over water. We believe this is due to the difference of the water structure in the two phases. In the external solution of nearly pure water the hydrocarbon tail of the alcohol interacts with the hydrogen-bonded water structure about as any hydrocarbon would, namely it tends to be pushed out of the way of the water structure into the less highly hydrogen-bonded structure in the resin phase.[10] That is, the presence of the hydrocarbon tightens up the water structure around it lowering both the enthalpy and the entropy of the water.[11,12] In the resin phase, the water structure is much less complete, due to the high concentration of ions there and to the fact that the resin matrix itself occupies about half of the volume, forcing the water into small layers and pores having at least one dimension of the order of only a few ångstroms. Because there is less water structure for the organic molecules to counter in the resin phase, positive values of ΔH and $T\Delta S$ should accompany their transfer from the aqueous into the resin phase, and the larger value of $T\Delta S$ should be the driving force,[13] just as with their transfer from an aqueous to an organic diluent phase.[11,12] The value of $T\Delta S$ should be larger, the larger the hydrocarbon tail. We believe this is the origin of the initial preferential uptake of alcohol by the resin, and the uptake does seem to be larger, the larger the alcohol. As the proportion of organic diluent is increased, however, the three-dimensional hydrogen-bonded water structure of the external phase is destroyed, both because the organic molecules occupy space (just like the resin matrix), and because the alcohol or dioxane molecules themselves can hydrogen-bond to water but form a much less extensive three-dimensional network. The main effect quickly becomes that of solvating the much higher concentration of ions in the resin phase, as described earlier, and a marked resin preference for water then shows.

Supporting evidence for the point of view expressed in the previous paragraph can be extracted from a study of ion-exchange resin separations of carboxylic acids by Davies and Owen[14] and from a study by Reichenberg and Wall[15] on the absorption of such acids and of alcohols by ion-exchange resins. They found that methyl, ethyl, and propyl alcohols and formic, acetic, propionic, butyric, and phenylacetic acids were absorbed by resins from aqueous solution, sometimes to well beyond the resin capacity and in order of increasing size. This behavior was attributed mainly to van der Waals interactions in the resin phase. But we believe the fact that the absorption decreases when dioxane is added to the system rules out the importance of such interactions in the resin phase (except for effects of the π electrons in

(8) "Handbook of Chemistry and Physics," R. C. Weast and S. M. Selby, Ed., Chemical Publishing Co., Cleveland, Ohio, 1966, p 61.

(9) E. Sjöström, L. Nykänen, and P. Laitinen, *Acta Chem. Scand.*, **16**, 392 (1962).

(10) B. Chu, D. C. Whitney, and R. M. Diamond, *J. Inorg. Nucl. Chem.*, **24**, 1405 (1962).

(11) D. D. Eley, *Trans. Faraday Soc.*, **35**, 1421 (1939).

(12) H. S. Frank and M. W. Evans, *J. Chem. Phys.*, **13**, 507 (1945).

(13) We are not aware of thermodynamic measurements of anion exchange involving an organic (hydrophobic) ion, but the free energies, enthalpies, and entropies of the cation exchange of sodium and tetraalkylammonium ions have been determined [G. E. Boyd and Q. V. Larson, *J. Amer. Chem. Soc.*, **89**, 6038 (1967)] and with the larger alkylammonium cations the entropy term is dominant.

(14) C. W. Davies and B. D. R. Owen, *J. Chem. Soc.*, 1681 (1956).

(15) D. Reichenberg and W. F. Wall, *ibid.*, 3364 (1956).

aromatics); we would not expect the presence of organic molecules mainly in the external phase to decrease the effect of van der Waals interactions in the resin phase. But if the absorption of alcohol or carboxylic acid is caused by rejection by the water structure in the external phase, it follows that the absorption would decrease with addition of organic diluent, as the diluent does destroy the water structure. This is precisely the unidentified factor mentioned by Reichenberg and Wall as necessary to explain why the order of the acid absorption reverses with increasing organic acid concentration.

Finally it should be mentioned that it is not necessarily true that water molecules provide better solvation for anions than all polar organic molecules. Formamide, *N*-methylformamide, and dimethylformamide, for example, have dipole moments of 3.37 D at 30° in benzene,[16] 3.86 D at 25° in benzene,[17] and 3.86 D at 25° in benzene,[18] respectively, compared to 1.85 D for water. Although the effectiveness for electrostatically solvating an anion may be more closely related to a bond dipole moment and its steric availability than to the overall molecular moment (and other important factors in the total solvation of the anion include hydrogen bonding when the organic solvent is capable of donating a proton, and dispersion force interactions when it has delocalized orbitals), any one of the above molecules may be more effective than water, on a 1:1 basis, in shielding an ion's charge. Water, however, has the advantage of the smaller molar volume, so that more water dipoles can pack around the ion. Inside Dowex 1 Cl^--form resin, these two factors must just about balance out for formamide and water, as little selectivity is shown in this case for distributing between the external solution and the resin phase over the entire range of diluent mixtures.[6] Dimethylformamide (DMF) cannot provide chemical (hydrogen-bonded) solvation for small anions, as can water and formamide, and is larger; it is discriminated against with respect to water by the resin when small counterions are involved. But when the resin form involves large, weakly basic anions, such as ClO_4^-, which do not require much hydrogen-bonded solvation, then the large bond moment and dispersion force interactions from the resonance

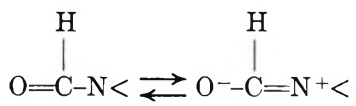

can dominate the solvation, and DMF becomes even slightly preferred by the resin phase.[6]

Although we did not determine the resin uptake for acetone–water mixtures, we would predict, on the basis of the reasoning given above, that our Cl^--form resin would preferentially take up water, and possibly even more strongly than with isopropyl alcohol, as the acetone cannot chemically solvate (hydrogen bond to) the Cl^- counterions in the resin phase. For nearly pure water solutions, however, acetone might well be taken up preferentially, as are the alcohols, and for the same reason. Fragmentary data (two points) in the literature[19] seem to indicate this behavior, and this is certainly true for uptake by a cation-exchange resin.[20]

Nonexchange Electrolyte Uptake. A plot of the LiCl resin invasion in milliequivalents of Cl^- per gram of dry Cl^--form resin *vs.* the equilibrium external-phase isopropyl alcohol mole fraction with a constant concentration of 0.010 *M* LiCl in the external solution is shown in Figure 2. The curve is somewhat similar to that with dioxane,[2] but with increasing organic-solvent mole fraction, the alcohol curve increasingly shows less resin invasion by nonexchange electrolyte. This is likely due to the higher dielectric constant of the alcohol–water mixtures[21] (also shown in Figure 2), for as a result, there will be less ion pairing in that system. Since ion pairs are not subject to the Donnan potential[22] and so to exclusion from the resin phase, to whatever extent there is less ion pairing of LiCl in the resin phase with alcohol–water mixtures over that with dioxane–water solutions, the amount of resin invasion by LiCl will be lower.

Anion Selectivity. Our basic premise, as with purely aqueous systems, is that the ion which most needs solvation (the smaller, more highly charged one) goes into that phase which provides the better solvation, and in the exchange pushes the other ion into the poorer solvating phase.[2,10,23,24] The primary exchange reaction is

$$X^- + \overline{Cl}^- \rightleftarrows \overline{X}^- + Cl^- \qquad (2)$$

with

$$\mathcal{K}_{X^-/Cl^-} = \frac{(\overline{X}^-)(\overline{Cl}^-)}{(X^-)(\overline{Cl}^-)} = \frac{[\overline{X}^-][Cl^-]\bar{\gamma}_{RX}\gamma_{LiCl}}{[X^-][\overline{Cl}^-]\gamma_{LiX}\bar{\gamma}_{RCl}} \qquad (3)$$

$$K_{X^-/Cl^-} = \frac{[\overline{X}^-][Cl^-]}{[X^-][\overline{Cl}^-]} \qquad (4)$$

$$D = \frac{[\overline{X}^-]}{[X^-]} = {}_{X^-/Cl^-}\frac{[\overline{Cl}^-]}{[Cl^-]} \qquad (5)$$

(16) W. W. Bates and M. E. Hobbs, *J. Amer. Chem. Soc.*, **73**, 2151 (1951).

(17) I. P. Gol'dshtein, Yu. M. Kessler, Yu M. Povarov, and A. I. Gorbanov, *Zh. Strukt. Khim.*, **4**, 445 (1963), as given in *Chem. Abstr.*, **59**, 5894 (1963).

(18) M. H. Hutchinson and L. E. Sutton, *J. Chem. Soc.*, 4382 (1958).

(19) D. G. Howery, G. Senum, and L. H. Madoff, *Anal. Lett.*, **3**, 483 (1970).

(20) C. W. Davies and B. D. R. Owen, *J. Chem. Soc.*, 1676 (1956).

(21) G. Akerlöf, *J. Amer. Chem. Soc.*, **54**, 4125 (1932).

(22) F. G. Donnan, *Z. Phys. Chem. (Leipzig)*, **A168**, 369 (1934).

(23) C. H. Jensen and R. M. Diamond, *J. Phys. Chem.*, **69**, 3440 (1965).

(24) R. M. Diamond and D. C. Whitney, "Resin Selectivity in Dilute to Concentrated Aqueous Solutions," in "Ion Exchange," Vol. I, J. Marinsky, Ed., Marcel Dekker, New York, N. Y., 1966.

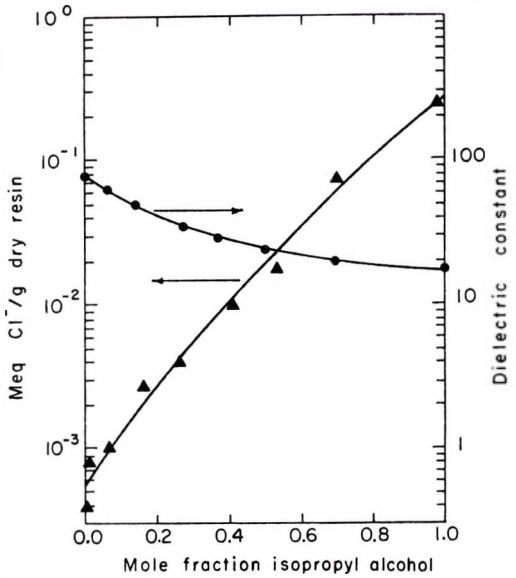

Figure 2. Uptake by the resin of nonexchange electrolyte from 0.010 *M* LiCl *vs.* isopropyl alcohol mole fraction. The left-hand ordinate scale is in milliequivalents of Cl^- per gram of dry Cl^--form resin, and the resin capacity is 4.04 mequiv/g of dry Cl^--form resin. Also shown is a plot of the dielectric constant (right-hand scale) *vs.* the isopropyl alcohol mole fraction.

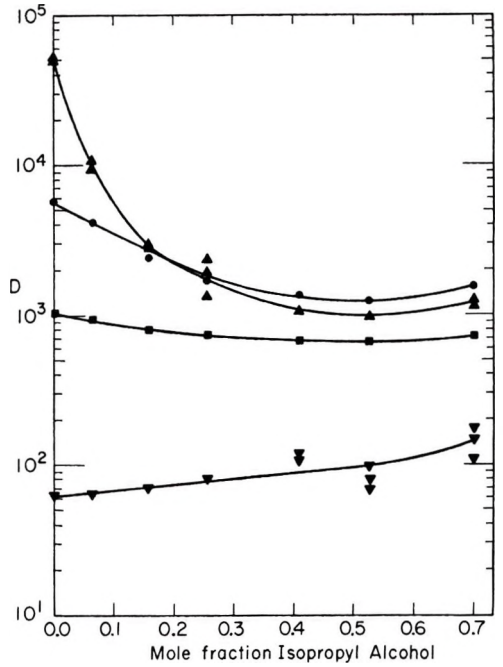

Figure 3. Plots of *D vs.* isopropyl alcohol mole fraction in the solution for 0.010 *M* LiCl and the tracer anions: F^-, ▼; Br^-, ■; I^-, ●; and ReO_4^-, ▲.

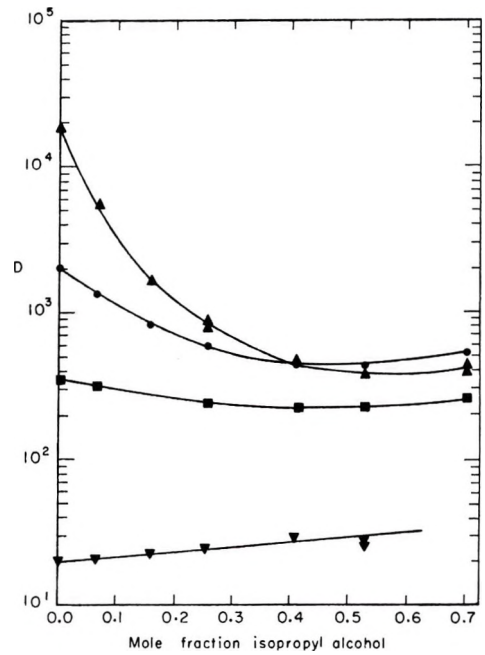

Figure 4. Plots of *D vs.* isopropyl alcohol mole fraction in the solution for 0.030 *M* LiCl and the same tracer anions and symbols as in Figure 3.

where parentheses indicate activities and brackets indicate concentrations.

For purely aqueous systems, solvation by water is best in the dilute external phase, and so the smaller, more highly charged, and more basic anions are held there. This leads to the predicted resin selectivity order, $AuCl_4^- > ReO_4^- = ClO_4^- > I^- > Br^- > Cl^- > F^-$, which is that observed experimentally. Now what happens when the water in the system is gradually replaced by alcohol? To answer this, we may perhaps start with a simpler example than anion exchange, namely the distribution of neutral hydrophilic organic molecules. Samuelson and his coworkers[25,26] have found that polyhydroxy substances such as sugars and polyalcohols distribute between the resin and the external solution, favoring the latter. These strongly hydrating substances find the best hydration there (just as do anions). But as alcohol replaces water in the system, the external-phase water mole fraction decreases more rapidly than that of the resin phase, so the polyhydroxy molecules decreasingly prefer that phase, and their uptake by the relatively water-rich resin phase increases. Similarly, a small, basic anion finds increasingly poorer solvation in the external phase as the organic mole fraction increases, and so its binding to the external solution decreases and its distribution into the resin increases. In an exchange, the distribution of the other larger, less basic ion (less in need of solvation) must correspondingly decrease, leading to a decrease in selectivity. It might be expected, however, that the decrease in distribution ratios, *D*, for the larger anions (and increase in *D* for F^- when Cl^- is the macroanion) would be less severe with isopropyl alcohol than with dioxane because the hydroxyl group of the former

(25) H. Rückert and O. Samuelson, *Acta Chem. Scand.*, 11, 315 (1957).

(26) M. Mattisson and O. Samuelson, *ibid.*, 12, 1386 (1958); 12, 1395 (1958).

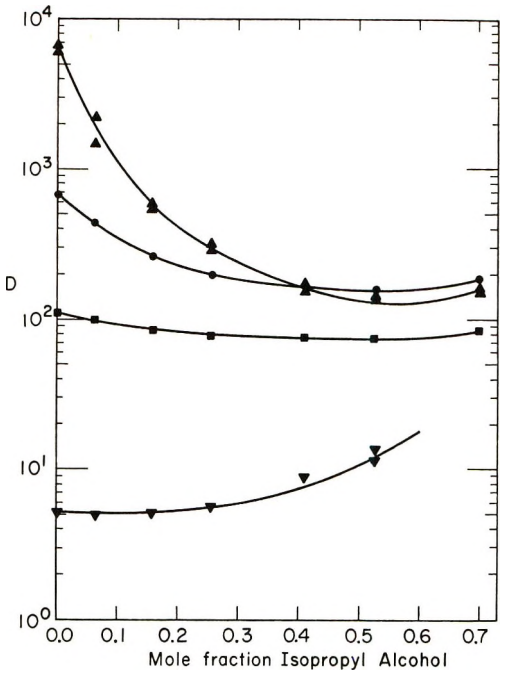

Figure 5. Plots of D *vs.* isopropyl alcohol mole fraction in the solution for 0.10 M LiCl and the same tracer anions and symbols as in Figure 3.

can hydrogen bond to the (smaller) anions and partially replace the chemical solvation lost with the gradual dehydration of the system. This would help to hold the smaller anions in the external solution and so would diminish the changes in D with increasing alcohol mole fraction, when compared with dioxane solutions.

Inspection of Figures 3–5 giving plots (for 0.010, 0.030, 0.10 M LiCl) of D *vs.* external-phase alcohol mole fraction show that the values of D for tracer ReO_4^-, I^-, and Br^- fall with increasing alcohol content, while that for F^- increases. Thus, the major result of adding isopropyl alcohol is the same as adding dioxane, and we think this is due, as already described, to the tendency of the smaller, more basic anions to follow the distribution of water into the resin phase. However, it must be noted that the values of the distribution ratios start to fall with the first addition of isopropyl alcohol, even though below an alcohol mole fraction of ~0.07 the resin phase prefers the alcohol somewhat to water. Possibly the water and organic molecules are not homogeneously distributed in the resin phase at low organic mole fraction. The individual waters may tend to cluster about the counterions and the resin-bound charge sites, while the organic molecules fit around the hydrocarbon matrix. Even though the stoichiometric proportion of water in the resin phase is slightly less than in the external solution, the small amount of organic solvent there may essentially act like a part of the hydrocarbon framework and leave the immediate vicinity of the resin-phase ions unchanged. Thus, the addition of a few mole per cent solvent to the resin phase would not greatly affect the solvation of resin-phase ions there. But in the external phase, the addition of the same proportion of organic molecules to a purely aqueous solution does decrease the secondary solvation of the ions there, thus decreasing the selectivity of the external phase for the smaller, more highly hydrated anions.

A comparison of Figures 3–5 with the corresponding figures in ref 2 for dioxane–water mixtures shows that the differences in results with dioxane–water and isopropyl alcohol–water mixtures are in the expected direction, but to us, are surprisingly small. The D's with alcohol solutions change almost as rapidly as with dioxane mixtures, while we expected a significantly slower rate. It is true that the dioxane curves are a little high (artificially) due to the larger nonexchange resin invasion with that solvent. For in the batch experiments, the invasion electrolyte comes from, and so diminishes, the external solution LiCl concentration and this increases D (eq 5). However, this is an effect of at most tens of per cent for the dioxane solutions of ~0.5 mole fraction. More importantly, the dielectric constant is lower for dioxane–water mixtures than alcohol–water mixtures, and so there is an increased possibility of ion pairing with Li^+. This will tend to hold Cl^- more firmly in the external phase, leaving the larger ions in the resin.

This is certainly part of the explanation. Another possibility involves an idea already in the literature.[27] The dioxane molecule normally exists in the chair form, and consequently the two bond moments oppose each other resulting in a small overall dipole moment, 0.45 D.[28] But there is a small amount of the boat form in the equilibrium mixture, and in this case the two bond moments tend to add. In the Coulomb field of the ions, the dioxane equilibrium is shifted toward the boat form, and so the dioxane molecules around the ions can provide much better (dipole moment) solvation for anions than would be expected from the properties (dipole moment and dielectric constant) of bulk dioxane. Such an idea has been used by Hyne[27] to explain the lower-than-expected ion-pair formation of n-Bu_4NBr in dioxane–water mixtures and was derived from similar reasoning employed earlier by Ramsey and coworkers[29] to explain the lower-than-expected ion pairing of n-$Bu_4N^+ClO_4^-$ in 1,2-dichloroethane. Yet another possibility is that we have greatly overestimated the ability of alcohol to hydrogen bond to small anions or the importance of such bonding.

To try to distinguish among these possibilities, particularly the last, we did some experiments with acetone–water mixtures. Acetone has a size, structure, and dielectric constant similar to isopropyl alcohol, but is missing the latter's hydroxyl hydrogen. As already

(27) J. B. Hyne, *J. Amer. Chem. Soc.*, **85**, 304 (1963).
(28) R. Sangewald and A. Weissberger, *Phys. Z.*, **30**, 268 (1929).
(29) Y. H. Inami, H. K. Bodenseh, and J. B. Ramsey, *J. Amer. Chem. Soc.*, **83**, 4745 (1961).

mentioned, we did not determine the solvent uptake by the resin for acetone–water mixtures, but almost certainly the anion-resin phase will take up water preferentially for the same reasons that it does so for dioxane–water and alcohol–water solutions (in fact, it appears to do so[19]). If the ability to hydrogen-bond to the anions is an important feature of solvating them, as we think, then the replacement of water by acetone in dilute solutions of LiCl should drive the smaller anions into the resin phase more strongly than when using isopropyl alcohol. Consequently, we would expect the values of D for the larger anions to decrease more sharply with increasing acetone mole fraction than with isopropyl alcohol mole fraction and to increase more rapidly for the small F^-. The results for tracer ReO_4^-, Br^-, and F^- with macro Cl^- (the external solution is 0.010 M LiCl) are shown in Figure 6, and it can be seen that these expectations are fulfilled. Apparently, acetone cannot solvate the F^- and Cl^- as well as isopropyl alcohol; the ability of the latter solvent to hydrogen-bond to anions makes a significant difference in the distribution ratios.

The problem that remains is why do the dioxane–water mixtures yield intermediate results rather than resembling the acetone solutions? But in fact, if one observes carefully the low mole fraction region of Figure 6, it can be seen that for both ReO_4^- and Br^- tracers the dioxane curves fall even more steeply than the acetone curves out to a solvent mole fraction of ~0.2. Then at higher mole fraction the curves for dioxane tend to level off, coming between those for acetone and isopropyl alcohol. This behavior indicates that dioxane solvates the small anions poorly, even more poorly than acetone (due to its smaller dipole moment), as originally expected, but that some other phenomenon comes into prominence at higher proportions of dioxane in the mixtures. We believe this latter effect is the result of ion pairing of the smaller anions with the lithium cation in the external phase, since the dioxane–water mixtures have considerably lower dielectric constants than the corresponding alcohol– or acetone–water mixtures. Because the lithium cations are mainly in the external phase, ion pairing with them tends to hold the Cl^- there; consequently, the values of D for ReO_4^-, I^-, and Br^- in dioxane–water mixtures tend to remain higher than they would otherwise, as observed.

But as can be seen in Figure 6, the main effect of adding any of the three organic solvents used (and for the reasons given above we believe this to be a general phenomenon) is to decrease the value of D for the larger, less basic (than Cl^-) anions and to increase it for the smaller, more basic ones. As a result, the selectivity coefficients become closer to unity (ReO_4^- and Br^- actually reverse their order in acetone–water and dioxane–water mixtures), and separations become poorer. This effect should be even more pronounced with anions differing still more widely in size and basicity. Thus,

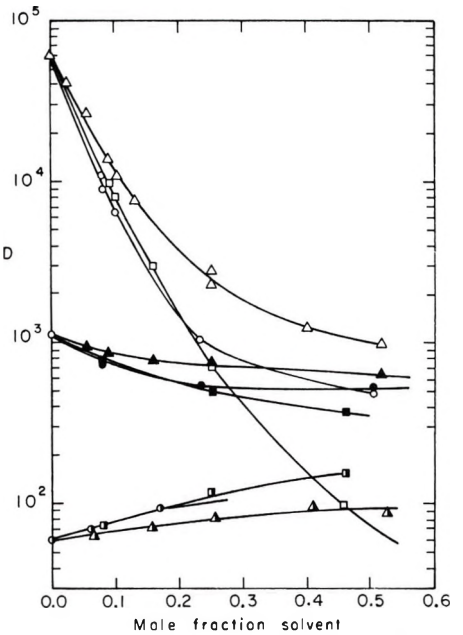

Figure 6. Plots of D *vs.* solvent mole fraction in the solution for 0.010 M LiCl and tracer F^- (half-filled symbols), Br^- (filled symbols), and ReO_4^- (open symbols). Data from isopropyl alcohol solutions are represented by triangles, from acetone by squares, and from dioxane solutions by circles.

a larger, still less hydrated species than ReO_4^-, such as $AuCl_4^-$, should show even a more marked decrease than ReO_4^- from the enormous distribution ratio it has in aqueous solution. Qualitatively, this behavior is shown in the work of Burstall, *et al.*,[30] who have reported on the very marked uptake and concentration of the cyano complexes of gold and silver on anion-exchange resins, and then the subsequent elution of these complexes from the resin by acetone–aqueous HCl solutions. Another example is furnished in a paper by Dobud, *et al.*,[31] where they show that the D for $AuCl_4^-$ on Amberlite IRA-400 from 4 M HCl falls by a factor of over 100 in going from aqueous solution to ~0.25 mole fraction *n*-propyl alcohol. This is certainly a larger drop than we observe for ReO_4^-. But the situation here is not so clear because of the use of concentrated HCl rather than dilute LiCl. Two additional effects must be considered, both related to association of the H^+ and Cl^- ions. One is that in the resin phase (with a large Cl^- concentration) some HCl and HCl_2^- will form;[32,33] the latter species especially will cause a decrease in the value of D for $AuCl_4^-$. This effect is now well known in aqueous anion resin systems where the use of moderately concentrated HCl leads to much smaller D's than are obtained with similar concentrations of LiCl.[32-35]

(30) F. H. Burstall, P. J. Forrest, N. F. Kember, and R. A. Wells, *Ind. Eng. Chem.*, **45**, 1648 (1953).

(31) P. Dobud, H. M. Lee, and D. G. Tuck, *Inorg. Chem.*, **9**, 1990 (1970).

(32) B. Chu and R. M. Diamond, *J. Phys. Chem.*, **63**, 2021 (1959).

(33) S. Lindenbaum and G. E. Boyd, *ibid.*, **66**, 1383 (1962).

The other effect is that as the effective dielectric constant in the external solution falls, the H^+ and Cl^- associate.[36] That is, the activity of HCl does not rise as rapidly as that of the same stoichiometric concentration of LiCl with increase in organic-solvent mole fraction.[37] This makes the value of D for the other anion (if less basic than Cl^-) larger than in LiCl. Thus, the two effects just described tend to cancel in anion-resin systems (but not in cation-resin systems). For example, plots of D *vs.* isopropyl alcohol mole fraction for tracer Br^- from 0.20 *M* HCl and 0.20 *M* LiCl (not shown) are not greatly different; that for HCl drops a little below the one for LiCl above 0.3 mole fraction alcohol.

In the paper on the exchange of $AuCl_4^-$ from 4 *M* HCl, already mentioned above,[31] the bulk dielectric constant was cited as a main parameter in explaining the decrease in D with increasing organic solvent content, both because of increased ion association and because of decreased (positive) electrostatic free energy of transfer of the smallest anion from the external solution to the resin phase. These certainly do have an influence; the second result does lead to a decrease in D and is encompassed in the change in free energy of solvation of the ions with organic-solvent mole fraction that we have discussed earlier. The first effect, however, leads to an increase in D for $AuCl_4^-$ (because HCl is surely more highly associated in the external solution than is $HAuCl_4$) and so is in opposition to experiment. In any case, a simple dependence on a bulk property like the dielectric constant is not likely to be useful beyond a homologous family of solvents, since it is the microscopic solvation properties that are important. These are more complicated, being related to the effective bond moments and their spatial arrangement, the dispersion-force interactions of mobile electrons such as the π electrons in aromatics, etc. Examples in point are the marked differences observed in this work with acetone and isopropyl alcohol solutions, though they have nearly the same bulk dielectric constants.

Finally, we can treat the situation in which a (labile) complex anion must be produced as well as exchanged. Plots of D *vs.* aqueous HCl and aqueous LiCl are shown in Figure 7 for Fe^{III}. At low Cl^- concentrations the iron is mainly in cationic complexes, and so there is little $FeCl_4^-$ present to exchange with the Cl^--form resin. As the Cl^- concentration increases, however, the proportion of $FeCl_4^-$ increases until this species is dominant. If it were not for resin invasion by the concentrated aqueous electrolyte and other "nonideal" behavior, the maximum in the distribution curve would represent the point where the *average* Fe^{III} species is electrically neutral.[38–40] Beyond that Cl^- concentration, the average iron species is anionic, and the decrease in D is due to the normal mass action effect on an anion of increasing the Cl^- concentration. In reality, resin invasion by the electrolyte may affect the

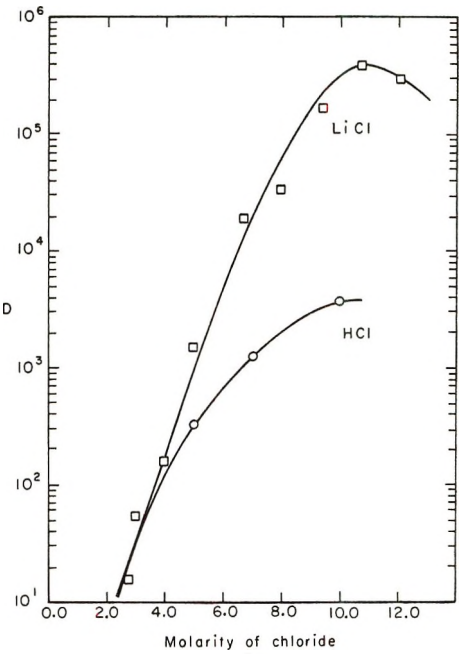

Figure 7. Plots of D for tracer Fe^{III} *vs.* chloride molarity in purely aqueous systems: LiCl, □; HCl, ○.

peak position, as will other effects. In Figure 7, the plot of D for aqueous HCl falls increasingly below that for LiCl at higher Cl^- concentration, due, as mentioned earlier, to the formation of HCl_2^- in the resin phase. If now at a particular HCl or LiCl concentration (below that of the maximum in the curve), the water is gradually replaced by an organic solvent, the activities of the ionic species will (at least initially) increase and the complexing equilibrium

$$Fe(H_2O)_x^{3+} + 4Cl^- \rightleftarrows FeCl_4^- + xH_2O$$

will be shifted to the right. This will occur because the addition of the organic substance lowers the dielectric constant and water activity of the solution, and the product has a lower charge and less hydration than the reactants (Le Chatelier's principle). Thus, above some minimum Cl^- value, we would expect a maximum in D for Fe^{III} to occur with an increase in organic mole fraction at constant Cl^- concentration. The value of D at this maximum would not necessarily be the same as when varying the Cl^- concentration in an aqueous system. If no additional effects are considered, the

(34) K. A. Kraus, F. Nelson, F. B. Clough, and R. C. Carlson, *J. Amer. Chem. Soc.*, **77**, 1391 (1955).

(35) R. A. Horne, *J. Phys. Chem.*, **61**, 1651 (1957); Y. Marcus and D. Magdan, *ibid.*, **67**, 979 (1963).

(36) H. S. Harned and B. B. Owen, "The Physical Chemistry of Electrolytic Solutions," 3rd ed, Reinhold, New York, N. Y., 1958, p 452.

(37) G. Akerlöf, *J. Amer. Chem. Soc.*, **52**, 2353 (1930).

(38) S. Fronaeus, *Sv. Kem. Tidskr.*, **65**, 1 (1953).

(39) Y. Marcus and C. D. Coryell, *Bull. Res. Council Israel*, **8A**, 1 (1959).

(40) K. A. Kraus and F. Nelson in "The Structure of Electrolyte Solutions," W. J. Hamer, Ed., Wiley, New York, N. Y., p 340.

value of D would be lower because the Cl^-, in the mixed external solution, would have a greater tendency to go into the resin phase and push out the larger anion than in a purely aqueous system (this is just our main argument for the decrease in D of large anions with increasing organic mole fraction). Figure 8 shows that this situation does hold for Fe^{III}. A maximum in D not much below the value at ~11 M aqueous LiCl is observed for a high fixed LiCl concentration and a low

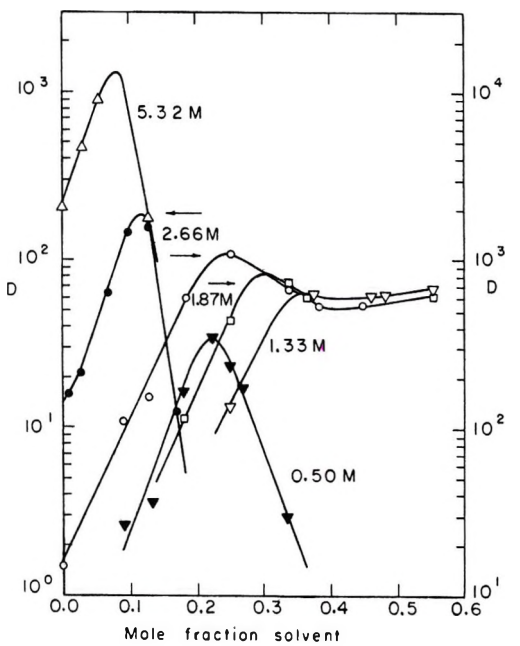

Figure 8. Plots of D for tracer Fe^{III} *vs.* solvent mole fraction for various concentrations of LiCl. The filled symbols represent acetone solutions, and values of D are to be read from the left-hand scale. Unfilled symbols indicate isopropyl alcohol solutions, and values of D are to be read from the right-hand scale. LiCl molarities for each curve are given near it.

isopropyl alcohol mole fraction; the peak value of D decreases for lower fixed values of LiCl and occurs at higher alcohol mole fractions. The same story appears to hold for acetone–water mixtures, except that the decrease of D on the high organic mole fraction side is even steeper than with isopropyl alcohol (corresponding to the steeper curves for ReO_4^- and Br^- with acetone), and so cuts off the maximum value of D at a lower value and at a lower organic mole fraction.

Summary

We have found that the strong-base resin in the Cl^- form preferentially takes up water from isopropyl alcohol–water solutions, just as from dioxane mixtures. The origin of this selectivity derives from the need to minimize the electrostatic free energy of the high concentration of charge in the resin phase and from the (hydrogen-bonding) solvation requirements of the resin counterion, Cl^-. The initial preference of the resin for the organic molecules as noted with the first few per cent mole fraction organic solvent is caused, we believe, by the hydrogen-bonded water structure in the dilute external solution pushing these molecules into the less-structured resin phase. As the water structure breaks down with increasing solvent mole fraction, this feature disappears.

Anion selectivity is considered to arise from the competition of the ions for that phase providing the most complete solvation; the smallest, highest charged, and most basic anion wins, leaving the other ion to go into the poorer solvating phase in the exchange. In a purely aqueous system, it is the dilute external phase that provides the most complete hydration, and so favors that ion most in need of solvation. But as alcohol (or dioxane or acetone) is added, the ability of the external phase to solvate anions decreases markedly while that of the (water-rich) resin phase decreases more slowly. As a result, the smaller anions are bound less strongly into the external phase, and so the distribution ratios for the larger anions fall. The ability of alcohols to hydrogen-bond to anions slows down the rate of decrease of D with organic mole fraction in comparison to the behavior with acetone, dioxane, and other aprotic solvents. Solvent mixtures with low dielectric constants, such as those with dioxane, introduce still another feature, namely ion pairing of the salts in the external phase. This, too, tends to hold the smaller, more basic anions in the external phase (lowers their activity) and so leads to a smaller decrease in D for the larger anions than would otherwise be expected.

Several rather general conclusions and predictions can be made. Most organic solvents will be discriminated against with respect to water by the anion-resin phase. This comes about because water molecules usually provide more complete ion solvation than the organic molecules (water has a moderately large dipole moment, a very small molar volume, and is capable of hydrogen bonding to the anion) and so are better able to lower the free energy of the concentrated resin phase. Such behavior is particularly true when the resin counterion is small and basic, *e.g.*, Cl^-, F^-, or OH^-. It is most likely to be violated when the counteranion is large, *e.g.*, ClO_4^-, as such an ion needs little (hydrogen-bonded) solvation.

With the usual organic solvents, the values of the distribution ratios of anions larger and less basic than the resin-phase counterion will decrease with an increase in organic-solvent mole fraction and the values of D for anions that are smaller and more basic will increase. Thus, selectivity coefficients will approach unity. This should also be true for complex ions if the operating con-

(41) The anion-exchange studies of C. W. Walter and J. Korkisch [*Mikrochim. Acta*, No. 1, 81 (1971); 137 (1971); 158 (1971); 181 (1971); 194 (1971)] on a number of metal cations with several mixed organic–aqueous solutions containing HNO_3 provide experimental confirmation of these last suggestions.

ditions are such that the average species is anionic (operating beyond the maximum in D for the complex ion). On the other hand, for the region below the maximum in D, where the average species is cationic, the value of D should increase with an increase in organic-solvent mole fraction.[41]

Conductometric Behavior of Tetraamylammonium Bromide and Potassium Picrate in Some Nonaqueous Solvents

by Paolo Bruno and Mario Della Monica*

Istituto di Chimica Analitica dell'Universita' di Bari, Bari, Italy *(Received June 28, 1971)*

Publication costs assisted by Centro di Chimica Analitica Strumentale, Bari, Italy

Conductance measurements are reported for n-Am_4NBr in dimethylformamide, formamide, and sulfolane, for KPi in dimethyl sulfoxide, formamide, and sulfolane, and for $KClO_4$ in dimethyl sulfoxide. The data were treated by the Fuoss–Onsager equation. The values of the ion-size parameter of all the salts were empirically corrected for the viscosity effect using the Einstein equation. Potassium picrate in sulfolane and tetraamylammonium bromide in sulfolane and in dimethylformamide exhibited values of the ion-size parameter which were smaller than the crystallographic radii of the salts; for the other salts the values of the ion-size parameter were close to the sum of the crystallographic radii of the salts. The Walden products of the large n-Am_4N^+ and Pi^- ions in the aprotic solvents show a regular increase as the medium viscosity increases. This effect is attributed to the structure breaking of the solvent molecules. In formamide the conductivity of these ions seems influenced by the protic character of this solvent.

Introduction

Tetraalkylammonium salts have been used recently to study the structural aspects of ion–solvent interaction in water and in nonaqueous solvents.[1] According to Frank and Wen,[2] large ions in water like tetraalkylammonium ions, because of their hydrophobic character, enforce the water structure, increasing the degree of hydrogen bonding around their hydrocarbon chains. The result is a comparatively lower mobility of these ions in water than in nonaqueous solvents.[3] A different behavior for the other ions has been suggested.[2] In aqueous solution the presence of ions, for instance the alkaline metal ions, introduces into the normally organized water two regions due to the more or less strong interaction among the ion and the solvent dipoles: close to the ion, the solvent molecules are strongly oriented; after this first zone loosely bound water molecules are found, characterizing a transition region, before the normally organized water which is still apart with respect to the central ion. When ions of different size are dissolved, the greater the ionic radius the larger the transition region becomes to the detriment of the first zone. Thus going along the alkaline series, whereas lithium ion has a net effect of water organizer because around it there is a broad region of firmly bound water molecules, rubidium and cesium ions which are not extensively solvated can be considered as structure breakers.

On the other hand, in aprotic solvents of different viscosity the comparative conductivities of tetraalkylammonium ions increase with the medium viscosity.[4] In these media tetraalkylammonium ions lose their peculiarity of enforcing the solvent structure *via* hydrogen bonding and they should conform to the structure breaker behavior due to their low charge density. They should, therefore, present a different behavior in protic and aprotic media as far as the solvent structure is concerned. Analogous considerations can be made in the case of large oxygenated anions which should present opposite character in these two kinds of solvents.

(1) P. G. Sears, E. D. Wilhoit, and L. R. Dawson, *J. Phys. Chem.*, **59**, 373 (1955); C. Treiner and R. M. Fuoss, *Z. Phys. Chem.*, **228**, 343 (1965); D. E. Arrington and E. Griswold; *J. Phys. Chem.*, **74**, 123 (1970); D. F. Evans and R. L. Kay, *ibid.*, **70**, 366 (1966); R. L. Kay, D. F. Evans, and G. P. Cunningham, *ibid.*, **73**, 3322 (1969); C. V. Krishnan and H. L. Friedman, *ibid.*, **73**, 3934 (1969).

(2) H. S. Frank and W. Y. Wen, *Discuss. Faraday Soc.*, **24**, 133 (1957).

(3) R. L. Kay, D. F. Evans, and G. P. Cunningham, *J. Phys. Chem.*, **73**, 3322 (1969).

(4) M. Della Monica and L. Senatore, *ibid.*, **74**, 205 (1970).

In this occurrence two salts, n-Am_4NBr and KPi, have been selected to study the conductometric behavior of n-Am_4N^+ and Pi^- ions in four solvents characterized by a large difference in viscosity (~0.008–0.1 P) and in the ability to form a hydrogen bond.

Experimental Section

Dimethylformamide (BDH for chromatography) was allowed to stand in contact with potassium hydroxide pellets for 3 days; the liquid was decanted and then fractionated at atmospheric pressure. The middle fraction obtained was distilled at 15 mm pressure. A fraction with a specific conductance 2×10^{-7} ohm^{-1} cm^{-1} was used.

Reagent grade (Rudi Pont) dimethyl sulfoxide was refluxed for 24 hr over calcium oxide and then fractionally distilled at 50° under reduced pressure (4 mm). The middle fraction had a specific conductance of 3×10^{-8} ohm^{-1} cm^{-1}.

Sulfolane (tetrahydrothiophene 1,1-dioxide), kindly supplied by Shell Italiana, was first distilled at reduced pressure (15 mm). Before heating, the sulfolane was pumped overnight to remove the volatile organic impurities. The final product was obtained by distillation under reduced pressure (1×10^{-4} Torr) over sodium hydroxide pellets.

According to the method of Notley and Spiro,[5] Baker Analyzed Reagent formamide was dried with molecular sieves 3A (Union Carbide) in the form of $^1/_{16}$-in. pellets. The column was heated electrically to 60° and the percolation rate was 1 l. in 4 hr. The formamide obtained in this way was used for the following operations: to wash and dehydrate the resins and to prepare sulfuric acid and sodium formamide solutions.

Deionization was performed by means of a mixed bed of Amberlite ion-exchange resins loaded, respectively, with H^+ and $HCONH^-$ ions and treated with formamide previously obtained. The final product had a specific conductance of 2×10^{-7} ohm^{-1} cm^{-1}, but its value changed in the course of experiments.

Eastman Kodak tetraamylammonium bromide was recrystallized three times from benzene and was dried for 48 hr in a vacuum oven at 40°.[6]

Fisher Certified Reagent potassium perchlorate was twice crystallized from conductivity water and dried in a vacuum oven at 130° for 24 hr.

Picric acid was recrystallized from benzene; the details of this purification are reported in the literature.[7] The picric acid obtained in this way was allowed to react with potassium hydroxide and the product was recrystallized three times from an ethanol–water mixture and dried under vacuum over phosphoric oxide at 100°.[8]

Apparatus. A Wavetek Function Generator Model 102 was coupled with a home-made conductivity bridge *via* a transformer in a grounded metal box. A General Radio tuned amplifier Type 1232-A was used as a null detector. The bridge of the Wheatstone type consisted of two General Radio Type 500 precision resistors plugged in the fixed arms. The chosen values of these resistors had to match the measured resistances as closely as possible. The cell, with a variable condenser in parallel, and a precision decade resistance box (121,111 ohms in 0.1-ohm steps) composed the other two arms. The bridge was properly screened and all connections were made with shielded coaxial cables. A corner of the bridge was properly grounded. Using a dummy cell, the dispersion of the components of the impedence was about $^1/_{10,000}$ in the frequency range 800–8000 Hz. The bridge was calibrated against General Radio Type 500 fixed precision resistors and the values were found to be within the specifications.

Two cells of the Daggett, Bair, and Kraus type[9] were used whose constants (about 0.5 and 0.05 cm^{-1}) were determined with aqueous KCl.[10] For the 0.05-cm^{-1} cell the value of the constant was also determined at 30° using a 0.01 demal aqueous solution of KCl and the Bremner and Thompson equation.[11] The cells were equipped with a side arm through which dry nitrogen was passed to prevent the immission of air when stock solution was added.

The four solvents used were distilled directly in the cell and the resistance of the pure solvents was measured with 10,000 and 20,000 ohms in shunt to the cell. Part of the pure solvent was used to prepare a stock solution which was added to pure solvent using a weight buret. All operations were performed in a drybox saturated with dry nitrogen; the weights were corrected to vacuum. In the calculations of the conductance of each solution allowance was made for the conductance of pure solvent. Since the conductance of pure formamide was continuously changing it was measured in a separate cell and the actual value was subtracted from the conductance of each solution.

The thermostat was an oil-filled bath kept at 25° for the measurements in dimethylformamide, dimethyl sulfoxide and formamide; in sulfolane the measurements were carried out at 30°.[12] The concentration of each solution in equivalents per liter was calculated assuming that the density of the solutions was the same as the pure solvent.

(5) J. M. Notley and M. Spiro, *J. Chem. Soc. B*, 362 (1966).

(6) A. C. Harkness and H. M. Daggett, *Can. J. Chem.*, **43**, 1215 (1965).

(7) S. R. Benedict, *J. Biol. Chem.*, **54**, 239 (1922).

(8) M. A. Coplan and R. M. Fuoss, *J. Phys. Chem.*, **68**, 1177 (1964).

(9) H. M. Daggett Jr., E. J. Bair, and C. A. Kraus, *J. Amer. Chem. Soc.*, **73**, 799 (1951).

(10) G. Jones and B. C. Bradshaw, *ibid.*, **55**, 1780 (1933).

(11) R. W. Bremner and T. G. Thompson, *ibid.*, **59**, 2372 (1937).

(12) M. Della Monica, L. Jannelli, and U. Lamanna, *J. Phys. Chem.*, **72**, 1068 (1968).

Results and Discussion

The measured equivalent conductance and corresponding electrolyte concentration have been filed with the ACS Microfilm Depository Service.[13]

Conductance data were analyzed using the Fuoss–Onsager equation[14] in the form

$$\Lambda = \Lambda_0 - Sc^{1/2} + Ec \log c + (J - F\Lambda_0)c \quad (1)$$

for unassociated electrolytes and in the form

$$\Lambda = \Lambda_0 - S(c\gamma)^{1/2} + Ec\gamma \log (c\gamma) + (J - F\Lambda_0)c\gamma - K_A f^2 c\gamma\Lambda \quad (2)$$

for associated electrolytes, where γ is the degree of dissociation, f is the mean activity coefficient, and K_A is the association constant, all other symbols having their usual meaning.

In the calculations the densities, viscosities, and dielectric constants of the four solvents were taken as: dimethylformamide, $d = 0.9439$,[15] $\eta = 0.00796$,[16] $\epsilon = 36.71$;[17] dimethyl sulfoxide, $d = 1.0956$,[18] $\eta = 0.01992$,[18] $\epsilon = 46.6$;[19] formamide, $d = 1.1296$,[20] $\eta = 0.0330$,[21] $\epsilon = 109.5$;[22] sulfolane, $d = 1.2618$,[23] $\eta = 0.1029$,[24] $\epsilon = 43.3$.[25]

Kay's least-squares program[26] was used to solve eq 1 and 2 for the parameters of interest, Λ_0 and $\mathring{a}$, and for associated electrolytes, K_A. The results are shown in Table I. Equation 2 gave positive association constants K_A for n-Am_4NBr in dimethylformamide and for KPi in sulfolane. For the other salts studied eq 2 gave negative association constants, so that conductance parameters have been calculated using eq 1.

Table I: Conductance Parameters

Solvent	Λ_0	J	a_j	K_A
	n-Am_4NBr			
Sulfolane	11.416 ± 0.002	30.0	1.60 ± 0.03	...
Formamide	22.95 ± 0.01	28.4	4.4 ± 0.6	...
Dimethyl-formamide	76.46 ± 0.08	691.9	3.1 ± 0.6	4 ± 2
	KPi			
Sulfolane	9.36 ± 0.03	46.2	3 ± 2	9 ± 7
Formamide	21.88 ± 0.01	25.2	3.9 ± 0.5	...
Dimethyl sulfoxide	31.43 ± 0.02	223.8	4.7 ± 0.1	...
	$KClO_4$			
Dimethyl sulfoxide	38.63 ± 0.01	235.9	4.08 ± 0.07	...

In the calculations, no allowance was made for the term F which takes into account the variation of viscosity for the added electrolyte. This fact does not alter the Λ_0 values, but only the value of $\mathring{a}$, the maximum approach distance of the ions, which is deduced from the J values. In this occurence precise values of distance a_j cannot be calculated, and the a_j values, as shown in Table I, are in all cases, except for $KClO_4$ in dimethyl sulfoxide, too low.

An attempt to calculate more correct a_j values can be tentatively made with the equation[13]

$$F = \frac{N\pi}{300}(R_+^3 + R_-^3) \quad (3)$$

where N is the Avogadro number and R_+ and R_- are the crystallographic radius of the cation and anion, respectively. This equation holds for large ions compared to the size of the solvent molecules and was derived for unhydrated solute species in a continuous medium.

Table II: Correction for the Viscosity Effect

Solvent	$F\Lambda_0$	J_{cor}	a_{cor}	$(R_+ + R_-)$
	n-Am_4NBr			
Sulfolane	11.2	41.2	2.1	7.24
Formamide	22.5	50.9	8.4	7.24
Dimethyl-formamide	75	655.8	2.9	7.24
	KPi			
Sulfolane	7.1	53.3	3.2	6.3
Formamide	17.6	42.8	7.0	6.3
Dimethyl sulfoxide	25.2	249	5.4	6.3
	$KClO_4$			
Dimethyl sulfoxide	3.9	239.8	4.16	4.25

(13) Equivalent conductance data will appear following these pages in the microfilm edition of this volume of the journal. Single copies may be obtained from the Business Operations Office, Books and Journals Division, American Chemical Society, 1155 Sixteenth St., N.W., Washington, D. C. 20036, by referring to author, title of article, volume, and page number. Remit check or money order for $3.00 for photocopy or $2.00 for microfiche.

(14) R. M. Fuoss and F. Accascina, "Electrolyte Conductance," Interscience, New York, N. Y., 1959.

(15) J. E. Prue and P. J. Sherrington, *Trans. Faraday Soc.*, **57**, 1795 (1961).

(16) D. P. Ames and P. G. Sears, *J. Phys. Chem.*, **59**, 16 (1955).

(17) G. R. Leader and J. F. Gormley, *J. Amer. Chem. Soc.*, **73**, 5731 (1951).

(18) D. E. Arrington and E. Griswold, *J. Phys. Chem.*, **74**, 123 (1970).

(19) P. G. Sears, G. R. Lester, and L. R. Dawson, *ibid.*, **60**, 1433 (1956).

(20) J. Thomas and D. F. Evans, *ibid.*, **74**, 3812 (1970).

(21) G. F. Smith, *J. Chem. Soc.*, 3257 (1931).

(22) G. R. Leader, *J. Amer. Chem. Soc.*, **73**, 856 (1951).

(23) U. Lamanna, O. Sciacovelli, and L. Jannelli, *Gazz. Chim. Ital.*, **94**, 567 (1964).

(24) R. Fernandez-Prini and J. E. Prue, *Trans. Faraday Soc.*, **62**, 1257 (1966); J. W. Vaughn and C. F. Hawkins, *J. Chem. Eng. Data*, **9**, 140 (1964).

(25) M. Della Monica, U. Lamanna, and L. Jannelli, *Gazz. Chim. Ital.*, **97**, 367 (1967).

(26) R. L. Kay, *J. Amer. Chem. Soc.*, **82**, 2099 (1960).

Table III: Conductances and Walden Products of n-Am_4N^+ and Pi^- Ions in Formamide, Dimethylformamide, Dimethyl Sulfoxide, and Sulfolane

	Solvents							
	Dimethylformamide		Dimethyl sulfoxide		Formamide		Sulfolane	
Ion	λ_0	$\lambda_0\eta$	λ_0	$\lambda_0\eta$	λ_0	$\lambda_0\eta$	λ_0	$\lambda_0\eta$
n-Am_4N^+	22.9	0.182	10.41[c]	0.206	5.81	0.192	2.50	0.257
Pi^-	37.5[a]	0.299	16.92[b]	0.335	9.13	0.301	5.28	0.544

[a] This mean value has been deduced from the Λ_0 of NaPi and KPi salts (P. G. Sears, R. K. Wolford, and L. R. Dawson, *J. Electrochem. Soc.*, **103**, 633 (1956)) and the λ_0 values of Na^+ and K^+ ions reported in the literature (ref 15). [b] This value has been calculated by the λ_0 value of ClO_4^- ion (M. Della Monica, D. Masciopinto, and G. Tessari, *Trans. Faraday Soc.*, **66**, 2872 (1970)) in combination with the values of $KClO_4$ and KPi salts reported in this work. [c] Reference 18.

These conditions can be assumed for n-Am_4N^+ and Pi^- ions and in some respects for Br^- and ClO_4^- ions, but not for the K^+ ion. However, since this correction should serve to give just an idea of the effect of the salt concentration on the solution viscosity, the crystallographic radii of Br^-, ClO_4^-, n-Am_4N^+, and also of K^+ ions have been used in eq 3.[27,28] The calculations of picrate ion radius have been based on the parameters of iodo-*s*-trinitrobenzene:[27,29] the radius of benzene ring = 1.39 Å; the maximum distance of C–N bond = 1.46 Å; the distance of N–O bond = 1.21 Å; the angle O–N–O = 120°; the van der Waals radius of oxygen atom = 1.40 Å. From these values a radius of the spheric envelope of picrate ion $\cong$5 Å is obtained.

After correction, the values of J_{cor} and then the a_{cor} values have been calculated and the results reported in Table II. A survey of Table II shows that the ion-size parameter a_{cor} is close to the sum of the crystallographic radii of the two ions for n-Am_4NBr and KPi in formamide and for KPi and $KClO_4$ in dimethyl sulfoxide. In dimethylformamide and sulfolane the salts studied have a_{cor} values that are too low and have no physical meaning.

According to Fuoss and Accascina,[14] a distance of maximum approach close to the sum of the crystallographic radii of the salts means that the ion–ion contacts occur between bare ions and not between their cospheres: in other words, the initial contact is between ions with their cospheres, but under the ionic fields, the solvent molecules of the cospheres can be expelled.

At the present time we have no convincing explanations to account for the small values of maximum approach distance found in the case of salts in dimethylformamide and sulfolane. Nevertheless, it seems that this fact is related to some solvent properties as can be deduced by the behavior of other salts in sulfolane.[30]

Starting from precise transference number measurements and conductivities of appropriate salts, the conductivities of n-Am_4N^+ and Pi^- ions in the various solvents have been deduced. These values and corresponding Walden products are reported in Table III. In the same table the equivalent limiting conductances and the Walden products of n-Am_4N^+ ion in dimethyl sulfoxide and Pi^- ion in dimethylformamide taken from the literature are also reported.

A survey of Table III shows that the Walden products of n-Am_4N^+ and Pi^- ions increase going from dimethylformamide to dimethyl sulfoxide and sulfolane; the same behavior is observed for other tetraalkylammonium ions in the same solvents.[4]

The anomalous conductivities of salts in viscous media have been explained in different ways. Very high Walden products found for some quaternary salts in cyanoethylsucrose–acetonitrile mixtures are explained by Fuoss and Treiner[31] with a greater ability of ions in cyanoethylsucrose rich mixtures to travel through the solvent molecules. The relative high mobility of Bu_4NPi in tricresyl phosphate is justified by Elliott and Fuoss[32] in terms of slipping of these ions between certain configurations of large solvent molecules. In order to explain the Walden product of Bu_4N^+ ion in formamide being higher than the corresponding values in water, methanol, ethanol, and nitromethane, Notley and Spiro[33] postulate iceberg formation which reduces the mobility of Bu_4N^+ ion in water and in the other solvents or, alternatively, the breaking of solvent structure in formamide.

Recently a study appeared on the viscosity of solutions of some tetraalkylammonium iodide in *N*-methylformamide.[34] The data obtained at various temperatures show a positive dependence on the temperature for the Jones and Dole equation[35] B coefficient.

A positive dB/dt implies a breaking effect on the solvent structure caused by the large tetraalkylammonium ions. If one assumes that the same structure-

(27) L. Pauling, "The Nature of the Chemical Bond," 2nd ed, Cornell University Press, Ithaca, N. Y., 1948.

(28) R. A. Robinson and R. H. Stokes, "Electrolyte Solutions," Academic Press, New York, N. Y., 1955.

(29) A. D. Mitchell and L. C. Cross, *Chem. Soc., Spec. Publ.*, **No. 11**, 189 (1958).

(30) R. Fernandez-Prini and J. E. Prue, *Trans. Faraday Soc.*, **62**, 1257 (1966).

(31) C. Treiner and R. M. Fuoss, *J. Phys. Chem.*, **69**, 2576 (1965).

(32) M. A. Elliott and R. M. Fuoss, *J. Amer. Chem. Soc.*, **61**, 294 (1939).

(33) J. M. Notley and M. Spiro, *J. Phys. Chem.*, **70**, 1502 (1966).

(34) P. P. Rastogi, *Bull. Chem. Soc. Jap.*, **43**, 2442 (1970).

(35) G. Jones and M. Dole, *J. Amer. Chem. Soc.*, **51**, 2950 (1929).

breaking effect is caused by these ions also in other nonaqueous solvents, then the anomalous Walden products reported in Table III can be understood. The breaking of the solvent structure decreases the viscosity around the ions and consequently, under an applied electrical field, they experience a resistance to motion smaller than that expected from Stokes' law.

The behavior of n-Am_4N^+ and Pi^- ions in formamide is no longer explainable with the above assumption alone. Formamide has a higher viscosity than dimethyl sulfoxide, but in this solvent the Walden product values of the two ions considered are not correspondently high. Formamide is a protic solvent with possibility of H-bonding lower than water but higher than alcohols.[20] The presence of the large n-Am_4N^+ ion can increase the degree of hydrogen bonding between the solvent molecules and enforce a shell of solvent around it in a two-dimensional structure. The above hypothesis is supported by the fact that in water, where a three-dimensional cage structure around the ions is possible, the Walden products of the tetraalkylammonium ions are very low.[36]

As far as the picrate ion in this solvent is concerned, the low value of the Walden product found is probably due to a strong hydrogen bonding interaction which occurs this time between the solvent molecules and the six oxygen atoms of picrate ions.

In conclusion, the results of this preliminary work suggest the idea that also in nonaqueous solvents the ions are able to act as structure breakers or structure makers, in whichever way the structure making effect caused by tetraalkylammonium ions seems limited to the protic solvents alone. More work is needed before definite conclusions can be drawn about this point.

Acknowledgment. We thank Dr. G. Tessari of this Institute for assistance and helpful suggestions.

(36) D. F. Evans and R. L. Kay, *J. Phys. Chem.*, **70**, 366 (1966).

Electrical Conductance and Ionization Behavior of Sodium Chloride in Dioxane–Water Solutions at 300° and Pressures to 4000 Bars[1]

by LeRoy B. Yeatts* and William L. Marshall*

Reactor Chemistry Division, Oak Ridge National Laboratory, Oak Ridge, Tennessee 37830 *(Received February 12, 1971)*

Publication costs assisted by the Oak Ridge National Laboratory, U. S. Atomic Energy Commission

Electrical conductance measurements were made of dilute sodium chloride (0.0005–0.01 m) in dioxane–water solutions to determine its ionization behavior in this solvent system at 300° and at pressures to 4000 bars. This conductance study is believed to be the first one made for any electrolyte in an organic–aqueous solvent above 100°. Estimates of dielectric constant, density, and viscosity under these conditions are given for the mixed solvent whose composition ranged from 34.7 to 75.0 wt % dioxane. These estimates were used with the conductance equation of Shedlovsky to determine limiting equivalent conductances (Λ_0) and conventional ionization constants (K_d). It was found that sodium chloride becomes a progressively weaker electrolyte both as the dioxane content in the solvent increases and as the pressure decreases. With hydration of the electrolyte species in solution considered an essential part of the ionization process, the value of the complete isothermal equilibrium constant (K^0) at 300° is $10^{-16.0}$, while the net change (k) on ionization in the number of solvated water molecules is 10.0. These values, appearing to be constant over the range of experimental conditions, are shown to be consistent with previous results for sodium chloride both in water (400–800°) and in dioxane–water (25–100°) at pressures up to 4000 bars. The values of k and K^0 *vs.* temperature provide required information for calculating the conventional thermodynamic functions over wide ranges of temperature and pressure.

Introduction

The earlier proposal[2,3] of a complete isothermal ionization constant (K^0), which includes the solvating polar solvent(s) in the ionic dissociation expression, has been applied successfully to describe numerous equilibria involving ions and ion pairs. These equilibria include the dissolution of several salts[3] in water and in dioxane–water solutions, the ionization of numerous

(1) (a) Research sponsored by the U. S. Atomic Energy Commission under contract with the Union Carbide Corp.; (b) presented before the Division of Physical Chemistry at the 162nd National Meeting of the American Chemical Society, Washington, D. C., Sept 12–17, 1971.

salts[2-4] in water and in dioxane–water, the ionization of quaternary ammonium salts in nitrobenzene–carbon tetrachloride,[2,3] the ionization in water of the weak base ammonia[5a] and of the acid HBr,[5b] and the ionization of water[6] itself. The experimental conditions for these studies cover the temperature range of 25–800° at pressures to 12,000 bars. This principle was recently used to calculate the complete isothermal rate constant[7] for several solvolysis reactions. The concentration of the polar solvent, generally water, is altered markedly during an investigation by changing the pressure on the system, by changing the ratio of polar to nonpolar constituents in the mixed solvent, or by doing both. The use of both methods to change the concentration of water, where the concentration of solute approaches zero [C(solute) $\rightarrow$ 0], provides a stringent test of the complete equilibrium constant approach, since the concept should apply, and has applied, in a continuous manner to water both above and below the critical temperature.

The adoption of the complete isothermal equilibrium constant also allows the determination of the net change (k) in the number of molecules of solvation which occurs during the ionization process. The values of k and K^0 have been described mathematically to be functions both of temperature and of pressure or C (solvating species).[8] Although k and K^0 may vary significantly with changes in temperature, they are observed experimentally to be constant over a wide range of pressure or of C (solvating species). Therefore, it was the purpose of this present study to evaluate k and K^0 over ranges of both pressure and dioxane–water composition and then to establish whether the values for sodium chloride in dioxane–water at 300° would provide a smooth transition between those obtained at 25° [2,3,8] and 100° [4d,e] in dioxane–water and those from 400 to 800° [4a] in pressurized water.[9]

Values of the conventional ionization constant (K_d) were calculated after measuring electrical conductances of dilute sodium chloride solutions (0.0005–0.01 m) in four different dioxane–water solvent compositions at 300° and at pressures to 4000 bars. These values of K_d were used to obtain a single value of both k and K^0. The results are consistent with those reported earlier at both lower and higher temperatures, even though estimates of the densities, dielectric constants, and viscosities for the various solutions at 300° had to be made to obtain values of K_d and hence k and K^0.

In addition to testing further the usefulness of a complete constant, this study of conductance and ionization behavior in an organic–aqueous solvent appears to be the first one for any electrolyte made at a temperature above 100°. The study therefore should be of value both in itself and in testing various theories of electrolyte behavior at high temperature. It is hoped that the estimates of the several physical properties of dioxane–water solvent mixtures, necessary for the calculations, will prove to be useful to others until actual experimental measurements of these properties are available.

Experimental Section

The preparation of sodium chloride–dioxane–water solutions,[4d] the conductance apparatus,[4a] and the experimental procedures[4a] have been described previously. The cell constants at 300° for the three inner electrodes used for the conductance measurements were determined with 0.01 demal KCl solutions to be 0.481, 0.493, and 1.96. All conductance measurements were made at a signal frequency of 2 kHz. Table I gives the smoothed specific conductances (κ) for the four solvent compositions prepared for this study. The values at saturation vapor pressure were obtained by extrapolating the curves of specific conductance *vs.* pressure below the lowest experimental pressure of about 500 bars. Four or five sodium chloride solutions, ranging from 0.0005 to 0.01 m, were studied at 300° and in solvent compositions of 34.7, 50.8, 61.5, and 75.0 wt % dioxane. The conductance measurements for these solutions were in the range of 0.1–2.4 mohm^{-1} (resistance = 400–10,000 ohms). Experimental values at 300° for density (d), dielectric constant (D), and viscosity (η) of either the solutions or the mixed solvent itself are not available. Therefore, estimates of these properties for the solvent at this temperature and at pressures to 4000 bars were made. The values of d, D, and η for the dilute sodium chloride solutions were assumed to be the same as those for the two component solvent. The methods used to estimate these three physical properties are discussed immediately below.

Estimations of Solvent Properties

Densities. Estimates of the densities of the dioxane–water solutions were based on the assumption that the two components form ideal solutions at 300°: solvent density = density of pure dioxane times volume fraction of dioxane plus density of pure water times volume fraction of water. The values used for water at pressures below 1000 bars are those compiled by Sharp,[10] while above

(2) W. L. Marshall and A. S. Quist, *Proc. Nat. Acad. Sci. U. S.*, **58**, 901 (1967).

(3) A. S. Quist and W. L. Marshall, *J. Phys. Chem.*, **72**, 1536 (1968).

(4) (a) A. S. Quist and W. L. Marshall, *ibid.*, **72**, 684 (1968); (b) *ibid.*, **72**, 2100 (1968); (c) L. A. Dunn and W. L. Marshall, *ibid.*, **73**, 723 (1969); (d) *ibid.*, **73**, 2619 (1969); (e) L. B. Yeatts, L. A. Dunn, and W. L. Marshall, *ibid.*, **75**, 1099 (1971); (f) E. U. Franck, *Z. Phys. Chem.* (*Frankfurt am Main*), **8**, 107, 192 (1956).

(5) (a) A. S. Quist and W. L. Marshall, *J. Phys. Chem.*, **72**, 3122 (1968); (b) *ibid.*, **72**, 1545 (1968).

(6) W. L. Marshall, *Rec. Chem. Progr.*, **30**, 61 (1969); A. S. Quist, *J. Phys. Chem.*, **74**, 3396 (1970).

(7) W. L. Marshall, *ibid.*, **74**, 346 (1970).

(8) W. L. Marshall, *ibid.*, **76**, 720 (1972).

(9) W. L. Marshall, *Rev. Pure Appl. Chem.*, **18**, 167 (1968).

(10) W. E. Sharp, "The Thermodynamic Functions for Water in the Range −10 to 1000° and 1 to 250,000 Bars," University of California Radiation Laboratory Report, No. UCRL-7118, 1962.

Table I: Properties of Dioxane–Water Solvent Compositions at 300° from Saturation Vapor Pressure to 4000 Bars

Dioxane, wt %	Pressure, bars: Satn VP[a]	500	1000	1500	2000	2500	3000	3500	4000
				Densities, g/cm³ [b]					
0	0.713	0.777	0.824	0.862	0.888	0.911	0.933	0.955	0.975
34.7	0.657	0.818	0.873	0.911	0.937	0.961	0.983	1.005	1.025
50.8	0.635	0.836	0.893	0.931	0.958	0.982	1.004	1.026	1.046
61.5	0.621	0.846	0.906	0.944	0.971	0.995	1.018	1.039	1.059
75.0	0.604	0.858	0.921	0.959	0.986	1.011	1.033	1.055	1.075
100	0.575	0.881	0.946	0.985	1.012	1.037	1.060	1.082	1.102
				Dielectric Constants[b]					
0	19.7	21.9	23.6	25.0	26.0	26.8	27.7	28.5	29.3
34.7	10.5	13.7	14.9	15.7	16.2	16.8	17.2	17.7	18.2
50.8	7.2	10.0	10.8	11.4	11.8	12.1	12.5	12.8	13.1
61.5	5.4	7.6	8.2	8.6	8.9	9.2	9.4	9.7	9.9
75.0	3.4	4.8	5.2	5.4	5.6	5.7	5.9	6.0	6.1
				Viscosities, cP[b]					
0	0.090	0.102	0.114	0.125	0.134	0.142	0.149	0.156	0.163
34.7	0.093	0.106	0.120	0.132	0.142	0.151	0.159	0.168	0.176
50.8	0.095	0.110	0.124	0.138	0.149	0.159	0.168	0.177	0.186
61.5	0.097	0.113	0.128	0.143	0.155	0.166	0.177	0.187	0.197
75.0	0.102	0.120	0.137	0.154	0.168	0.182	0.194	0.206	0.218
100	0.124	0.155	0.185	0.216	0.242	0.271	0.298	0.323	0.352
				Specific Conductances of Solvent,[c] ohm^{-1} cm^{-1} × 10^6					
34.7	(2.0)[d]	3.6	4.3	5.7	7.3	8.9	10.6	12.3	14.0
50.8	(1.1)	1.3	1.6	1.8	2.0	2.3	2.5	2.8	3.1
61.5	(0.2)	0.7	1.0	1.2	1.4	1.7	1.9	2.1	2.4
75.0	(0.2)	0.3	0.3	0.4	0.5	0.6	0.7	0.8	0.9

[a] Saturation vapor pressures are 86 bars for water and 43 bars for dioxane; estimated saturation vapor pressures are 82, 78, 75, and 70 bars for 34.7, 50.8, 61.5, and 75.0 wt % dioxane solvent compositions, respectively. [b] Calculated values (see Experimental Section of text). [c] Values derived from experimental measurements. [d] Parentheses enclose extrapolated values, since reliable measurements could not be made below about 500 bars.

1000 bars the data of Maier and Franck[11] were used.[12] The density of liquid dioxane at 300° and saturation vapor pressure was read from the orthobaric curve of Højendahl.[13] The method of Lydersen, Greenkorn, and Hougen,[14a] which is discussed by Reid and Sherwood,[14b] was then used to calculate the densities of dioxane up to 1500 bars of pressure. Since this pressure was the upper limit for the method in this instance, densities from 1500 to 4000 bars were estimated by assuming that the density of dioxane changes with pressure by the same absolute amount as does that of water. With these densities for the pure components, the densities of dioxane–water solutions were estimated at various pressures to 4000 bars from the initial assumption of the formation of ideal solutions at 300°. (The liquid–vapor critical temperatures of dioxane and water are 312[13] and 374°, respectively.) These densities are presented in Table I.

Dielectric Constants. Upon plotting the dielectric constants (D) for dioxane–water solutions of Åkerlöf and Short[15] at 20 and 80° and estimated by Dunn and Marshall[4d] at 100° as log (D − 1) *vs.* log C_{H_2O} (moles/liter), it was found that straight lines with nearly identical slopes could be drawn at each temperature up to about 90 wt % dioxane. Therefore, it was assumed that the line at 300° would have the same slope as the one at 100°. With this slope of the line at 100°,[4e] the value of the dielectric constant of water at 300° (19.66) from Åkerlöf and Oshry,[16] and the density of water at 300°, the equation for the new line was obtained

(11) S. Maier and E. U. Franck, *Ber. Bunsenges. Phys. Chem.*, **70**, 639 (1966).

(12) The more recent densities for water of C. W. Burnham, J. R. Holloway, and N. F. Davis, *Amer. J. Sci.*, **267A**, 70 (1969), are approximately 1% lower than those we used. Our choice was prompted by a desire to maintain consistency with the previous publications from this laboratory. The use, however, of these more recent densities of water would change negligibly the estimated values of dioxane–water density in Table I and would not have any significant effect upon the calculated values of Λ_0 or of log K_d given in Table III.

(13) K. Højendahl, *Kgl. Dansk. Videnskab. Selsk., Mat.-Fys. Medd.* **24**, No. 2, 3 (1946).

(14) (a) A. L. Lydersen, R. A. Greenkorn, and O. A. Hougen, "Generalized Thermodynamic Properties of Pure Fluids," College of Engineering, University of Wisconsin, Engineering Experimental Station, Report No. 4, Madison, Wis., Oct 1955; (b) R. C. Reid and T. K. Sherwood, "Properties of Gases and Liquids," McGraw-Hill, New York, N. Y., 1958, pp 60–65.

(15) G. Åkerlöf and O. A. Short, *J. Amer. Chem. Soc.*, **58**, 1241 (1936).

(16) G. C. Akerlöf and H. I. Oshry, *ibid.*, **72**, 2844 (1950).

$$\log (D - 1) = -0.85303 + 1.32965 \log C_{H_2O} \quad (1)$$

The molar concentration of water was determined from the composition of the solvent and the previously estimated solvent density at a given pressure to 4000 bars. Since the solutions did not exceed 75 wt % dioxane, eq 1 was used to estimate the dielectric constants listed in Table I.

Viscosities. To obtain estimated values of viscosity, it was again assumed that dioxane and water formed ideal solutions at 300°. We chose the relationship

$$\ln \eta = N_{Dx} \ln \eta_{Dx}^0 + N_{H_2O} \ln \eta_{H_2O}^0 \quad (2)$$

where η, η_{Dx}^0, and $\eta_{H_2O}^0$ are the viscosities of the binary solvent, pure dioxane, and pure water, respectively, and N_{Dx} and N_{H_2O} are the mole fractions of dioxane and water, respectively.[17] The viscosities of pure water at various pressures which were used in the calculations are those reported by Dudziak and Franck,[18] extrapolated to 4000 bars.

Experimentally determined viscosities for dioxane above 80° were not found in the literature. Therefore, Geddes' equation[19] relating the fluidity ($1/\eta$) of dioxane at temperatures up to 80° was used to estimate the viscosity of dioxane at 300° and saturation vapor pressure. (Højendahl's simpler equation[13] for calculating the viscosity of dioxane at temperatures up to 70° produced a value at 300° within 5% of this one.) Estimates of the viscosities of pure dioxane as a function of pressure were obtained by assuming that the fluidities of dioxane decrease in absolute value, with an incremental rise in pressure, to the same extent as do the fluidities of water. Estimates of viscosities for the four dioxane–water solvent compositions at different pressures were then calculated with eq 2. These values are listed in Table I.

Saturation Vapor Pressures. The saturation vapor pressures at 300° which are given in Table I were estimated from ideal solution behavior

$$p = N_{Dx} p_{Dx}^0 + N_{H_2O} p_{H_2O}^0 \quad (3)$$

where p, p_{Dx}^0, and $p_{H_2O}^0$ are the saturation vapor pressures of the binary solvent, pure dioxane, and pure water, respectively. A value of 85.92 bars reported by Vukalovich[20] was used for the saturation vapor pressure of water at 300° and a value of 42.8 bars for dioxane, reported by Højendahl.[13]

Results and Discussion

Conductances Correlated with Ion Association and Viscosity. The measured conductances were converted to resistances and corrections were made both for the resistance of the electrical leads and for a slight dependence (1–2%) of conductance upon signal frequency. From these results along with the cell constants, specific conductances were calculated which were corrected finally for solvent conductance. (For a detailed description of treating the original data, see ref 4a.) Typical curves for the pressure dependence of the specific conductance of sodium chloride at 300° in dioxane–water are shown in Figure 1. Although the molality of sodium chloride is essentially the same in these solutions, there is a marked decrease in specific conductance at constant pressure as the fraction of dioxane in the solvent increases. This behavior is due to the decreased water concentration of the solution, which favors ion association, along with the increased solution viscosity (see Table I), which decreases ionic mobilities. At 34.7, 50.8, and 61.5 wt % dioxane, the specific conductance curves show sharp increases with pressure up to about 1000 bars and then pass through shallow maxima as the pressure continues to rise. As the pressure increases until the specific conductance reaches a maximum, the effect of increasing density (water concentration) outweighs the effect of increasing solution viscosity; beyond the maximum specific conductance, the viscosity effect predominates slightly as the pressure rises. At 75.0 wt % dioxane, the effect of increasing density (water concentration) prevails throughout as the pressure rises. These results at 300° are in sharp contrast to those at 100° [4e] where the specific conductance of sodium chloride in dioxane–water continues to decrease from the outset as the pressure increases. The

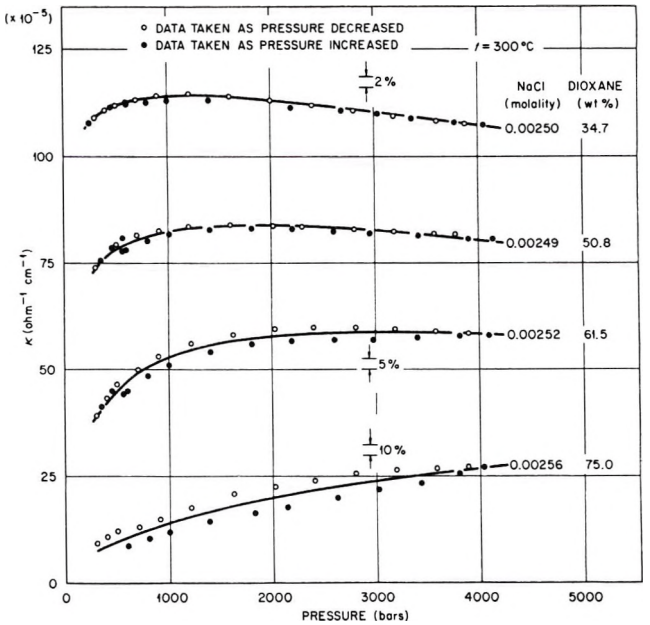

Figure 1. Dependence of specific conductance of NaCl solutions upon pressure in various dioxane–water solvent compositions at 300°.

(17) J. Kendall, *Medd. K. Vetenskapsakad. Nobelinst (Stockholm)*, 2, 1 (1913); see *Chem. Abstr.*, 7, 2714 (1913); also see S. Glasstone, "Textbook of Physical Chemistry," 2nd ed, Van Nostrand, Princeton, N. J., 1946, p 500; J. O. Hirschfelder, C. F. Curtiss, and R. B. Bird, "Molecular Theory of Gases and Liquids," Wiley, New York, N. Y., 1954, p 630.

(18) K. H. Dudziak and E. U. Franck, *Ber. Bunsenges. Phys. Chem.*, 70, 1120 (1966).

(19) J. A. Geddes, *J. Amer. Chem. Soc.*, 55, 4832 (1933).

(20) M. P. Vukalovich, "Termodinamicheskie Svoistva Vody i Vodianogo Para," 6th ed, Vebverlag Technik, Berlin, 1958.

Table II: Specific Conductances (ohm^{-1} cm^{-1}) × 10^6 of NaCl in Dioxane–Water Solutions at 300° from Saturation Vapor Pressure to 4000 Bars

Dioxane, wt %	NaCl, $m \times 10^3$	Pressure, bars							
		Satn VP[a]	500	1000	1500	2000	2500	3000	3500	4000
34.7	1.003	(39.9)[b]	47.4	48.0	47.8	47.3	46.8	46.1	45.5	44.7
	1.808	(69.4)	83.0	84.3	84.2	83.8	83.1	82.3	81.3	80.4
	2.500	(93.0)	111.5	113.8	113.4	112.5	111.6	110.3	108.7	107.0
	9.998	(336.)	401.	418.	423.	423.	421.	418.	414.	409.
50.8	0.4975	(15.9)	19.9	20.2	20.1	20.0	19.9	19.8	19.6	19.4
	0.9969	(29.0)	36.0	37.6	37.5	37.2	37.0	36.8	36.6	36.4
	2.496	(62.5)	80.8	85.9	87.1	87.2	86.7	85.8	84.7	83.5
	5.013	(99.0)	141.	156.	161.	162.	162.	162.	161.	159.
	10.03	(167.)	238.	262.	281.	287.	289.	289.	288.	287.
61.5	1.013	(16.9)	24.3	26.6	27.9	28.3	28.4	28.3	28.0	27.5
	2.521	(30.1)	44.2	52.8	56.2	57.8	58.4	58.6	58.5	58.4
	5.043	(47.3)	76.9	91.7	98.6	103.	105.	106.	108.	109.
	10.09	(72.1)	128.	159.	177.	186.	191.	195.	198.	202.
75.0	1.034	(3.4)	5.9	8.8	10.5	11.8	12.8	13.5	14.2	14.8
	1.539	(4.3)	8.3	11.7	14.0	15.7	17.1	18.3	19.3	20.3
	2.555	(4.5)	9.5	14.3	17.5	20.0	21.8	23.5	25.4	27.0
	5.124	(5.6)	15.6	22.8	28.5	33.3	37.8	41.9	46.0	50.0
	10.26	(7.4)	24.0	35.7	44.9	53.8	62.4	69.4	74.8	79.4
	10.26	(7.4)	22.4	33.7	42.8	50.8	58.5	65.6	72.7	79.5

[a] See footnote *a*, Table I. [b] See footnote *d*, Table I.

curves of specific conductance *vs.* pressure for the sodium halides,[4a,b,c] as well as for other alkali halides,[21] in aqueous solutions at 300° have also shallow maxima. In these cases it is not until temperatures of 400° and greater are reached that the effect of increasing water concentration outweighs the effect of increasing viscosity upon specific conductance throughout the pressure range.

The specific conductances of 0.001 *m* sodium chloride in 50.8 wt % dioxane are approximately twice as high at 300° as they are at 100°.[4c] From this representative behavior, it is concluded that as the temperature rises the increasing ionic mobilities far outweigh the effect of the reduction in ionic concentrations from a decreasing density and from expected increasing association. Raising the pressure (1–4000 bars) as the temperature increases from 100 to 300° would not appear to void this conclusion.

It can be seen in Figure 1 that, in general, the conductance readings which were taken upon increasing the pressure on the system are somewhat lower than those taken after decreasing the pressure. This slight "hysteresis" effect, which increases as the dioxane content of the solution increases, cannot be explained at this time, although efforts were made to eliminate it by improving the temperature control and by permitting sufficient time to elapse to assure that an equilibrium pressure was reached. Several repeated runs on different days with the same composition of solvent and of NaCl, but with a fresh solution, gave essentially identical results. It was thought that the best values might be those extrapolated to zero time. However, since a constant temperature is necessary, it was decided that the best procedure would be to report the average value of the first sets of measurements at increasing and decreasing pressure.

Graphs similar to Figure 1 were made from the data for each solution of sodium chloride in the four dioxane–water solvent compositions. Smoothed specific conductances were read from these curves at increments of 500 bars up to 4000 bars and are presented in Table II. It should be noted that data collected at pressures below about 500 bars showed too much scatter to be considered reliable for extrapolating to obtain specific conductances at saturation vapor pressure. Therefore, the values of specific conductance reported in Table II for saturation vapor pressure were calculated from values of equivalent conductance (Λ) obtained from extrapolations of the curves of Λ *vs.* pressure, presented below. These latter curves do not show as high a pressure dependence at the low pressures as do the specific conductance curves; hence, extrapolations of the Λ *vs.* pressure curves should be more exact.

Unique Behavior of Equivalent Conductances. Equivalent conductances of the sodium chloride solutions were calculated from the smoothed specific conductances, the molalities, and the estimated densities of the solvent, which also were considered to be the densities of these dilute solutions. The pressure dependence of the equivalent conductance can be seen in

(21) A. S. Quist and W. L. Marshall, *J. Phys. Chem.*, **73**, 978 (1969).

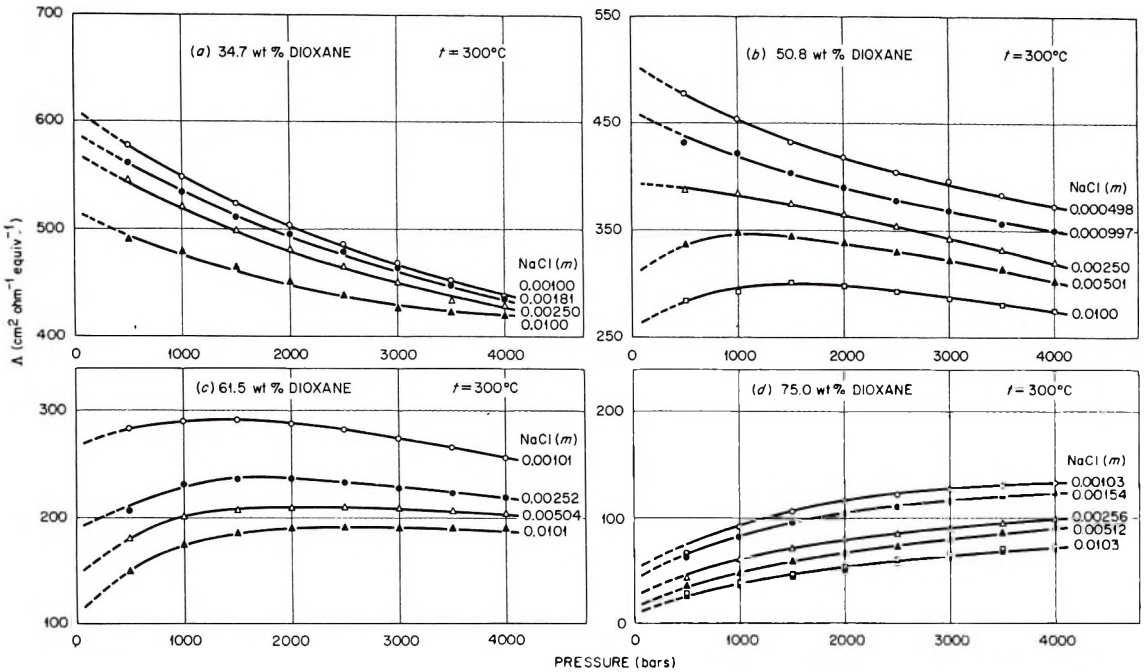

Figure 2. Equivalent conductances of NaCl as a function of pressure for several dioxane–water compositions at 300°.

Figure 2; note that the curves are extrapolated from 500 bars to saturation vapor pressure. As the dioxane content of the solvent increases from 34.7 to 75.0 wt %, the equivalent conductances of all the solutions are seen to change from *decreasing* with increasing pressure to *increasing* with rising pressure. This behavior indicates that at 34.7 wt % dioxane the effect of an increase in viscosity with increasing pressure, accompanied by lower ionic mobilities, predominates, while at 75.0 wt % dioxane the effect of an increase in the concentration of water with increasing pressure, accompanied by greater ionization, prevails. At 100°, however, no such pressure effect upon the equivalent conductance for sodium chloride was observed. Rather, the equivalent conductances *decreased steadily* with increasing pressure at the five solvent compositions from 29.7 to 70.5 wt % dioxane.[4e] The lower compressibilities of the solvent mixtures at 100° disallowed a sufficiently large change in water concentration, and accordingly the effect of viscosity predominated at all pressures and solvent compositions.

The curves for the equivalent conductances of sodium chloride at various molalities in 50.8 and 61.5 wt % dioxane are particularly interesting, since here a gradual transition between the above two extremes of pressure dependence is seen. In 50.8 wt % dioxane, as the pressure increases the equivalent conductances decrease at the lower salt molalities due to the predominant effect of increasing viscosities which lower the ionic mobilities. In the same solvent at the higher salt molalities where ionic association is greater, the initial rise in the equivalent conductances is related to the predominant effect of increasing ionization from raising the concentration of water by increasing the pressure. The form of the curves for equivalent conductance *vs.* pressure in 61.5 wt % dioxane for all molalities shows the effects both of increasing ionization at low pressures and of increasing viscosity at high pressures as the pressure continually rises.

Curves showing maxima, as in Figure 2, are observed also for aqueous solutions of 1:1 electrolytes at supercritical temperatures (400–800°), as described for sodium chloride.[4a] In this region of high temperature at pressures to 4000 bars, the predominant effects of ionization at low pressures and of viscosity at high pressures are always observed in the same curve. The wide range of fluid density over 1–4000 bars, resulting from the high compressibility of supercritical water, allows both effects to be observed in water as solvent. It was found also[4a] that the maxima in the curves of isothermal equivalent conductance *vs.* pressure for aqueous sodium chloride shift to higher densities with increasing electrolyte molality. That this behavior is also true for sodium chloride in dioxane–water at 300° can be seen in Figure 2b and c. This effect is presumed to be due to a greater degree of ionic association created by a higher concentration of electrolyte.

Limiting Equivalent Conductances; Rectilinear Dependence on Water Concentration. Considerable association or ion-pair formation by Na^+ and Cl^- is anticipated in these dioxane–water solvent compositions at 300°. This expectation is based on the results of the previous study[4e] at 100° and the fact that at these higher temperatures ion association in general increases as the temperature of an aqueous solution increases. Therefore, it was considered necessary once again to

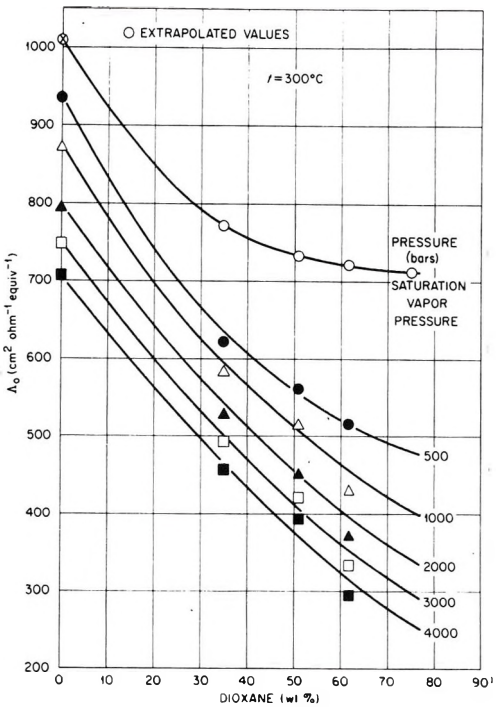

Figure 3. Limiting equivalent conductances of NaCl in dioxane–water solutions as a function of solvent composition and pressure at 300°. (The size of points indicates the estimated uncertainty in each value.)

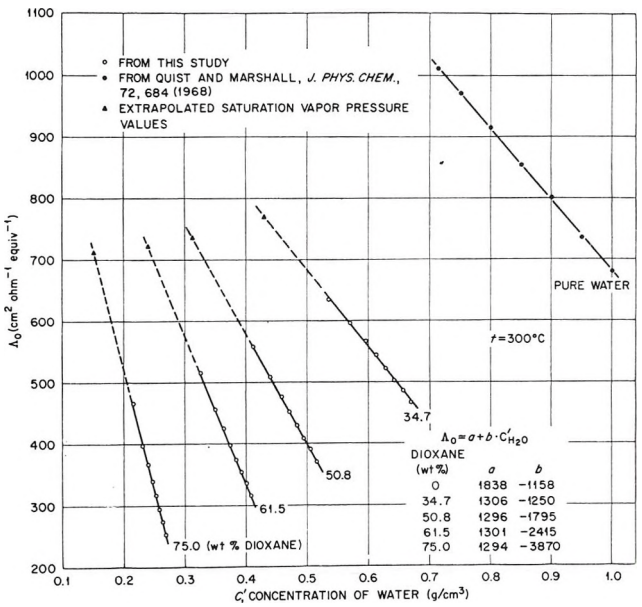

Figure 4. Dependence of the limiting equivalent conductances of NaCl on the concentration of water in several dioxane–water compositions at 300° from saturation vapor pressure to 4000 bars.

adopt a conductance equation which embodies both the limiting equivalent conductance (Λ_0) and the conventional ionization or dissociation constant (K_d) of NaCl to interpret our data. For reasons given in the previous paper,[4e] Shedlovsky's[22] equation was used in the form

$$1/\Lambda S(z) = 1/\Lambda_0 + C\Lambda S(z) f_\pm^2/K_d\Lambda_0^2 \quad (4)$$

where C is the stoichiometric normality and $f_\pm$ is the mean molar activity coefficient of the ions, defined by

$$\log f_\pm = -(\mathrm{DHS})C^{1/2}\Theta^{1/2}/(1 + C^{1/2}\Theta^{1/2}) \quad (5)$$

Here DHS is the Debye–Hückel limiting slope and Θ is the fraction of salt ionized, given by

$$\Theta = S(z)\Lambda/\Lambda_0 \quad (6)$$

$$S(z) \equiv (z/2 + [1 + (z/2)^2]^{1/2})^2 \quad (7)$$

$$z = [8.21 \times 10^5\Lambda_0/(DT)^{3/2} + 82.5/\eta(DT)^{1/2}]C^{1/2}\Lambda^{1/2}/\Lambda_0^{3/2} \quad (8)$$

A computer was used to solve eq 4 simultaneously for Λ_0 and K_d; the average standard errors for Λ_0 and log K_d were approximately 2.5% and 0.06 logarithm (base 10) unit, respectively.

The strong dependence of Λ_0 (NaCl) upon solvent composition at several pressures is evident from Figure 3. (Values for sodium chloride in pure water as solvent are from data given elsewhere.[4a]) There are no data points plotted for 75.0 wt % in this figure because it was not possible to obtain mathematical convergence upon solving simultaneously for Λ_0 and K_d with the experimental Λ values. This difficulty is in part due to the fact that the specific conductances of the most dilute sodium chloride solution (0.001034 m) in 75.0 wt % dioxane (Table II) are so low that the experimental error is relatively high. Also, since 0.001034 m NaCl is our most dilute solution at this solvent composition, its specific conductances unfortunately have the strongest effect upon these particular Λ_0 values. Furthermore, sodium chloride is such a weak electrolyte at this solvent composition that it would be highly desirable to obtain conductance measurements of solutions lower than ~0.001 m for a reliable limiting equivalent conductance; such low reliable measurements were not possible with our present apparatus. Shedlovsky[22] also stated that his conductance equation is applicable in general to associated electrolytes whose ionization constant (K_d) is not less than 10^{-4}. We now know that sodium chloride in 75.0 wt % dioxane has K_d values less than this value below 2500 bars pressure (see Table III), indicating another source of the problem encountered. The limiting equivalent conductances at saturation vapor pressure plotted in Figure 3 are extrapolated values taken from Figure 4.

Table III lists the smoothed limiting equivalent conductances at several pressures which were read from either Figure 3 or similar plots. These values for sodium chloride in dioxane–water at 300° are greater than those at 100° [4e] by a factor of ~2.5 under the same conditions of pressure and solvent composition.

(22) T. Shedlovsky, *J. Franklin Inst.*, **225**, 739 (1938); R. M. Fuoss and T. Shedlovsky, *J. Amer. Chem. Soc.*, **71**, 1496 (1949).

Table III: Limiting Equivalent Conductances and Conventional Ionization Constants for NaCl in Dioxane–Water from Saturation Vapor Pressure to 4000 Bars at 300°

Dioxane, wt %	Pressure, bars: Satn VP[a]	500	1000	1500	2000	2500	3000	3500	4000
	Limiting Equivalent Conductances, cm² ohm⁻¹ equiv⁻¹								
34.7	(771)[b]	634	596	566	544	522	502	486	467
50.8	(736)	557	508	476	451	429	408	391	370
61.5	(722)	515	456	425	397	374	354	336	316
75.0	(712)	(466)	(397)	(367)	(339)	(317)	(294)	(274)	(253)
	Negative Logarithm of Conventional Ionization Constants								
34.7	2.29	1.36	1.07	0.89	0.75	0.51	0.14	0.44	−0.061
50.8	3.31	2.56	2.26	2.05	1.90	1.76	1.61	1.50	1.21
61.5	4.18	3.41	3.07	2.89	2.74	2.63	2.52	2.41	2.27
75.0	5.94	4.93	4.52	4.26	4.11	3.96	3.82	3.68	3.53

[a] See footnote *a*, Table I. [b] See footnote *d*, Table I; also, all values of Λ_0 at 75.0 wt % dioxane are extrapolated values (see text).

Figure 4 shows a plot of the limiting equivalent conductance of sodium chloride *vs.* the concentration of water (grams per cubic centimeter) in the dioxane–water solvent compositions and in pure water as solvent as the pressure is varied at 300°. The concentration of water is defined as the weight per cent of water times the density of the solvent. The rectilinear relationship which results over the density range of 0.15–1.0 g/cm³ for water is consistent with the results obtained previously for sodium chloride in dioxane–water at 100° [4e] and in water from 100 to 800°,[4a] as well as for $KHSO_4$,[23] NaBr,[4b] NaI,[4c] NH_4OH,[5a] and HBr[5b] in water solutions. The systems with dioxane–water, but not water alone, as solvent are noted in Figure 4 to have extrapolated Λ_0 values which are 1299 ± 6 cm² ohm⁻¹ equiv⁻¹ at a water concentration of zero. The line representing values of Λ_0 in water extrapolates to 1838 cm² ohm⁻¹ equiv⁻¹, or about 40% higher than the mean value from the dioxane–water solvents. However, analogous plots for results at 100° [4e] produce a value from water solvent within the range of those from dioxane–water. This difference in behavior at 300° cannot be explained at the present time.

Ionization Constants and Complete Equilibrium Constant of NaCl. Since dioxane is assumed here to be a diluent which is nonsolvating in the presence of water,[24,25] the ionization equilibrium of sodium chloride in dioxane–water may be given by the equations

$$\mathrm{NaCl(aq)} + k\mathrm{H_2O} \overset{K^0}{\rightleftharpoons} \mathrm{Na(aq)^+} + \mathrm{Cl(aq)^-} \quad (9)$$

$$K^0 = K_d/C_{\mathrm{H_2O}}{}^k,\ C(\text{solute}) \longrightarrow 0 \quad (10)$$

$$\log K_d = \log K^0 + k \log C_{\mathrm{H_2O}} \quad (11)$$

where K^0 is the complete equilibrium constant, K_d is the conventional constant, k is the net change in the number of solvating water molecules when one hydrated NaCl ion pair forms hydrated ions, and $C_{\mathrm{H_2O}}$ is the molar concentration of water in the mixed solvent. For application of eq 10 or 11, both solute and solvent species are restricted to thermodynamic reference states of infinite dilution for solute species and of pure substance (or solvent mixture) for the solvent. The activity coefficients are therefore defined to be unity, and units of concentration (moles/liter) are used to express both solute and solvent species in a complete mass action expression represented by K^0. A mathematical derivation of K^0 shows that, unless there is uniquely only a single solvated species for each separate class of solute species, k and K^0 cannot be independent of pressure or of solvent composition (X).[8] Thus, in reality, k and K^0 should be written as $k(P, T, X)$ and $K^0(P, T, X)$ to show these dependencies in addition to the dependency on temperature. Nevertheless, isothermal constancies of k and K^0 have been observed experimentally over wide ranges of pressure and of $C_{\mathrm{H_2O}}$, as shown in previous papers,[2-9] and therefore k and K^0 are considered to be experimental constants in this context.

The negative logarithms to base 10 of the conventional ionization constants (K_d) recorded in Table III were calculated using the smoothed limiting equivalent conductances in the same table by again applying the Shedlovsky equation. A plot of log K_d *vs.* log $C_{\mathrm{H_2O}}$ according to eq 11 is given in Figure 5. This figure shows that the results for sodium chloride in 34.7, 50.8, and 61.5 wt % dioxane adhere well to a straight line, in agreement with behavior described elsewhere,[2-9] but in 75.0 wt % dioxane there is some deviation at pressures above saturation vapor pressure. This deviation is believed to be due to the fact that the conventional ionization constants of sodium chloride in this solvent composition are below the stated limit for the applica-

(23) A. S. Quist and W. L. Marshall, *J. Phys. Chem.*, **70**, 3714 (1966).

(24) T. W. Davis, J. E. Ricci, and C. G. Sauter, *J. Amer. Chem. Soc.*, **61**, 3274 (1939).

(25) A. Fratiello and D. C. Douglass, *J. Chem. Phys.*, **39**, 2017 (1963).

tion of Shedlovsky's conductance equation, as discussed above. The deviation from linearity of the two log K_d values at higher pressures (3000 and 4000 bars) in 34.7 wt % dioxane are indicative of the difficulty in making sufficiently accurate conductance measurements as the equilibrium constant approaches a value of unity. There is no apparent explanation for the log K_d values of sodium chloride in 34.7 and 75.0 wt % dioxane at saturation vapor pressure adhering unusually well to the relationship expressed by eq 11, while the results in 50.8 and 61.5 wt % dioxane for the same condition adhere somewhat poorly. The line drawn in Figure 5 yields a net change in waters of hydration, k, of 10.0 and a log K^0 of -16.0.

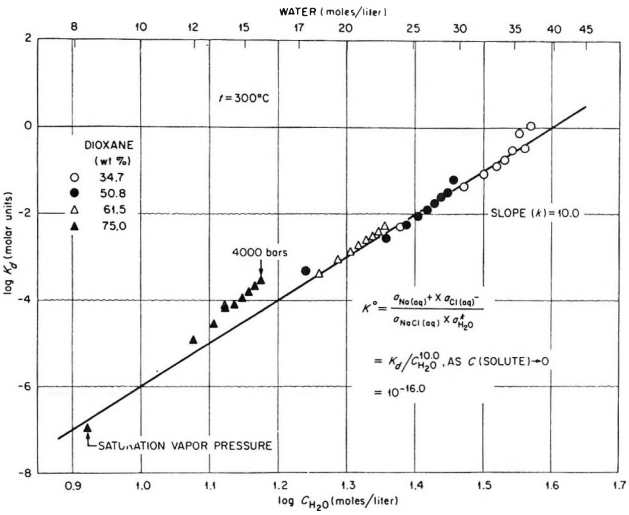

Figure 5. Variations of the logarithm of the conventional ionization constant for NaCl with the logarithm of the molar concentration of water in various dioxane–water solvent compositions at 300° from saturation vapor pressure to 4000 bars. (The size of points indicates the estimated uncertainty in each value.)

Conventional Thermodynamic Functions. The values of k and log K^0 for sodium chloride at 300° are compared in Figure 6 with the corresponding constants in dioxane–water at 25°[2,3,8] and 100°[4d,e] and in pure water over the range of 400–800°.[4a] The smooth change of k with the inverse of the absolute temperature seen here appears to indicate that dioxane is not solvating sodium chloride to any significant degree but is acting as a diluent only. Furthermore, the fact that both k and log K^0 are smooth, continuous functions of $1/T$ as the solvent composition changes from dioxane–water to water at high pressure suggests that k and K^0 values which are obtained for salts in dioxane–water solvents can be applied directly to ionization behavior in water at high pressures, and conversely. Therefore, a knowledge of the pressure–volume–temperature (PVT) relations of water and the curves in Figure 6 can be used to calculate, over wide ranges of temperature and pressure, the

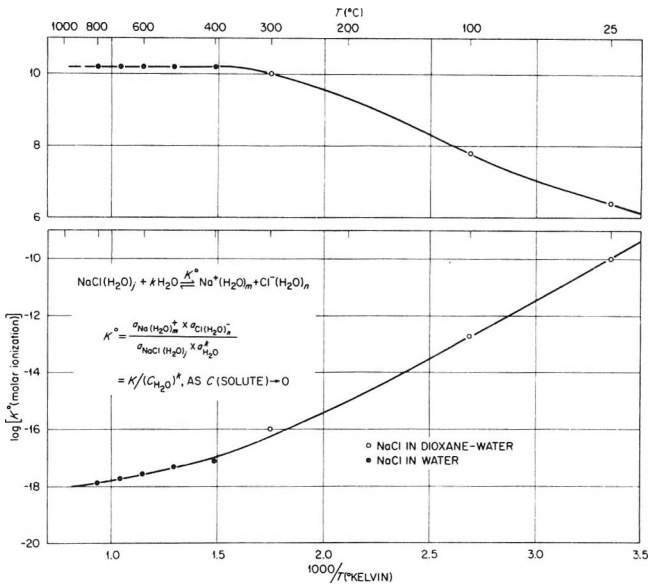

Figure 6. Variation with temperature of the complete molar ionization constant (K^0) and the net change (k) in waters of solvation for sodium chloride in aqueous solutions, 25–800°.

standard enthalpy change[7] (ΔH) for the conventional ionization equilibrium of *aqueous* sodium chloride which excludes the solvent (water) as a reactant

$$\Delta H = -R\left[\frac{\mathrm{d} \ln K^0}{\mathrm{d}(1/T)} + \ln C_{H_2O} \frac{\mathrm{d}k}{\mathrm{d}(1/T)} + k\alpha T^2\right] \quad (12)$$

where α is the coefficient of thermal expansion for pure water. The standard free energy changes for the complete ionization expression (ΔG°) and the conventional ionization expression (ΔG), respectively, can be calculated from the equilibrium constants K^0, in Figure 6, and K_d, determined with the use of eq 10. With the above information and the isothermal compressibilities (β) derived from the PVT properties of water, all additional thermodynamic functions of the conventional ionization equilibrium for sodium chloride at infinite dilution in pure water can in principle be calculated,[7] and the description of these equilibria is considerably simplified.

Effects of Errors in Physical Properties. The effects of errors in the estimated values of density, dielectric constant, and viscosity upon equivalent conductance, limiting equivalent conductance, and, finally, the conventional dissociation constant have been discussed in detail elsewhere.[4e] Therefore, a summary of these effects will simply be given here. Both the equivalent and limiting equivalent conductances of sodium chloride calculated in this paper from specific conductances are inversely proportional to the estimated densities of the solutions. The calculated values of K_d at different pressures in the solvent of lowest weight per cent dioxane (34.7), where the fractions of salt ionized in the solutions are the largest, are particularly sensitive to any errors in density. It can be seen from eq 11 and also from Figure 5 that both k and K^0 will reflect errors

in K_d and in the concentration of water in the solvent calculated from the estimated solvent densities. Errors in the estimated dielectric constants and viscosities can be quite high without changing the limiting equivalent conductance appreciably. For example, a variation in the assigned values of D and η of $\pm 20\%$ created differences of less than 1% and less than 0.5%, respectively, in Λ_0. However, the conventional ionization constant is much more sensitive to changes in these two properties, particularly as K_d approaches unity, which is the case for sodium chloride in 34.7 wt % dioxane at 300°.

Conclusions

Although the four physical properties of the solvent mixtures are estimates, they should prove useful to those needing the properties of dioxane–water solvents at high temperatures and pressures. However, experimental measurements of these properties of dioxane–water under the above conditions are certainly to be encouraged.

The straight-line relationships of limiting equivalent conductance *vs.* concentration of water in the several dioxane–water solvents (Figure 4) support earlier, similar observations for 1:1 electrolytes in water, and in dioxane–water at 100°. An explanation for these straight-line relationships is not immediately apparent.

The interpretation of the conductance curves presented in Figure 2 is consistent with all previously observed conductance behavior of 1:1 electrolytes in the solvent water, and in dioxane–water at 100°. It appears, however, to be almost impossible to observe the complex conductance behavior shown in this figure at lower temperatures either in water or in dioxane–water solvents because of the low compressibilities of these solvents at the lower temperatures.

Finally, this work is believed to represent the first study of electrical conductances and ionization behavior of any electrolyte in a mixed organic–aqueous solvent at a temperature above 100°. The results for sodium chloride in dioxane–water at 300° to high pressures therefore are of interest in themselves and may be of further use to others for evaluating electrolyte theories. These conductance data are used to determine the conventional ionization constants of sodium chloride, which in turn are shown to produce a complete equilibrium constant that is experimentally independent of pressure and solvent composition over the range studied. A mathematical derivation, however, shows that K^0, and k, cannot be absolutely constant.[8]

Structure in Concentrated Solutions of Electrolytes. Field-Dielectric-Gradient Forces and Energies

by Lowell W. Bahe

Department of Chemistry, University of Wisconsin—Milwaukee, Milwaukee, Wisconsin 53201
(Received July 22, 1971)

Publication costs assisted by the University of Wisconsin—Milwaukee

The gradient of dielectric constant near the surface of an ion immersed in water is shown to interact with the electric field generated by another ion in such a way that a repulsive force exists between every pair of ions; this force is proportional to $1/R^4$. The combination of this repulsive force with the classic coulombic force between charged ions leads to a description of uni-univalent ionic solutions in terms of a "loose" face-centered cubic lattice. X-Ray scattering curves are compatible with this structure in solution. Activity coefficient data agree with this model over a very large concentration range, from a lower concentration of at least 0.01 M to concentrations of 3 M or higher for several simple electrolytes in water.

Introduction

Throughout the past 50 years repeated attempts have been made to interpret the properties of solutions of electrolytes in terms of a cube-root law.[1-5] Invoking such a cube-root law usually implied the existence of some kind of structure, commonly referred to as a pseudolattice or statistical lattice. After the publication of Debye and Hückel's classic paper in 1923[6] these

(1) G. C. Ghosh, *J. Chem. Soc.*, **113**, 449, 627, 707, 790 (1918).

(2) N. Bjerrum, *Z. Elektrochem.*, **24**, 321 (1918); *Z. Anorg. Allg. Chem.*, **109**, 275 (1920).

interpretations became less common, although they did appear periodically.

X-Ray data indicate the existence of actual structure in concentrated solutions of electrolytes. Activity coefficient data agree with this structure down to concentrations at least as low as 0.01 M and perhaps even to lower concentrations. An explanation of this behavior can be found in the interactions between the electric fields of the ions and the gradient of dielectric constant near the surface of ions in solution.

Dielectric Constant near an Ion

The fields generated by ions in solution in water will change the dielectric constant of the medium surrounding the ions. The effects of this change in dielectric constant have been considered by various authors. Hückel[7] showed that a linear term in the concentration could be added to the Debye–Hückel limiting law if the decrease of dielectric constant in the medium surrounding the ions were proportional to the concentration of ions. Harned and Owen[8] and Robinson and Stokes[9] both consider the linear term empirical. To understand the properties of concentrated solutions, where the linear term becomes important or even predominant, the source and significance of the linear term need to be specified.

Debye and Pauling[10] showed that a change in dielectric constant near the ion would not change the limiting law. Frank[11] confirmed the conclusion of Debye and Pauling and extended the analysis to an interpretation of activities of electrolytes in terms of association equilibria.

The dielectric constant of the medium near an ion and the change of dielectric constant with distance from the ion do not lend themselves to direct experimental measurement. However, indirect results can give a reasonable semiquantitative picture of behavior. Ritson and Hasted[12] calculated the dielectric constant of water as a function of distance from a point electronic charge, using two different models. Both models led to similar values for the local dielectric constant. The dielectric is saturated up to about 2 Å from the point charge (dielectric constant of perhaps four or five), and then rises rapidly so that beyond a distance of about 4 Å the dielectric constant reaches the ordinary bulk value of water.

A similar conclusion was reached by Padova,[13] who used a function given by Grahame[14] to estimate that the dielectric constant of water changes from a very small value (perhaps 3) at the surface of the ion to the value of the bulk dielectric constant within a distance of about 3 Å from the surface of a singly charged ion. This change results from the saturation of the dielectric under the influence of the very large fields near the surface of the ions.

Owen, Miller, *et al.*,[15] measured the change of dielectric constant of water with pressure. If their equation for the dielectric constant as a function of pressure is extrapolated considerably beyond the maximum pressure used in their experiments, the dielectric constant increases with pressure up to about 7000 bars and then decreases at higher pressure. This very long extrapolation is unfair with the data available, but it does indicate qualitatively that the dielectric constant of water might be expected to decrease under the influence of very large pressures (or correspondingly under the influence of very large electric fields).

We can therefore reach a semiquantitative measure of the change of dielectric constant with distance from an ion. We picture this effect as given in Figure 1 for an ion with a radius of 1.5 Å. The change of dielectric constant in region I results from dielectric saturation. The change in region II results from the compressibility of water with more dipoles being crowded into a unit volume. Region III is that of the normal, static dielectric constant of bulk water. This picture is only semiquantitative, but seems reasonable in view of the experimental data available.

Forces and Energies

In the development below, the following symbolism has been used: $\bar{F}_v$ = volume force vector, $\bar{E}$ = electric field vector, ρ = charge density or depth of gradient sea, $\epsilon_0 = {}^1/_2\pi$, E = electric field, $\bar{\nabla}$ = vector gradient operator, k = dielectric constant or Boltzmann constant, k_0 = dielectric constant at surface of ion, g = mass density, R = distance of ionic separation or distance from an ion, r = radius of ion or unit cell length, V = volume, q_+, q_- = charge subscripted for positive or negative, Z = atomic number, $s = (4\pi/\lambda)\sin\theta$, θ = Bragg angle, and F = force.

The volume force vector acting on a region of space in a dielectric is given by[16]

$$\bar{F}_v = \rho\bar{E} - \frac{\epsilon_0}{2}E^2\bar{\nabla}k + \frac{\epsilon_0}{2}\bar{\nabla}\left(E^2\frac{\mathrm{d}k}{\mathrm{d}g}g\right) \qquad (1)$$

(3) H. S. Frank and P. T. Thompson in "The Structure of Electrolytic Solutions," W. J. Hamer, Ed., Wiley, New York, N. Y., 1959, p 113.

(4) E. Glueckauf in ref 3, p 97.

(5) J. E. Desnoyers and B. E. Conway, *J. Phys. Chem.*, **68**, 2305 (1964).

(6) P. Debye and E. Hückel, *Phys. Z.*, **24**, 185 (1923).

(7) E. Hückel, *ibid.*, **26**, 93 (1925).

(8) H. S. Harned and B. B. Owen, "The Physical Chemistry of Electrolytic Solutions," 3rd ed, Reinhold, Princeton, N. J., 1958, pp 508–509.

(9) R. A. Robinson and R. H. Stokes, "Electrolyte Solutions," 2nd ed (revised), Butterworths, London, 1959, p 231.

(10) P. Debye and L. Pauling, *J. Amer. Chem. Soc.*, **47**, 2129 (1925).

(11) H. S. Frank, *ibid.*, **63**, 1789 (1941).

(12) D. M. Ritson and J. B. Hasted, *J. Chem. Phys.*, **16**, 11 (1948).

(13) J. Padova, *ibid.*, **39**, 1552 (1963).

(14) D. C. Grahame, *ibid.*, **21**, 1054 (1953).

(15) B. B. Owen, R. C. Miller, C. E. Milner, and H. L. Cogan, *J. Phys. Chem.*, **65**, 2065 (1961).

(16) W. K. H. Panofsky and M. Phillips, "Classical Electricity and Magnetism," Addison-Wesley, Reading, Mass., 1955, p 95.

The first term on the right of eq 1 is the standard Coulomb term, the second term is of interest to us, and the third term is the electrostriction term which we shall ignore (ignoring the third term is equivalent to assuming that $dk/dg = 0$, or that the fluid is incompressible).

We use the following model. (1) The ions are incompressible spheres with charge located at the center. (2) The water is a continuous dielectric medium with the properties of liquid water, the most important of which is the dielectric constant behavior given in Figure 1.

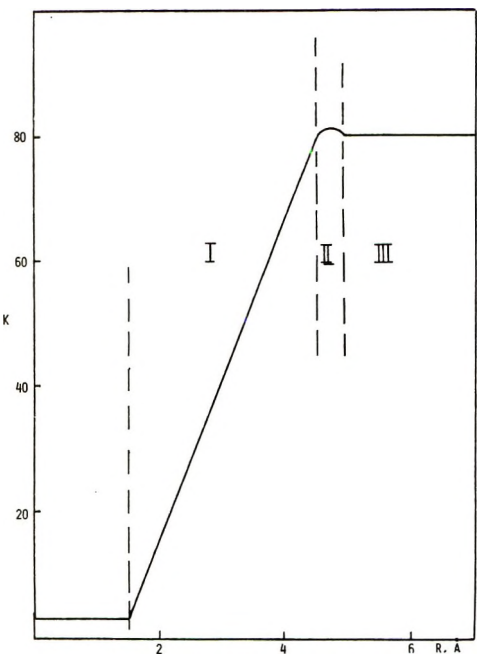

Figure 1. Variation of dielectric constant with distance from the center of the ion with radius 1.5 Å.

Consider a spherical unit positive ion and a spherical unit negative ion of equal size (radius r) immersed in water as a dielectric medium a distance R (center to center) apart. Consider the negative ion (arbitrary choice) as being surrounded by the variation of dielectric constant shown in Figure 1. The field acting on the negative ion is that generated by the positive ion. To find the forces operating on the negative ion, eq 1 must be integrated over the volume. The only part of the volume which contributes to the integral of the first term on the right of eq 1 will be that part containing charge. The only part of the volume which will contribute to the integral of the second term on the right of eq 1 will be that part containing a gradient in the dielectric constant. As shown in Figure 2, the negative ion is a sphere of radius r surrounded by a sea of dielectric gradient of depth ρ (perhaps 3 Å deep, as estimated by Padova[13]) in which the dielectric constant changes from the static bulk value at $(r + \rho)$ to some

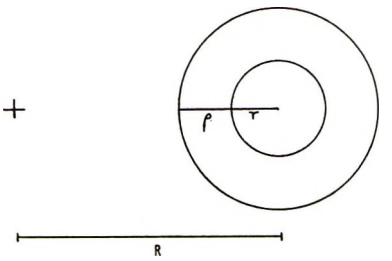

Figure 2. Spherical anion of radius r surrounded by a region of dielectric gradient over the distance ρ.

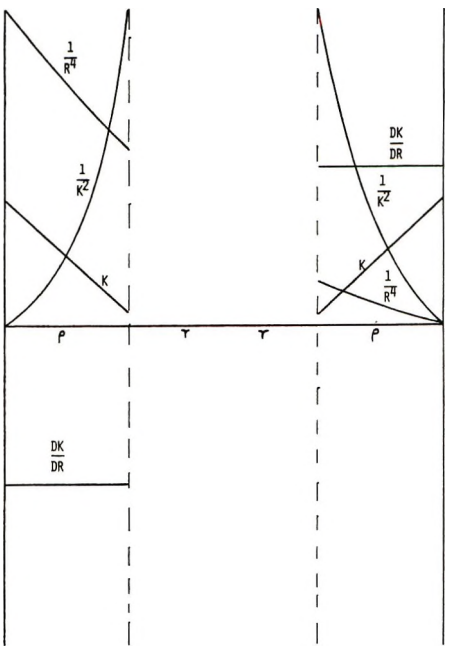

Figure 3. Schematic representation of the parameters near the surface of an ion.

much smaller value (perhaps 3[12]) at r. We assume the slope in dielectric constant to be roughly constant within ρ, as drawn in Figure 1.

The integral of the first term on the right of eq 1 gives the classical Coulomb result shown in eq 2 for point charges. The force is along the line of centers.

$$\int \rho \bar{E} dV = \int \frac{q_+ \rho}{kR^2} dV = \frac{q_+ q_-}{kR^2} \qquad (2)$$

The integral of the second term on the right of eq 1 can be expressed in terms of the significant parameters as shown in

$$\int -\frac{\epsilon_0}{2} E^2 \bar{\nabla} k dV = -\frac{\epsilon_0}{2} q_+^2 \int \frac{1}{k^2 R^4} \frac{\overline{dk}}{dR} dV \qquad (3)$$

In all regions of space except within the "gradient sea," the gradient in the dielectric constant is zero, so we need consider the integration only over the volume of the gradient sea. Let us consider the one-dimensional problem first. The quantities in eq 3 are shown schematically in Figure 3 as they would occur along a line through the centers of the two ions. Each of the

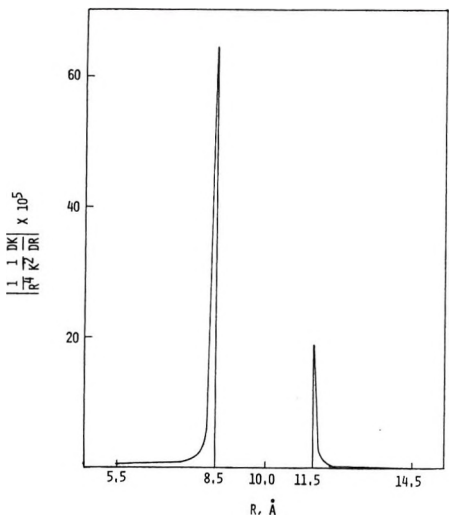

Figure 4. Areas under the curves represent forces acting on an ion in the one-dimensional case.

quantities in the integrand of eq 3 can be estimated as follows: $R = 10$ Å, $r = 1.5$ Å, $\rho = 3$ Å, $k_{bulk} = 93$, $k_0 = 3$, $dk/dR = 30/$Å. Figure 4 shows the estimated absolute value of the integrand of eq 3 plotted against R. For the one-dimensional problem, the areas under the curve represent the integral of eq 3. Because the gradient is negative on the left and positive on the right, the area on the left represents a repulsive force and the area on the right an attractive force. From the relative areas under the curves, it can be seen that the net force on the negative ion under these conditions is repulsive.

The three-dimensional problem is more complex. The model being used here indicates that the roughly half of the sea on the side of the negative ion nearest the positive ion will contribute a positive, repulsive force, while the roughly half of the sea on the side of the negative ion farthest from the positive ion will contribute a smaller attractive force. As shown in Appendix I, the integral in eq 3 gives, at least to a first approximation, the result in eq 4 for the field-dielectric-gradient force

$$\int -\frac{\epsilon_0}{2} E^2 \bar{\nabla} k \mathrm{d}V = \frac{3}{4} \epsilon_0 \frac{q_+^2}{k_0^2} \left| \frac{\mathrm{d}k}{\mathrm{d}R} \right| V_{sea} \frac{1}{R^4} \qquad (4)$$

between the two ions along the line of centers. The total force between the two ions results from the combination of eq 2 and eq 4 to give eq 5. The energy of

$$F = \frac{q_+ q_-}{k} \frac{1}{R^2} + \frac{3}{4} \epsilon_0 \frac{q_+^2}{k_0^2} \left| \frac{\mathrm{d}k}{\mathrm{d}R} \right| V_{sea} \frac{1}{R^4} \qquad (5)$$

the two ions can be obtained by integrating eq 5 from $R = \infty$ (zero point of electric energy) to the final position $R = R$ to give eq 6. As Panofsky and Phillips make

$$\text{energy} = \frac{q_+ q_-}{k} \frac{1}{R} + \frac{\epsilon_0}{4} \frac{q_+^2}{k_0^2} \left| \frac{\mathrm{d}k}{\mathrm{d}R} \right| V_{sea} \frac{1}{R^3} \qquad (6)$$

clear,[17] the energy in eq 6 is the free energy. This will be the Helmholtz free energy, but for ionic solutions will also be essentially the Gibbs free energy.

The model that results from this analysis can be summarized as follows. An ion in solution has two significant features. One of these is the charge itself and the other is the gradient in dielectric constant surrounding that ion and existing only in the immediate vicinity of that ion (Figure 2). Both the charge on the ion and the gradient in dielectric constant associated with that ion will interact with an electric field according to eq 1. When the electric field is generated by another ion, the forces and energies of interaction are given approximately by eq 5 and 6. The dielectric constant of the water between the ions (beyond about 4 or 5 Å from the center of each ion) will retain the bulk dielectric constant of water.[12,13]

From this description of the interaction of ion pairs immersed in the dielectric medium of water, we can proceed to a consideration of many ions immersed in water to form a solution. As equation 5 indicates, each ion pair will feel a coulombic force that drops off as the inverse of R^2 and each ion pair simultaneously will feel a field-dielectric-gradient force that drops off as the inverse of R^4. The coulombic force will be attractive or repulsive depending on whether the two ions have opposite or like signs, and the field-dielectric-gradient force between ion pairs will always be repulsive. Because of the way in which these forces vary with R, the field-dielectric-gradient repulsive force should become important or even predominate when R is small, or therefore when solutions are concentrated.

Structure in Solution

This description of forces resembles the description applied to solid ionic substances[18] and leads to a closer examination of the evidence for ionic structure in concentrated solutions of simple ions in water. In analogy with many solid 1:1 electrolytes, we might look for a face-centered cubic structure in concentrated solutions. The ions near a central ion would assume positions corresponding to those of a face-centered cubic structure, but the regularity of this structure would disappear as the distance from the central ion increased. The X-ray diffraction pattern from this "loose" face-centered cubic structure would not be exactly that expected from a well-defined face-centered cubic (fcc) solid, but would have elements of a dispersion curve of a liquid with the near-neighbor distances corresponding to the near sites in a fcc structure.

Ideally, the Wierl equation[19] should be applied to an infinite array of lattice points, the Wierl equation being modified to take into account a "temperature

(17) W. K. H. Panofsky and M. Phillips in ref 16, p 90.

(18) L. Pauling, "The Nature of the Chemical Bond," 2nd ed, Cornell University Press, Ithaca, N. Y., 1948, p 337 ff.

(19) See, for example, G. M. Barrow, "Physical Chemistry," 2nd ed, McGraw-Hill, New York, N. Y., 1966, p 381.

factor" that would allow for the greater fluctuation of ions (and therefore a decrease of electron density or scattering power) as the distance from the central ion increased. Since the infinite array of lattice points is computationally difficult to handle, we have limited our calculations to the eight unit cells surrounding a central point in a fcc lattice. We have modified the Wierl equation as shown in eq 7 to include an arbitrary

$$I \propto \sum_i \sum_j \frac{Z_i Z_j e^{-a^2 r_{ij}^2} \sin sr_{ij}}{sr_{ij}} \qquad (7)$$

exponential factor which decreases the contribution of a particular term in the Wierl equation as the distance increases. This factor was chosen to resemble that used by Vaughn, Sturdivant, and Pauling[20] to allow for temperature effects. If the salt being considered is chosen from a group which has one ion with a large atomic number (scattering factor) and the counterion a small atomic number, then only the ions with the large atomic number need be considered. For such a system, the 63 significant lattice points in the eight unit cells surrounding a central ion give eq 8,

$$I \propto \frac{2Z^2}{sr}\left[\sum_{n=1}^{13,16-18,24} \frac{a_n}{\sqrt{\frac{n}{2}}} e^{-(n/2)a^2r^2} \sin \sqrt{\frac{n}{2}} sr + \frac{63}{2} sr\right] \qquad (8)$$

which, in combination with the coefficients given in Table I, is a shorthand representation of the results of carrying out the summations of eq 7. The symbol

$$\sum_{n=1}^{13,16-18,24}$$

in eq 8 means that the summation is carried out over the integral values of n from one to 13, from 16 to 18, and the value 24. The 17-term eq 8, without the $(^{63}/_2)sr$ term, was programmed on a Wang 700 programmable desk calculator, and a quantity proportional to I obtained as a function of sr at various values of a^2r^2 (r is the unit cell distance). The results are shown in Figure 5. The curve for $a^2r^2 = 0$ is that which would be obtained for a "molecule" that consisted of eight unit cells of a fcc ionic structure in which the ion with the large scattering factor is the central ion and the ion with the small scattering factor is the counterion; the prominent features of this curve are the maximum at sr slightly greater than 11 with fine structure on both sides of this principal maximum. As a^2r^2 increases in size, the maximum at $sr = 11.15$ decreases in intensity, the curve around the maximum broadens somewhat, and the fine structure on both sides of the maximum washes out. Although the principal maximum decreases in intensity, the value of sr at which this maximum occurs changes negligibly as a^2r^2 increases. As a^2r^2 increases above zero, the curves are approximations to an infinite array of fcc lattice points which has a contribution to the dispersion curve from the points separated by distances up to the order of $2r$ and no contribution for points separated by greater distances.

Table I: Coefficients of Eq 8

n	a_n	n	a_n
1	252	9	156
2	114	10	84
3	324	11	60
4	150	12	60
5	228	13	72
6	68	16	18
7	288	17	24
8	39	18	12
		24	4

Hyman and Vaughn[21] reported the dispersion curves for aqueous solutions of chloroplatinic acid. Thermodynamic data, which will be reported later, indicate that 2:1 and 1:2 electrolytes assume a fluorite structure in solution. The X-ray diffracting anions in chloroplatinic acid can therefore be examined as an fcc lattice with a unit cell length of the corresponding fluorite cell. Hyman and Vaughn report their concentrations in molal units, but their Table I gives the "nearest neighbor distance if close-packed" which allows the determination of the unit cell length at each concentration. The maximum from eq 8 at $(sr)_{max} = 11.15$, when applied to Hyman and Vaughn's data, predicts maxima at the following points: 2.9690 m at $\sin \theta/\lambda = 0.062$, 2.0016 m at $\sin \theta/\lambda = 0.056$, and 1.0035 m at $\sin \theta/\lambda = 0.046$. In Figure 5, the left-hand minimum occurs at $(sr)_{min} = 5.90$ for the curve with $a^2r^2 = 1$. This minimum would occur in Hyman and Vaughn's results at the following points: 2.9690 m at $\sin \theta/\lambda = 0.033$ and 2.0016 m at $\sin \theta/\lambda = 0.030$. Though not resolved, one can see some evidence for what could be minima at these points. Finally, the ratio of the intensity of the maximum to the intensity of what could be a minimum in Hyman and Vaughn's 2.9690 curve can be estimated at near six and the ratio of the intensity of the maximum to the intensity of the minimum in the $a^2r^2 = 1$ curve in Figure 5 is about seven. If one restricts his attention to region A of Hyman and Vaughn's data, the agreement between the data and the predictions of eq 8 is quite good.

Beck[22] has reported X-ray photometric curves for concentrated solutions of LiBr and LiCl. The most concentrated solution of LiBr was 12.3 M. His curve shows a distinct peak at about $2\theta = 21°$. At a

(20) P. A. Vaughn, J. H. Sturdivant, and L. Pauling, *J. Amer. Chem. Soc.*, **72**, 5477 (1950).

(21) A. Hyman and P. A. Vaughn, "Small-Angle Scattering, Proceedings of the Conference Held at Syracuse University, June, 1965," Gordon and Breach, New York, N. Y., 1967, p 477.

(22) J. Beck, *Phys. Z.*, **40**, 474 (1939).

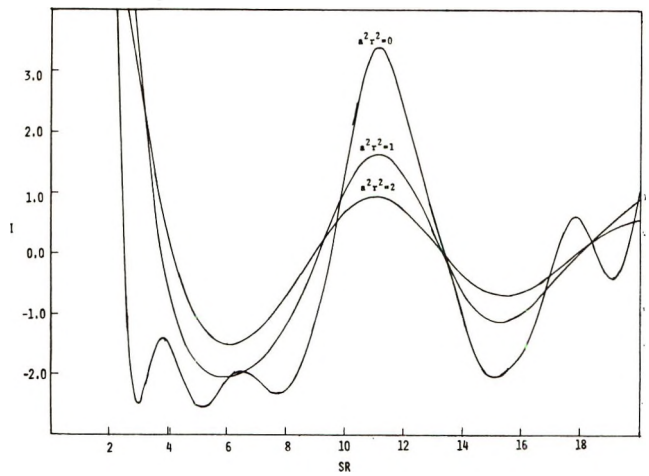

Figure 5. The intensity of scattered X-rays as a function of sr as given by the modified Wierl equation for the eight unit cells around a central point in the fcc system. The three curves show the effect of increasing values of a^2r^2.

concentration of 12.3 M, the unit cell length of an fcc structure would be 8.14 Å. With $(sr)_{max}$ = 11.15, this corresponds to 2θ = 19.4°. The most concentrated solution of LiCl was 13.3 M. Beck's curve shows a less distinct maximum at about 2θ = 19°. At a concentration of 13.3 M, the unit cell length of an fcc structure would be 7.94 Å. With $(sr)_{max}$ = 11.15, this corresponds to 2θ = 19.8°. At lower concentrations, the maximum would be expected to shift to lower angles and to become broader and less intense. With a little imagination, Beck's curves for LiBr and LiCl at lower concentrations (down to perhaps 6 M) in the regions between 2θ = 16° and 2θ = 30° can be interpreted as composed of two broad peaks, the peak from the loose fcc structure superimposed on the water peak at 2θ = 28°. Beck interpreted his curves in terms of peaks corresponding to the results obtained from solid $LiBr \cdot H_2O$ and $LiCl \cdot H_2O$. The agreement between Beck's experimental results and the predictions of eq 8 is satisfactory considering the difficulty of reading the published curves accurately. We are presently attempting a greater resolution of the X-ray dispersion curves from concentrated aqueous solutions of LiBr. We also intend to look for scattering curve evidence at larger angles though the decrease of intensity with angle, the interference from the water structure, and the interference from the intraionic structure of polyatomic ions may make such a search futile.

In both of these cases of X-ray data on solutions of electrolytes in water, the results are compatible with a loose face-centered-cubic structure of the ions in solution.

Harned and Owen[23] note that certain features of partial molar volume behavior can be interpreted in terms of a lattice structure: "If this is the case, the concept of the ionic atmosphere might be replaced by a statistical lattice structure, except at high dilutions."

Free Energy of Salts in Solution

The X-ray evidence indicates that simple 1:1 electrolytes in concentrated aqueous solutions assume a loose fcc structure. Further evidence for structure in solutions can be obtained from activity coefficient data. For perfect structure in solution, eq 6 can be used to find the electrical free energy of the ions by inserting a Madelung constant in the coulombic term and a Madelung-like constant in the second term to give eq 9, where A'' and B'' are those appropriate constants. It should be noted in eq 9 that the partial molar Gibbs

$$\frac{\bar{G}_{elect}}{N} = A''\frac{q_+q_-}{k}\frac{1}{R} + B''\frac{\epsilon_0}{4}\frac{q_+^2}{k_0^2}\left|\frac{dk}{dR}\right| V_{sea}\frac{1}{R^3} \quad (9)$$

free energy was equated directly, which is in contrast to the procedure used by Frank and Thompson[3] and Glueckauf.[4] The total free energy of n_2 moles of electrolyte will be n_2 times the right-hand side of eq 9. The derivative of the total free energy with respect to n_2 must be taken at constant R, since R is an intensive variable in this system, to obtain the partial molar free energy, and this is the result in eq 9.

Since we have let R represent the shortest distance between a cation and an anion in the fcc structure, we can replace $1/R$ by $(2Nc/1000)^{1/3}$, where c is the concentration in moles/liter and N is Avogadro's number, giving

$$\frac{\bar{G}_{elect}}{N} = A''\frac{q_+q_-}{k}\left[\frac{2N}{1000}\right]^{1/3} c^{1/3} + B''\frac{\epsilon_0}{4}\frac{q_+^2}{k_0^2}\left|\frac{dk}{dR}\right| V_{sea}\frac{2N}{1000}c \quad (10)$$

The symbolism and equations of Harned and Owen[24] have been used in the following development. Following the usual assumption that the deviations from ideal behavior result from electrical interactions, the deviations from ideal behavior are related to the stoichiometric mean ionic mole fraction activity coefficient (rational activity coefficient) as given in eq 11. Combining eq 10 and 11 and converting to logarithms to the base 10 gives eq 12 and 13, where A, the coefficient

$$\frac{\bar{G}_{elect}}{N} = \frac{RT}{N}\ln f_\pm^2 \quad (11)$$

$$\frac{\log f_\pm}{N} = A''\frac{q_+q_-}{2(2.3)RTk}\left[\frac{2N}{1000}\right]^{1/3} c^{1/3} + B''\frac{\epsilon_0}{2(2.3)(4)RT}\frac{q_+^2}{k_0^2}\left|\frac{dk}{dR}\right| V_{sea}\frac{2N}{1000}c \quad (12)$$

$$\log f_\pm = -A(c)^{1/3} + Bc \quad (13)$$

of $c^{1/3}$, has the value 0.28894 at 25° in H_2O and B, the

(23) H. S. Harned and B. B. Owen, "The Physical Chemistry of Electrolytic Solutions," 3rd ed, Reinhold, Princeton, N. J., 1958, p 367.

(24) H. S. Harned and B. B. Owen in ref 23, p 10 ff.

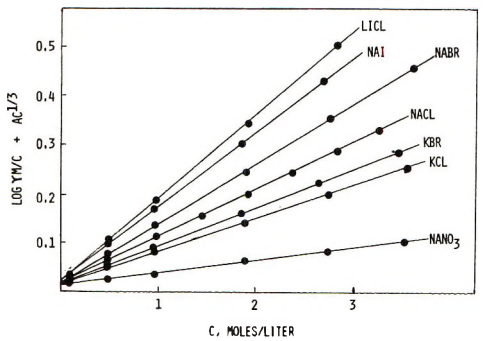

Figure 6. The left-hand side of eq 12 plotted against the molar concentration for several uni-univalent electrolytes at 25°. The data were taken from Harned and Owen.[8]

coefficient of c, can be estimated (as will be done below), but at this point remains an adjustable parameter to be determined from experimental data. Activity coefficients are usually reported in terms of $\gamma_{\pm}$, the mean molal ionic activity coefficient, and m, the molality. Combining eq 13 with the classical relationships among the kinds of activity coefficients gives eq 14. A plot of the left-hand side of eq 14 against c is

$$\log \frac{m\gamma_{\pm}}{c} + A(c)^{1/2} = -\log\left[d + \frac{c(2M_1 - M_2)}{1000}\right] + Bc \quad (14)$$

shown in Figure 6, and very satisfactory straight lines are obtained for several simple electrolytes in water. KI was not drawn in Figure 6, since the line almost superimposes that of NaCl. The slopes, B, and the intercepts, determined by the method of least squares, are shown in Table II. Table II also shows the result for HCl which was obtained from the original data of Harned and Ehlers.[25] A plot of the left-hand side of eq 15, the EMF equation incorporating eq 13 converted

$$\mathcal{E} + \frac{2(2.3)RT}{n\mathfrak{F}} \log c - \frac{2(2.3)RT}{n\mathfrak{F}} A(c)^{1/2} = \mathcal{E}^0 - \frac{2(2.3)RT}{n\mathfrak{F}} Bc \quad (15)$$

for molar units (but ignoring a small log term), is shown in Figure 7 and again gives a satisfactory straight line.

From Table II it can be seen that the values of B range from 0.02 to 0.2. By counting only the ions and distances in the eight unit cells (the same cells used in evaluating the Wierl eq 7) around a central point in an fcc structure, we find that $\Sigma(1/R_i^3) \simeq 18/R^3$, where R is the shortest plus-minus distance so that the constant in the repulsive term (B'' in eq 9) which resembles the Madelung constant has approximately the value of 18. We can estimate the other quantities in the repulsive term of eq 12 as $k_0 = 3$, $r = 1.5$, $\rho/r = 0.1$, and $dk/dR = 30/\text{Å}$. Using these estimates, B has the

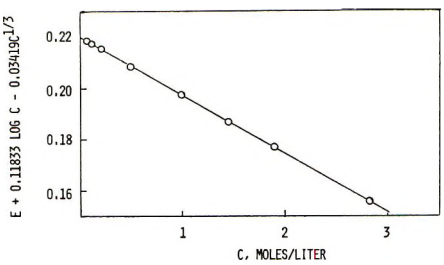

Figure 7. The left-hand side of eq 13 plotted against the molar concentration for the cell Pt, H_2|HCl (m)|AgCl, Ag at 25°. The data were taken from Harned and Ehlers.[25]

Table II: Summary of Results Obtained for B and Intercept from Tabulated Values of Activity Coefficients for Various 1:1 Salts along with the Results from Emf Measurements for HCl

Electrolyte	B	Intercept
HCl	0.1890	
LiCl	0.1713	0.019
NaCl	0.0970	0.017
KCl	0.0680	0.015
NaBr	0.1230	0.016
KBr	0.0785	0.016
NaI	0.1540	0.020
KI	0.0967	0.021
$NaNO_3$	0.0270	0.013

calculated value of 0.065 l./mol which falls within the range of the experimental results.

As indicated by eq 15 and Figure 7, extrapolation using these equations will result in a new value for the E^0 of a cell and therefore will result in a completely new set of values for activity coefficients. It will also, for example, change redox potentials for half cells from those presently in the literature. No attempt has been made in this paper to carry out these adjustments. The significance of these changes is discussed below.

Discussion

The differences between the development in this paper and the Debye–Hückel development will be considered first, and then comparison to other developments will be made. First, the existence of a field-dielectric-gradient force has not been recognized explicitly previously and therefore was not included in the Debye–Hückel treatment. The inclusion of this field-dielectric-gradient force led to an expression for the activity coefficient that included a linear term (eq 12 and 13) which had not been satisfactorily explained previously,[8,9] and which does not follow directly from the Debye–Hückel theory.

Second, though both the Debye–Hückel treatment and the treatment presented here take into account the

(25) H. S. Harned and R. W. Ehlers, *J. Amer. Chem. Soc.*, **55**, 2179 (1933).

coulombic interaction, the results of the analyses lead to different conclusions about the variation of the coulombic interaction with concentration. Whereas the Debye–Hückel treatment finds a variation of the electrical free energy with the square root of concentration, the present treatment finds that the field-dielectric-gradient effect leads to a "loose" face-centered cubic structure and therefore to a variation of the coulombic part of the electrical free energy with the cube root of the concentration.

Third, an advantage of the Debye–Hückel theory is that it includes the effect of temperature on the ionic distribution through the Boltzmann factor, while the temperature effects in the present treatment are accounted for only secondarily through the inclusion of an exponential factor in the modified Wierl equation. However, temperature effects on the fundamental distribution can apparently be disregarded and satisfactory agreement with experimental data obtained. More will be said about this below.

It is surprising that ionic solutions behave as if the fcc structure persisted to the lowest concentrations for which data have been obtained. In 0.01 *M* solutions, the shortest cation–anion distance in the fcc structure is about 43 Å. The linear, field-dielectric-gradient term in eq 13 is 1–3% of the cube-root, coulombic term at this concentration. Though small, the gradient effect still cannot be completely disregarded compared to the coulombic effect until even lower concentrations have been reached. At this distance of 43 Å, the electrical energies should be small, especially compared to kT, and the thermal motions would be expected to predominate. One possible explanation for the observed agreement in spite of the fact that thermal effects would be expected to interfere is the nature of the interactions as given by the development in this paper. It is well known from electrostatics that a spherically symmetrical distribution of charge can be treated as if the charge were located at a point in the center. Though the separation of 43 Å in 0.01 *M* solution is large, any tendency for the ions to close this distance would be accompanied by a rapid increase in the repulsive force between these ions. The statistical average distribution of charge may be spherically symmetrical about the lattice points, which would allow the energy calculation as if perfect structure obtained.

In addition, if we apply eq 6 to the one-dimensional system of two positive charges at a fixed separation with a negative charge assuming all possible points between the fixed positive charges, we find an energy curve which is very flat over most of the distance and very steep near the two cations. The anion, because of the strong repulsive forces as the distance decreases, can approach a cation to only a limited degree. Between these two limits, the energy is almost independent of position of the anion. The energy can be calculated as if the anion were at the center, even though it may "slide around" over a relatively large distance.

In spite of these possibilities, at the ultimate limit of zero concentration, the field-dielectric-gradient repulsion must become insignificant compared to the coulombic effects, and at concentrations very close to zero the Debye-Hückel theory will apply. The question that needs to be answered, then, is: what is the maximum concentration for the validity of the Debye–Hückel limiting law, or what is the minimum concentration above which structure applies? Appeal to experimental results is not conclusive, since experimental data up to concentrations of perhaps 0.1 *M* have been fit to a Debye–Hückel type of equation (though commonly additional terms not directly following from the Debye–Hückel treatment have been added to the limiting term to improve the fit), while the "loose" lattice equations presented in this paper fit down to the lowest concentrations for which data have been reported. The fit extends to much higher concentrations with the present equations, but that does not justify the low end. We have no satisfactory answer to this question at this time.

In view of this dilemma, another question must be considered: what are the consequences of extrapolating data to zero concentration according to the equations in this paper if the equations do not apply below a concentration of the order of perhaps 0.001 *M*? Fortunately, the application of thermodynamics to the experimental data is independent of the method of extrapolation, *i.e.*, the choice of reference function and reference state is arbitrary.[26] However, certain choices are more convenient than others. Extrapolating data to zero concentration according to eq 13 (as has been done in Figure 7) merely establishes the reference state as that state which would exist if structure persisted to infinite dilution. This is no more arbitrary than establishing the reference state as that state which would exist if the Debye–Hückel limiting law were obeyed to infinite dilution. The choice is rather one of convenience. Since the equations developed in this paper are reasonably simple and apply over a considerable concentration range, choosing the reference state as that of the persisting structure (whether or not it actually persists) seems more convenient and therefore the better choice.

Other authors have also considered forces and energies between ions in addition to the classic coulombic interaction. Levine and Rozenthal[27] considered a contribution which would result from the difference between the dielectric constant of the ion complex and

(26) F. T. Wall, "Chemical Thermodynamics," 2nd ed, W. H. Freeman, San Francisco, Calif., 1965, p 372 ff.

(27) S. Levine and D. K. Rozenthal in "Chemical Physics of Ionic Solutions," B. E. Conway and R. G. Barradas, Ed., Wiley, New York, N. Y., 1966, p 119.

the dielectric constant of the surrounding normal water. Their analysis resulted in an interaction energy which included the coulombic energy along with additional terms which could be expressed as a series, the leading term of which showed the energy varying as $1/R^4$. Their equations did not explicitly take into account the effect of the dielectric gradient.

Friedman recognized that the region of dielectric saturation around an ion would make a positive contribution to the free energy of interaction between ions.[28] He also correctly noted that this contribution would be positive whether the interacting ion pair had the same or different signs, as is the case for the field-dielectric-gradient effect used in this paper. Friedman did not develop this model beyond these qualitative considerations, though he did point out that further progress in understanding ionic solutions would depend upon calculating the extracoulombic interactions from a reasonable physical model.

Friedman and Ramanathan[29] have included four terms in their ion–ion pair potential considerations: one is the classical coulombic term, a second is the cavity term[27] (discussed above), a third is a core repulsion term,[18] and a fourth is the Gurney cosphere overlap term.[30] Both the third and fourth terms depend upon a very close approach of ions to each other and would therefore be most important in very concentrated solutions. In such solutions at least these two terms would need to be included. The approximations and model used in developing eq 6 would break down at such short distances and a much more detailed treatment would be required to take into account all of these interactions.

The most significant parts of this paper concern (1) the demonstration that ions in solution in water assume a "loose" lattice structure; (2) the development of equations which give a quantitative measure of the forces and energies of interaction that result from the electrical field generated by an ion acting on the charge and the dielectric gradient associated with another ion; and (3) the development of equations which will simplify and make more convenient the application of thermodynamics to ionic solutions. In addition, though there is presently more hope than demonstrated reality in this statement, a more detailed knowledge of these forces and energies will lead to a greater understanding of the properties of concentrated ionic solutions. In regard to this extension of understanding, we have obtained preliminary results on the heats of dilution and relative partial molar enthalpies of ionic solutions in water that appear very promising.

Acknowledgment. The patience of Glenn Schmieg, with whom many valuable discussions were held, is gratefully acknowledged, as is the assistance of many senior chemistry majors who helped with the calculations.

Appendix

The model we use is drawn in Figure 8. The anion is a sphere of radius r surrounded by a "gradient sea" of depth ρ. The dielectric constant changes from the bulk value, k, at $(\rho + r)$ to the low value, k_0, at r. The rate of change of k with distance within ρ is assumed to be constant; therefore, the gradient, except

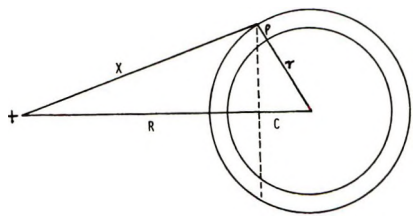

Figure 8. Model for the ion and its gradient sea used for purposes of integration.

for direction, is constant within ρ. The gradient sea is acted on by the field generated by a cation whose center is a distance R from the center of the anion. The integral to be evaluated is

$$\int -\frac{\epsilon_0}{2}E^2\bar{\nabla}k\,\mathrm{d}V = -\frac{\epsilon_0}{2}q_+^2\int\frac{1}{x^4k_0^2}\frac{\overline{\mathrm{d}k}}{\mathrm{d}R}\,\mathrm{d}V \quad \text{(A1)}$$

where the integral must be taken over the volume of the sea. We do this by integrating over the volume of the sphere with radius $(\rho + r)$ and subtracting the integral over the sphere with radius r.

We choose the volume element as the cylinder (dotted line in Figure 8) at $(R - c)$ having the circular base with radius $(r + \rho)\sin\theta$ and height dc. Since $c = (r + \rho)\cos\theta$, the volume element is $\mathrm{d}V = \pi(r + \rho)^2 \sin^2\theta\,\mathrm{d}c = -\pi(r + \rho)^3 \sin^3\theta\,\mathrm{d}\theta$. Applying the law of cosines we find that

$$x^2 = (R^2 + (r + \rho)^2)\left(1 - \frac{2R(r + \rho)\cos\theta}{R^2 + (r + \rho)^2}\right) \quad \text{(A2)}$$

k is assumed to have the constant value k_0. As was seen in the one-dimensional problem above, the volume immediately adjacent to the ion (ρ very small) makes the most significant contribution to the integral and over this short ρ we assume k_0 is constant and has the value at the surface of the ion. Since we are interested in the force along the line of centers, the vector $(\overline{\mathrm{d}k}/\overline{\mathrm{d}R})$ can be written $\mathrm{d}k/\mathrm{d}R\cos\theta$. The integral therefore becomes

(28) H. L. Friedman, "Ionic Solution Theory," Interscience-Wiley, New York, N. Y., 1962, p 121.

(29) H. L. Friedman and P. S. Ramanathan, *J. Phys. Chem.*, 74, 3756 (1970).

(30) R. W. Gurney, "Ionic Processes in Solution," Dover, New York, N. Y., 1953, p 251.

$$\frac{\epsilon_0}{2}\frac{q_+^2}{k_0^2}\left|\frac{dk}{dR}\right|\frac{1}{R^4}\left(\frac{\pi(r+\rho)^3}{\left[1+\left(\frac{r+\rho}{R}\right)^2\right]^2}\int_0^\pi \frac{\cos\theta\sin^3\theta\,d\theta}{(1-b\cos\theta)^2} - \frac{\pi r^3}{\left[1+\left(\frac{r}{R}\right)^2\right]^2}\int_0^\pi \frac{\cos\theta\sin^3\theta\,d\theta}{(1-a\cos\theta)^2}\right) \quad \text{(A3)}$$

where

$$b = \frac{2(r+\rho)}{R^2+(r+\rho)^2}$$

and

$$a = 2r/(R^2+r^2)$$

Both integrals have the same form and can be solved in the general case.

$$\int_0^\pi \frac{\cos\theta\sin^3\theta\,d\theta}{(1-a\cos\theta)^2} = \int_0^\pi \frac{\cos\theta\,(-d\cos\theta)}{(1-a\cos\theta)^2} - \int_0^\pi \frac{\cos^3\theta\,(-d\cos\theta)}{(1-a\cos\theta)^2} \quad \text{(A4)}$$

Integrating by parts, we find that the first integral on the right in eq A4 gives

$$\int_0^\pi \frac{\cos\theta\,(-d\cos\theta)}{(1-a\cos\theta)^2} = \frac{2}{a}\left(\frac{1}{1-a^2}\right) - \frac{2}{a^2}\ln(1+a) + \frac{1}{a^2}\ln(1-a^2) \quad \text{(A5)}$$

which, if $a \ll 1$, can be approximated to -1.

The second integral on the right in eq A4 can be integrated by parts to give

$$\int_0^\pi \frac{\cos^3\theta\,(-d\cos\theta)}{(1-a\cos\theta)^2} = \frac{1}{a^2}\frac{1}{(1-a^2)} - \frac{3}{a^2}\ln\frac{(1+a)}{(1-a)} + \int_0^\pi \frac{6}{a^2}\cos\theta\ln(1-a\cos\theta)\,d\theta \quad \text{(A6)}$$

If we use the approximation that $\ln(1-a\cos\theta) = -a\cos\theta$, we get

$$\int_0^\pi \frac{\cos^3\theta\,(-d\cos\theta)}{(1-a\cos\theta)^2} = \frac{1}{a}\frac{2}{(1-a^2)} - \frac{3}{a^2}\ln\left(\frac{(1+a)^2}{(1-a^2)}\right) + \frac{4}{a} \quad \text{(A7)}$$

which approximates (when $a \ll 1$) to

$$\int_0^\pi \frac{\cos^3\theta\,(-d\cos\theta)}{(1-a\cos\theta)^2} = -3 \quad \text{(A8)}$$

The total integral (A3), therefore, becomes

$$\frac{\epsilon_0}{k_0^2}\left|\frac{dk}{dR}\right|\frac{1}{R^4}\left(\frac{\pi(r+\rho)^3}{\left[1+\left(\frac{r+\rho}{R}\right)^2\right]^2} - \frac{\pi r^3}{\left[1+\left(\frac{r}{R}\right)^2\right]^2}\right) \quad \text{(A9)}$$

When $[(r+\rho)/R]^2 \ll 1$ and $(r/R)^2 \ll 1$, eq A9 gives

$$\frac{\epsilon_0}{k_0^2}\left|\frac{dk}{dR}\right|\frac{1}{R^4}(\pi(r+\rho)^3 - \pi r^3) \quad \text{(A10)}$$

or

$$\frac{\epsilon_0}{k_0^2}\left|\frac{dk}{dR}\right|\frac{1}{R^4}\frac{3}{4}V_{sea} \quad \text{(A11)}$$

Alkali Ion Mobility and Exchange Equilibria in Silica Glass

by D. R. Flinn and K. H. Stern*

Electrochemistry Branch, Naval Research Laboratory, Washington, D. C. 20390 *(Received July 19, 1971)*

Publication costs assisted by the Naval Research Laboratory

The temperature dependence of the Na:K ion mobility ratio in fused silica has been measured using dc conductance techniques over the temperature interval 450–850°. Below 550°, the mobility ratio was time and temperature dependent. Above 550°, the temperature dependence of the steady-state Na:K ion mobility ratio indicated that the activation energy for potassium ion conduction was greater than that for sodium ion conduction by approximately 6 kcal mol^{-1}. Below 550°, this same activation energy difference was noted as the glass was cooled from above 550° over a few-hour time period. However, the steady-state measurements below 550° indicated a greater activation energy for sodium ion conduction than for potassium ion conduction. The difference in activation energy for conduction determined from steady-state measurements compared to that determined from transient temperature measurements is attributed to changes in the glass structure. These structural changes require significant time to attain equilibrium after a change in temperature. Ion-exchange equilibria were measured for potassium–sodium exchange in fused silica from several sodium and potassium molten salt mixtures over a temperature range of 550–815°. The ion-exchange equilibrium constants were shown to be dependent on the temperature and the nature of the melt anion.

Introduction

The use of membrane potential measurements for the determination of ion-exchange equilibria at molten salt–glass interfaces depends on the ability to measure the true ionic mobility ratio in the glass for the cations involved.[1-3] The membrane potential, made up of a boundary potential and a diffusion potential, may be represented by the equation[1]

$$E_M = \frac{RT}{F} \ln \{ [A^+(s)]^{1/n} + k^{1/n}[B^+(s)]^{1/n} \}^n + \text{constant} \quad (1)$$

where $[A^+(s)]$ and $[B^+(s)]$ represent the melt ion activities of the two cations exchanging with the glass, k is the electrode selectivity constant, and n is a constant.

The electrode selectivity constant, k, is given by

$$k = K_{A^+-B^+} \left(\frac{u_{B^+}}{u_{A^+}} \right)^n \quad (2)$$

where $K_{A^+-B^+}$ is the ion-exchange equilibrium constant for the reaction

$$A^+(g) + B^+(s) \rightleftarrows A^+(s) + B^+(g) \quad (3)$$

and u_{B^+}/u_{A^+} is the mobility ratio of the ions in the glass. $A^+(g)$ and $B^+(g)$ represent the ions contained in the glass phase. The equilibrium constant for the reaction given in eq 3 may be expressed in the form

$$K_{A^+-B^+} = ([A^+(s)]/[B^+(s)])(X_B(g)/X_A(g))^n \quad (4a)$$

where $X_i(g)$ denotes the mole fraction of ion i in the glass. The mole fraction term arises from the assumption that the activities of the ions in the glass are proportional to the nth power of the mole fraction of that ion in the glass. This n value, given in eq 1, 2, and 4, is the "thermodynamic factor," $\partial \ln [A^+(g)]/\partial \ln X_A(g)$ used by Doremus.[2]

A complete check of the validity of eq 1–4 requires that membrane potentials, ion mobility ratios, and ion-exchange equilibrium constants be determined independently. Because of the great amount of time required to make such measurements, and since few electrode systems are available for use in making membrane potential measurements, few such studies have been carried out.[1,2] However, good agreement was found between experiment and theory for the cases studied.

Previously reported experimental investigations most frequently measured the dependence of the membrane potential on the activities of the melt cations exchanging at the membrane surface. Then, either the ion mobility ratio[4] or the ion exchange equilibrium constant[5] is measured independently, and the remaining term obtained through the use of eq 2.

Although the ion-exchange equilibrium constant is independent of cationic activities in the melt, it does vary with the melt anion.[4,6,7] This relationship is most readily apparent when one considers that ΔG° for eq 3 contains a contribution $\Delta G_f^\circ(AX) - \Delta G_f^\circ(BX)$, which depends on the nature of the anion X. For this reason, the Na^+–K^+ ion exchange from several melts having

(1) G. Eisenman in "Glass Electrodes for Hydrogen and Other Cations," G. Eisenman, Ed., Marcel Dekker, New York, N. Y., 1966, Chapter 5.

(2) R. H. Doremus, *J. Phys. Chem.*, **72**, 2877 (1968).

(3) R. H. Doremus in ref 1, Chapter 4.

(4) K. H. Stern, *J. Phys. Chem.*, **74**, 1323 (1970).

(5) H. M. Garfinkel, *ibid.*, **73**, 1766 (1969).

(6) Y.-F. Y. Yao and J. T. Kummer, *J. Inorg. Nucl. Chem.*, **29**, 2453 (1967).

(7) G. Eisenman, *Biophys. J.*, **2** (2), 259 (1962).

different anions was studied. In order to calculate the temperature dependence of the electrode selectivity constant k, the ion mobility ratio and $K_{A^+-B^+}$ were determined over a range of temperatures. Using different sodium and potassium salts enabled us to cover a sufficiently wide range. Apparent discrepancies in the temperature dependence of the Na:K ion mobility ratio, reported for a borosilicate glass by a single investigator,[8,9] indicated that this measurement might be very sensitive to some unrecognized factors. For this reason the effect of temperature on the Na:K ion mobility ratio in fused silica was studied in detail.

In this work we have determined the Na:K ion mobility ratio in fused silica by measuring the electrical dc conductance of the glass when it contained exclusively one or the other of the cations of interest. The conductance determined for each of the cations was then used to determine the composition of the glass when mixtures of the two ions were present by use of the relation[2,8,10]

$$\sigma_t = X_A(g)\sigma_A + X_B(g)\sigma_B \quad (5)$$

where σ_t is the observed conductance $(1/R)$ when ions A and B are both present, σ_A and σ_B are the conductances observed when either ion A or ion B is the only cation present in the glass, and $X_A(g)$ and $X_B(g)$ are the mole fractions of the two ions when both are present in the glass. It is assumed that $X_A(g) + X_B(g) = 1$ and that the self-mobilities of ions A and B are independent of mole fraction.[8] The composition of the glass was determined from eq 5 for a series of melt ion activities. This equation has been shown to be applicable to sodium–silver exchange between fused silica and molten nitrate mixtures.[2] Equation 4a is used to calculate the ion-exchange equilibrium constant by rewriting it in the form

$$\log K_{A^+-B^+} = \log \frac{[A^+(s)]}{[B^+(s)]} + n \log \frac{X_B(g)}{X_A(g)} \quad (4b)$$

A plot of the logarithm of the melt ion activity ratio against the logarithm of the ion mole fraction in the glass yields the n value from the slope and the K value from the intercept.

The activation energy for conduction was determined from the temperature dependence of the conductance. The electrical conductivity of a system in which the current is carried by only a single ion is given by[10,11]

$$\sigma = z^2F^2Dc/RTf \quad (6)$$

where z is the ionic charge, D is the diffusion coefficient, c is the concentration of the ion species in the glass, F is the faraday, R is the gas constant, T is the temperature, and f is a correlation factor.

In a defect mechanism the diffusion coefficient may be expressed in the form[10,11]

$$D = N\nu \exp(\Delta S^{\ddagger}/R) \exp(-\Delta H^{\ddagger}/RT) \quad (7)$$

where $\Delta S^{\ddagger}$ and $\Delta H^{\ddagger}$ are the entropy and heat of activation for conduction, N is the defect concentration, and ν is the vibrational frequency of the diffusing ion. Equations 6 and 7 may then be combined to yield

$$\sigma = \frac{z^2F^2c}{RTf} N\nu \exp(\Delta S^{\ddagger}/R) \exp(-\Delta H^{\ddagger}/RT) \quad (8)$$

It is assumed that $\Delta S^{\ddagger}$, N, ν, and c are approximately temperature independent. The enthalpy of activation for conduction is then obtained from the slope of the log σT *vs.* $1/T$ relationship.[12]

The conductance–temperature data may also be fitted to an empirical Arrhenius-type equation of the form[13]

$$\sigma = A \exp(-E_a/RT) \quad (9)$$

where A is a constant. No particular relationship between ion conduction and diffusion is implied by this equation. As will be shown, the data obtained in this work fit eq 8 and 9 about equally well.

Experimental Methods

U-shaped cells were made from 13-mm o.d. General Electric 204 fused silica tubing. The cell arms were separated by a fused silica membrane of approximately 1-mm thickness. Subsequent examination of these membranes after use showed them to be of rather uniform thickness over a 9-mm diameter, with rapidly increasing thickness at the cell walls. Since the exact dimensions of the active membrane were unknown, the resistance and conductance data reported in this paper are the actually measured values, *i.e.*, $\sigma = 1/R$, where R was determined from the slope of the I–E plots.

Each cell was suspended in air from a transite block in a furnace controlled to within ±2°. The membrane temperature was monitored by a thermocouple placed in a well fused to the cell adjacent to the membrane. For measurements at temperatures below 600°, the cell was shielded from ac pickup by a grounded silver cylinder between the furnace and cell.

Known weights of reagent grade salts were placed in each arm of the cell. Electrodes of 20–30-mil platinum wire were placed in each arm of the cell. A potential was applied between the Pt electrodes to introduce either sodium or potassium ions into the glass, and the current was monitored to determine when a steady-state resistance was reached. Standard floating power supplies with up to 320-V output capability were used

(8) H. M. Garfinkel, *Phys. Chem. Glasses*, **11**, 151 (1970).
(9) H. M. Garfinkel, *J. Phys. Chem.*, **74**, 1764 (1970).
(10) R. H. Doremus, *ibid.*, **68**, 2212 (1964).
(11) R. H. Doremus in "Modern Aspects of the Vitreous State," Vol. II, J. D. Mackenzie, Ed., Butterworths, London, 1962, p 1.
(12) R. J. Charles, *J. Appl. Phys.*, **32**, 1115 (1961).
(13) E. Rasch and F. W. Hinrichsen, *Z. Elektrochem.*, **14**, 6 (1908).

for applying the potential across the cell. A Keithley 150B microvolt ammeter was used for most current measurements. This ammeter proved very satisfactory for use in current measurements because of its low input impedance, low leakage to ground, and complete isolation from ground when used in the battery mode. The current was monitored on a Rustrak Model A galvanometer recorder driven through the 150B ammeter output. Applied potentials were measured on standard voltmeters. All instruments were calibrated by the NRL instrument repair facility prior to use, so that all meter readings were accurate to at least $\pm 2\%$.

All salts were reagent grade and were vacuum dried at about 200° overnight before use. Although most cells were open to the atmosphere, one cell containing sodium and potassium nitrates was run under a steady flow of dry helium to displace the air over the molten salts in the cell. No difference was noted in this cell compared to the other cells containing the same melt.

In two consecutive cases the potassium nitrate salt was apparently contaminated with some material which rendered the membrane surface in contact with this melt virtually nonconductive with respect to passage of potassium or sodium ions into the membrane. Conduction of cations from the other side through the membrane was unaffected. Although no impurity was discovered in the salt by emission spectrographic analysis, the salt was triply recrystallized from water and subsequently did not show this behavior. No other salt was found to give this effect.

Results and Discussion

(*A*) *Conductance Studies.* At temperatures above approximately 750°, the conductance of fused silica was found to be sufficiently high so that irreversible changes could be produced in the glass with current densities exceeding about 30 μA cm^{-2}. Figure 1 illustrates the phenomena observed in one case for a sodium-containing membrane at 805°. The electrolysis current for given applied voltages followed the lower line and was time independent at currents below 30 μA, while the points at higher currents were very time dependent. The time-dependent points along the lower current–potential line were obtained up to an applied potential of 10 V, pausing only long enough at each potential to read the current. While a potential of 10 V was applied to the cell for 1.5 hr, the observed current slowly rose to 262 μA. The potential was then lowered, again pausing at each potential just long enough to read the current, and the current followed the upper line. Even after several days at open circuit, the membrane resistance increased to only about 90% of the original value. In another instance after a membrane was subjected to a high current overnight at 800° the activation energy for sodium ion conduction was found to be only 14.6 kcal mol^{-1}, a value much below that which was normally observed for sodium conduction. Even though

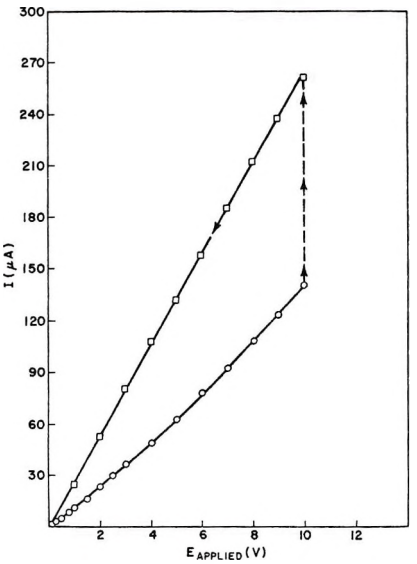

Figure 1. Example of irreversible resistance change caused by excessive current for fused silica which contains sodium ion; $t = 805°$.

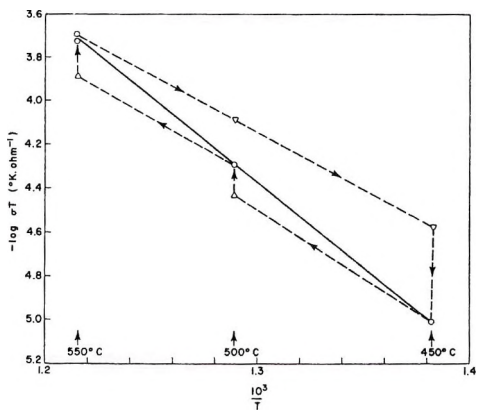

Figure 2. Temperature dependence of the conductance for sodium ion in fused silica observed for a typical membrane; cycle begun at upper right: (▽) cooling, (△) heating, (○) steady state.

no similar effect was noted at the lower temperatures, electrolysis currents were always kept below 10–15 μA cm^{-2} for all further experiments.

The temperature dependence of the conductance for sodium and potassium containing membranes was first examined over the temperature interval of 450–550°. The solid line in Figure 2 shows the long-term steady-state conductance values for sodium ion observed in a typical cell. With only sodium ions in the glass, a steady current for a constant applied potential (steady-state conductance) was established at 550°. The glass was then cooled over a period of about 6 hr to 450°, during which time the two points on the upper dashed line were determined. The temperature was maintained at 450° and the current was monitored until a steady current was observed for a constant applied potential. At 450° a period of about 4 days was

required before a steady current (conductance) was established. The membrane was then heated to 500° over a period of about 4 hr. The conductance rose from the point shown on the lower dashed line to the steady-state value within 12 hr. The membrane was then heated to 550°. At this temperature the conductance rose to the steady value along the solid line within a few hours. The steady-state conductance values were reproducible within a few per cent. Although the transient conductances over this temperature interval were not particularly reproducible, the general form of the response of the conductance to transient temperature changes was always of the form shown in Figure 2. The possibility of a polarization contribution to the measured conductance was eliminated by determining the steady-state conductance at each temperature for at least two constant applied potentials differing by a factor of two or more. The conductance was always independent of potential within experimental error.

The activation enthalpy given by the solid line in Figure 2 for sodium ion conduction in the steady-state case is 35 kcal mol^{-1}. Over the temperature interval 130–280°, Doremus[14] found an activation energy, E_c, of 35 kcal mol^{-1} for sodium ion conduction in fused silica. The dashed lines in Figure 2 show that the apparent activation energy for sodium ion conduction is time dependent, being much greater in the steady state than in the transient case. We postulate that these transient activation energies are more characteristic of sodium ion conduction in (nearly) the same glass structure, whereas the steady-state activation energies include a contribution from glass structures which are different at each steady-state temperature. Given sufficient time at any temperature, the glass "accommodates" itself to ion transport at that temperature so that the silicate network relaxes around the ion.

Douglas[15] has shown that, although normal thermal expansion of fused silica occurs rapidly, a distinctive time-dependent density effect is observable. Such a long-time effect may influence the ionic conductivity mechanism. As seen in Figure 2, the activation energy for sodium ion conduction as determined from the slope of any one of the rapid cooling or heating lines is much less than the steady-state value, even though it varies slightly with the rate at which the temperature is changed. If the activation energy is indeed approximately a constant, then assuming that N, ν, f, and c are not time and/or temperature dependent, the entropy as defined in eq 8 must be less in the steady-state glass than in the newly cooled glass at 450°. Charles[16] found the opposite result from his diffusion measurements for a complex lime glass.

The difference between the steady-state and transient conductance values for sodium ion conduction decreased with increasing temperature. For example, 1 day was required to attain a steady conductance at 500°, while above 550° no difference was found in the transient and the steady-state conductances.

In order to attain a steady-state current at temperatures above 550° during replacement of sodium ion in the glass with potassium ion by electrolysis, it was necessary to electrolyze about twice the amount of charge through the glass as had been anticipated from the previously determined mobile cation impurity concentration in this glass.[17] However, when sodium ion was electrolyzed into a membrane which initially contained only potassium ion, the passage of approximately ten times the amount of anticipated charge was required in order to attain a steady current. It is likely that since the sodium ion is much more mobile in the membrane this ion overtakes and becomes mixed with the slower potassium ions during this replacement. In the case of replacement of sodium ion by the potassium ion, the ions apparently do not mix, so that the potassium ion moves into the membrane in a rather well defined layer. An analysis of this case was carried out by Doremus.[14]

After potassium ions replaced the sodium ions in the silica, an E_c value of 30 kcal mol^{-1} ($\Delta H^{\pm}$ = 32 kcal/mol) for the conduction process was found over the 450–550° interval. This E_c value is identical with that found by Doremus[14] at slightly lower temperatures. In contrast to the sodium case, this activation energy was found to be only very slightly time dependent.

The temperature dependence of the conductance for a series of sodium-containing or potassium-containing membranes was measured and log σ *vs.* $1/T$ and log σ T *vs.* $1/T$ plots were prepared which gave good straight lines, with no evidence of curvature over the temperature ranges investigated. The data were then computer fitted to the linear relationships of eq 8 and 9 by the method of least squares. A comparison of the E_c and $\Delta H^{\pm}$ activation energies of these membranes is shown in Table I. The variance is given in all cases except for the data from Figure 2. Since the exact dimensions of the membrane were not known, the conductance rather than the specific conductivity was determined, so that the preexponential A term of eq 9 and the similar grouping of constants of eq 8 are not included in the table. The heat of activation values ($\Delta H^{\pm}$) were consistently larger by about 2 kcal mol^{-1} than the corresponding E_c values. The variance in $\Delta H^{\pm}$ and in E_c was identical for each set of data, consequently eq 8 and 9 both describe the conduction process equally well.

For both sodium ion and potassium ion the activation energies for conduction decrease with increasing temperature. Frischat[18] observed the same trend for

(14) R. H. Doremus, *Phys. Chem. Glasses*, **10**, 28 (1969).

(15) R. W. Douglas and J. O. Isard, *J. Soc. Glass Technol.*, **35**, 206 (1951).

(16) R. J. Charles, *J. Amer. Ceram. Soc.*, **45**, 105 (1962).

(17) K. H. Stern, *J. Phys. Chem.*, **72**, 2256 (1968).

(18) H. Frischat, *J. Amer. Ceram. Soc.*, **51**, 528 (1968).

Table I: Temperature Dependence of Conductance

Conducting ion	Temp interval, °C	E_a,[c] kcal mol^{-1}	$\Delta H^{\pm}$,[d] kcal mol^{-1}
Na^+ [a]	450–550	32	35
Na^+ [b]	450–550	24–27	26–28
Na^+	500–620	26.8 ± 0.7	28.4 ± 0.7
Na^+	745–861	21.5 ± 0.2	23.6 ± 0.2
K^+	510–620	29.5 ± 0.3	31.2 ± 0.3
K^+	838–914	24.9 ± 1.2	27.2 ± 1.2

[a] Figure 2, steady state. [b] Figure 2, transient. [c] Activation energy for conduction from eq 9. [d] Enthalpy for conduction from eq 8.

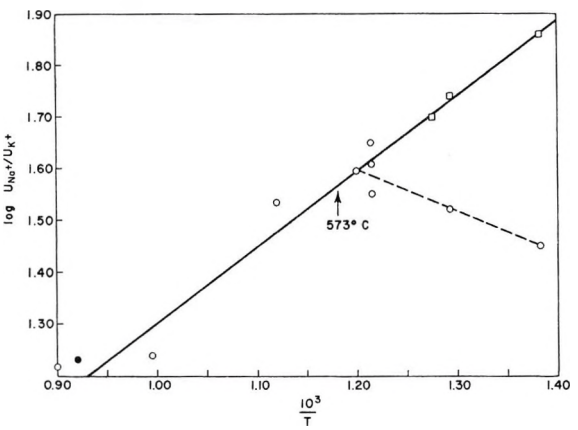

Figure 3. Temperature dependence of the Na:K ion mobility ratio for fused silica containing these ions: (○) steady-state values, (□) transient values, (●) steady-state values for Vycor reported by Stern, ref 19, (---) steady-state values for temperatures below 550°. Arrow indicates α–β quartz transition temperature.

the temperature dependence of sodium ion diffusion in fused silica.

A factor which may be directly compared for all of the cells examined is the mobility ratio, since absolute membrane dimensions are then unimportant. The temperature dependence of the Na:K ion mobility ratio for six different cells is shown in Figure 3. The solid point was obtained from data on Vycor reported earlier by Stern,[19] which will be more fully discussed later. The data on the portion of the solid line below 550° were obtained under rapid (less than 8 hr) cooling, while the points on the dashed line are the final steady-state values. Above 550° the points along the solid line are steady-state points. The points along the solid line indicate a constant difference in the activation energies for conduction of 6.03 ± 0.30 kcal mol^{-1}, with the potassium ion having the greater activation energy. Thus the potassium ion mobility approaches the sodium ion mobility as the temperature is increased. The limiting high-temperature intercept ($T \rightarrow \infty$) of the mobility ratio from the least-squares determination is near unity (1.1 ± 0.2). An analysis of this fact in terms of the model proposed by eq 8 suggests that ν and $\Delta S^{\pm}$ are very similar over this temperature range for the sodium- and the potassium-containing glasses. In the steady-state case below 550°, the apparent activation energy for conduction for sodium ion is greater than that for potassium ion by about 4.6 kcal mol^{-1}. This time and temperature dependence of the mobility ratio below 550° has important consequences with respect to possible errors in the true long-time equilibrium parameters when such parameters are measured using short-time techniques.

Our conductance results may be compared with those found by Doremus.[14] He determined the dc conductance of fused silica containing only sodium, lithium, or potassium ions at temperatures below 500°. He found that the activation energy for sodium ion conduction was greater than that for potassium ion conduction over the temperature interval studied. The activation energy for potassium ion conduction was found to be independent of temperature. However, above 300°, the activation energy for sodium ion conduction was found to decrease with increasing temperature so that at higher temperatures the Na:K ion mobility ratio would be expected to decrease with increasing temperature, in the direction found in the present investigation.

Garfinkel[8] studied the diffusion of potassium and sodium ions into a borosilicate glass and found that the mobility ratio decreased with increasing temperature. In an earlier paper by Garfinkel,[9] just the opposite temperature dependence was reported. However, ref 9 contains an error in eq 2 which renders eq 4, 7, and 8 of ref 9 unusable, so that the mobility ratios shown in Figure 2 of ref 9 are not correct. From the present study, the ion mobility results given in ref 8 have the expected temperature dependence.

It is recognized that the two mobility ratio–temperature lines shown in Figure 3 meet in the area of 560°, near the 573° α–β quartz transition point. Frischat[18] observed a less definite discontinuity at this temperature in his sodium diffusion experiments in fused silica (Infrasil), which he attributed to "quartz-like" precrystalline elements in the SiO_2 glass structure. Owen and Douglas[20] observed a sharp discontinuity in this temperature region for their measurements of the relaxation of the dielectric constant of Thermal Syndicate OS synthetic fused silica which contained a significant amount of bound water. In the present work the glass membranes were examined under a microscope after use. Although some slight surface devitrification occurred, the membrane bulk was still quite strong and clear, with no indication of devitrification.

The results of the mobility study were utilized in the determination of ion exchange equilibrium constants for

(19) K. H. Stern, *J. Electrochem. Soc.*, **112**, 208 (1965).

(20) A. E. Owen and R. W. Douglas, *J. Soc. Glass Technol.*, **43**, 159T (1959).

sodium and potassium ions on fused silica from nitrate, bromide, and chloride melts.

(*B*) *Ion-Exchange Equilibria.* With pure sodium salt on one side of the membrane and a pure potassium salt on the other side, the mobility ratio for the two ions was first measured as before. Mixtures of the potassium and sodium salts were then prepared on each side of the cell by the addition of weighed amounts of the required salt. The steady-state resistance was determined for each addition. The steady-state resistance (conductance) for each known melt mixture and the conductance of the membrane containing only one kind of ion were then used in eq 5 to determine the mole fraction of each ion present in the glass at each melt composition. The melt ion activities were determined from the thermodynamic data given by Lumsden.[21] These activity and mole fraction data were then plotted for each cell in the form given by eq 4b. Figure 4 shows such a log–log plot for a series of $NaNO_3$–KNO_3 mixtures at 550°. The line for the upper set of points was drawn using all points except those for cells 13 and 15. Cells 1, 7, 8, 9, and 11 were new cells. Cell 9 was reused for two more runs following treatment after each run with 10% aqueous HF solution for 4–5 hr at room temperature to remove surface devitrified layers. The results of these runs are shown on Figure 4 as cells 13 and 15. Cell 1, which was made by the glassblower at the same time as several of the other cells used, is seen to have an entirely different response compared to the other cells, exhibiting a much greater preference for sodium ion over potassium ion. Unfortunately, in studying cell number 1 only sodium nitrate was added to the potassium nitrate side, so that asymmetry effects across the membrane were not studied. Mixtures of these salts were studied for both membrane surfaces for most of the other cells. For the individual cells (excluding cell 1) the minimum n value was 1.21 with a corresponding $K_{K^+-Na^+}$ of 0.91 for cell 11, while the maximum n value was 1.7 with a corresponding $K_{K^+-Na^+}$ of 0.32 for cell 15. Since the mobility ratio is 41 at 550°, the electrode selectivity constant for Na^+–K^+ exchange favors sodium in all cases studied. The value of the electrode selectivity constant determined from the upper solid line of Figure 4 is $k = 111$.

Real variations in mobility ratios, n, and in absolute conductances for the individual ions could all be responsible for the rather large scatter of the data shown in Figure 4. The results of the series of points obtained with the same original cell, cells 9, 13, and 15, indicate that aging (temperature cycling) affects the selectivity, so that the n value increases and the preference for potassium increases ($K_{K^+-Na^+}$ decreases).

As individual conductance values were determined from different sides of the membrane in order to determine the ion mobility ratio, we considered the possibility of somewhat different ionic-transfer characteristics from the two sides of the membrane. However,

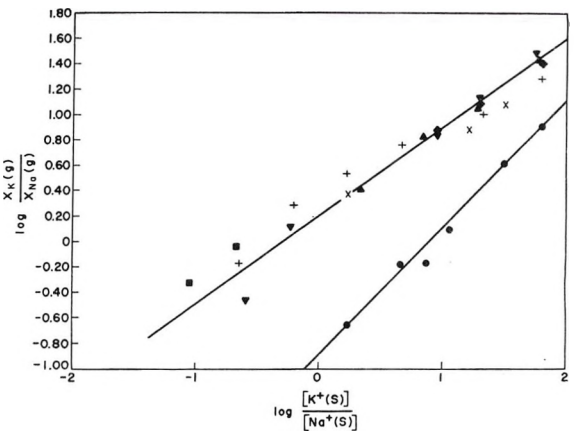

Figure 4. Dependence of the log K:Na ion mole fraction ratio in silica on the log K:Na ion melt activity ratio for $NaNO_3$–KNO_3 mixtures at 550°; individual cells studied are given the following symbols: (●) 1, (▲) 7, (■) 8, (◆) 9, (▼) 11, (×) 13, (+) 15.

a cell was run using a mixture of KNO_3 + 0.4 mol fraction of $NaNO_3$ in both sides of the cell. Continued electrolysis from one side and then the other revealed only a few per cent difference in the measured resistivities.

Although the majority of data was collected on ion exchange from nitrate-containing melts, two other melt systems were examined. In Figure 5 the determination of n and K for NaCl–KCl mixtures was made in the same manner as in Figure 4. Using the $n = 0.97$ and $K = 0.89$ values determined from Figure 5 and the mobility ratio of 15 from Figure 3 gives a k value of 12.3 at 815°.

Ion-exchange equilibria were also examined in NaBr–KBr mixtures. The results of the two cells studied were very different. Cell 6, examined at 747°, gave $n = 0.99$, $K_{K^+-Na^+} = 9.26$, while at 805° cell 10 yielded $n = 1.26$, $K_{K^+-Na^+} = 0.58$. Thus, cell 6 had properties similar to those of cell 1, while cell 10 seems to have properties more in line with most of the remaining cells. As all cells studied were made by the same glassblower under as equivalent conditions as possible, the reason for the high sodium preference for cells 1 and 6 is not known.

The results of the NaCl–KCl exchange may be compared to results obtained earlier by Stern,[19] where Vycor was used as the exchanger in this melt mixture at 814 and 890°. Stern[19] measured the resistance of Vycor membranes as a function of temperature and melt composition after allowing the membrane to come to ion exchange equilibrium with the melt by diffusion, with no electrolysis through the membrane. Assuming the validity of our eq 5, the $X_{Na}(g)$ and $X_K(g)$ values were determined from the data contained in Figures 1, 2, and 4 of ref 19. These data are plotted in Figure 6.

(21) J. Lumsden, "Thermodynamics of Molten Salt Mixtures," Academic Press, London, 1966.

Table II: Comparison of Ion-Exchange Equilibria Constants

Cell	Salt mixture	Temp, °C	n	$K_{K^+-Na^+}$	k
1[a]	$NaNO_3$–KNO_3	550	0.99 ± 0.06	8.14 ± 0.40	323
7–9, 11[a]	$NaNO_3$–KNO_3	550	1.47 ± 0.07	0.470 ± 0.072	111
2[b]	NaCl–KCl	815	0.965 ± 0.024	0.894 ± 0.058	12.3
6	NaBr–KBr	747	0.994 ± 0.012	9.26 ± 0.12	170
10	NaBr–KBr	805	1.26 ± 0.04	0.579 ± 0.049	19.0
Stern[c]	NaCl–KCl (Vycor)	814	0.958 ± 0.019	0.511 ± 0.022	7.30
Stern[c]	NaCl–KCl (Vycor)	890	1.015 ± 0.017	0.447 ± 0.017	5.62
Stern[d]	NaCl–KCl	560–585	1–1.2	0.52	71

[a] Figure 4. [b] Figure 5. [c] Figure 6. [d] Stern, ref 4.

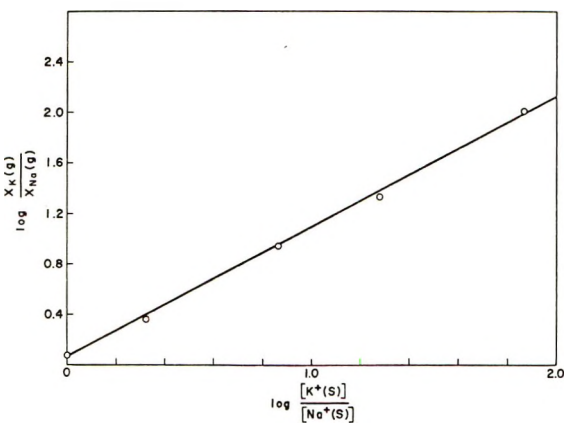

Figure 5. Dependence of the log K:Na ion mole fraction ratio in silica on the log K:Na ion melt activity ratio in NaCl–KCl mixtures at 815°.

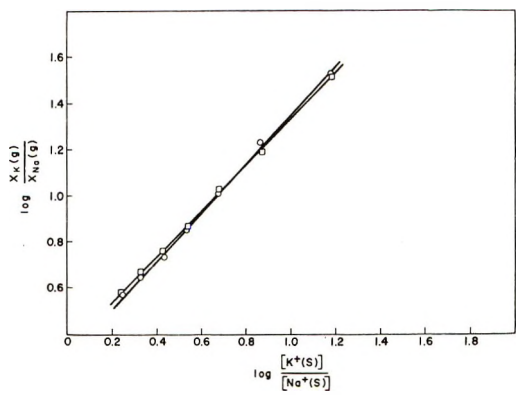

Figure 6. Dependence of the log K:Na ion mole fraction ratio in Vycor on the log K:Na ion melt activity ratio for NaCl–KCl mixtures: (○) 814°, (□) 890°. Data were obtained from Figures 1, 2, and 4 of ref 19.

For both temperatures n is very near unity, and $K_{K^+-Na^+} = 0.51$ at 814° and 0.45 at 890°. Although the $K_{K^+-Na^+}$ value is almost independent of temperature, k changes from 7.3 at 814° to 5.6 at 890°, due primarily to a decrease in the ion mobility ratio over this interval.

The ion-exchange equilibria data are tabulated in Table II together with the computer calculated least squares variances. The calculated mean value of k is also listed for each determination. For comparison purposes equilibrium data from an earlier paper by Stern[4] are included which were obtained from membrane potential and mobility ratio measurements for Ag^+–Na^+ and Ag^+–K^+ exchange. Since the n values were different for the two cells he studied, with $n = 1.2$ for K^+–Ag^+ exchange and unity for the Na^+–Ag^+ exchange, the $K_{K^+-Na^+}$ values are not exactly comparable with the present investigation. However, the ratio of k values for the two cells yields an expected $k = 71$ for the sodium–potassium exchange which compares well with the present results, even though Stern used a chloride melt. The good agreement between the directly measured exchange value and the one determined by Stern[4] through the use of a third ion (Ag^+) indicates that a true exchange equilibrium must have been obtained in both investigations.

The high-temperature $K_{K^+-Na^+}$ values found for cells 2 and 10 may be compared to the values in Vycor determined for the resistance data of Stern[19] (our Figure 6) by which the membrane came to exchange equilibrium by diffusion. The good agreement indicates that the diffusion or the electrolysis method appear to be equally valid means by which exchange equilibrium may be established throughout a glass membrane.

Although the $K_{K^+-Na^+}$ values given in Table II are rather independent of temperature, the n values seem to approach unity at higher temperatures. The k values decrease with increasing temperature because of the decrease in the Na:K ion mobility ratio in the glass.

For mole fractions of exchangeable ions A and B in a glass between about 0.1 and 0.9, with $X_A + X_B = 1$, and assuming the ion exchanger to be a regular solution, Garrels and Christ[22] developed the relation $n = 1 - W_{A-B}/RT$, where, following the notation of Garfinkel,[23] W_{A-B} is the excess interaction energy of neighboring A and B ions in the glass. Our results indicate

(22) R. M. Garrels and C. L. Christ, "Solutions, Minerals, and Equilibria," Harper and Row, New York, N. Y., 1965, pp 272–279.

(23) H. M. Garfinkel, *J. Phys. Chem.*, **72**, 4175 (1968).

Table III: $\Delta G_f^\circ(AX)_l - \Delta G_f(BX)_l$ and $\Delta G_f^\circ[A^+(g)] - \Delta G_f^\circ[B^+(g)]$ for the reaction $A^+(g) + B^+(s) = A^+(s) + B^+(g)$

No.	$K_{A^+-B^+}$	$A^+(g)-B^+(g)$	$\Delta G_f^\circ(AX)_l - \Delta G_f^\circ(BX)_l$, kcal mol^{-1}	$\Delta G_f^\circ[A^+(g)] - \Delta G_f^\circ[B^+(g)]$, kcal mol^{-1}	T, °K	Glass	Melt anion
1[a]	0.47	K^+–Na^+	−6.30	−7.50	823	Fused silica	NO_3^-
2[a]	8.14	K^+–Na^+	−6.30	−2.87	823	Fused silica	NO_3^-
3[a]	9.26	K^+–Na^+	−6.20	−1.68	1020	Fused silica	Br^-
4[a]	0.58	K^+–Na^+	−5.38	−6.55	1078	Fused silica	Br^-
5[a]	0.89	K^+–Na^+	−4.48	−4.73	1088	Fused silica	Cl^-
6[b]	0.52	K^+–Na^+	−5.55	−6.63	833	Fused silica	Cl^-
7[c]	0.51	K^+–Na^+	−4.47	−5.93	1087	Vycor	Cl^-
8[c]	0.45	K^+–Na^+	−3.98	−5.84	1163	Vycor	Cl^-
9[d]	0.91	K^+–Na^+	−7.33	−7.55	653	Pyrex–borosilicate phase	NO_3^-
10[d]	0.71	K^+–Na^+	−7.55	−8.04	738	Pyrex–borosilicate phase	NO_3^-
11[e]	1.06	K^+–Na^+	−7.08	−6.98	773	Na-aluminosilicate, Na/Al = 1.2	NO_3^-
12[f]	27.0	K^+–Na^+	−7.33	−3.0	651	Na-aluminosilicate, Na/Al = 3.6	NO_3^-
13[f]	74.0	K^+–Na^+	−7.33	−1.6	651	Na-aluminosilicate, Na/Al = 0.74	NO_3^-
14[d]	204.	K^+–Na^+	−7.33	−0.43	653	Pyrex–high-silica phase	NO_3^-
15[d]	1850.	K^+–Na^+	−7.58	+3.00	708	Pyrex–high-silica phase	NO_3^-
16[g]	7.98	K^+–Na^+	−7.20	−4.54	643	K_2O–$4SiO_2$	NO_3^-
17[e]	0.28	Li^+–Na^+	−6.79	−8.49	673	Li-aluminosilicate, Li/Al = 0.69	NO_3^-
18[e]	0.27	Li^+–Na^+	−6.79	−8.54	673	Li-aluminosilicate with 4% MgO, Li/Al = 0.51	NO_3^-
19[e]	0.02	Li^+–Na^+	−6.79	−12.0	673	Crystallized form of number 18	NO_3^-
20[h]	0.46	Ag^+–Na^+	76.0	+75.0	610	Fused silica	NO_3^-
21[b]	3000.	Ag^+–Na^+	58.1	71.3	833	Fused silica	Cl^-
22[i]	0.62	Ag^+–Na^+	75.9	75.4	608	Pyrex–borosilicate phase	NO_3^-
23[e]	0.39	Ag^+–Na^+	76.0	74.9	573	Na-aluminoborosilicate, Na/(Al + B) = 0.46	NO_3^-
24[i]	0.0043	Ag^+–Na^+	75.9	69.4	608	Pyrex–high silica phase	NO_3^-
25[j]	0.003	Ag^+–Na^+	76.1	68.9	627	Na–K-aluminosilicate, (Na + K)/Al = 8	NO_3^-
26[b]	5900.	Ag^+–K^+	63.6	78.0	833	Fused silica	Cl^-
27[b]	714.	Ag^+–Li^+	60.7	71.6	833	Fused silica	Cl^-
28[e]	0.32	Ag^+–Li^+	81.4	80.1	573	Li-aluminosilicate, Li/Al = 0.69	NO_3^-

[a] This investigation. [b] Stern, ref 4. [c] Stern, ref 19. [d] Garfinkel, ref 5. [e] Garfinkel, ref 23. [f] Locardi and Lama, ref 29. [g] Stern, unpublished results. [h] Doremus, ref 2. [i] R. H. Doremus, *J. Phys. Chem.*, **72**, 2665 (1968). [j] G. Schulze, *Ann. Phys.* (*Leipzig*), **40**, 335 (1913).

that W_{A-B} decreases with increasing temperature and is not independent of the melt present. Since so few ions are present in the fused silica compared to other glasses it is expected that n should be near unity.[4] It is not known why n should depend on the particular melt present. It is possible that the presence of different melts affects the number or distribution of surface bonding (exchange) sites so that n is melt and temperature dependent.

As the exchange equilibrium constants were determined from several different melts it is difficult to compare the results directly. However, it is possible to compare all of the cells studied with respect to the differences in the standard free energy of formation of fused silica that contains only potassium ions compared with fused silica containing only sodium ions.[6] This determination simply involves the use of the free energy change of eq 3. This free energy change is given by

$$-RT \ln K_{A^+-B^+} = \Delta G_1^\circ \qquad (10)$$

where $K_{A^+-B^+}$ is the exchange equilibrium constant of eq 4a. The free energy change of eq 3 may be set equal to the left-hand side of eq 10. The resulting equation may be rearranged to yield

$$\Delta G_f^\circ[K^+(g)] - \Delta G_f^\circ[Na^+(g)] = RT \ln K_{K^+-Na^+} - [\Delta G_f^\circ[NaX]_l - \Delta G_f^\circ[KX]_l] \qquad (11)$$

where $\Delta G_f^\circ[K^+(g)] - \Delta G_f^\circ[Na^+(g)]$ is the free energy change per mole when potassium ion replaces sodium ion in the glass, and $\Delta G_f^\circ[NaX]_l - \Delta G_f^\circ[KX]_l$ is the difference in the free energies of formation of the pure molten salts at the temperature of interest.

In order to illustrate the importance of viewing the energetics of the overall exchange equilibrium described by eq 11, ion-exchange equilibria data from a number of workers were collected from the literature and compared to the results of the present investigation. The required thermochemical data for the liquid salts at the required temperature were obtained from several sources.[24-28]

Table III lists the equilibrium constants and the

calculated free energy differences for a number of pairs of ions in a wide range of glasses determined from nitrate and halide melts over a 400° temperature range. Where available, the data for each pair of exchanging ions are arranged according to the type of glass in the following general order: (1) fused silica, (2) Vycor, (3) Pyrex, borosilicate phase, (4) alkali borosilicates or aluminosilicates having compositions of Na:Al or Na:B near unity; (5) alkali silicate glasses, including the high silica phase of Pyrex. The numbers in the first column of Table III are for discussion purposes and do not necessarily correspond to the earlier cell numbers.

Although some of the individual equilibrium values seem to be somewhat in disagreement, certain very definite trends are apparent for the Na^+–K^+ exchange. In agreement with the Eisenman theory,[7] the fused silica, Vycor, and the borosilicate phase of Pyrex all appear to have about the same properties. The glasses which contain appreciable amounts of sodium and aluminum, as well as the high-silica phase of Pyrex, are quite variable in their properties, but all have definitely less negative $\Delta G_f^\circ[K^+(g)] - \Delta G_f^\circ[Na^+(g)]$ values compared to the fused silica. The potassium silicate glass, number 16 of Table III, also has a less negative free energy change for this process, in agreement with the Eisenman theory, which predicts that the sodium should be more strongly bonded in a silicate structure compared to a boro- or aluminosilicate structure. Although the free energy change in the glass calculated from the Locardi and Lama[29] work appears to be somewhat too positive compared to the other data, the trend is that expected from the Eisenman theory, that is, the glass with Na:Al = 3.6 prefers sodium less than the glass with the lower sodium content. The small $\Delta G_f^\circ[K^+(g)] - \Delta G_f^\circ[Na^+(g)]$ values found for numbers 2 and 3 of Table III (corresponding to cells 1 and 6 of Table II) indicate the possibility of alkali ion contamination of the fused silica for these cells.

Since $\Delta G_f^\circ[K^+(g)] - \Delta G_f^\circ[Na^+(g)]$ is negative for all cases except number 15, it is misleading to say that the glasses "prefer" sodium to potassium ion just because $K_{K^+-Na^+} > 1$. In fact, from free energy considerations, the glasses "prefer" potassium ion in all cases shown except number 15. The overall free energy of the exchange reaction must be considered rather than the equilibrium concentration of ions in the glass and melt phases separately. This point was well developed by Yao and Kummer,[6] but the significance of their work seems to have been overlooked by many workers. For all of the cases considered in Table III, the free energy of formation for each potassium salt was more negative than that of the corresponding sodium salt, so that $\Delta G_f^\circ(KX)_1 - \Delta G_f^\circ(NaX)_1$ was always negative.

The Eisenman theory[1,7] is based on the assumption that in the type of glasses considered here ions are bonded to SiO^- type or $(AlOSi)^-$ type anionic sites in the glass by electrostatic forces, so that the bonding strength anticipated for both types of anionic sites is $Li^+ > Na^+ > K^+$. The order of bonding strengths indicated by the data of Table III is $Li^+ > K^+ > Na^+$. Even if one considers the possibility of anionic sites larger or smaller than the SiO^- or $(AlOSi)^-$ sites as was done by Eisenman,[7] any of the predicted possible orders of bond strengths is not that which is observed. This raises the question of whether or not the basic theory is in error. If the Eisenman theory is correct and the equilibrium data are also correct, the possibility of a different type bonding for potassium ion compared to sodium ion in these glasses is indicated.

The $\Delta G_f^\circ[Li^+(g)] - \Delta G_f^\circ[Na^+(g)]$ values calculated from the lithium–sodium exchange agree closely with the value predicted by the Eisenman theory for $(AlOSi)^-$ sites. Number 19 of Table III is a crystallized form of number 18, the crystal structure of which is more stable when it contains the lithium ion.

The silver–alkali ion exchange values listed in Table III indicate that the silver containing glass is very unstable with respect to the alkali ion containing glass. The results from the silver–sodium exchange in the high-silica glasses, numbers 24 and 25, indicate that the silver ion is more stable in these glasses than in fused silica. Numbers 20 and 21 of Table III illustrate the large change in $K_{Ag^+-Na^+}$ resulting primarily from a change in the melt anion.

With the exception of one of the Ag^+–Li^+ exchange values, number 27, the other silver–alkali ion exchange equilibria and glass free energy differences are in the order expected when compared to the alkali ion–alkali ion exchange equilibria.

It is possible that some of the data contained in Table III were not obtained under truly reversible conditions. Most of the exchange measurements were carried out in one direction only, without determining whether an ion placed into the glass by exchange would come out. In the present work this determination was made, so that there is no question but that the Na^+–K^+ exchange in fused silica is reversible.

Conclusions

(1) It has been shown that irreversible changes in the resistance and in the activation energy for sodium

(24) D. R. Stull, Ed., "JANAF Thermochemical Tables," The Dow Chemical Co., Midland, Mich., 1965.

(25) K. H. Stern, "High-Temperature Properties and Decomposition of Inorganic Salts. Part 3. Nitrates and Nitrites," *J. Phys. Chem. Ref. Data*, in press.

(26) "Selected Values of Chemical Thermodynamic Properties," National Bureau of Standards Circular 500, U. S. Government Printing Office, Washington, D. C., 1952.

(27) W. J. Hamer, M. S. Malmberg, and B. Rubin, *J. Electrochem. Soc.*, **103**, 8 (1956).

(28) K. K. Kelley, U. S. Bureau of Mines Bulletin 584, U. S. Government Printing Office, Washington, D. C., 1960.

(29) B. Locardi and A. Lama, *Phys. Chem. Glasses*, **11**, 71 (1970).

ion conduction may occur in a fused silica membrane when subjected to current densities exceeding approximately 30 μA cm^{-2} at temperatures above 750°.

(2) The activation energy for sodium ion conduction was found to be time dependent over the temperature interval 450–550°, and time independent at higher temperatures. The activation energy for potassium ion conduction was found to be time independent over the 450–850° range investigated, so that the steady-state temperature dependence of the Na:K ion mobility ratio below 550° was opposite to that found above 550°.

(3) Ion-exchange equilibrium constants were measured for Na^+–K^+ exchange between NO_3^-, Br^-, and Cl^- melts and fused silica. Although the ion-exchange equilibrium constant was found to be only slightly dependent on the temperature, the electrode selectivity constants were shown to be temperature dependent because of the mobility ratio term. The ion-exchange equilibrium constant was shown to be dependent on the melt anion.

(4) Consideration of the overall free energy changes involved in the ion-exchange reaction allowed the comparison of many ion-exchange equilibria constants reported in the literature. The dependence of the ion-exchange equilibrium constant on the melt anion is satisfactorily explained by the difference in free energy of formation of the respective salts.

Differential Scanning Calorimetric Studies of the System Poly-γ-benzyl-α,L-glutamate–Dimethylformamide

by J. H. Rai and W. G. Miller*

Department of Chemistry, University of Minnesota, Minneapolis, Minnesota 55455 *(Received November 8, 1971)*

Publication costs assisted by the National Institutes of Health

Differential scanning calorimetry has been used to investigate the thermal behavior of the system polybenzyl-glutamate–dimethylformamide in the temperature range −30 to +120° and the composition range 0–30 vol % polymer. Irrespective of the initial state (isotropic or liquid crystalline) at room temperature, exotherms were obtained invariably when solutions were cooled to the biphasic region. The thermograms yielded heats of polymer–solvent mixing which were small and endothermic. The observed heats were fitted adequately by a van Laar binary contact heat of mixing expression. From these data a *maximum* of 5 cal/mol was placed on the latent heat of the isotropic to liquid crystal phase transition.

Introduction

Several studies on the system poly-γ-benzyl-α,L-glutamate (PBLG)–dimethylformamide (DMF) have been reported.[1-6] Recently Wee and Miller[5] determined the temperature–composition phase diagram for this system in the temperature range −20 to +140° and the composition range 0–30 vol % polymer. At higher polymer concentration solvent activity as a function of temperature and composition has been determined.[6] Although a wide variety of experimental techniques have been employed to investigate the PBLG–DMF system, direct thermal analysis of the system using thermoanalytical methods, such as differential thermal analysis and differential scanning calorimetry (DSC), has not been reported. In this communication, we report the results of a DSC study on the system in the temperature range −30 to +120° and composition range 0–30 vol % polymer. Both heating and cooling experiments have been carried out. The temperature at which the polymer solution begins to generate or absorb heat is correlated with the phase diagram. The heats determined are compared with that expected for binary contacts assuming a van Laar form for the heat of mixing.

(1) A. E. Elliott and E. J. Ambrose, *Discuss. Faraday Soc.*, 9, 246 (1950).

(2) V. Luzzati, M. Cesari, G. Spach, F. Mason, and J. Vincent, *J. Mol. Biol.*, 3, 566 (1961).

(3) P. J. Flory and W. J. Leonard, Jr., *J. Amer. Chem. Soc.*, 87, 2102 (1965).

(4) K. G. Goebel and W. G. Miller, *Macromolecules*, 3, 64 (1970).

(5) E. L. Wee and W. G. Miller, *J. Phys. Chem.*, 75, 1446 (1971).

(6) J. H. Rai and W. G. Miller, *Macromolecules*, 5, 45, (1972).

Experimental Section

PBLG (M_w = 310,000) was obtained from New England Nuclear Corp. and was vacuum dried for 24 hr at 55° before use. It was of the same lot as was used in determining the phase diagram.[5] Dimethylformamide (ACS Certified, Fisher Scientific Co.) was vacuum distilled over $CaSO_4$. Samples were prepared having concentrations of 2, 5, 8, 9.3, 12, 20, and 30 vol % polymer. In calculating volume concentration the specific volume of PBLG was taken as 0.787 ml g^{-1}.[7] Solutions were prepared in a drybox at room temperature. After homogenous solution was obtained, about 10–20 mg of the solution was transferred to a DSC aluminum sample pan. The pan was hermetically sealed to prevent solvent loss. The sample was then stored in a desiccator for 15–20 hr before use. Weight loss due to vaporization of DMF was not detectable.

A Du Pont Model 900 differential scanning calorimeter was used for all measurements. The instrument was calibrated by using indium, gallium, mercury, and water as standards. Cooling and heating experiments were carried out at scanning rates of 4–10°/min. For cooling experiments a Dry Ice, water, and methanol mixture was used as a cooling source. In a typical run involving subambient temperatures the sample was heated slowly (1–2°/min) from room temperature to 40° and then cooled at a specific, preselected rate. After the sample was cooled to about −30°, the cooling attachment was removed, and the sample was heated at the same rate to room temperature. For a given sample the same procedure was repeated two or three times to observe the reversibility of the system. In DSC studies from room to higher temperatures no heat sink was necessary.

Results

Typical thermograms are shown in Figures 1–3 for runs between room and subambient temperatures. These clearly indicate that the observed heat was associated with a reversible transition. Thermograms from 25° to temperatures as high as 120° gave no indication of heat release or absorption and were indistinguishable from thermograms on inert materials. Thermograms for pure DMF and for pure solid PBLG showed no evidence of thermal transitions.

Although the thermograms in Figures 1–3 indicate a reversible process, the onset of exothermicity in the cooling curves does not come at the same temperature as the onset of endothermicity in the heating curves. Runs with the calibrating materials indicated that this was a result of supercooling and thermal lag. Gallium (mp 29.5°), water, and mercury (mp −38.9°) showed initial freezing at +14, −15, and −40°, respectively, upon cooling. However, heating curves indicated the onset of endothermicity occurred within 2–3° of the melting point. By analogy the onset of endothermicity was taken as the approximate "transition temperature"

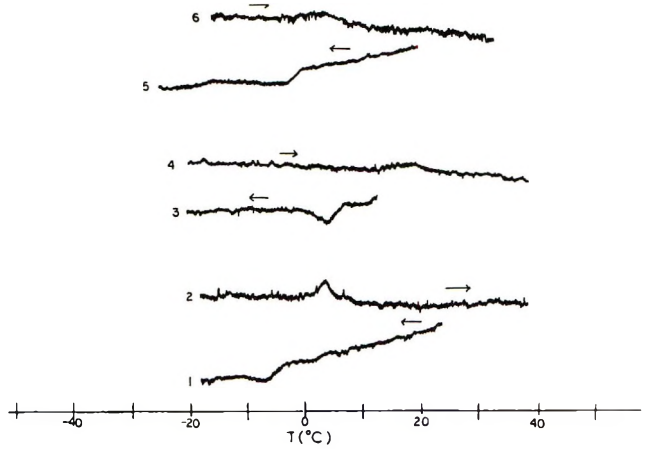

Figure 1. Typical DSC thermograms for 5% (1, 2), 8% (3, 4), and 9.3% (5, 6) solutions. Arrows indicate direction of temperature scan. Temperature scanning rate was 6 (1–5) or 10°/min (6).

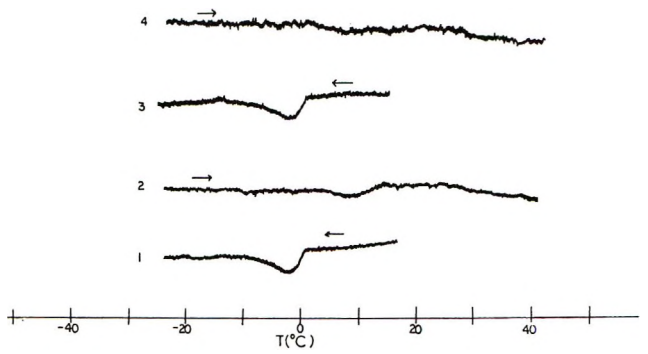

Figure 2. Consecutive series of DSC thermograms on a 12% solution. Scanning rate was 6°/min.

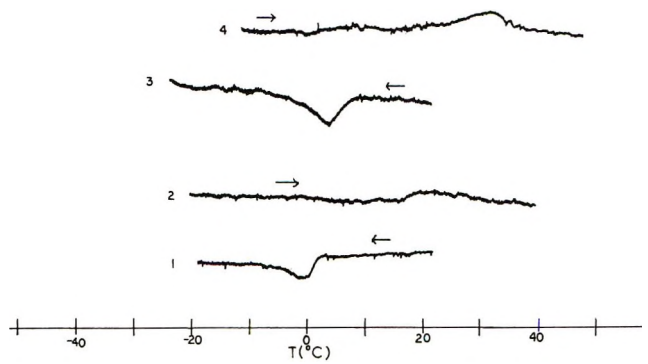

Figure 3. Typical thermograms for 20 (1, 2) and 30 (3, 4) vol % solutions. Scanning rate was 6 (1–3) or 8°/min (4).

for the DMF–PBLG thermograms. These are shown in Figure 4 superimposed on the phase diagram. The coincidence of the "transition temperature" with the phase boundaries indicates that the observed thermal transition is associated with the crossing of the phase boundary.

(7) A. Elliott, E. M. Bradbury, A. R. Downie, and W. E. Hanby, "Polyamino Acids, Polypeptides and Proteins," M. A. Stahmann, Ed., University of Wisconsin Press, Madison, Wis., 1962, pp 255–269.

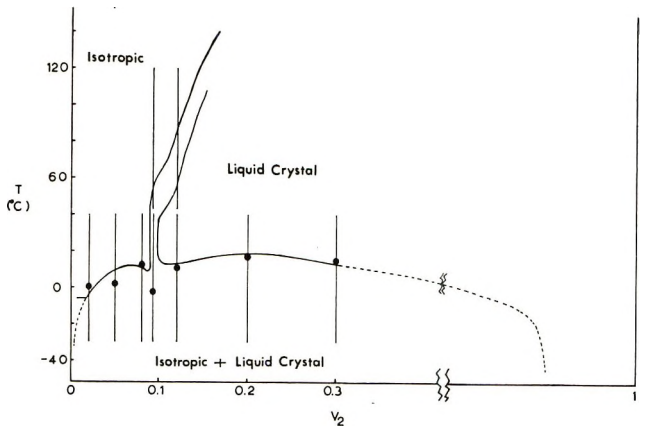

Figure 4. Phase diagram for the system PBLG–DMF.[5] Circles indicate onset of endothermicity in DSC thermograms. Vertical lines indicate the range of temperature scanning. Dashed lines are *hypothetical* extension of phase boundaries.

The shape of the DMF–PBLG cooling curves indicates supercooling not unlike that observed with the calibrating materials. Inasmuch as this leads to a more clearly defined "peak" the transition heat from the cooling curves was more reliably measured than from the heating curves. The heats determined from the exotherms are tabulated in Table I.

Table I: Observed Heats as a Function of Concentration

Polymer concn, vol %	Observed heat: Cal/g of solution	Observed heat: Cal/g of polymer	ΔH_{mix}(obsd), cal/mol of solution[b]
2	−0.06 ± 0.03	−2.3 ± 1	5 ± 2
5	−0.14 ± 0.01	−2.2 ± 0.2	11 ± 1
5	+0.13 ± 0.02[a]	+2.0 ± 0.4[a]	10 ± 2
8	−0.23 ± 0.02	−2.2 ± 0.2	18 ± 2
9.3	−0.34 ± 0.04	−1.9 ± 0.3	27 ± 3
12	−0.44 ± 0.04	−2.9 ± 0.3	36 ± 4
20	−0.70 ± 0.07	−2.8 ± 0.3	62 ± 6
30	−0.93 ± 0.09	−2.6 ± 0.3	59 ± 10

[a] Determined from endotherm. [b] Polymer concentration taken as moles of monomeric units.

Discussion

Origin of the Thermal Transition. The thermal transitions observed by differential scanning calorimetry correlate well with the phase boundaries as shown in Figure 4. However the heating of the 9.3 or 12 vol % solutions from 25 to 120° gave no indication of a thermal transition, even though phase boundaries were crossed also. The origin of the thermal transition can be understood with aid of the phase diagram. Although the phase boundaries have not been determined at low temperature, it is clear that at −30° the liquid crystal phase is in equilibrium with an isotropic phase that is nearly pure solvent. As the line bounding the isotropic phase must be nearly vertical in this temperature region, its composition as well as the composition of the liquid crystal phase with which it is in equilibrium must be nearly temperature independent. Thus as a sample is warmed from −30° there is little change in composition or in the relative amounts of the two phases until a temperature of 0° or above is reached. Then there is a rapid change in composition. If equilibrium is maintained, all samples except the 9.3 one will turn into a single phase system. The heat observed in heating a solution from −30 to +40° can be described as the heat of mixing two phases of very different compositions to obtain a single phase. This heat of mixing corresponds to mixing nearly pure solvent with a phase rich in polymer, though containing an unknown amount of solvent. Since the polymer-rich phase contains some solvent, the observed heat of mixing will presumably contain little if any contribution from the heat of fusion of the polymer. The cooling curves represent the reverse process, or a heat of unmixing. As can be seen from Table I the heats are very small.

The interpretation presented above also explains why no thermal transition is observed on crossing high-temperature phase boundaries. These high-temperature phase boundaries represent a relatively small difference in composition; consequently, the heat associated with mixing or unmixing when crossing such a boundary will be negligible. The fact that no heat is observed when a liquid crystal phase is turned into an isotropic phase sets limits on the enthalpy associated with the liquid crystal–isotropic phase transition. This will be discussed later.

ΔH_{mixing} and $\Delta \bar{H}_1$. In discussing the heat of mixing it is convenient to consider the −30° state of the system as the initial state and the 40° state as the final state, *i.e.*, initially the system is biphasic whereas it is a single phase system in the final state. The observed heats of mixing are small and endothermic irrespective of whether the final state is isotropic or liquid crystalline. Frequently small, endothermic heats of mixing can be fitted to a binary contact, van Laar type of treatment. Due to ease of treatment the enthalpy contribution to lattice model approaches to the thermodynamics of random coil as well as stiff chain polymers[8] has typically been handled in this manner. In Flory's treatment[8] of stiff chain polymers the polymer–solvent interaction parameter χ is assumed to be independent of whether or not the system is an isotropic or a liquid crystalline phase. If we further assume that the χ parameter is independent of composition as well as phase, a comparison can be made between the experimental heats and that predicted from a van Laar expression. Thus the heat of mixing polymer and solvent to form a solution of volume fraction ν_2 is given by

$$\Delta H_{mix}(\nu_2) = RT\chi n_1 \nu_2 \qquad (1)$$

(8) P. J. Flory, *Proc. Roy. Soc., Ser. A*, **234**, 73 (1956).

where n_1 is the number of moles of solvent. In the system studied the observed heat of mixing is given by

$$\Delta H_{mix}(obsd) = RT\chi(n_1\nu_2 - n_1^{I}\nu_2^{I} - n_1^{LC}\nu_2^{LC}) \quad (2)$$

where n_1 and ν_2 refer to the final state of the system, n_1^{I} and ν_2^{I} to the initial isotropic phase, and n_1^{LC} and ν_2^{LC} to the initial liquid crystal phase. The values of ν_2^{I} and ν_2^{LC} are fixed, and n_1^{I} and n_1^{LC} are related through a tie line relationship to give the correct overall composition. In the case of the 9.3 vol % sample the final state is biphasic. This results in an inconsequentially altered eq 2.

By assuming values for ν_2^{I} and ν_2^{LC} $\Delta H_{mix}(obsd)$ may be calculated, using arbitrary values of χ, for comparison with the experimental heats determined from the cooling curves $[-\Delta H_{mix}(obsd)]$. Results of such calculations are shown in Figures 5 and 6 superimposed on the experimental data. For a given χ the maximum heat would be obtained if $\nu_2^{I} = 0$ and $\nu_2^{LC} = 1.0$. To a first approximation it is possible to fit the data using a constant value of χ, independent of phase and concentration. More precise measurements of the heats and a definitive knowledge of ν_2^{I} and ν_2^{LC} might dictate the need for a slightly varying χ, which frequently is the case with random coil polymers.

The χ values estimated here represent the enthalpy contribution to the free energy of mixing. Previously smaller χ values have been estimated from osmotic pressure[4] and phase equilibrium[5] studies. These values are a measure of excess free energy and hence contain entropy as well as enthalpy contributions. In the Flory expression for the mixing of rod polymers with solvent[8] no account is taken of solvent–polymer side-chain mixing, which is known now to contribute to the solution thermodynamics of helical polypeptides.[3,6] As the solvent–polymer side-chain mixing will make a negative contribution to the excess free energy of mixing, it is reasonable that measurements yielding an excess free energy χ will be smaller than those yielding an enthalpic χ.

At low overall polymer concentration and at low temperature the solvent is nearly quantitatively in the isotropic phase, a state with $\nu_2^{I} \approx 0$. Therefore at low concentration the observed molar heat of mixing, column 5 in Table I, approaches $\Delta\bar{H}_1$. These values may be compared with other determinations.

The temperature dependence of the osmotic second virial coefficient may be used to evaluate $\Delta\bar{H}_1$. Unfortunately $\Delta\bar{H}_1$ so determined can only cover the concentration range where higher terms to the osmotic pressure equation are not needed. Analysis of osmotic pressure data[4] indicates $\Delta\bar{H}_1$ is less than 1 cal/mol for a 0.5 vol. % solution, the highest concentration for which the second virial coefficient adequately describes the osmotic pressure data. The DSC data extrapolated to this concentration fall in the same range.

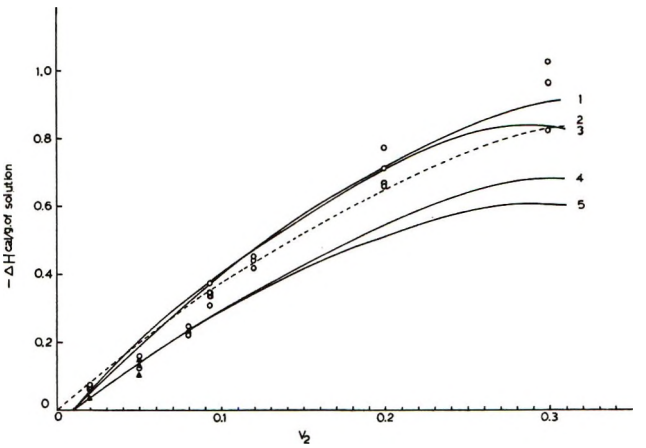

Figure 5. The observed heat per gram of solution. For the 2 and 5% solutions endotherms (▲) as well as exotherms (O) were sufficiently well defined for area determination. Lines calculated from eq 2 with ν_2^{I}, ν_2^{LC}, and χ being, respectively, 0.01, 0.9, and 0.8 (1); 0, 1.0, and 0.6 (2); 0.01, 0.7, and 1.1 (3); 0.01, 0.9, and 0.6 (4); 0.01, 0.7, and 0.8 (5).

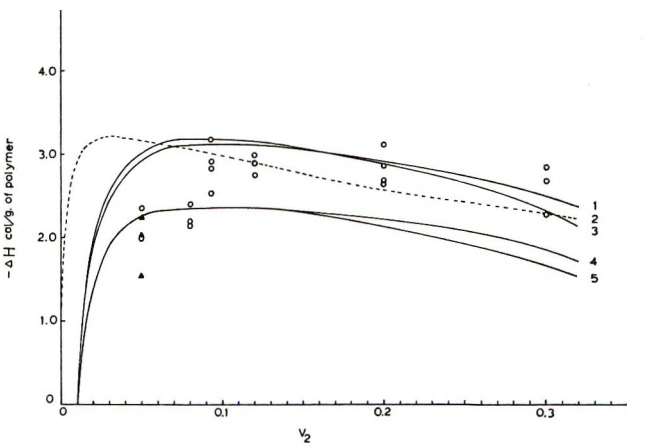

Figure 6. The heat per gram of polymer. Notation same as in Figure 5.

The temperature dependence of solvent activity determined from vapor sorption is yet another method for determining $\Delta\bar{H}_1$. Vapor sorption data[6] taken in the concentration range 70–100 vol % polymer indicate that the temperature dependence of the solvent activity at constant solution composition is less than the experimental error, which is about 3%. Using this 3% value as a maximum variation in activity with temperature, $\Delta\bar{H}_1$ must be less than 400 cal/mol in this concentration range. The DSC data can be extrapolated to the same concentration region through use of the van Laar expression and the parameter which best fits the DSC data. Using a χ value of 0.8, a value of 200–400 cal/mol is estimated for the concentration range 70–100 vol % polymer.

The three types of experimental data, covering the entire composition range, are in satisfactory agreement as far as $\Delta\bar{H}_1$ is concerned.

The Latent Heat of the Isotropic–Liquid Crystal Phase Transition. The Flory treatment of the statistical thermodynamics of rod polymers predicts that it should be possible to have a first-order isotropic–liquid crystal phase transition with no latent heat. From the nature of the phase diagram (Figure 4) one can see that there is no manner in which this can be studied by direct thermal measurements. There is no temperature or composition at which the isotropic phase can be completely converted into the liquid crystal phase. A maximum value for the heat can be estimated, however, from the DSC studies. If the data for the heat of mixing to form the isotropic phase are extrapolated into the liquid crystal range, nonoverlap of the two curves corresponds to the heat of the isotropic–liquid crystal phase transition. The values for the 5 and 8% solutions (isotropic) were extrapolated to 12% and compared to the 12% (liquid crystal) value. This difference corresponds to about 0.06 cal/g of solution or 5 cal/mol of solution. Extension of these calculations to higher concentrations will yield somewhat larger estimates of the maximum latent heat. However, the scatter in the DSC data and the uncertainty in the phase boundaries at low temperatures make such extensions meaningless. The high-temperature thermogram on the 12% solution is consistent with a small latent heat in that even a rapid scan across the biphasic region, resulting in a rapid conversion of the sample from a single phase, liquid crystal solution into a single phase, isotropic solution, gave no evidence of a thermal transition. It is clear that the latent heat associated with the isotropic to liquid crystal phase transition is indeed small if not zero.

Acknowledgments. We would like to thank Dr. R. Moore, Department of Laboratory Medicine, University of Minnesota, for use of the Du Pont 900 differential thermal analyzer.

COMMUNICATIONS TO THE EDITOR

Concentration Dependence of Ionic Vibration Potentials: Consequences for the Determination of Ionic Partial Molal Volumes[1]

Publication costs assisted by the U. S. Office of Naval Research

Sir: In a recent communication,[2] Panckhurst has questioned the use of experimental partial molal volumes and transport numbers at *infinite* dilution and 25° with ionic vibration potential data at *finite* concentrations and 22° in our calculation[3] of individual ionic partial molal volumes. Panckhurst further states that "in view of their (Zana and Yeager) weighting procedure it is reasonable to consider the above points at 0.3 N, as has been done for some of them by Millero." According to Panckhurst, it then follows that the "Zana and Yeager method (as presently developed) does not do more than support the claim that $\bar{V}_{H^+}{}^0$ is probably in the range 0 to -5 cm^3 mol^{-1} and does not justify the CDV (Conway, Desnoyers, and Verrall)[4] extrapolation against molecular weight."

The purpose of this note is to present arguments to show that the values for ionic partial molal volumes calculated by us from ionic vibration potentials are much more reliable than Dr. Panckhurst's note would indicate.

We wish first to call attention to the fact that the experimental values for the ionic vibration potentials per unit velocity amplitude reported in our paper[3] are essentially constant within the accuracy of the measurements over the concentration range 1×10^{-3} to 3×10^{-1} N for almost all of the electrolytes examined. (The experimental values were constant within ± 0.1 μV cm^{-1} sec at concentrations of 3×10^{-3} to 1×10^{-1} N for 26 of the 32 electrolytes for which the concentration dependence was examined and constant to within ± 0.3 μV cm^{-1} sec over the range 1×10^{-3} to 3×10^{-1} N for all except NaF.) With the exception of NaF, the ionic vibration potentials used in the calculation of the ionic partial molal volumes correspond to those at 3×10^{-3} N within ± 0.1 μV cm^{-1} sec even though the data were weighted somewhat toward higher concentrations (3×10^{-2} to 1×10^{-1} N).

At 3×10^{-3} N the value of $\phi_V - \phi_V{}^0$ is of the order of 0.1 cm^3/mol for 1–1 electrolytes and the error in using $\phi_V{}^0$ instead of ϕ_V is small relative to the experimental accuracy. (In our paper,[3] the precision (and also the accuracy) of the measured values of the ionic vibration potentials was taken, perhaps somewhat conservatively, as $\pm$ 0.3 μV cm^{-1} sec, which for a 1–1 electrolyte corresponds to a maximum error in the calculated ionic partial molal volumes of ± 2 cm^3/mol.) A similar situation also exists with respect to the transport numbers. Likewise for the 1–1 electrolytes the dependence of the transport numbers and partial molal volumes on temperature is sufficiently small that the difference between 22 and 25° contributes only a small error to the overall final calculation of the ionic partial molal volumes, compared to that arising from the limited accuracy of the ionic vibration potential measurements.

In our original work[3] seven 1–1 chlorides were examined. The root-mean-square deviation of the values of $\bar{V}_{Cl^-}$ for these seven salts was 1.2 cm^3/mol. The determination of the ionic partial molal volume for any one ion, however, requires measurements in only one electrolyte. Therefore, if the optimum accuracy is desired from the vibration potential data in combination with partial molal volumes for 1–1 electrolytes, probably the best procedure is not to average the data for a given anion with a variety of cations but rather to choose one or two salts which should come closest to being ideal. Rubidium and cesium chlorides exhibit no detectable dependence of the ionic vibration potential on concentration from 10^{-3} to 3×10^{-1} M and furthermore have transference numbers each very close to 0.5. The data for both these two electrolytes yield partial molal volume results for the Cl^- ion of 23.5 cm^3/mol as compared to a value of 23.7 cm^3/mol obtained from averaging seven electrolytes and to a value 23.6 cm^3/mol as obtained by the extrapolation procedure of Conway, Desnoyers, and Verall.[4] This very close agreement (0.1 cm^3/mol) is partially fortuitous. The accuracy of the mean value of the ionic vibration potentials for the RbCl solutions measured over the concentration range 10^{-3} to 10^{-1} M is considerably better than that of the individual measurements and statistically should be ± 0.1 μV cm^{-1} sec, corresponding to an accuracy of ± 1 cm^3/mol for the partial molal volume of the Cl^- ion. The situation is the same for the CsCl solutions. Thus the ionic partial molal volume of the Cl^- ion appears to be accurate to at least ± 1 cm^3/mol but not necessarily much better. Since our absolute values for ionic partial molal volumes were

(1) Partially based on research supported by the U. S. Office of Naval Research.

(2) M. H. Panckhurst, *J. Phys. Chem.*, **75**, 3035 (1971); see also M. H. Panckhurst, *Rev. Pure Appl. Chem.*, **19**, 45 (1969).

(3) R. Zana and E. Yeager, *J. Phys. Chem.*, **71**, 521 (1967).

(4) B. Conway, J. Desnoyers, and R. Verrall, *ibid.*, **75**, 303 (1971); *Trans. Faraday Soc.*, **62**, 2738 (1966).

reported,[3] two more papers reporting absolute ionic partial molal volumes have appeared from other laboratories[5,6] in addition to ref 4 with values for $\bar{V}_{H^+}^0$ which agree with our value to within 1 cm³/mol.

The small or negligible concentration dependence found for ionic vibration potentials in the range 1×10^{-3} to 1×10^{-1} N is not surprising particularly for 1–1 electrolytes. (Artifacts interfere with measurements[3] much below 10^{-3} N.) A treatment[7] has been developed incorporating correction terms for ionic atmosphere relaxational and electrophoretic forces and diffusion. These terms amount to not more than 10% for a 1–1 electrolyte at 10^{-1} N, and usually tend to cancel out when the cation and anion transference numbers are nearly equal.

For electrolytes with equal cation and anion charge, the effect of the ionic atmosphere on the ionic partial molal volume is the same for both ions, within the limits of the simple Debye–Hückel theory, and hence the difference in the partial molal volumes of cation and anion is essentially constant. If the transference numbers of both ions are nearly equal, the ionic vibration potential depends only on the difference in the cation and anion partial molal volumes to a good approximation. Therefore under these circumstances even the relatively small ionic atmosphere effects on the ionic partial molal volumes tend to cancel out at least to a first approximation with the result that ionic atmosphere effects do not cause any appreciable concentration dependence of the ionic vibration potentials with such electrolytes up to concentrations of 10^{-1} M. Ion pairing may become appreciable at such concentrations, however, and it is not taken into account even in the more extensive theoretical treatment.[7] On the other hand, for 1–1 electrolytes, ion pairs do not contribute directly to the observed effect, since they have no net charge. Furthermore, on the basis of theory and also experimental studies of mixtures of salts,[3] the effects of charge ionic aggregates are expected to become appreciable only when their concentration approaches within an order of magnitude of the concentration of the major ionic species. Consequently, the small concentration dependence observed for asymmetric electrolytes also is not surprising.

Taking into account these points and other aspects of the development of the working equations used in our paper,[3] one can put forth a strong argument favoring the use of the ionic partial molal volumes and transference numbers at *infinite* dilution as yielding a better approximation than the corresponding values at *finite* concentrations when applying these equations to interpret experimental measurements at concentrations up to 10^{-2} N and perhaps even 10^{-1} N in 1–1 electrolytes.

In conclusion, we believe that our set of absolute values of ionic partial molal values is among the most reliable available because of the freedom of the experimental approach from questionable assumptions.

(5) E. J. King, *J. Phys. Chem.*, **74**, 4590 (1970).
(6) F. Millero, *ibid.*, **75**, 280 (1971).
(7) J. Bugosh, E. Yeager, and F. Hovorka, *J. Chem. Phys.*, **15**, 592 (1947).

CHEMISTRY DEPARTMENT
CASE WESTERN RESERVE UNIVERSITY
CLEVELAND, OHIO 44106
ERNEST YEAGER*

CENTRE DE RECHERCHES
SUR LES MACROMOLECULES
STRASBOURG, FRANCE
RAOUL ZANA

RECEIVED OCTOBER 21, 1971

Photochemistry of Nitrosobenzene

Publication costs borne completely by The Journal of Physical Chemistry

Sir: Two reports indicate that the photochemistry of nitrosobenzene gives rise to azoxybenzene and 2-hydroxyazobenzene.[1,2] The latter has been known to result from the direct photolysis of azoxybenzene.[3] In both investigations the authors concluded that phenylhydroxylamine does not arise as a photoproduct. In view of our continuing interests in the photochemistry of aromatic nitro compounds it appeared in analogy to the photochemical behavior of nitrobenzene that hydrogen abstraction by the nitrosobenzene n,π^* triplet should lead to phenylhydroxylamine as the only photochemical product. Although Mauser and Heitzer[1] used monochromatic excitation at 313 and 366 nm, the identification of photoproducts was based on large-scale photolysis. The experiments of Tanikaga[2] were performed with broad range uv excitation, which because of the dominance of secondary photochemical effects resulted in 10 photoproducts. We have reinvestigated the photochemistry of this molecule in 2-propanol with the aim of elucidating the detail photochemistry of nitrosobenzene. Irradiations in 1-cm cells were performed at 313 nm in vacuum-degassed solutions of 2-propanol in the concentration range 10^{-3} to 10^{-5} M, and contrary to previous reports phenylhydroxylamine is the only photoproduct formed and its growth can be seen very clearly in the uv spectrum. The photochemical disappearance of the 281- and 306-nm peaks of C_6H_5NO is accompanied by the grow-in of the 238- and 281-nm peaks of C_6H_5NHOH; see Figure 1. Of particular interest is that the oxidation of C_6H_5NHOH in the presence of air leads to a return of C_6H_5NO, which occurs as a dark reaction, as is evident in Figure 1. The known coupling reaction between C_6H_5-

(1) H. Mauser and H. Heitzer, *Z. Naturforsch. B*, **20**, 200 (1965).
(2) R. Tanikaga, *Bull. Chem. Soc. Jap.*, **42**, 210 (1969).
(3) G. M. Badger and R. G. Buttery, *J. Chem. Soc.*, 2243 (1954).

NHOH and C_6H_5NO accounts for the formation of azoxybenzene during the large scale photolysis of C_6H_5NO. At 258 nm there is evidence for an isosbestic point during these reversible changes, which is suggestive of a simple photochemical process.

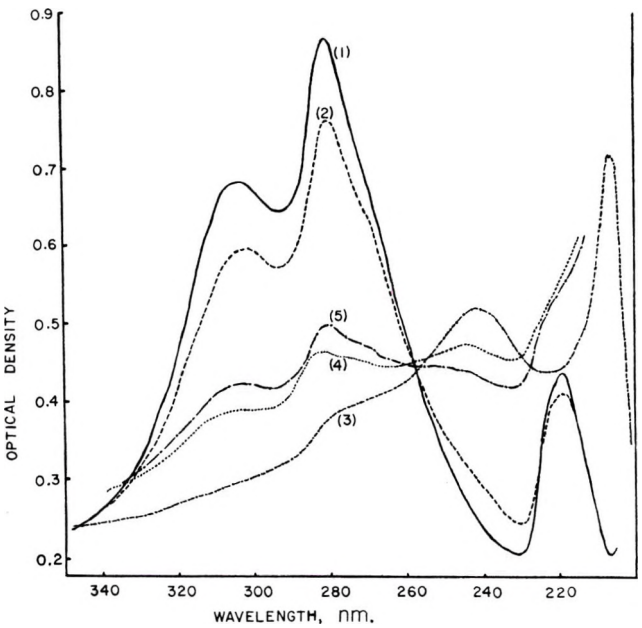

Figure 1. Spectral changes during the photoreduction of nitrosobenzene in 2-propanol; degassed, 313-nm excitation: 1, initial solution 6.3×10^{-5} *M*; 2, 60-min photolysis; 3, 390-min photolysis; 4, 36-hr dark reaction after opening cell to air; 5, 60-hr dark reaction.

In analogy to our results on the photoreduction of nitrobenzene in 2-propanol,[4] which proceeds through an n,π^* triplet, we believe the same reactive state to be responsible in nitrosobenzene.[5] We have been unable to observe phosphorescence from C_6H_5NO in EPA at 77°K, which suggests a short-lived triplet state similar to nitrobenzene.[6] We have also attempted to measure the triplet yield of nitrosobenzene by energy transfer to *cis*-piperylene, but the method was inapplicable because of the coupling reaction between donor and acceptor.[7] The following scheme is presented to account for the photoreduction of C_6H_5NO in 2-propanol.

$$C_6H_5NO \xrightarrow{313\ nm} C_6H_5NO^{*1} \rightsquigarrow C_6H_5NO^{*3} \quad (1)$$

$$C_6H_5NO^{*3} \rightsquigarrow C_6H_5NO \quad (2)$$

$$C_6H_5NO^{*3} + (CH_3)_2CHOH \longrightarrow C_6H_5\dot{N}OH + (CH_3)_2\dot{C}OH \quad (3)$$

$$C_6H_5\dot{N}OH + (CH_3)_2\dot{C}OH \text{ [or } (CH_3)_2CHOH] \longrightarrow C_6H_5NHOH + (CH_3)_2CO \text{ [or } (CH_3)_2\dot{C}OH] \quad (4)$$

The photochemistry of C_6H_5NO is particularly interesting since its uv absorption spectrum exhibits its lowest energy singlet at 760 nm (ϵ 44 in heptane), which has been assigned as an n,π^* state.[8] Although irradiation at 313 nm leads to C_6H_5NHOH, we have been unable to observe any photochemical activity with 730-nm excitation. It appears, therefore, that in nitrosobenzene excitation into the lowest singlet state leads to radiationless deactivation, whereas excitation into the second excited singlet state leads to photochemistry *via* the lowest n,π^* triplet. Another possibility is that photochemistry is occurring from the second triplet state.

The measured quantum yields for disappearance of C_6H_5NO are 0.047 ± 0.002 and 0.033 ± 0.002 in degassed and air saturated solutions, respectively.[9] Although nitroso compounds are known to exhibit a monomer–dimer equilibrium, the constancy of the measured quantum yield over the hundredfold change of concentration studied indicates that only the characteristic green monomeric nitrosobenzene participates in the observed photoreduction.

(4) R. Hurley and A. C. Testa, *J. Amer. Chem. Soc.*, **88**, 4330 (1966).

(5) Although no distinct n,π^* absorption band in the uv has been assigned to nitrosobenzene, we believe that it is probably buried under the long wavelength side of the strong absorption appearing at 308 mm.

(6) R. Hurley and A. C. Testa, *J. Amer. Chem. Soc.*, **90**, 1949 (1968).

(7) M. Ahmad and J. Hamer, *J. Org. Chem.*, **31**, 2829 (1966).

(8) K. Tabei and S. Nagakura, *Bull. Chem. Soc. Jap.*, **38**, 965 (1965).

(9) Quantitative determination of the disappearance of C_6H_5NO was made by polarographic measurements.

DEPARTMENT OF CHEMISTRY
ST. JOHN'S UNIVERSITY
JAMAICA, NEW YORK 11432

K. PAK
A. C. TESTA*

RECEIVED NOVEMBER 22, 1971

Here is the ideal way to obtain the ***most reliable reference data available today!*** *All you need is a subscription to the new*

JOURNAL OF PHYSICAL AND CHEMICAL REFERENCE DATA

published by the American Chemical Society and the American Institute of Physics for the National Bureau of Standards.

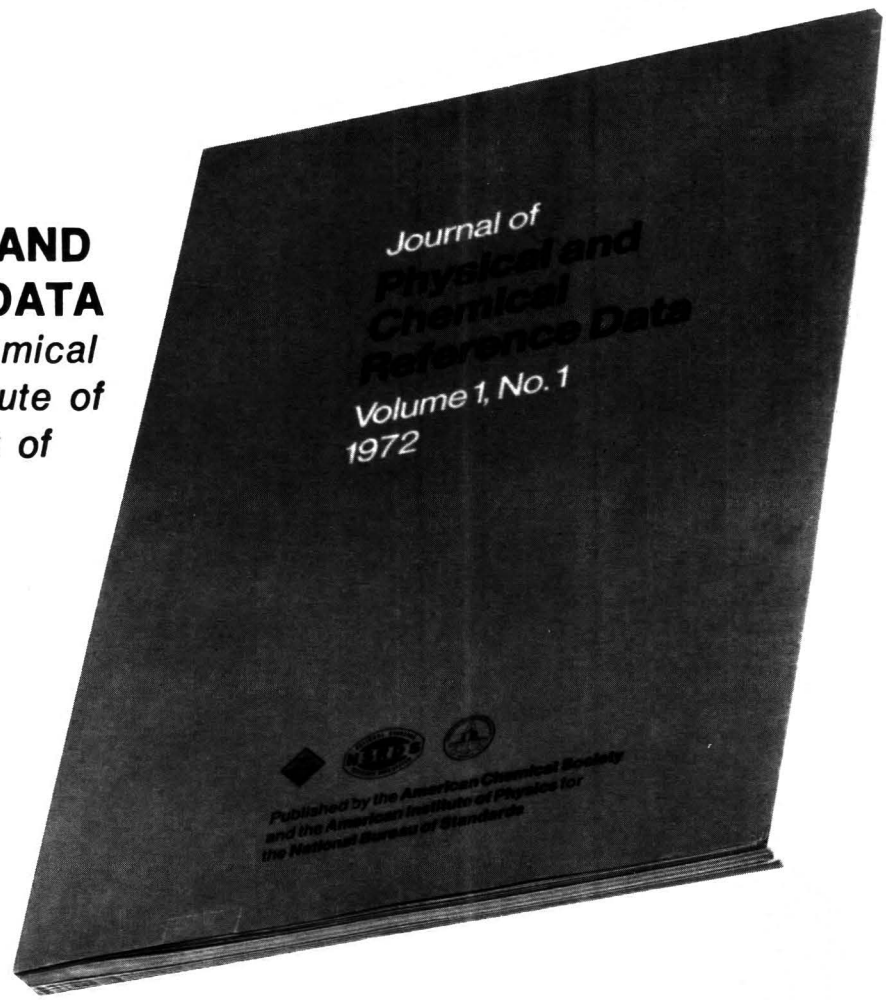

The *Journal of Physical and Chemical Reference Data* fills an important gap in the literature of the physical sciences. Its subject matter is the quantitative numerical data of physics and chemistry. As the new publication vehicle of the National Standard Reference Data System, the *Journal* will contain carefully evaluated data, with recommended values and uncertainty limits chosen by experts in each field. Critical commentary on methods of measurement and sources of error, as well as full references to the original literature, will be an integral part of each compilation.

Examples of some of the critical compilations scheduled for publication in the four issues of Volume I (1972) include:

- Tables of Molecular Vibrational Frequencies, Part 5, T. Shimanouchi
- Gaseous Diffusion Coefficients, by T. R. Marrero and E. A. Mason
- The Spectrum of Molecular Oxygen, by P. Krupenie
- Thermal Conductivity of the Elements, by C. Y. Ho, R. W. Powell and P. E. Liley
- Selected Values of Critical Supersaturation for Nucleation of Liquids from the Vapor, by G. M. Pound
- Gas Phase Reaction Kinetics of the Hydroxyl Radical, by W. E. Wilson, Jr.
- Selected Values of Heats of Combustion and Heats of Formation of Organic Compounds Containing the Elements CHNOPS, by E. S. Domalski
- Microwave Spectra of Molecules of Astrophysical Interest: Formaldehyde, Formamide, Thio-Formaldehyde, by D. R. Johnson, F. J. Lovas and W. H. Kirchhoff

Future compilations are expected to cover areas such as the following:

Band gaps in semiconductors
Nuclear moments
Atomic energy levels and transition probabilities
Diffusion in metals
Electron swarm data
Elastic constants of metals
Surface tension of liquids
Properties of molten salts
Activity coefficients of electrolytes
Equation of state of atmospheric gases
Ionization and appearance potentials

The *Journal of Physical and Chemical Reference Data* is intended to be a definitive source of reliable data on physical and chemical properties. Just fill in the order form at the bottom of this page to receive this invaluable reference source.

JOURNAL OF PHYSICAL AND CHEMICAL REFERENCE DATA
AMERICAN CHEMICAL SOCIETY
1155 Sixteenth Street, N.W.
Washington, D.C. 20036

Yes, I would like to receive the JOURNAL OF PHYSICAL AND CHEMICAL REFERENCE DATA at the one-year rate checked below:

	U.S.	Canada	PUAS	Other Countries
AIP and ACS members	$20.00	$20.00	$23.00	$23.00
Nonmembers	$60.00	$60.00	$63.00	$63.00

Bill me ☐ Bill company ☐ Payment enclosed ☐

Name _____

Street _____ Home ☐ Business ☐

City _____ State _____ Zip _____

JP 72

If you had to choose just one publication...

naturally, it would be the Journal of the American Chemical Society...

This internationally respected biweekly journal ranks number one in the field of chemistry . . .

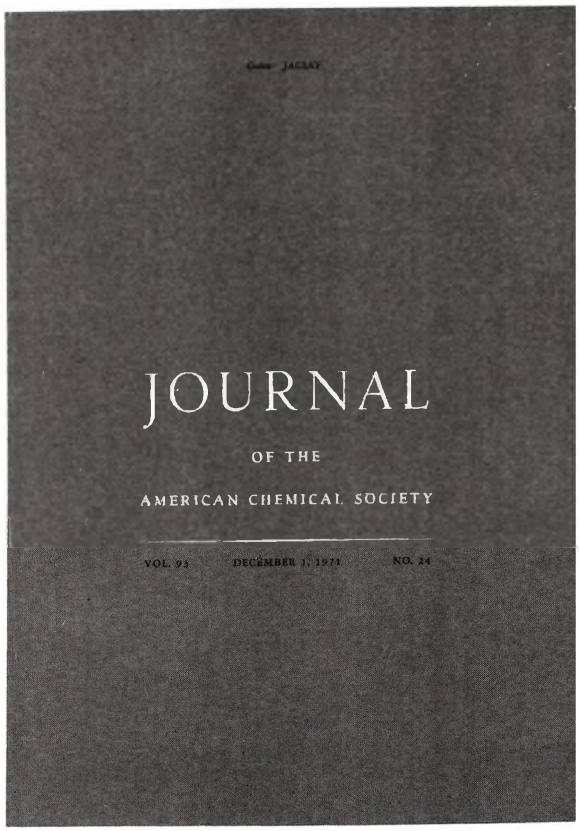

Since 1879 it has been presenting significant original research that cuts across ALL chemical research areas. It is the only ACS research journal designed to appeal across the board.

Despite the highest manuscript rejection rate among ACS journals, JACS published 6600 pages in 1971 alone. The JACS subscriber pays less per page than for any other major journal in the world.

You'll welcome its biweekly offering of both definitive articles and concise, timely communications. You'll get prompt reports on important results.

To order the Journal of the American Chemical Society, just complete and return the form below.

American Chemical Society / 1155 Sixteenth Street, N.W., Washington, D.C. 20036

Please send me the Journal of the American Chemical Society at the following subscription rates:

ACS Members: ☐ U.S. $22.00 ☐ Canada, PUAS $27.00 ☐ Other Nations $28.00

Nonmembers: ☐ U.S. $66.00 ☐ Canada, PUAS $71.00 ☐ Other Nations $72.00

Note: Subscriptions at ACS Member Rates are for personal use only.

name _____ position _____

address _____

city _____ state/country _____ zip _____

your company _____ nature of company's business _____

☐ I am an ACS member ☐ I am not an ACS member ☐ Bill me for $ _____

☐ Payment enclosed in the amount of $_____ (payable to American Chemical Society). Payment must be made in U.S. currency, by international money order, UNESCO coupons or U.S. bank draft; or order through your book dealer.

J3A